University of Nevada, Reno

A New Congenital Mouse Model to Study Laminin Protein Therapy for Muscular Dystrophy

A dissertation submitted in partial fulfillment of the

requirements for the degree of Doctor of Philosophy in

Cellular and Molecular Pharmacology and Physiology

By Caroline B. M. Coffey

Dr. Dean J. Burkin/Dissertation Advisor

December 2015

THE GRADUATE SCHOOL

We recommend that the dissertation
prepared under our supervision by

CAROLINE B. M. COFFEY

Entitled

A New Congenital Mouse Model to Study Laminin Protein Therapy for Muscular Dystrophy

be accepted in partial fulfillment of the
requirements for the degree of

DOCTOR OF PHILOSOPHY

Dean J. Burkin, Ph.D., Advisor

Sean M. Ward, Ph.D., Committee Member

Normand LeBlanc, Ph.D., Committee Member

Josh E. Baker, Ph.D., Committee Member

Subhash C. Verma, Ph.D., Graduate School Representative

David W. Zeh, Ph. D., Dean, Graduate School

December, 2015

ABSTRACT

Merosin deficient congenital muscular dystrophy type 1A (MDC1A) is caused by the loss of laminin-211 and laminin-221 heterotrimers which are most abundant in skeletal and cardiac muscle basal lamina; mutations in the LAMA2 gene cause the loss of these laminin isoforms. This absence of laminin-211/221 in MDC1A reduces the capacity for myofiber adhesion, loss of sarcolemmal integrity and subsequently the ability of the skeletal muscle syncytium to generate force in a coordinated and efficient manner. Patients experience progressive muscle wasting which confines them to a wheelchair at an early age and respiratory failure that leads to their untimely death. Currently, there is no effective treatment or cure for this devastating disease.

Previous studies have shown that laminin-111, an embryonic form of laminin, delivered before disease onset can reduce muscle pathology and improve viability in the *dy^{W}-/-* mouse model of MDC1A. These studies suggested that laminin-111 may act to strengthen and reinforce the sarcolemma and provide a protective niche for muscle repair. Since most patients are diagnosed with MDC1A after disease onset, we determined if laminin-111 could be beneficial after disease onset. Our studies suggest *dy^{W}-/-* mice treated with laminin-111 after disease onset show improvement in muscle function and histology. Results from this study along with an understanding of laminin-111 pharmacokinetics will help pave the way in developing this protein as an exciting potential therapeutic for MDC1A patients.

Duchenne Muscular Dystrophy (DMD) is the most common X-linked disease affecting 1 in 3,300 live male births. Patients with DMD suffer from severe, progressive muscle wasting and weakness with clinical symptoms first detected between 2 to 5 years of age; as the disease progresses patients are confined to a wheelchair in their teens and die in their early 20s mainly due to cardiopulmonary complications. DMD is caused by the loss of the sarcolemmal protein dystrophin (427kDa) due to mutations in the dystophin gene. When present, dystrophin acts as a scaffold linking the cell cytoskeleton to the extracellular matrix. This loss of dystrophin in DMD results in patients experiencing greater susceptibility to muscle damage via reduced structural and functional integrity of their muscle.

One potential therapeutic avenue that needs to be explored involves increasing the levels of the α7β1 integrin in order to compensate for the loss of dystrophin. To test this hypothesis, a muscle cell-based assay was developed in order to report α7 integrin promoter activity with the intent of identifying molecules that promote α7 integrin expression. Laminin-111 was identified as an enhancer of α7 integrin expression. Theoretically, the identification of α7 integrin enhancing compounds that help boost α7β1 integrin expression as part of drug-based therapies may lead to a novel therapeutic approach for the treatment of this disease.

Systemic laminin-111 treatment significantly reduces myofiber degeneration in both forms of MDC1A and DMD muscular dystrophy. This dissertation reinforces the potential of laminin-111 as a systemic protein therapy,

capable of restoring sarcolemmal integrity thus reducing muscle disease progression. The importance of α7 integrin in skeletal and cardiac muscle was highlighted here through the generation of the α7-/-:: laminin-α2-/- double knockout mouse model. This mouse has never been studied before and could prove to be another important mouse model needed to explore therapeutic avenues for muscular dystrophy.

DEDICATION

To my Mum, Dad, Dearest Family and Friends

I will be forever grateful for your continuous love and support.

Thank you with all my heart. I hope that I have made you proud.

Non Providentia Sed Victoria.

ACKNOWLEDGEMENTS

A special thanks to Dr. Dean Burkin for giving me this wonderful opportunity. Notwithstanding, my sponsor Tracy McCausland, founder of Struggle Against Muscular dystrophy (SAM) charity in Northern Ireland for providing me with a fellowship to carry out the research for my dissertation. Tracy's determination to save her son, Sam who currently suffers from MDC1A inspired me to take the challenges regards finding a cure. Throughout the course of my dissertation, I would like to express sincere gratitude to CureCMD and all scientists worldwide for all their commitment and hard work trying to find cures for diseases. My undergraduate students Vivian Cruz, Annemarie Vogedes, and Chelsea Lamb. I would also like to thank Dr Jachinta Rooney whom I had the opportunity to work under for a year when I was an undergraduate and also Dr. Jinger Doe for her unstinting support with my work.

I want to thank my dissertation committee Dr. Sean Ward, Dr. Normand Leblanc, Dr. Subhash Verma and Dr. Josh Baker. I would like to thank Dr. Ward especially for helping me towards the later stages of my PhD. Without you, I would not have been able to have a place to finish my lab work. I will always be grateful to you for giving me the opportunity to arrive at UNR all those years ago for the International Undergraduate research Program (IURP). It was the most exciting time of my life and I am truly indebted to you for helping me in my hour of need in recent times.

Dr. Sang Don Koh offered me very helpful advice a few months ago, science involves passion, pain and perseverance. There are many people I wish to thank and I will try to include everyone in this next paragraph. Please accept my apologies if I have left anyone out as I really do appreciate those who have helped me. Dr. Leonie Corrigan, a big thank you to you for guiding me through CMPP. Yulia Bayguinov and Dr. Sung Jin Hwang for their continuous help within the lab this past year. Also special thanks to Sima, Breeana & Mark, Jolie, Lara & Peter, Caroline, Robert, Jon, Monica, Robyn, Prabath, and Rahul and to everyone who helped provide me with transport in order to go purchase groceries from time to time; I really appreciated it! Queen's University Belfast, Dr. Tom Gardiner whose unstinting encouragement and support inspired me and also Dr. Mihaela Ghita, Dr Guiseppe Schettino and Dr. Kevin Prise, Pro-Vice Chancellor Dr. Patrick Johnston, and Dr. Stephen McCullough. Lab animal medicine especially Dr. Walt Mandeville and his team for their expertise and care of the mice I worked with. Dr. Kent Sanders and Dr Iain Buxton for their constructive and helpful advice. All the physiology and pharmacology administrative staff, Dr. Paul Brewer, and Dr. Andrea Agarwal for echocardiography data analysis. Dr. David Zeh for his time and helpful advice. I would like to thank Dr. Joseph Fass and Dr. Ryan Kim for generating and processing the RNA-Seq data at the UC Davis Genome center. UNR Campus escort service, IT staff, Janitors in the medical school for always being so friendly and providing a clean environment to work in.

Thank you to Kevin Van Ry and Thomas Knapp for their much needed muscle power when I had to move apartments. Office of International Students and Scholars (OISS), my Japanese friends at Intensive English Language center (IELC). My hairdresser Antonio for always being a friendly person. Canteen staff for providing delicious snacks. I would also like to give shout out to the UNR bus drivers especially to Tina and KJ who supported me throughout and became two of my best friends, for always getting me safely to my destination on campus and always with a smile ☺. My medical team for their much needed support through this past year. You are all so wonderful!

Thank you to my Mum, Donna, my Dad, James and my younger sister, Natalie for listening to me and providing support for me on the phone 24/7 no matter what happened throughout the entire course of my PhD. To my extended family, Bernadette, Nicola, Carmela, Jim, Maureen, Stefin, Mary in Co. Donegal Ireland. My American family, Eamonn, Lisa, Liam and Zara for their continued support in San Francisco (and for letting me stay each time I was there!)..... I have some really great memories there with you all and will never forget them.

It only feels like yesterday that I was graduating from Queen's University Belfast. There is one very poignant message that I will never forget from the graduation speech delivered to all the graduants that day. The life message was "Sail away from the great harbor, catch the trade winds in your sails. Dream, Explore and Discover" ~Mark Twain. I aim to follow this approach throughout my life and I hope never to forget that.

UNR has been an amazing journey and I am so glad that I embarked on this adventure. I got to meet some truly inspirational people from all corners of the globe and embrace their cultures whilst I was living, studying and working independently in Reno. As a young girl growing up in Northern Ireland, I honestly never thought that I would be able to visit USA let alone be making a life for myself here 5,000 miles away from my home. It's been an emotional rollercoaster driving me through some very happy and indeed some incredibly dark times. But despite this I am grateful for this life journey that I have experienced. I hope to be able to have many more adventures in the future. Not only did the PhD help me to develop as an academic but also into an independent young woman who is constantly learning. All my friends and family here in USA, United Kingdom and scattered across the world; thanks for keeping in contact with me.

Thank you to my parents for teaching me to always stand up for what is true no matter what the consequence; one essential part of life. I would like to thank everyone who helped me at every stage throughout my PhD journey. Your help was much appreciated. I thank the people of Reno for making me feel so welcome. I will miss you lots but I'll be back to visit one day. Thank you to everyone who believed in me. I am truly grateful.

Sláinte!

TABLE OF CONTENTS

List of Figures

List of Tables

Chapter I

Introduction

Muscular Dystrophy

There are many different types of muscular dystrophy which are all caused by genetic defects within the contractile machinery or cell-matrix adhesion components in skeletal muscle[1–23]. Despite extensive research over the years, only palliative care is available which proves to be expensive as there is still no cure for these neuromuscular diseases[24-26].

Myogenesis and Muscle development

Myogenesis happens when the myotome is formed from a portion of somites[27–30]. Muscle development regulates α7 integrin and α7β1 integrin has been shown to participate in the formation of skeletal muscle during development with detection of α7β1A integrin occurring when myocytes migrate to the peripheral targets from the myotome[30,31]. Several rounds of proliferation are carried out by muscle precursor cells prior to myoblast fusion to form myofibers[27,32]. Formation of myofibers happens in two processes, primary and secondary myogenesis. There is alignment of primary myoblasts into rows and their subsequent fusion to form multinucleated cells which are then ensheathed by a basal lamina enriched by laminin[33,34]. Secondary myoblasts fuse forming binucleate cells and then there is insertion of additional myoblasts along the entire length of the myofiber in order to help elongate the developing muscle cell[35]. It is thought that the α7β1 integrin helps to home primary myoblasts to regions of myofiber formation and to laminin during development[27,29,36–38].

Differentiation happens whenever the muscle cells become quiescent[35]. Once this occurs, there is an increase in the accumulation of muscle-specific genes and myofiber proteins of the contractile apparatus[39]. Motor units therefore start to form via differentiation of the dynamic developing cells[39,40].

Skeletal muscle

Skeletal muscle is responsible for almost all movements made under voluntary control[41]. It is made up of bundles of muscle fibers which are formed when myoblasts fuse into long cylindrical multi-nucleated cells which are held together by connective tissue. Satellite cells are ever present in the periphery of the muscle in order to help regenerate the muscle after damage[42]. The satellite cell supply becomes exhausted whenever there is too much repetitive damage occurring to the muscle and therefore there is a much more exaggerated clinical phenotype in dystrophic patients[43–47].

Sarcolemma

The sarcolemma consists of at least three systems that are able to protect the muscle during the sheer forces of muscle contraction[48–51]. The three systems couple the contractile apparatus to the muscle membrane and surrounding extracellular matrix[48–52,53]. These complexes form molecular associations with laminin in the basal lamina that surrounds each myofiber to cytoskeletal F-actin within myofibers[58-56]. The sarcolemmal complexes are known as the dystrophin glycoprotein (DGC) complex, utrophin protein complex and the α7β1 integrin

complex[48–51] (Figure 1). The α7β1D integrin is found to be enriched around costameres where they are thought to be able to facilitate transmission of lateral contractile force[62-68].

α7β1 integrin

The α7β1 integrin is a heterodimeric cell surface receptor member of the large family of integrins[60] (Figure 1). The α chain and β chain are noncovalently linked and integrins in general are evolutionarily conserved[55,61]. Integrins act as receptors for a variety of cellular components to include, leukocytes, RGD, collagen and laminin[55]. The α7β1 integrin is prevalent within skeletal, cardiac and vascular smooth muscle. There are many splice variants of α7β1 integrin that exist. There are 3 intracellular (α7A, α7B and α7C) and 2 extracellular (X1 and X2) splice variants[28,62,63,64]. The β1 integrin possesses variants β1A and β1D, with β1D being the major isoform in mature skeletal muscle[51]. The α7β1 integrin complex is elevated in order to compensate for the instability of the dystrophin glycoprotein (DGC) laminin binding complex due to loss of dystrophin in Duchenne Muscular dystrophy (DMD)[50]. α7 integrin overexpression is able to rescue the severe dystrophic phenotype of *mdx*/*utr* $^{-/-}$ mice and improve the viability of these mice[51]. MDC1A patients have decreased α7β1 integrin expression[65]. This integrin is found localized at costameres, myotendinous junctions and neuromuscular junctions[59,60].

Dystrophin glycoprotein laminin binding complex

The dystrophin glycoprotein (DGC) complex is found in skeletal, cardiac and vascular smooth muscle (Figure 1). It plays a very important function in providing structural integrity and signaling roles to all of these muscle types, especially skeletal muscle[66]. Laminin in the extracellular matrix binds to this DGC complex[49]. Dystrophin (427 kDa) protein is a major component to this complex and links laminin in the extracellular matrix to cytoskeletal F-actin[56]. The N-terminus binds to actin and the C-terminus of dystrophin associates with β-dystroglycan which is a transmembrane protein and it interacts with α-dystroglycan, the sarcoglycans and sarcospan[67]. α-dystroglycan can bind extracellular matrix components such as laminin, perlecan and agrin[67]. The C-terminus of α-dystroglycan interacts with cytoplasmic proteins to include dystrobrevins and syntrophins[11].

Dystrophin plays a structural role within muscle by providing a link between myofibers and the ECM. This structural scaffold helps aid muscle contraction and strength to withstand the sheer mechanical stress associated with normal contraction. Dystrophin is more prevalent around costameres of the sarcolemma, myotendinous junctions and neuromuscular junctions[68,69]. Signaling pathways become mis-regulated whenever dystrophin is missing which causes weakness within the structure of muscle[67]. Muscular dystrophy arises when there is any loss of DGC protein causing weakness in this link between cytoskeletal F-actin and the extracellular matrix. The DGC proteins are not able to compensate

for the loss of dystrophin which is the main gatekeeper for the entire structure and function of the DGC complex needed for integrity of muscle.

Laminin-α2

Laminin- α2 is also produced by Schwann cells in the Peripheral Nervous System (PNS). In MDC1A, the laminin- α2 deficiency means that the Schwann cells are unable to myelinate the nodes of Ranvier on the nerves. As a consequence, peripheral neuropathy and impaired conduction velocity ensue[70]. Laminin- α2 is the major laminin chain in the basement membrane of adult skeletal muscle[71]. MDC1A is caused by mutations in the laminin- α2 gene. This laminin- α2 deficiency has been modeled in mice to include the *dy^{W} -/-* mouse model which is described and studied in this dissertation. This mouse model is able to emulate the symptoms experienced by MDC1A patients which include muscle weakness, hypotonia from birth and joint contractures at an early age. With these symptoms in mind, this mouse model offers a good baseline to study MDC1A due to its overt phenotype. Two protein complexes rely on this association of laminin- α2 binding to myofibers[72,73]. These complexes are known as the dystroglycan and α7β1 integrin. Laminin-α2 is the major ligand for the α7β1 integrin although it can interact with alternative isoforms of laminin to include laminins α1, α4 and α5 as well as galectin-1 and fibronectin[32].

Cardiac muscle

Cardiac muscle is very similar to skeletal muscle as it contains sarcomeres due to precise alignment of actin and myosin filaments, although

cardiac organization is not as regular and only offers involuntary contractions vital to its function. Cardiac muscle is the most extensively used muscle within the body having to contract more than 3×10^9 throughout the life of an average human. Cardiomyocytes express specific isoforms of myosin and actin. Serious heart disease can occur even with very subtle changes in these contractile apparatus proteins. Because of the frequency of repetition in the cardiac muscle, such tiny abnormalities in the contractile apparatus can gradually degrade the heart over time causing serious health defects such as familial hypertrophic cardiomyopathy as a result of 1 of 40 subtle point mutations in genes encoding cardiac β myosin heavy chain or contractile proteins causing cardiac arrhythmias[74]. Dilated cardiomyopathy can also result in heart failure due to minor missense mutations in the cardiac actin gene. These are only a few examples to emphasize how subtle changes can cause detrimental effects[41,52,75].

Adherens junctions anchor the actin bundles of the contractile apparatus and act in parallel to desmosome junctions to link the contractile cells end-end. Stained light-microscope sections show these cell-cell adhesions very clearly as they are visible as intercalated discs which are a unique characteristic of cardiac muscle[76–78]. Action potentials fired along cardiac muscle typically last > 200 msec[53] allowing the cardiac muscle to relax during a refractory period before blood filling again whereas many skeletal muscle action potentials are fired typically lasting 1-5 msec.

Laminins

Laminins comprise a large family of heterotrimeric glycoproteins comprised of an α chain, β chain and γ chain. They are highly conserved extracellular matrix proteins throughout evolution[79]. To date, 16 different laminin heterotrimers have been identified with which there are different combinations of 5 α, 2 β and 3 γ chains[80,51]. The isoforms of laminin have different preferences for their tissue distribution[80,81]. The α chain is the most variable and dictates binding specificity of the laminin heterotrimer[80]. α1 and α5 chains are important for embryonic development and organogenesis while α2, α3 and α4 are critical for postnatal developmental processes[82]. The basal lamina underlying epithelia, nerve and muscle, is essentially composed of laminins, collagen IV, nidogens, perlecan and agrin[71]. Laminins have special functions in creating structural integrity through cell-extracellular matrix adhesions and cell signaling such as tissue proliferation, survival, migration and differentiation[71].

Two major receptors for laminins- 111, 211 and 221 are α-dystroglycan (a member of the dystrophin glycoprotein (DGC) laminin binding complex) and the α7β1 integrin. α-dystroglycan interacts with laminin-α2 via the G-domain (COOH-terminus)[71,72]. The polymerization of individual laminin proteins occurs at the N-terminus of laminin. Laminin is a distinct membrane protein which can be separated from collagens and fibronectin in their description[72].

Muscle contraction and Force transduction

Normal muscle function requires very precise organization of all the contractile machinery within the muscle ultrastructure. The muscle syncytium needs to be able to contract in unison for efficient movement. Skeletal muscle is controlled by the central nervous system (CNS). Each myofiber is innervated by an α motor neuron. The neuromuscular junction forms at a specialized cholinergic synapse at an α neuron called an end-plate. An action potential is produced in a myofiber after neuromuscular transmission[74,75]. A motor unit comprises of the motor nerve and all the muscle fibers innervated by the nerve. It is described as the functional contractile unit because all the myofibers within a motor unit contract synchronously when the motor unit fires an action potential. Activation of varying numbers of motor units within a muscle is one way in which muscle tension can be controlled[74,75].

Acetylcholine released from the motor neuron initiates an action potential < 5 msec in the myofiber that rapidly spreads along the length of the myofiber[74]. The short duration of the skeletal muscle action potential allows very rapid contractions of the myofiber and provides a mechanism by which the force of contraction can be increased. This increasing muscle tension by repetitive stimulation of the muscle is called tetanus[74]. The method by which skeletal muscle contracts is known as excitation-contraction coupling. It is when an action potential is transmitted along the sarcolemma and then into T-tubules, Ca^{2+} is then released from the terminal cisternae sarcoplasmic reticulum (SR) into the myoplasm and binds to Troponin C. This release of Ca^{2+} from the SR raises

intracellular Ca^{2+} which in turn promotes actin-myosin interaction and contraction called a twitch. Relaxation of skeletal muscle occurs as intracellular Ca^{2+} is resequestered by the SR[74].

The process of skeletal muscle contraction is not only regulated by intracellular calcium but also by the thin filament actin. Once Ca^{2+} released from the SR binds to troponin C there is a movement of tropomyosin initiated towards the cleft of the actin myofilament[74]. This movement exposes the myosin binding site on the actin filament and allows a cross-bridge to generate tension. Troponin C has 4 Ca^{2+} binding sites in total and two of these sites have a high affinity for Ca^{2+} switch their preference to Mg^{2+} at rest. These sites control interactions with troponin I and troponin T. The other two binding sites have a lower affinity for Ca^{2+} but bind Ca^{2+} when it is released from the SR. Tropomyosin gets further shifted due to myosin heads binding to actin filaments. It is thought that one myosin head binding to actin filaments can cause a shift in tropomyosin perhaps exposing myosin binding sites for up to 14 actin molecules[74].

Actin filaments get moved towards the center of the sarcomere due to ATP-dependent conformational changes of myosin molecule after myosin and actin have bound to each other. Such movement of actin results in sarcomere shortening and therefore contraction of the myofiber. These repetitive movements are known as cross-bridge cycling-sarcomere shortening[74]. The collective term for the entire process is the sliding filament theory because the myosin cross-bridge is pulling the actin thin filament toward the center of the

sarcomere thereby sliding the thin filament past the myosin thick filament[74]. The skeletal muscle syncytium means that each one of these muscle twitches described get amplified into a huge force generation within the muscle which is needed for movement.

Merosin Deficient Congenital Muscular Dystrophy

Merosin deficient congenital muscular dystrophy (MDC1A) is caused by the loss of Laminin-211 and Laminin-221 heterotrimers which are most abundant in skeletal and cardiac muscle basal lamina; mutations in the *LAMA2* gene cause the loss of these Laminin isoforms. This reduction of laminin reduces the capacity for myofiber adhesion, loss of sarcolemmal integrity and subsequently affects the ability of the skeletal muscle syncytium to generate force in a coordinated and efficient manner[3,5,73,91-87]. Patients, from birth, experience progressive muscle wasting which confines them to a wheelchair at an early age and respiratory failure that leads to their untimely death. Currently, there is still no effective treatment or cure for this devastating disease.

Merosin deficient congenital muscular dystrophy (MDC1A) affects approximately 0.89/100,000 individuals worldwide (1:100,000 - 1:500,000) and is thought to be the most common form of congenital muscular dystrophy affecting 30-40% of all diagnosed CMD cases[88]. Loss of merosin (Laminin-α2 protein) is caused by mutations occurring in the *LAMA2* gene which is located on chromosome 6q22-23 spanning ~260 kb with 64 exons [73,89-100]. This loss of Laminin-α2 protein in MDC1A results in the absence of Laminin-211 and

Laminin-221 heterotrimers which are abundant in skeletal and cardiac muscle basal lamina. Patients, also experience demyelinating neuropathy, muscle atrophy, limited eye movement and also respiratory failure that leads to their untimely death which can be as early as the first decade of life [88,92–94]. There is an increased likelihood of seizures occurring after six months of age due to changes in white matter of the brain [97,101-102]. Symptoms depend on where the mutation occurs and a mutation which results in no laminin-α2 protein being produced will result in a more severe clinical phenotype compared to a mutation which produces a truncated form of laminin-α2. Currently, there is still no effective treatment or cure for this cruel disease [24,88].

Duchenne Muscular Dystrophy

Duchenne Muscular Dystrophy is a genetic disorder that affects the skeletal and cardiac muscle. Duchenne Muscular Dystrophy (DMD) is the most common type of muscular dystrophy in boys[95]. It is an X-linked disorder that affects 1 in every 3,300 live male births. This disorder results from a mutation in the DMD gene which produces three isomers of the protein Dystrophin. Dystrophin is a protein that connects muscle fiber cytoskeleton to surrounding laminin in the extracellular matrix. This connection provides structural integrity during muscle contractions. The failure to produce dystrophin results in the inability for the formation of the dystrophin-laminin binding complex which results in severe muscle weakness[96]. Children with DMD are not able to walk and are wheelchair-bound by their teenage years[95]. The progressive nature of DMD leads

to feeding tube placement, cardiomyopathy, ventilator assistance and results in the untimely death of DMD patients[97-98]. Although the dystrophin gene has been known for well over 20 years there is still no effective treatment or cure for this disease.

Mouse models

Mdx

The *mdx* mouse model has a point mutation in the dystrophin gene that produces a nonsense codon, resulting in a premature termination of translation and a lack of dystrophin protein[99,100]. *Mdx* mice have a very different phenotype to DMD patients. The *mdx* mice exhibit a near normal lifespan and the dystrophy phenotype they exhibit is relatively mild compared to that of DMD patients. The mdx mouse goes through rounds of muscle degeneration followed by complete regeneration between 3 and 10 weeks of age. After this time-point, muscle degeneration ceases in limb muscles and lack of evidence of scar tissue formation[110-111]. Diaphragm muscle harvested from *mdx* mice does however retain muscle pathology throughout its lifetime[112-113]. The GRMD dog model recapitulates the disease in DMD patients and is considered the gold standard to mouse muscle pathology and therapeutics[105].

dy^W -/-

The *dy^W-/-* mouse is a knockout mouse model for which there are other models offered. Three other mouse models offer spontaneous mutations to study[106–111]. *dy^W-/-* mice have decreased transcript and protein levels of the α 7

integrin chain and the β1D integrin isoform is thought to be responsible for a more differentiated state in *dy^{W}-/-* mice. Protein levels of α7 integrin are also decreased in laminin- α2 deficient patients. Utrophin, dystrophin and associated proteins remain unchanged in laminin-α2 deficient *dy^{W}-/-* mice and MDC1A patients[73,112]. There is significant strain variation noticed across published studies for *dy^{W}-/- dy/dy, dy^{2J}/dy^{2J}* and *dy3k-/-.*

α7dy

The *α7dy* double knockout mouse model of both laminin-α2 and α7 integrin talked about in this dissertation is the first known study of its kind for this particular *dy^{W}-/-* mouse model.

Laminin-111

Isolation and identification of laminin-111 from Engelbreth-Holm Swarm (EHS) mouse sarcoma was the first time that the laminin family was described[113]. Laminin-111 (α1, β1 and γ1) is the predominant laminin isoform during embryonic development and is replaced by laminins 211 and 221 in mature differentiated skeletal muscle[71,114–116] (Figure 2). This genetic switch from laminin-111 to laminin-α2 occurs at embryonic day 11 in mice and within humans it is at 7 weeks gestation with maximal expression at 21 weeks gestation[117–119]. The role of embryonic laminin-111 and laminin-α2 is to anchor the myofibers to the basement membrane. Laminin-α2 is highly glycosylated due to post-translational modifications before being secreted by myofibers[71]. In MDC1A patients, laminins α4 and α5 are upregulated[71,120].

In MDC1A, apoptosis is a common characteristic due to the laminin- α2 deficient myotubes being unable to anchor myofibers to the extracellular matrix therefore causing instability within the muscle[130-123]. *In vitro* studies support this claim due to laminin- α2 deficient C2C12 myoblasts being unable to form stable myotubes and whenever laminin- α2 expression is reinstated then myotube stability is returned[121]. Laminin- α2 deficient myotubes are also responsible for decreased regenerative capacity after injury[124].

Summary

The main hypothesis of this dissertation is that laminin-111 will act as an effective replacement protein therapy for the loss of laminin-α2 in the *dy^{W}-/-* model of MDC1A and dystrophin in *mdx* model of DMD. Similar to how experimental animals were designed as double knockouts to lack both dystrophin and α7 integrin (*mdx/α7$^{-/-}$)* and resulted in a more severe phenotype than single knockout animals, a double knockout of both laminin-α2 and α7 integrin was created in order to study the full extent to which α7 integrin plays in laminin-α2 deficient muscle.

Chapter 2 discusses laminin protein therapy after disease onset. Laminin-111 treatment was effective in reducing percentage (%) muscle fatigue in 8 week old *dy^{W}-/-* mice. Treatment with laminin also helped to improve the overall integrity of the muscle whilst helping to reduce scar tissue formation. This in turn helped to improve activity of these animals post-treatment after disease onset.

Chapter 3 looks at transcriptional changes within diaphragm muscle in a *dy^{W}-/-* mouse model treated before disease onset. RNA-Seq experiments helped to identify osteoactivin (GPNMB) as a novel biomarker of MDC1A disease progression. Our results also reemphasized the role of Galectin-3 as a biomarker in this disease. Laminin-111 treatment also helped to restore many sarcolemmal proteins and improved muscle function by reducing muscle fibrosis. This study will help pave the way in teasing out the molecular pathways associated with MDC1A disease progression and treatment.

Chapter 4 looks at long term laminin treatment of *mdx* mice. This study basically showed that extensive treatment with laminin-111 had no added benefit compared to short-term treatments in younger mice. The lack of significance in the results for laminin treated animals could reflect the fact that the *mdx* mice have no overt dystrophic phenotype after 10 weeks of age. Repetitive treatment over a period of 1 year was expected to have a positive effect but the data was disappointing and may be explained by receptor desensitization. However, there was elevated EBD uptake and increased kyphosis within PBS treated animals. Laminin treatment helped to reduce muscle hypertrophy at 10 weeks old. Treatment also reduced muscle fatigue experienced and there was an increase in the sarcolemmal protein, β-DG.

Chapter 5 studies the new mouse model α7 integrin -/-:: laminin-α2 -/- double knockout for muscular dystrophy. This study analyzes the effects on skeletal and cardiac muscle with severe kyphosis and atrial flutter/fibrillation

occurring within this new double knockout mouse model[125–130]. There was also elevated scar tissue deposition within cardiac muscle and embryonic lethality experienced. Laminin-α2 presence proved to be most critical for prevention of MDC1A disease severity.

Chapter 6 offers conclusions and future directions associated with this work. In summary, this dissertation provides evidence that laminin-111 is beneficial with treatment before disease onset by reducing muscle pathology and increasing functional activity within mice. It is also the first time that the α7 integrin -/-:: laminin-α2 -/- double knockout mouse model has been studied and described for this particular *dy^{W}*-/- mouse model.

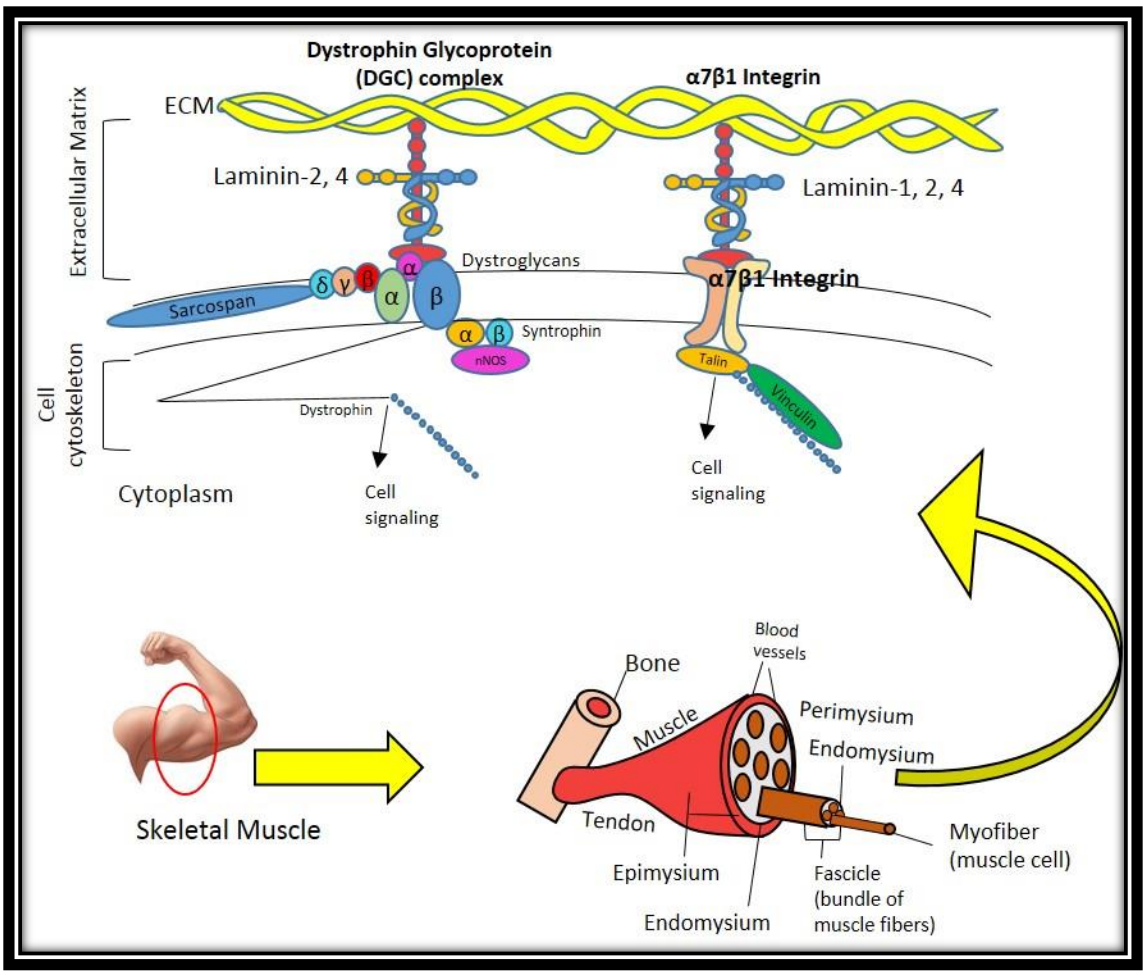

Figure 1. Main sarcolemmal proteins associated with both the extracellular matrix and intracellular cytoplasm present in each individual myofiber

Diagrammatic representation of skeletal muscle which is magnified in order to show how the skeletal muscle is attached to the bone via tendons. Bundles of myofibers (fascicles) are surrounded by connective tissue called the perimysium, which is in turn enveloped by the epimysium. Individual myofibers are surrounded by connective tissue known as endomysium. At the top of the diagram, there is a schematic diagram highlighting the main sarcolemmal proteins present in each healthy individual myofiber.

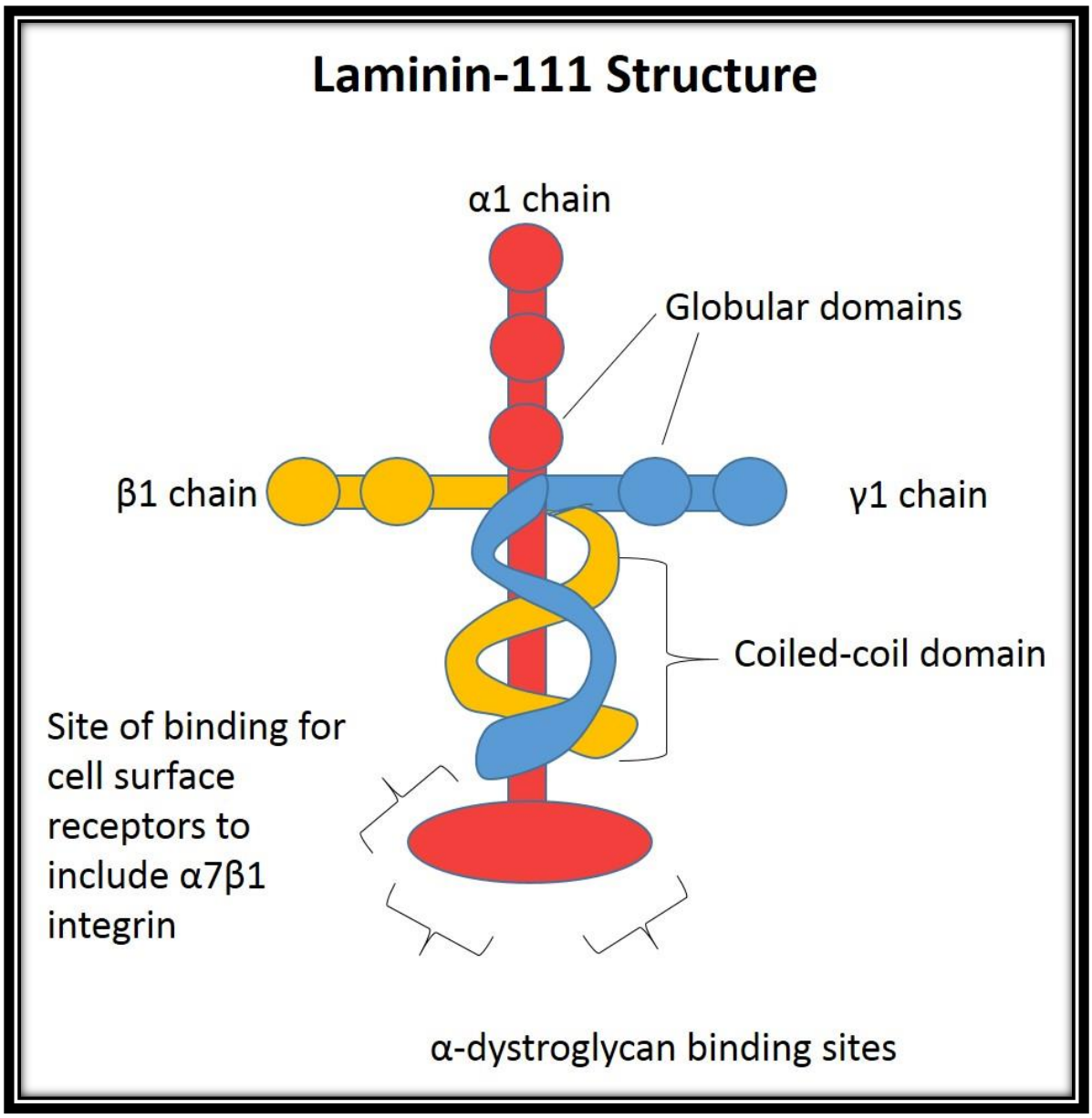

Figure 2. Schematic structure of laminin-111 protein

Laminin-111 protein consists of three chains (α1, β1, γ1) that each have their own globular domains. The overall laminin-111 protein shape and coiled-coil domain, contributes to its very distinctive cruciform structure. The base of laminin-111 cruciform provides binding sites for cell surface receptors such as α7β1 integrin and sarcolemmal proteins such as α-dystroglycan.

Chapter II

Laminin-111 protein therapy after disease onset in the *dy^{W}* mouse model for MDC1A

ABSTRACT

Merosin deficient congenital muscular dystrophy type 1A (MDC1A) is caused by the loss of laminin-211 and laminin-221 heterotrimers which are most abundant in skeletal and cardiac muscle basal lamina; mutations in the LAMA2 gene cause the loss of these laminin isoforms. This absence of laminin-211/221 in MDC1A reduces the capacity for myofiber adhesion, loss of sarcolemmal integrity and subsequently the ability of the skeletal muscle syncytium to generate force in a coordinated and efficient manner. Patients experience progressive muscle wasting which confines them to a wheelchair at an early age and respiratory failure that leads to their untimely death. Currently, there is no effective treatment or cure for this devastating disease.

Previous studies have shown that laminin-111, an embryonic form of laminin, delivered before disease onset can reduce muscle pathology and improve viability in the *dy*^{W}*-/-* mouse model of MDC1A. These studies suggested that laminin-111 may act to strengthen and reinforce the sarcolemma and provide a protective niche for muscle repair. Since most patients are diagnosed with MDC1A after disease onset, we determined if laminin-111 could be beneficial after disease onset. Our studies suggest *dy*^{W}*-/-* mice treated with laminin-111 after disease onset show improvement in muscle function and histology. Results from this study along with an understanding of laminin-111 pharmacokinetics will help pave the way in developing this protein as an exciting potential therapeutic for MDC1A patients.

INTRODUCTION

Patients with MDC1A are usually diagnosed after disease onset whenever little children are not able to walk properly and fall over easily. Previous studies have shown that laminin-111, an embryonic form of laminin, delivered before disease onset can reduce muscle pathology and improve viability in the *dy^{W}-/-* mouse model of MDC1A[131]. These studies suggested that laminin-111 may act to strengthen and reinforce the sarcolemma and provide a protective niche for muscle repair. Because systemic laminin-111 treatment was able to have many beneficial effects before disease onset (previously published)[131,132], we therefore carried out this study to investigate whether laminin-111 protein would be able to have the same beneficial effects when treatment was started after disease onset in *dy^{W} -/-* mice. This study would be a step towards trying to link what happens at the patient bedside to one of the current accepted mouse models used to study this disease[124,133].

MATERIALS AND METHODS

Generation of laminin-α2 -/- mice

All experiments involving mice were performed under an approved protocol from the University of Nevada, Reno Institutional Animal Care and Use Committee. The *dy^{W}+/-* mice were a gift from Eva Engvall via Paul Martin (The Ohio State University, Columbus, OH, USA). Male and female heterozygous mice were bred. In order to genotype mice, genomic DNA was isolated from tail snips

or ear notches using a Wizard SV DNA purification system (Promega, Madison, WI) following manufacturers instructions. To detect the mutation in the laminin-α2 gene, the following primers were used: DYWF (5'-ACTGCCCTTTCTCACCCACCCTT-3'), LAMA2exonR1 (5'-GTTGATGCGCTTGGGAC-3') and Lac/ZR2 (5'-GTCGACGACGACAGTATCGGCCTCAG-3'). PCR conditions were as follows: 95°C for 5 minutes then 33 cycles of 94°C for 20 seconds, 62°C for 30 seconds and 72°C for 45 seconds. After these cycles, then 72°C for 10 minutes. A wild-type band was 250 bp whereas the laminin- α2 targeted allele produced a 480 bp band.

Experimental procedures were performed once mice were 4 weeks of age with weekly weighing until the end of study which was at 8 weeks of age where all mice were subject to *in vivo* experiments. To reduce experimental bias, investigators assessing and quantifying experimental outcomes were blinded to the treatment and control groups.

Animal husbandry

dy^{W} -/- mice were housed with their wild-type littermates alongside the provision of mashed kibble and access to water. Husbandry and protocols were carried out via IACUC approval. Knockout mice that lost ≥ 20% body weight (g) were euthanized. Pups were genotyped at 10 days old and at the end of each study, the female WT and *dy^{W}-/-* mice were euthanized by CO_2 inhalation in accordance with a protocol approved by the University of Nevada, Reno Animal

Care and Use Committee. The diaphragm muscles from these mice were dissected, flash-frozen in liquid nitrogen and stored at -80°C as previously reported by [134].

Laminin-111 protein treatments

dy^{W} -/- mice were intraperitoneally injected with 0.01 mg/g/week of laminin-111 protein (Invitrogen). Laminin-111 was stored at -80°C and thawed slowly at 4°C overnight before use. *dy*^{W} -/- mice were intraperitoneally injected (weekly) from 4 weeks old until 8 weeks old.

Experimental Design

4 week old female Wild-type (n=22) and *dy*^{W} -/- (n=10) mice systemically treated with (0.01 mg/g/week) EHS mouse laminin-111 until 8 weeks old. Alongside this treatment group *dy*^{W} -/- control mice (n=14) were systemically injected with a volume of sterile Phosphate buffered saline (PBS) that equated to such in the laminin-111 treatment group. At 8 weeks of age, PBS and laminin-111 treated *dy*^{W} -/- mice were sacrificed following a protocol approved by the Animal Care and Use Committee at the University of Nevada, Reno. Analysis of WT, PBS and laminin-111 treatment groups at 8 weeks of age was planned with the hope of identifying what changes occur within the functional activity and muscle pathology of these animals.

Weights

Weights for all mice of each genotype were recorded on a weekly basis. Softened kibble was provided fresh daily in a petri dish on the bottom of the cage in order to ensure there was no significant weight loss within the mice.

Muscle Strength

Muscle strength assessed at 10 weeks of age using the Chatillon DFE Digital Force Gauge (San Diego Instruments Inc., San Diego, CA). A total of six measurements per mouse were recorded and all results averaged for each group. The mice were analyzed by grasping a horizontal platform with their forelimbs and pulled backwards. The peak tension (grams of force) was recorded on a digital force gauge as mice released their grip.

Functional and activity

Opto-Varimex 4 Activity Meter (Columbus Instruments) offered unbiased data due to the machine possessing lasers that monitor and auto-track the activity of each mouse for a period of 30 minutes.

Plethysmography

Animals were subjected to plethysmography at 8 weeks of age. Animals for each genotype were used. Animals were placed in the plethysmography chamber (unrestrained) and then subjected to increasing does of aerosolized Acetyl-methacholine (6.25, 12.5, 25, 50 and 100 mg/mL), after an initial time

period to acclimatize in the chamber[135,136,137]. First mice were exposed to aerosolized PBS to gather baseline data. Experimental values were automatically generated by the pneumograph in the wall of the chamber. FinePointe software (Buxco©) was used to collect all data.

Hematoxylin and Eosin staining

Tibialis Anterior muscle was cryosectioned and 10 µm sections were placed on surgipath microscope slides. Tissue sections were fixed with ice-cold 95 % ethanol for 2 minutes followed by 70 % ethanol for 2 minutes and then re-hydrated in running water for 5 minutes. Gill's hematoxylin (Fisher Scientific, Fair Lawn, NJ) was then used to stain the sections and rinsed in water for 5 minutes. Scott's solution (0.024 M $NaHCO_3$, 0.17 M $MgSO_4$) was then applied for 3 minutes and rinsed in water for 5 minutes. Tissue cryosections were then immersed in eosin solution (Sigma-Aldrich, St. Louis, MO) for 2 minutes. Sections were then dehydrated in ice cold 70 % and 95 % ethanol for 30 seconds each, followed by 100 % ethanol for 2 minutes. Xylene was then used to clear the sections for 5 minutes prior to mounting with DepeX mounting medium (Electron Microscopy Services, Washington, PA). Centrally located Nuclei were counted from images composing representative montages for each mouse. Images were assessed at 100 X magnification by bright field microscopy. The number of centrally located nuclei per muscle fiber was determined by counting each image which contributed to myofibers being counted per treatment group. At least 4 animals from each treatment group were analyzed.

Isolation of skeletal muscle

8 week old female wild-type and *dy*^{W} -/- mice were euthanized by CO_2 inhalation in accordance with a protocol approved by the University of Nevada, Reno Animal Care and Use Committee. Muscles from these mice were dissected, flash-frozen in liquid nitrogen and stored at -80°C.

Sirius Red Staining

TA muscle sections were stained with Sirius Red to measure fibrosis in the skeletal muscle tissue. 10 µm cryosections on slides were fixed in 100% ethanol and then hydrated through an alcohol series (95 and 80% ethanol) and rinsed in tap water. The sections were stained with Sirius Red (0.1% in saturated aqueous picric acid solution, Rowley Biochemical Institute, Danvers, MA, USA) for 30 min followed by two washes in acidified water. The sections were dehydrated through an alcohol series, rinsed in xylene and mounted with DEPEX Mounting media (Electron Microscopy Science, Hat- field, PA, USA). Representative montages were captured and analyzed using Axiovision 4.8 software. Montages were assembled using Photoshop and Microsoft Powerpoint. Images were captured at 100 X magnification. Areas of red in the TA were considered fibrotic. Circled fibrotic areas were added together, and any non-fibrotic fibers within the fibrotic area were subtracted from the calculated area. The percentage of muscle fibrosis was quantified in treated and control muscles as a percentage of total TA muscle area. Sirius red slides were also used to measure minimal feret's diameter for mice of all 4 genotypic groups. All muscle

fibers within an entire TA montage were used to determine the minimal feret's diameter.

Statistical Analysis

All averaged data are reported as the mean ± s.d or as denoted on specific figures as mean ± SEM. *P*-values of < 0.05 were considered to be statistically significant. One-way or Two-Way *ANOVA* statistical testing alongside a student *t*-test was used.

RESULTS

Treatment regime and analysis of muscle strength in 8 week old WT, *dy^{W}*-/- + PBS and *dy^{W}*-/- + mLAM-111 mice

Female *dy^{W}* -/- mice were treated from 4 weeks of age with weekly systemic injection of laminin-111 (0.01 mg/g) in Figure 4 A. Littermate control *dy^{W}* -/- mice were also injected with the same volume of sterile Phosphate buffered saline (PBS). There was not much difference between PBS or laminin treatment groups with regards forelimb grip strength (Figure 4 B) and stand-up activity (Figure 4 C). There was however a trend towards WT with Percentage (%) forelimb muscle fatigue (Figure 4 D) but overall laminin-111 treatment did not improve muscle performance relative to WT muscle.

Histological Analysis Quantifying Centrally Located Nuclei in 8 week old WT, *dy^{W}*-/- + PBS and *dy^{W}*-/- + mLAM-111 mice

Representative montages for Tibialis anterior (TA) muscle stained with H & E (Figure 5 A) for each treatment group revealed that laminin-111 treatment did help to halt any further muscle degeneration (Figure 5 A). There was a steep elevation in the Percentage (%) of centrally located nuclei (CLN) (Figure 5 B), this could be a possible halt in degradation or indeed *de novo* muscle formation and these centrally located nuclei represent this muscle fusion of new myotubes. Due to the heterogeneity of the myofiber sizes and the fact that mature skeletal muscle is formed by the fusion of myoblasts into myotubes. Mature skeletal muscle possesses many nuclei along the periphery of each myofiber. Only when there is degeneration or regeneration will nuclei move into the center of each myofiber and in the case of mice, the nuclei will stay there permanently once they have moved into the center.

Fibrotic tissue reduced in 8 week old Tibialis Anterior muscle by laminin-111

Even after disease onset, treatment with laminin-111 helped to halt any further degradative environment of fibrotic scar tissue deposition within dy^{W} -/- mice (Figure 6 A). This finding was proven to be statistically significant (Figure 6 B), the PBS treated animals had 12.91 % fibrotic tissue ± 1.481 % whilst mLAM-111 treated animals had 9.363 % fibrotic tissue ± 0.9431 %. This was alongside an elevation in the size of myofibers by minimal feret's diameter measurements (Figure 6 C). Minimal feret's diameter is a method for measuring the size of the

myofibers. When comparing PBS and mLAM-111 treated animals their myofiber sizes were 25.67 µm ± 0.2741 µm and 26.92 µm ± 0.2397 µm respectively.

Activity and Function of 8 week old WT, *dy^{W}*-/- + PBS and *dy^{W}*-/- + mLAM-111 mice

There was a slight increase with the distance (cm) and speed (cm/sec) with which moved for *dy^{W}* -/- mice treated with laminin-111 compared to PBS treated *dy^{W}* -/- mice (Figure 7). WT moved 9937 cm ± 2844.267 cm, PBS treated animals moved 3693.55 cm ± 1877.44 cm and mLAM-111 treated animals moved 4477 cm ± 234.98 cm. Laminin treatment created a 21.21 % improvement in distance moved compared to PBS treated animals. Laminin treatment also caused a 7 % increase in the speed with which moved by the mice compared to PBS controls.

Respiratory function of 8 week old WT, *dy^{W}*-/- + PBS and *dy^{W}*-/- + mLAM-111 mice

Plethysmography analysis of important respiratory parameters in Figure 8 proved to be significant for all three parameters, frequency of breathing, PenH, and TVb when compared to wild-type. However, there was no significant difference between laminin treated and PBS treated *dy^{W}* -/- mice. Treatment after disease onset was not effective in targeting and importantly relieving a main marker in disease progression.

DISCUSSION

As mentioned at the start, patients with MDC1A are usually diagnosed after disease onset. Because systemic laminin-111 treatment was able to have many beneficial effects before disease onset (previously published)[131,132], we carried out this study to investigate whether laminin-111 protein would have the same beneficial effects when treatment was started after disease onset in the *dy*^{W} -/- mice.

This study would be a step towards trying to link what happens at the patient bedside to one of the current mouse models used to study this disease. As with all scientific studies it is important that they correlate to what is currently experienced in the medical field. Our studies suggest *dy*^{W}-/- mice treated with laminin-111 protein after disease onset show improvement in muscle function by reducing the percentage of forelimb muscle fatigue (Figure 4 D) and reduced fibrosis as shown in the histology data presented in Figure 6 A.

Overall laminin-111 protein delivered after disease onset is not as effective as treatment before disease onset. As with any disease there needs to be early detection and treatment before disease progression in order to see a significant beneficial effect. Galectin-1 protein, a modifier in apoptosis and inflammation, has been recently been shown to be beneficial in the treatment of *mdx* mice[138]. Perhaps this galectin-1 protein in combination with laminin-111 protein delivered as a cocktail therapy may prove to be a beneficial avenue of investigation for the treatment of MDC1A. Omigapill has been shown to block

apoptosis which is a primary cell process involved in MDC1A disease progression[139,140]. An enzyme called GAPDH is heavily involved with apoptosis and omigapill was found to bind directly to GAPDH and blocking its actions therefore preventing the cell death pathway[141]. Additionally, apoptosis inhibitors and mini-agrin have been proven to be effective in the treatment of congenital muscular dystrophy[1].

Results from this study along with an understanding of laminin-111 pharmacokinetics will help pave the way in developing this protein as an exciting potential therapeutic for MDC1A patients.

ACKNOWLEDGEMENTS

I would like to thank Vivian Cruz and Chelsea Lamb for their technical assistance with histological staining and analysis. Rebecca Evans for genotyping and providing the mice for this study. Dr Cherie Singer for kindly allowing access to the Buxco whole body plethysmography (WBP) system.

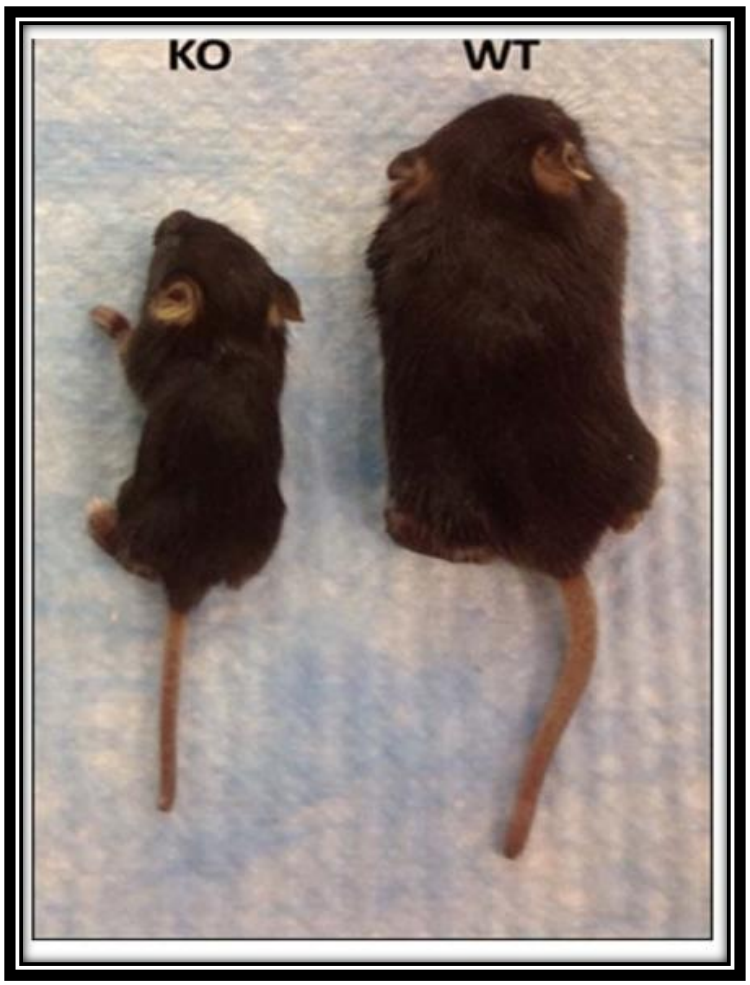

Figure 3. *Dy^{W}-/-* mice display greatly reduced body size and mass

The *dy^{W} -/-* mutant mouse, shown here on the left lacks laminin-α2. Notice the fragility of the mutant mouse (left) compared to the WT mouse (right). Both mice are 8 weeks old.

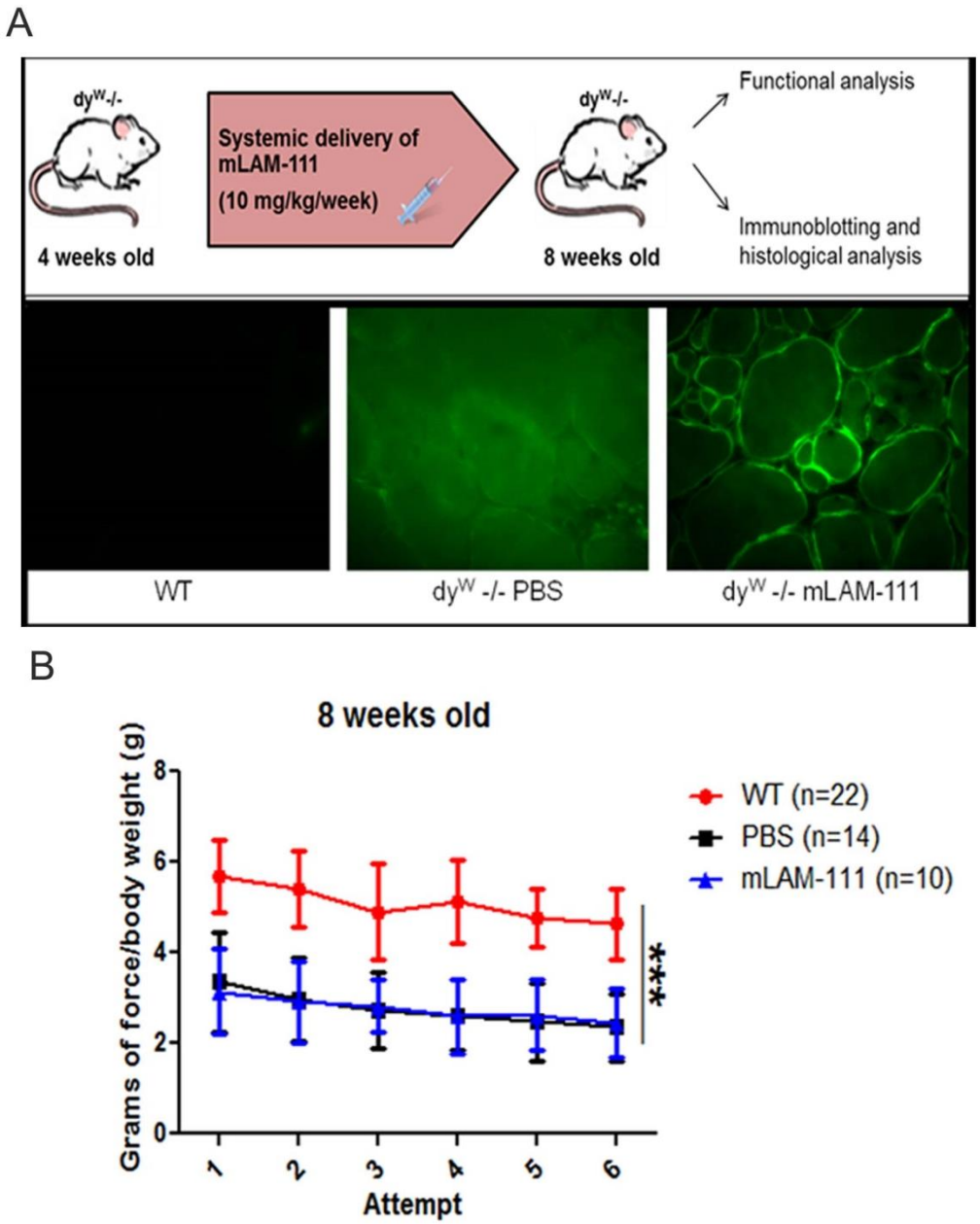

Figure 4. Treatment regime and analysis of muscle strength in 8 week old WT, *dy^{W}-/-* + PBS and *dy^{W}-/-* + mLAM-111 mice

A) Laminin-111 protein was detected in Tibialis Anterior cryosections of 8 week old *dy^{W}* -/- mice after intraperitoneal treatment. The treatment regime was started

after disease onset with intraperitoneal injection of 0.01 mg/g/week EHS mLAM-111 from 4 weeks old to 8 weeks old. Upon completion of the study, mice were subjected to functional studies and then were sacrificed for immunohistochemical and Western analysis. B) Functional activity was recorded at 8 weeks old to include grip strength. There was no difference in grip strength between mLAM-111 treated and untreated dy^{W}-/- mice. Significance in grip strength for dy^{W}-/- mice compared to WT mice was indicated with a *p*-value <0.001 after Two-way *ANOVA* was performed.

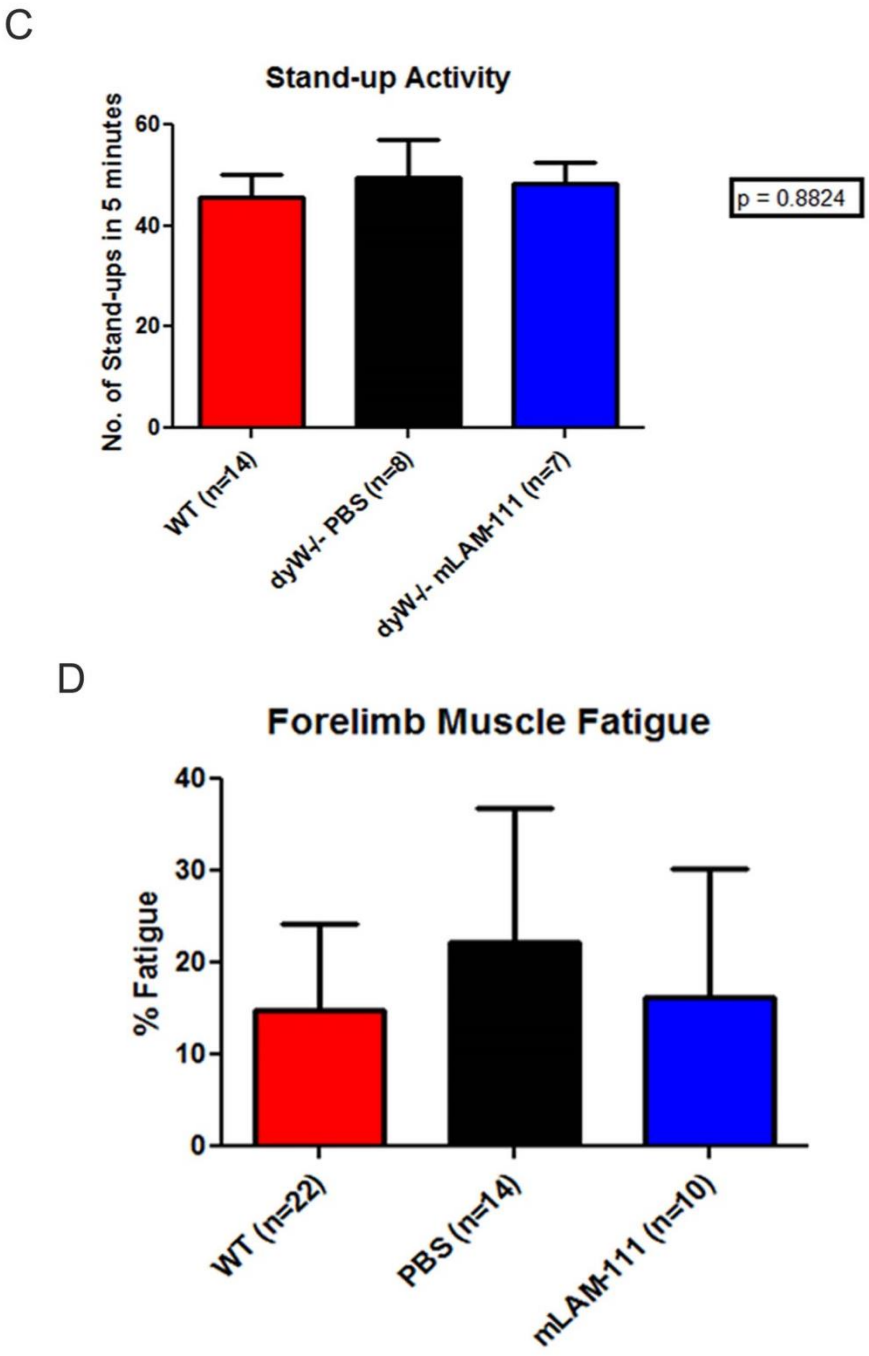

Figure 4. Treatment regime and analysis of muscle strength

C) Stand-up activity was recorded for a period of 5 minutes. The number of stand-ups accomplished by each 8 week old mouse was noted. There was no statistical significance found between the treatment groups (*P*-value= 0.8824).

Mean ± SEM for each treatment group were as follows: PBS (49.63 stand-ups ± 7.442), mLAM-111 (48.29 stand-ups ± 4.150). D) Percentage (%) forelimb muscle fatigue was calculated based on the previous grip strength data in Figure 4 B, gathered at 8 weeks of age.

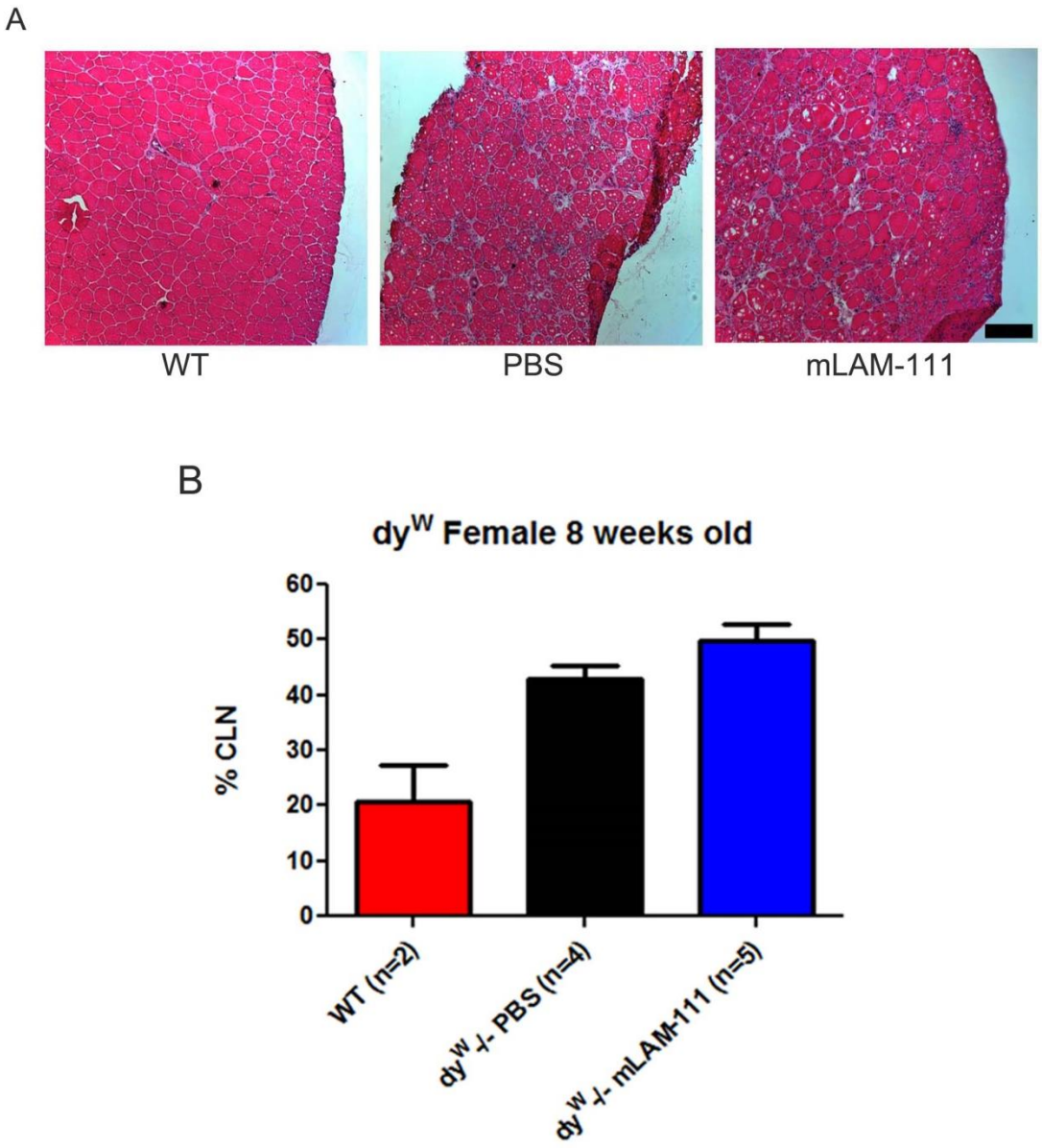

Figure 5. Histological Analysis Quantifying Centrally Located Nuclei

A) Hematoxylin and Eosin staining on 10 µm 8 week old TA cryosections. Magnification: 100 X, scale bar = 200 µm. B) Percentage (%) myofibers with centrally located nuclei (CLN) were quantified as CLN are used as a marker of degeneration and regeneration. A *t*-test was performed to compare PBS (42.9 % CLN ± 2.296 %) treated and mLAM-111 treated animals (49.96 % CLN ± 2.852

%) and there was no statistical significance with the generated *P*-value of 0.0749. There was however statistical significance upon One-way *ANOVA* analysis of the 3 treatment groups generating a *P*-value = 0.0003.

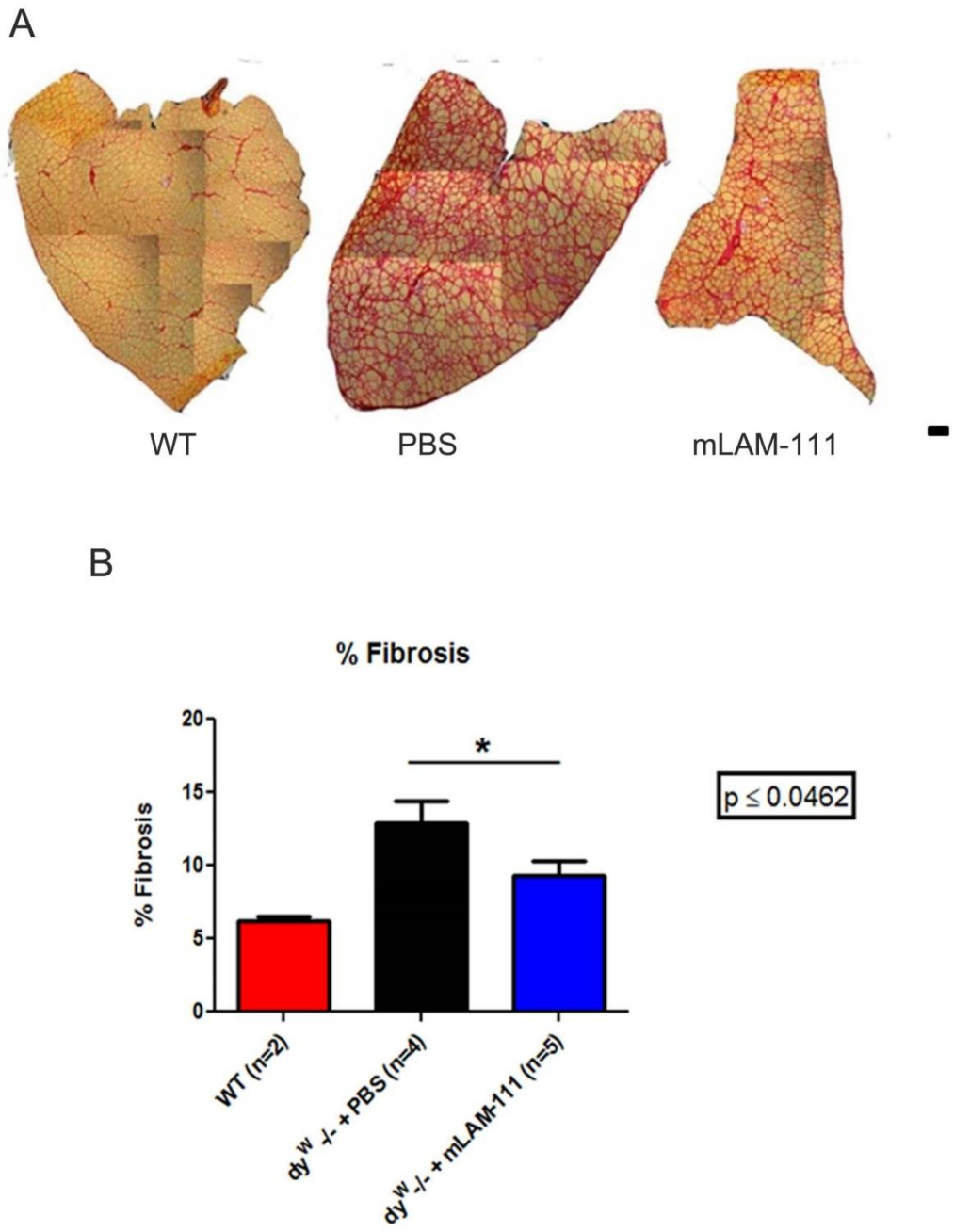

Figure 6. Fibrotic tissue reduced in 8 week old Tibialis Anterior muscle by laminin-111

A) Sirius red staining on 10 µm TA cryosections was used to calculate percentage (%) of fibrosis. Magnification 100 X, scale bar 200 µm. B) The PBS

treated animals had 12.91 % fibrotic tissue ± 1.481 % whilst mLAM-111 treated animals had 9.363 % fibrotic tissue ± 0.9431 %. The *P*-value generated was 0.0462 using a *t*-test to compare PBS and mLAM-111 treatment groups.

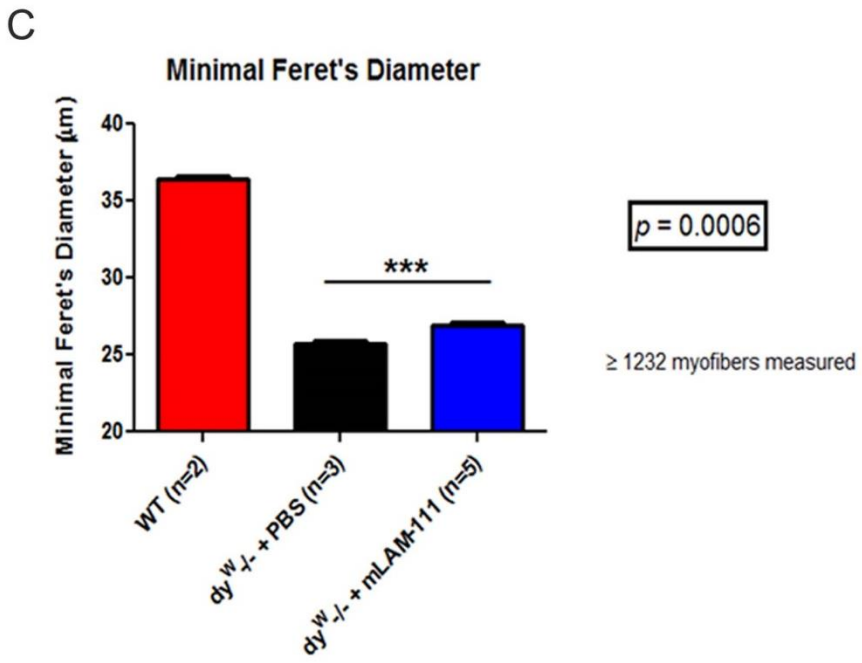

Figure 6. Fibrotic tissue reduced in 8 week old Tibialis Anterior muscle by laminin-111 C) Sirius red stained 10 µm TA cryosections were used to measure minimal feret's diameter (µm). Minimal feret's diameter is a method for measuring the size of the myofibers. When comparing PBS and mLAM-111 treated animals their myofiber sizes were 25.67 µm ± 0.2741 and 26.92 µm ± 0.2397 respectively. The *P*-value was 0.0006 using a *t*-test. Using One-way *ANOVA* statistical testing for all 3 groups the *P*-value generated was <0.0001.

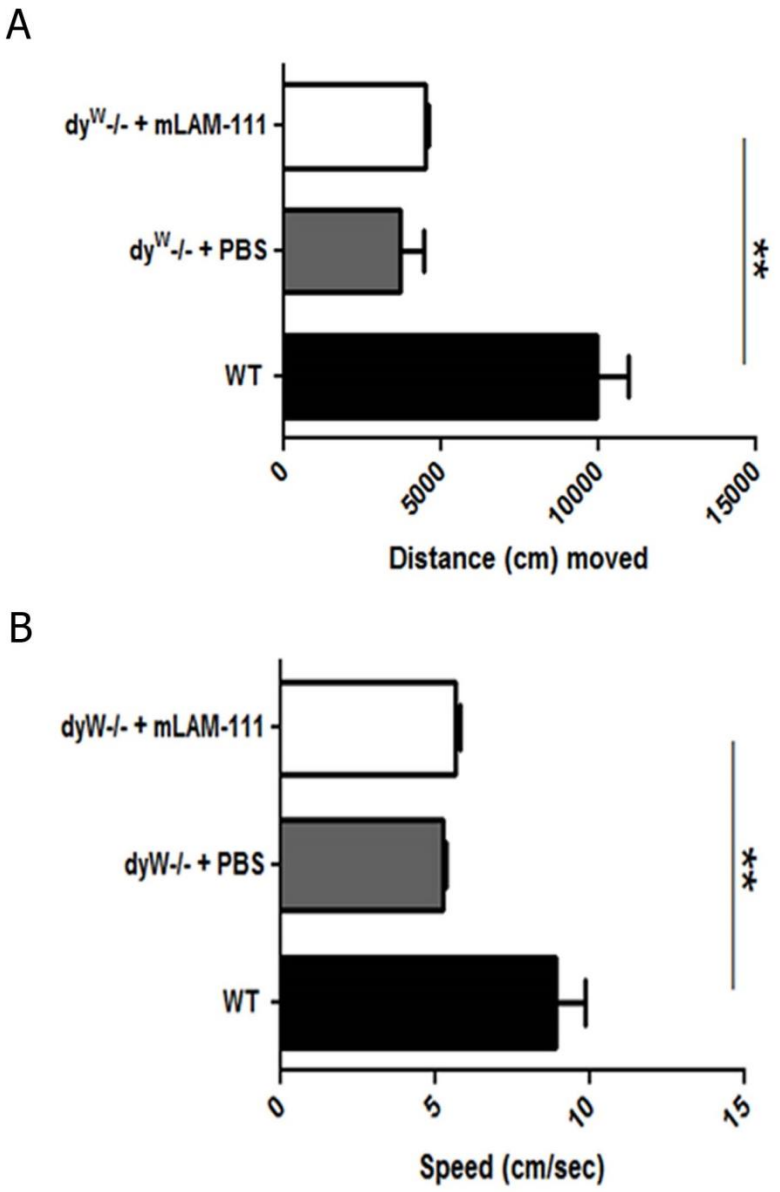

Figure 7. Activity and Function of 8 week old WT, *dy^{W}-/-* + PBS and *dy^{W}-/-* + mLAM-111 mice

Activity box data showing distance (cm) (Figure 7 A) and speed (cm/sec) (Figure 7 B) with which the 8 week old mice moved for each treatment group. WT moved 9937 cm ± 2844.267 cm, PBS treated animals moved 3693.55 cm ± 1877.44 cm and mLAM-111 treated animals moved 4477 cm ± 234.98 cm. Laminin treatment

created a 21.21 % improvement in distance moved compared to PBS treated animals. Laminin treatment also caused a 7 % increase in the speed with which moved by the mice compared to PBS controls. *P*-values for both distance (cm) and speed (cm/sec) with which moved comprised of comparing all 3 treatment groups were <0.05 with One-way *ANOVA* and a Bonferroni's Multiple comparison test.

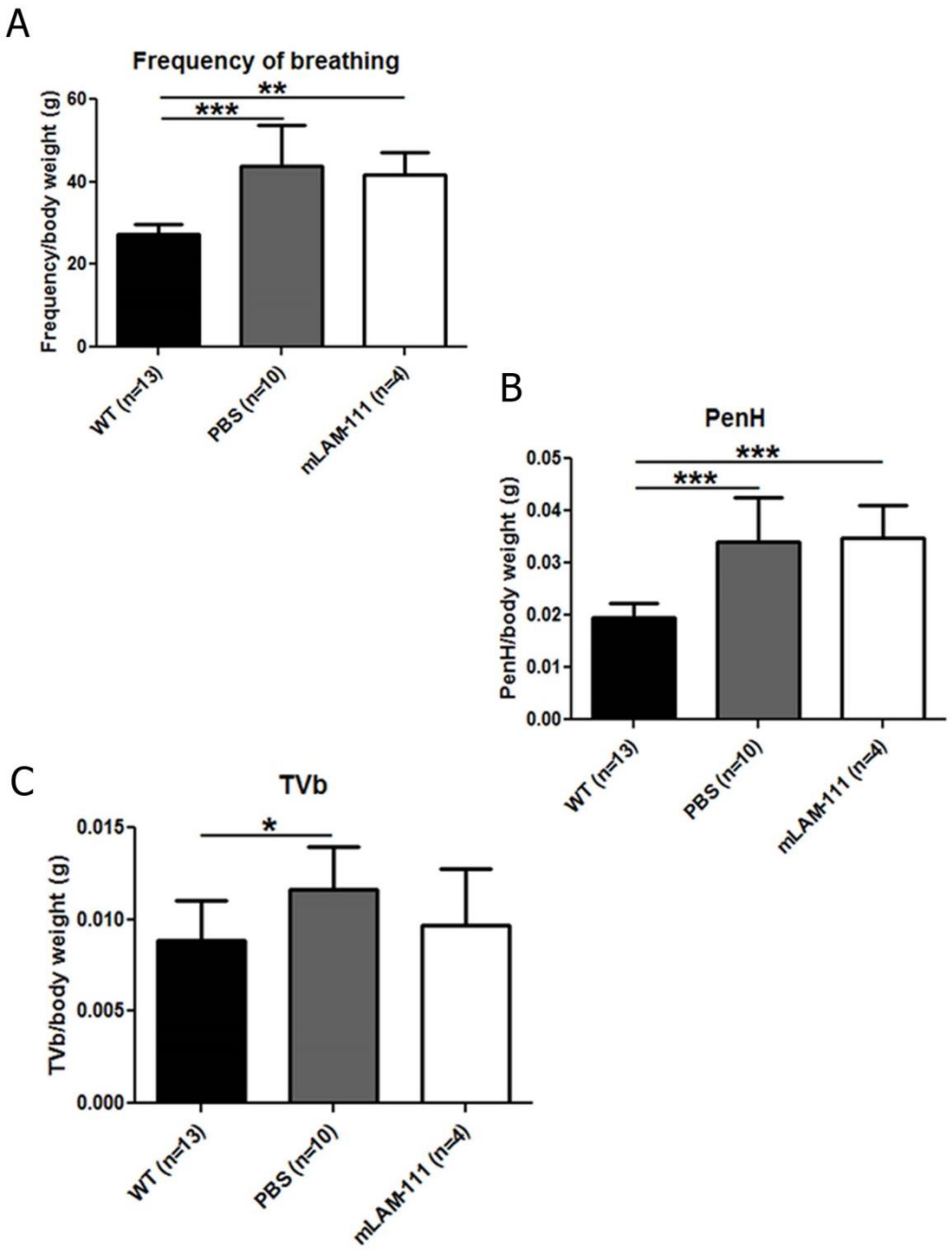

Figure 8. Respiratory function of 8 week old WT, *dy^{W}-/-* + PBS and *dy^{W}-/-* + mLAM-111 mice

Plethysmography data are presented here showing important respiratory parameters for 8 week old mice. Frequency of breathing (Figure 8 A), PenH

(Figure 8 B) and Tidal volume (TVb) (Figure 8 C) were recorded and normalized to body weight (g). PenH (enhanced pause) is correlated to but not a direct measurement of airway resistance. There was a 5.1 % decrease in Frequency of breathing, a 2.3 % increase in PenH and a 16.4 % decrease in Tidal volume when treated with laminin-111 compared to PBS treatment. There was no statistical significance between PBS and laminin-111 treated animals but *P*-values were <0.05 with One-way *ANOVA* and a Bonferroni's Multiple comparison test of the 3 treatment groups.

Chapter III

Laminin-111 Treatment Modifies Transcriptional Changes in the Diaphragm Muscle of a Mouse Model of MDC1A

ABSTRACT

Merosin deficient congenital muscular dystrophy type 1A (MDC1A) is caused by loss of laminin-211 and laminin-221 within the basal lamina of skeletal and cardiac muscle. This absence of laminin-211/221 reduces the capacity for myofiber adhesion resulting in loss of sarcolemmal integrity and subsequently the ability of the skeletal muscle to generate force in a coordinated and efficient manner. Patients experience progressive muscle wasting resulting in loss of ambulation and death from respiratory failure. Currently, there is no effective treatment or cure for this devastating disease. Recently we have shown that laminin-111, an embryonic form of laminin, can act as a protein replacement therapy in the *dy*^{W} mouse model of MDC1A. This study set out to determine the transcriptional changes that occur within the diaphragm muscle during MDC1A disease progression and after laminin-111 treatment using RNA-Seq technology. Our results show major transcriptional changes with age in pathways associated with immune response, cell growth and survival and muscle repair. Galectin-3 is known to help stabilize myofibers and these transcripts were found to be upregulated (six-fold) in diseased muscle compared to wild-type muscle. Together, this study will help to identify novel therapeutic targets that may be useful in the treatment of MDC1A.

INTRODUCTION

Merosin deficient congenital muscular dystrophy (MDC1A) is caused by the loss of Laminin-211 and Laminin-221 heterotrimers which are most abundant

in skeletal and cardiac muscle basal lamina; mutations in the *LAMA2* gene cause the loss of these laminin isoforms.Laminin-211/221 are critical to muscle integrity and loss of these heterotrimers causes reduced muscle function, ability to repair and myofiber loss. Patients experience progressive muscle wasting from birth which confines them to a wheelchair at an early age and leads to respiratory failure. Currently, there is no effective treatment or cure for this devastating disease.

Merosin deficient congenital muscular dystrophy (MDC1A) affects approximately 0.89/100,000 individuals worldwide (1:100,000 - 1:500,000) and is considered to be one of the most common forms of congenital muscular dystrophy. Loss of merosin (Laminin-α2 protein) is caused by mutations occurring in the *LAMA2* gene which is located on chromosome 6q22-23 [73,89]. This results in the absence of Laminin-211 and Laminin-221 heterotrimers which are abundant in skeletal and cardiac muscle basal lamina. Patients also experience demyelinating neuropathy, muscle atrophy, limited eye movement and also respiratory failure that leads to their untimely death which can be as early as the first decade of life[88,92,94]. There is an increased likelihood of seizures occurring after six months of age due to changes in white matter of the brain [88,92,93]. Recently we have shown that laminin111, an embryonic form of laminin, can act as a protein replacement therapy in a mouse model of MDC1A [142]. The presence of laminin-111 prevented muscle disease progression and improves muscle repair [132,142]. To explore the on-target and off-target activity of laminin-111, we conducted RNA-seq analysis to identify transcript changes in the

diaphragm muscle of *dy*^{W} mice. Our results showed 828 transcripts changed significantly in the diaphragm muscle of untreated *dy*^{W} animals compared to wild-type mice with 81 transcripts changes that were specific only to laminin-111 treatment. This study identifies transcript changes caused by disease progression in the diaphragm muscle and on- and off-target activity of laminin-111 protein therapy.

MATERIALS AND METHODS

Animal Care and Laminin-111 Treatment Schedule

The *dy*^{W}-/- mice used in the study were generated by crossing *dy*^{W}+/- x *dy*^{W}+/- animals. The *dy*^{W}-/- mice were housed with wild-type littermates under a protocol approved by the Animal Care and Use Committee at the University of Nevada, Reno. Pups were genotyped at 10 days old and genotypes confirmed at the end of the study. In order to genotype mice, genomic DNA was isolated from tail snips or ear notches using a Wizard SV DNA purification system (Promega, Madison, WI) following manufacturers instructions.

To detect the mutation in the laminin- α2 gene, the following primers were used: DYWF (5'-ACTGCCCTTTCTCACCCACCCTT-3'), LAMA2exonR1 (5'-GTTGATGCGCTTGGGAC-3') and Lac/ZR2 (5'-GTCGACGACGACAGTATCGGCCTCAG-3'). PCR conditions were as follows: 95°C for 5 minutes then 33 cycles of 94°C for 20 seconds, 62°C for 30 seconds and 72°C for 45 seconds. After these cycles, then 72°C for 10 minutes. A wild-

type band was 250 bp whereas the laminin- α2 targeted allele produced a 480 bp band.

Experimental procedures were performed once mice were 10 days and 2 weeks of age with weekly weighing until the end of study which was at 2 weeks and 5 weeks of age where all mice were subject to *in vivo* experiments. To reduce experimental bias, investigators assessing and quantifying experimental outcomes were blinded to the treatment and control groups.

Mice were euthanized by CO_2 inhalation in accordance with a protocol approved by the University of Nevada, Reno Animal Care and Use Committee. Tissues from these mice were dissected, flash-frozen in liquid nitrogen and stored at -80°C as previously reported by [134]. All mice used in these studies were female.

Two separate experimental mouse groups were included in this study. One experimental data group included wild-type (WT; n=5) and dy^W -/- (n=5) mice which were untreated and sacrificed at 14 days of age. A second experimental data group consisted of mice treated weekly with either Lamin-111 (dy^W *-/-)* or Phosphate buffered Saline (PBS; WT and dy^W *-/-)* from 10 days old until 5 weeks old, at which time mice were sacrificed. Laminin-111 was stored at -80°C and thawed slowly at 4°C overnight before use. Mice were injected intraperitoneally (i.p.) with 0.01 mg/g/week of laminin-111 protein (Invitrogen) or an equal volume of PBS. This experimental group consisted of Laminin-111 treated dy^W -/- (n=5) or PBS-treated WT (n=4) and dy^W -/- (n=4).

Immunofluorescence

TA and gastrocnemius muscles were embedded in Tissue-Tek OCT and 10 µm cryosections were cut using a Leica CM 1850 cryostat (Leica, Wetzal, Germany). Sections were placed on pre-cleaned Surgipath slides (Surgipath Medical Industries, Richmond, IL) and fixed using 4% paraformaldehyde (PFA). ERK1/2 was detected using a rabbit anti-mouse ERK polyclonal antibody (Cell Signaling, 1:100) followed by a FITC-conjugated goat anti-rat-IgG secondary antibody (1:5000; Li-Cor Biosciences).

Osteoactivin was detected using rabbit anti-osteoactivin antibody (AbCAM; 1:100) overnight followed by fluorescein isothiocyanate (FITC)-conjugated anti-rabbit IgG secondary antibody. These slides were also treated with Texas Red labeled wheat germ agglutinin (WGA, 1:250, Molecular Probes, Invitrogen detection technologies, Eugene, OR). Slides were mounted using Vectashield Hard Set with DAPI (Vector Laboratories Inc., Burlingame, CA).

Images were captured using an Olympus FluoviewFV1000 Laser scanning biological confocal microscope using the Olympus micro FV10-ASW 3.1 software. Representative images for publication were taken at 400 X using the Olympus FluoviewFV1000 Laser scanning biological confocal microscope.

Immunoblotting

The TA muscles were carefully dissected and protein extracted using RIPA buffer supplemented with protease inhibitors. Proteins were separated using an 8% SDS-PAGE gel electrophoresis, transferred to nitrocellulose

membrane and blocked using 2.5% Coronation dry milk in TBST for 1 hour. Blots were incubated with primary antibody overnight before being incubated with secondary antibody for 1 hour and then washed with 1X TBST buffer. Proteins were imaged using the LiCor Odyssey system.

RNA-Seq

Diaphragm tissue was homogenized and suspended in TRIzol reagent (GibcoBRL, Life Technologies). Total RNA was isolated following the manufacturer's instructions (Gibco BRL, Life Technologies). The RNA samples were treated with 5 units of DNase I and purified using RNeasy Mini Spin Columns (Qiagen) according to the manufacturer's instructions. Total RNA concentration and purity was assessed by measuring A260/280. RNA was pooled equally for each experimental group (2-week untreated WT, 2-week untreated *dy^{W}-/-*, 5-week PBS WT, 5-week PBS *dy^{W}-/-,* and 5-week Laminin-111 *dy^{W}-/-)* and sent to UC Davis Genome Center (UC Davis Genome Center, 451 Health Sciences Drive, Davis, CA 95616). UC Davis made libraries from the pooled RNA with indexes following Illumina's TruSeq library prep kit and libraries were sequenced for single end 50 bases using Illumina HiSeq2000 following manufacturer's standard procedures. Illumina reads were aligned to the reference using Bowtie 20 with end-trimming enabled and indels penalized with a score equivalent to 3 mismatches. The best alignments were retained for downstream analysis for read counts and variant calls using filtering criteria for polymorphisms that required at least 8 uniquely aligned reads to call the variant

within a given sample, with an average quality of >= 20 for bases calling the variant, and having a variant frequency of >=%20 within all reads covering that position in that sample. Changes in the transcriptome were compared between disease and control data sets. Excess Total RNA was stored separately at -80°C for later individual qRT-PCR assessment of highly affected transcripts.

Statistical Analysis of RNA-Seq data

Each sample was subjected to alignment and counting of mapped reads. For this, TopHat was used for alignment to the genome, then reads were counted per locus (all isoforms counted together for one gene) using htseq-counts. In order to adjust for large differences in the number of mapped reads in each sample (with the sample with the most reads having more than 6 times as many reads as the sample with the fewest reads), prior to analysis, counts were down-sampled using binomial sampling as described by[143]. Genes with less than 1 count per million reads in all 8 samples were filtered from the counts table, leaving 15,026 genes in the analysis. Differential expression analysis was conducted using the Bioconductor package edgeR, version 3.4.2[144–147]. Analysis was conducted using a multifactorial GLM with factors for time, group (WT, PBS treated *dy^{W}-/-* and LAM-111 treated *dy^{W}-/-*), and their interaction. This multifactorial method was chosen during analysis as it is considered to be more powerful than running each discrete comparison. Due to the lack of replication, tagwise dispersion parameters were estimated from a multifactorial GLM with factors for time and group but no interaction effect. *P*-values were adjusted for

multiple testing using the false-discovery rate (FDR) method of Benjamini and Hochberg (1995)[148]. Log2-fold changes and FDR-adjusted p-values less than 0.1 for all 15,026 genes included in the analysis.

qRT-PCR

Quantitative Real Time PCR (qRT-PCR) was used to confirm individual mouse changes from cherry picked transcripts identified as altered in the RNA-seq study. Individual mouse diaphragm cDNA was made from previously isolated Total RNA using Superscript III (Invitrogen) following standard procedures. qRT-PCR using SYBR-green PCR mix (VWR) and primers (IDT DNA) against Aggrecan, GPNMB (Osteoactivin), Elane, MMP8, MMP9, BGLAP1, BGLAP2, PRTN3, DMP1, CALCA1, SERCA1, SERCA2, IBSP, LAMA2, Tenascin C, LGALS3, WISP1, and ADAM8 transcript Ct values were normalized to GAPDH (Doe et al.) Ct values in order to establish a fold-difference between treatment groups.

Muscle transcripts

The muscle transcript ontology groups of interest included: Integrin signaling, Inflammation, Fibrosis, Apoptosis (ILK, AKT), Extracellular Matrix signaling, Cell surface receptors and signaling (integrins and dystrophin and utrophin glycoproteins) and Cell Survival pathways (AKT).

Data Analysis

Microsoft Excel and Ingenuity Pathway Analysis (IPA) software were employed in order to visualize the signaling pathways affected within the treatment groups. Protein expression levels were analyzed and processed using GraphPad Prism software. Fold-changes in protein were calculated using changes in intensity within ImageJ software.

RESULTS

Transcriptional changes in the diaphragm muscle of laminin-α2 deficient Mice

Previous studies have shown laminin-111 can act as a protein replacement therapy for the loss of laminin-211/221. In this study we sort to identify transcriptional changes during disease pathogenesis in the diaphragm muscle of *dy*^{W} mice at 2 and 5-weeks of age. Compared to wild-type animals, 2 week old *dy*^{W} mice show 138 transcript changes in the diaphragm muscle (Table 5). 27 transcripts were reduced more than 4-fold and 111 transcripts were increased more than 4-fold. These changes include increased transcripts associated with immune response, muscle apoptosis in 2 week old animals and muscle necrosis in 5 week old animals. Of special interest were genes associated with muscle necrosis at 5 weeks old which are involved in creating and recruiting signaling players for a cyclical degradative environment which ultimately destroys muscle.

Laminin-111 alters the transcript profile in *dy^{W}* diaphragm muscle

We next compared transcriptome changes caused by normal disease progression with the impact laminin-111 protein therapy has on transcript levels. RNAseq studies revealed 468-specific transcripts in total were altered by laminin-111 treatment (Table 6). 356 transcripts were increased more than 4-fold and 112 transcripts were reduced more than 4-fold. Transcripts associated with bone growth and maintenance, muscle and ECM associated genes. These include tenascin N, elastase, aggrecan, MMP8, MMP9, MMP13, proteinase-3 were significantly altered.

Osteoactivin is increased in laminin-α2 deficient muscle

Our RNAseq study identified that osteoactivin transcript (GPNMB) is significantly upregulated in the *dy^{W}* -/- diaphragm. Osteoactivin is a transmembrane protein that promotes bone formation by increasing the activity of osteoblasts[149,150]. Osteoactivin can induce transdifferentiation of myoblasts into osteoblasts and has recently been shown to protect muscle from degeneration. That has been reported to be associated with integrins.

Transcriptome data analysis encompassed changes in 5 week old diaphragm tissue harvested from PBS treated *dy^{W}* -/- mice versus LAM-111 treated *dy^{W}* -/- mice. There were relatively few significant changes (~275 total genes), most genes had little to do with muscle or the extracellular matrix (ECM). However there were many genes found misregulated that were associated with

bone growth and maintenance. Of the few muscle and ECM associated genes found to be significantly altered, were tenascin N, elane (elastase), aggrecan, MMP8, MMP9, MMP13, proteinase-3. There were several genes associated with neuronal signaling that were found to be altered in the disease state. Our results at this age may represent individual disease state changes and not changes specifically associated with Laminin-111 treatment. 5 week old diaphragm from Wild-type versus Untreated *dy^{W} -/-* changes: Over 15,000 genes were significantly altered, current analysis is continuing on the known functions for all genes on the list but one of the most interesting genes that were upregulated in the *dy^{W} -/-* diaphragm is osteoactivin (*GPNMB*).

RNA-Seq summary (WT vs *dy^{W}-/-*, 2 week, 5 week and 8 week): sets baseline transcripts

2 week *dy^{W}-/-* transcripts that are upregulated include Ankyrin (Ankrd1), Myosin Heavy chain 3 (Myh3), Interleukin-8 (IL-8), Dyenin (Dnahc1), Troponin T type 2 (Tnnt2) (Supplemental Table 1). Interleukin 8 and laminin-α2 transcripts are downregulated. These results are good in offering a baseline view of what happens in *dy^{W}-/-* before disease onset.

2 week ≥ 4–fold changes summary

A summary of 138 transcripts misregulated ≥4–fold between WT and *dy^{W}-/-* at 2 weeks old were narrowed down to 14 transcripts shown in Supplemental Table 2.

5 week ≥ 4-fold changes summary

A summary of 169 transcripts misregulated ≥4–fold between *dy^{W} -/-* PBS treated and *dy^{W}-/-* laminin treated mice at 5 weeks old were narrowed down to 34 transcripts shown in Supplemental Table 3.

RT-PCR results confirming important transcriptional changes in genes associated with the extracellular matrix in 2 week old and 5 week old WT and *dy^{W}-/-* + PBS mice

In Figure 9, *LAMA2* transcript was confirmed to be decreased in *dy^{W}-/-* mice which is as expected due to the deficiency of laminin-α2. Tenascin C and LGAL3 transcripts were highly elevated in *dy^{W}-/-* mice. GPNMB (Osteoactivin) was upregulated consistently within 2 week old *dy^{W} -/-* TA and 5 week old TA and Gastroc muscles which supports data provided in Figures 9 - 14.

Immunofluorescence on critical protein changes identified from gene transcripts in TA muscle from 5 week old WT, *dy^{W}-/-* + PBS and *dy^{W}-/-* + mLAM-111 treated mice

Osteoactivin (GPNMB) protein is also elevated amongst PBS treated *dy^{W}-/-* TA muscle and also MDC1A diseased patient tissue. As the disease progresses we have shown the stage where Osteoactivin (OA) becomes misregulated. In normal wild-type muscle, osteoactivin is a type I transmembrane protein which can interact with integrins and other receptors[149,151]. It is maintained as an intact protein. Loss of laminin-211 causes a transcript increase

osteoactivin transcription, but the protein is cleaved by ADAM12[152–155] giving rise to two fragments which is previously known. The internal fragments we see in patient muscle are completely osteoactivin positive and often surrounded by fibrotic tissue. The external peptide fragment activates myofibroblasts to secrete MMPs, especially MMP3 (this is known) and pathways (TGFβ) that promote fibrosis. When mice are treated with laminin-111, although we do not see a reduced osteoactivin transcript in Figure 10 A, there is a change in protein localization. All the osteoactivin is now back at the membrane (as in wild-type muscle) suggesting it is no longer cleaved. So laminin-111 treatment possibly prevents ADAM12 activity[152,153] and preserves the intact osteoactivin protein.

Immunoblotting for ERK and phospho-ERK protein

Protein levels of total ERK were decreased for Laminin treated animals, and in addition the levels of phospho-ERK protein steeply increased upon laminin-111 treatment (Figure 11). This data suggests that increased phospho-ERK will restore MAPK signaling and increase survival by laminin-111 treatment.

Immunoblots on critical protein changes identified from transcripts for 5 week old *dy^{W}-/-* mice

Quantification of changes in protein expression as a direct result of laminin-111 treatment of *dy^{W}-/-* mice is shown in Figure 12. Statistical analysis via One-way *ANOVA* showed significance in LAM-111 treated animals relative to

PBS treated animals in α7A, α7B and αDG expression with *p*-values (0.0032, 0.0165, 0.0016) respectively.

RNA-Seq data for *dy*^{W}-/- +PBS vs *dy*^{W}-/- +LAM-111

This data in Supplemental Table 4 presents an overview of gene expression changes discovered for 2 week old *dy*^{W}-/- mice between WT and laminin-α2 deficient mice. Gene expression changes were tabulated for 5 week old *dy*^{W} -/- mice between PBS treated and mLAM-111 treated groups. 5 week old *dy*^{W}-/- transcripts of interest include: Integrin binding Sialoprotein (Ibsp), Osteocalcin (Bglap), MMP-13 (MMP13), Cartilage Oligomeric Matrix Protein (Fam150b), WNT Inhibitory Factor 1 (Adra1b), Calcitonin (BC089597), Integrin B (Bhmt2), Ficolin (Akr1b7), Interleukin-8 (IL-8) and Vitamin D (Ugt1a5).

RT-PCR results confirming important transcript changes in 5 week old LAM-111 treated *dy*^{W}-/- mice

Presented in Supplemental Table 5, is a comparison of expression changes (MMP8, MMP9, Aggrecan, IBSP and BGLAP2) as disease progresses in treated versus untreated *dy*^{W}-/- genes. This data is good at showing whether the gene expressions changes we observe are global or are they indeed due to one mouse skewing the data.

Histology and functional data obtained from 5 week old *dy*^{W} mice

Activity box data distance (cm) and speed (cm/sec) with which moved showed that there was more than a trend towards wild-type activity upon laminin-

111 treatment of *dy*^{W}*-/-* mice (Figure 13). *P*-values were (0.0221 and 0.0190) respectively with One-way *ANOVA*. Grip strength displayed as grams of force (g) normalized to body weight (g) was quantified for each treatment group. The results proved to be statistically significant for the comparison of *dy*^{W}*-/-* mice treated with either PBS or laminin-111. This data showed that laminin treatment improved forelimb muscle strength in *dy*^{W}*-/-* mice. *P*-values were (< 0.0001 and 0.05) respectively with Two-way *ANOVA*. Percentage (%) fatigue was quantified based on grip strength recorded but there was no statistical significance observed with this specific result.

Histology and respiratory function in 5 week old WT, *dy*^{W}*-/-* + PBS and *dy*^{W}*-/-* + mLAM-111 treated mice

Sirius red staining of TA cryosections showed visually that there was a reduction in fibrotic area for laminin-111 treated mice compared to PBS treated *dy*^{W}*-/-* mice (Figure 14 A). Despite this, there was no significance in regards myofiber sizes regardless of the treatment group in question (Figure 14 B). Percentage (%) fibrosis showed a trend towards WT upon laminin-111 treatment. This was statistically significant with One-way *ANOVA* and *p*-value of 0.002. Plethysmography data was obtained using the Buxco system (Figure 14 C). Parameters of interest included: Frequency of breathing, Tidal Volume (TVb) and PenH. Each parameter was normalized to body weight (g). There was a significant peak in breath frequency in laminin treated *dy*^{W}*-/-* mice. *P*-value was 0.0126 with One-way *ANOVA*.

Model of Laminin-111 action on Osteoactivin (OA) restoration

A model of Laminin-111 protein action on Osteoactivin restoration is presented in Figure 15. WT muscle possesses intact Osteoactivin (OA) protein. Loss of laminin-α2 in *dy*^{W}*-/-* muscle causes increased Osteoactivin transcription but the protein is cleaved into two fragments by ADAM12. The internal fragment is visible in fibrotic patient tissue. The external fragment is free to activate myofibroblasts that secrete matrix metalloproteinases and trigger fibrotic pathways. Treatment with laminin-111 does not affect Osteoactivin transcription but does however change Osteoactivin protein localization. With LAM-111 treatment, Osteoactivin moves back to the sarcolemma like WT therefore suggesting that ADAM12 cleavage is prohibited and there is intact Osteoactivin protein.

DISCUSSION

Merosin deficient congenital muscular dystrophy (MDC1A) is a common congenital muscular dystrophy with an incidence estimated at 0.89/100,000. MDC1A is caused by mutations in the *LAMA2* gene which encodes laminin-α2 protein. The *LAMA2* gene is located on human chromosome 6q22-23, spans approximately 260kb and is encoded by 64 exons (Helbling-Leclerc et al., 1995; Naom et al., 1997). Loss of laminin-α2 protein in MDC1A results in the absence of laminin-211/221 (merosin), a major component of the basal lamina, that surrounds skeletal and cardiac muscle. MDC1A patients exhibit severe muscle weakness from birth, demyelinating neuropathy, muscle atrophy and limited eye

movement [88,92–94,117]. Patients exhibit feeding problems and/or respiratory difficulties and often require the placement of a feeding tube and/or ventilator assistance [93]. Most MDC1A patients are unable to walk without assistance and are confined to a wheelchair [88]. There is currently no cure or treatment for this devastating muscle wasting disease.

Recently we have shown that EHS derived mouse laminin-111 protein can act as a substitution therapy in laminin-α2 deficient mice [142]. Our studies showed that *dy^{W}-/-* mice treated with laminin-111 showed reduced muscle pathology, maintained muscle strength and dramatically increased longevity [142]. In this study we investigated the transcriptional changes that occur during disease progression within diaphragm muscle of the *dy^{W}-/-* mouse model of MDC1A. We also examined how treatment with laminin-111 protein altered transcriptional changes in the diaphragm muscle to identify on-target and off-target drug action.

Using RNAseq technology we were able to show that more than 800 transcripts were altered as a result of disease progression in the diaphragm muscle of 2 week old *dy^{W} -/-* mice. Our studies showed that at 2 weeks of age transcript variability in the diaphragm muscle between animals is low. At 5 weeks of age there is significant variability in transcript abundance in the diaphragm muscle between animals. QRT-PCR data analysis on individual animals revealed the variability observed at 5 weeks of age occurred due to one animal. Laminin-111 treatment reduced the number of transcripts that changed and we identified several specific transcripts that changed as a result of laminin-111 treatment.

An interesting transcript that changed as a result of disease progression was osteoactivin. Osteoactivin is a (*Dchil*) dendritic-cell associated heparin sulphate proteoglycan- dependent integrin ligand [155,156]. In humans, Osteoactivin is known as the *GPNMB* gene. The osteoactivin gene encodes a protein of 572 amino acids and is localized to the membrane as a Type-1 transmembrane glycoprotein [151,156]. Osteoactivin is expressed in osteoblasts actively involved in bone matrix production and mineralization. Osteoactivin is also necessary for osteoblast differentiation *in vitro* [150]. Syndecan-4 is a receptor on T-cells for Osteoactivin which therefore initiates an inhibitory function on T cell activation [157]. Osteoactivin is upregulated in muscle denervation and unloading stress. The regulatory mechanisms of Osteoactivin in muscle and bone have not yet been determined, however the role of Osteoactivin in transdifferentiation of myoblasts into osteoblasts has been alluded to in a published study[149]. Interestingly, osteoblast differentiation is characteristically identified by expression of markers which include Osteoactivin (*Gpnmb*) and Osteocalcin (*Bglap*) [158]. Transdifferentiation is the manner in which a somatic cell retains plasticity and can be transformed into another somatic cell. This process can also described as lineage reprogramming. It was first demonstrated whenever mouse embryonic fibroblasts became myoblasts by forced expression of MyoD [159].

Given the transcript and protein level changes in Osteoactivin observed during disease progression in the dy^{W} -/- mouse model, we next wanted to confirm that this occurred on patient muscle. Immunofluorescence for Osteoactivin using muscle from an MDC1A patient and unaffected control

showed that Osteoactivin is normally located in the extracellular matrix in unaffected muscle, but in the MDC1A muscle it is localized within the muscle cells. This may cause misregulation of MAPK signaling (and potentially activation of TGF-beta and fibrotic pathways) in muscle cells. Although laminin-111 treatment did not change transcript levels, treatment in mice appears to restore normal localization of Osteoactivin in skeletal muscle and therefore would potentially restore MAPK signaling in muscle and prevent further fibrosis.

In this study we show that loss of laminin-211/221 in the diaphragm muscle of mice results in a large number of transcript changes that may serve as markers for disease progression and to report the efficacy of potential therapies. At early stages of muscle disease, the transcriptome changes are relatively uniform, however as disease progresses there is increasing variation in transcript abundance between individuals. Laminin-111 treatment results in changes in transcripts that are mis-regulated in dystrophic muscle and in addition restores that localization of proteins in which may negatively impact muscle integrity and survival. These studies identify potential new markers to track disease progression in MDC1A. In addition we identify on- and off-target activity for laminin-111 protein therapy and potential new therapeutic targets that may be useful in the treatment of MDC1A.

The aim of this study was to identify transcriptional changes within diaphragm muscle for the MDC1A mouse model compared to wild type controls. Muscle contraction causes acute damage to the integrity of the sarcolemma within healthy skeletal muscle resulting in myofiber rupture that releases many

susceptible candidates for immune targeting. This process may be aberrantly activated in the progressive disease state of Laminin-α2 deficient skeletal muscle resulting in chronic injury with the prolonged release of many intracellular molecules including proinflammatory cytokines, growth factors and cytosolic calcium which is directly involved in the activation and recruitment of t-lymphocytes facilitating a positive feedback mechanism for further myofiber contraction, rupture, apoptosis and fibrotic scar tissue formation. It is unclear from past and current studies what exact role or what key immune players have in the pathophysiology of MDC1A. Treatment with Laminin-111 (found embryonically) reduces muscle pathology and improves viability in the *dy^{W}-/-* MDC1A mouse model. Laminin-111 helps to strengthen and reinforce the sarcolemma in the *dy^{W}-/-* mouse during prolonged progressive muscle injury induced by contraction offering a protective niche against the occurrence of this degenerative scenario by reducing inflammation, fibrosis and apoptosis via improved matrix-mechanotransduction.

At 2 weeks of age the variability between animals is low and the RNA-Seq data appears uniform. At 5 weeks of age there is significant variability between mice and the RNA-Seq data requires more interpretation. The changes observed in some of the transcripts were the result of only one mouse in the 5 week study. RT-PCR data analysis confirms this result. Osteoactivin is involved in differentiation of skeletal and muscle tissue and may serve as a novel biomarker for disease progression. RT-PCR confirmed that it is increased in mice and also now in an MDC1A patient muscle that we have in our tissue archive.

Laminin-111 is the predominant Laminin isoform found in the basal lamina of developing embryonic skeletal muscle [115]. However in adult skeletal and cardiac muscle Laminin-111 is replaced by Laminin-211 and Laminin-221 isoforms which help to anchor myofibers to the basement membrane and form neuromuscular junctions [116,160]. Laminin-α2 protein is an essential component of the basal lamina that surrounds muscle fibers and is composed of α, β, and γ heterotrimers [161]. MDC1A is caused by the loss of Laminin-α2 protein. Regeneration of Laminin-α2 deficient muscle is also dependent on the presence of Laminin [124,162]. Molecules that reinforce muscle-basal lamina interactions and restore normal survival signaling pathways are likely candidates for drug-based therapeutics for MDC1A.

Laminin-111 can be systemically delivered to all major muscles affected in MDC1A patients helping to enhance muscle integrity and addresses the primary defect of cellular adhesion in MDC1A. Laminin-111 is unlikely to elicit an immune response since it is naturally expressed during embryonic development and in the adult kidney basement membrane [142]. Treatment with Laminin-111 has been shown recently to reduce muscle pathology and improve viability in the (*dy^{W}-/-)* MDC1A mouse model [131]. In one such study, Evan's Blue Dye uptake was used to examine the integrity of the sarcolemma and Laminin-111 treatment had beneficial effects in Laminin-α2 deficient muscle by causing a 7.3-fold reduction in sarcolemmal rupture. The α7β1 integrin is the major Laminin-binding integrin in cardiac and skeletal muscle [163]. MDC1A patients and *dy^{W}-/-* mice have reduced levels of α7 integrin contributing to severe muscle pathology [160] Laminin-111 has

been shown to increase α7 integrin expression in mouse and human muscle cells [164].

Immunofluorescence for Osteoactivin using muscle from an MDC1A patient and unaffected control showed that Osteoactivin is normally located in the ECM in unaffected muscle, but in the MDC1A muscle it is localized within the muscle cells. This may cause misregulation of MAPK signaling (and potentially activation of TGF-beta and fibrotic pathways) in muscle cells. Laminin-111 treatment in mice appears to block Osteoactivin expression and therefore would potentially restore MAPK signaling in muscle and prevent further fibrosis. The immunofluorescence data confirms in patients the mouse RNA-Seq data and RT-PCR studies.

ACKNOWLEDGEMENTS

Dr. Ryan Wuebbles for assistance with RNA-Seq and qRT-PCR studies. I would like to thank Dr. Joseph Fass and Dr. Ryan Kim for generating and processing the RNA-Seq data at the UC Davis Genome center. I would also like to thank Dr. Paul Brewer for kindly performing the ERK immunoblots and Rebecca Evans for genotyping the *dy*^{W}-/- mice.

Gene Name	Forward Primer	Reverse Primer
Aggrecan	actgccttcgccagtgagga	Atgtcagagagtatctggtggagcct
GPNMB	gaagagccttcaatgggtctggcac	tggagatcaggacaccattcactgct
Elane	agcgcactcgacagacctt	Cgttaatggtagcggagccattga
MMP8	ttcatatctctgttctggcccttccta	Cttgctgcaggtcatagccact
MMP9	cttggtgtagcacaacagctgacta	cctcaaagatgaacgggaacacaca
BGLAP1	cagcagcttggcccagaccta	ctttgtcagactcagggccgct
BGLAP2	gaccctctctctgctcactctgct	gtagcgccggagtctgttcacta
PRTN3	gaagttcaccatcagtcaggtcttcca	ggacagagtctggtcctgct
DMP1	ggtgatttggctgggtcacca	cagctcctctccagattcactgct
CALCA1	catgggcttcctgaagttctcccct	caggcgaacttcttcttcactgagagt
SERCA1	atggcctggactgtgaggtcttt	Atccgcagtagggactggttct
SERCA2	ttgctgttggtgacaaagttcctg	Ggacagggtcagtatgcttgatga
IBSP	cagaagaaaatggagacggcgatagt	ggaaagtgtggagttctctgcct
LAMA2	Doe *et al.*	Doe *et al.*
Tenascin C	Doe *et al.*	Doe *et al.*
LGALS3	Doe *et al.*	Doe *et al.*
WISP1	ctgcacagaggctgccatctgt	Aggactcgccattggtgtagcgt
ADAM8	cagatctgaaaactgctctgctaaatgca	ctgcttgttcatctgatacatctgcca

Table 1: Primer oligonucleotide sequences that were used to confirm RNA-Seq data

This table was kindly provided by Dr. Ryan Wuebbles.

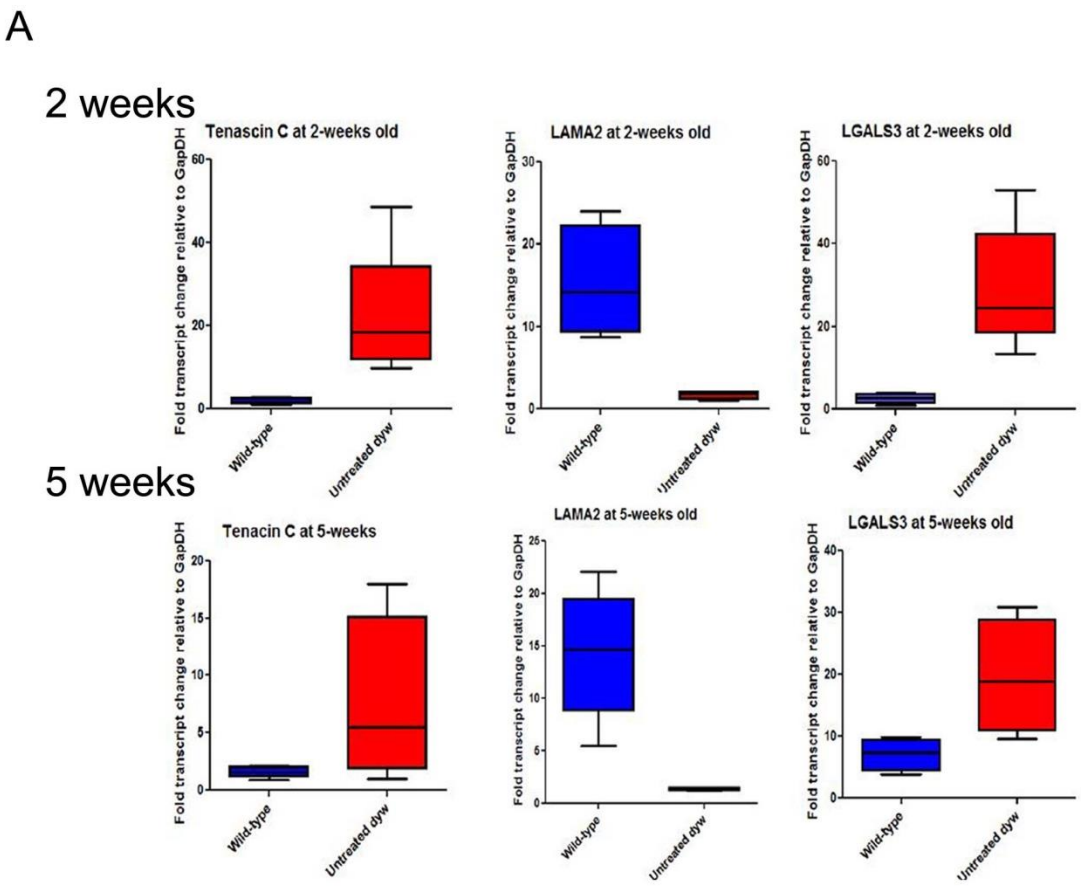

Fig 9. RT-PCR results confirming important transcriptional changes in genes associated with the extracellular matrix in 2 week old and 5 week old WT and *dy^{W}*-/- + PBS mice

A) Both 2 week old and 5 week old *dy^{W}* -/- mice show similar trends for fold-changes in Tenascin-C, LAMA2 and LGAL3. These RT-PCR results were necessary to compare previous published findings. The results presented here helped to suggest that the RNA-Seq data used in this study were reliable based on these initial changes. The data and figure were kindly provided by Dr. Ryan Wuebbles.

B i.

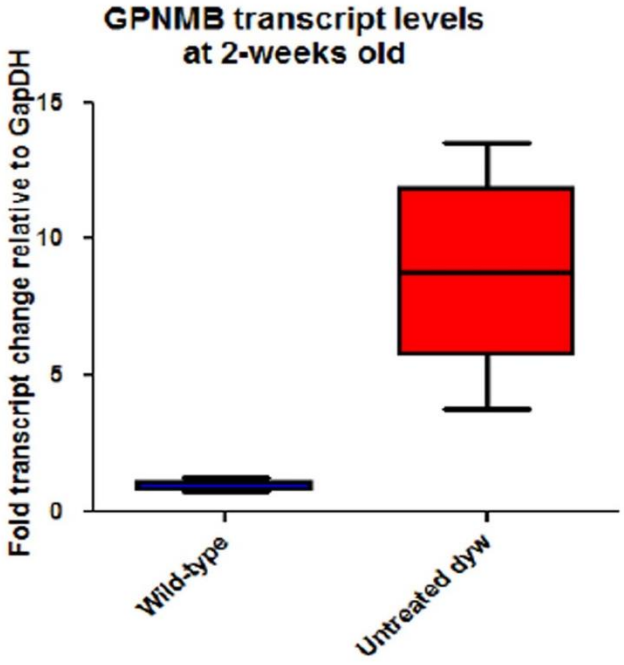
GPNMB transcript levels
at 2-weeks old
Fold transcript change relative to GapDH
15
10
5
0
Wild-type
Untreated dyw

B ii.

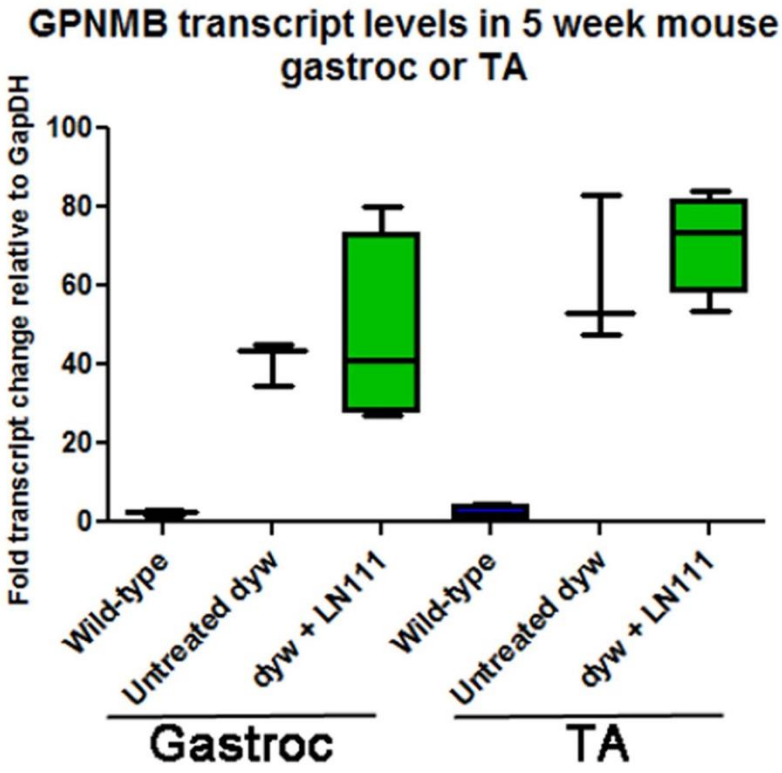
GPNMB transcript levels in 5 week mouse
gastroc or TA
Fold transcript change relative to GapDH
100
80
60
40
20
0
Wild-type
Untreated dyw
dyw + LN111
Wild-type
Untreated dyw
dyw + LN111
Gastroc
TA

Fig 9. RT-PCR results confirming important transcriptional changes in genes associated with the extracellular matrix in 2 week old and 5 week old WT and *dy^{W}-/-* + PBS mice

B) i) Osteoactivin (GPNMB), the transcript of interest, was shown to be elevated in TA muscle of 2 week old *dy^{W}-/-* mice compared to WT. ii) Osteoactivin (GPNMB), at 5 weeks old was shown to be elevated in *dy^{W}-/-* Gastroc and TA muscle. Laminin-111 treatment did not cause a significant change in GPNMB transcript levels compared to PBS treated animals. The data and figure were kindly provided by Dr. Ryan Wuebbles.

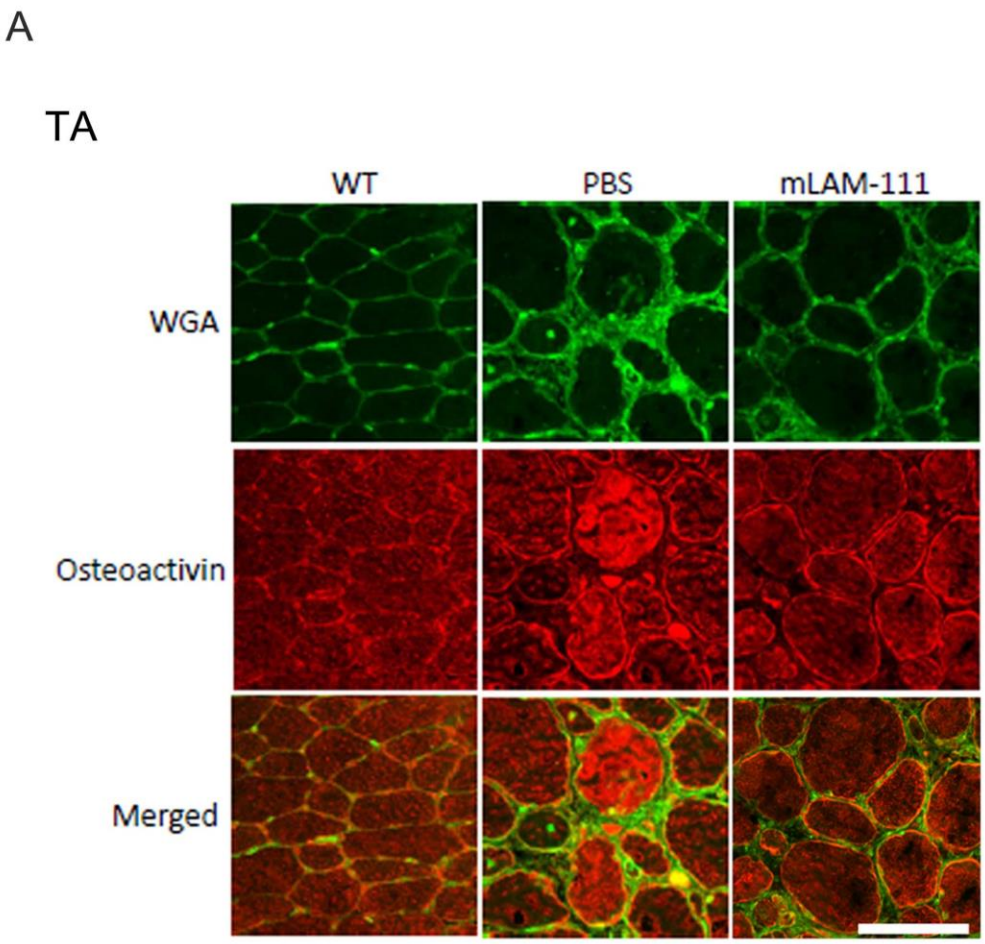

Fig 10. Immunofluorescence on critical protein changes identified from gene transcripts in TA muscle from 5 week old WT, *dy^{W}*-/- + PBS and *dy^{W}*-/- + mLAM-111 treated mice

A) Osteoactivin protein detection in 10 µm TA cryosections shown in red. Wheat-germ Agglutinin (WGA) shown in green was used to outline the myofibers. Scale bar =100 µm Magnification = 400 X. PBS treated *dy^{W}*-/- muscle showed elevated Osteoactivin and an increase in the localization of Osteoactivin protein within the myofibers suggesting that the Osteoactivin protein is cleaved and able to enter the ruptured myofibers. Laminin-111 treated muscle showed that the sarcolemma

is stabilized and therefore osteoactivin is unable to enter the myofibers and is located around the periphery of the myofibers.

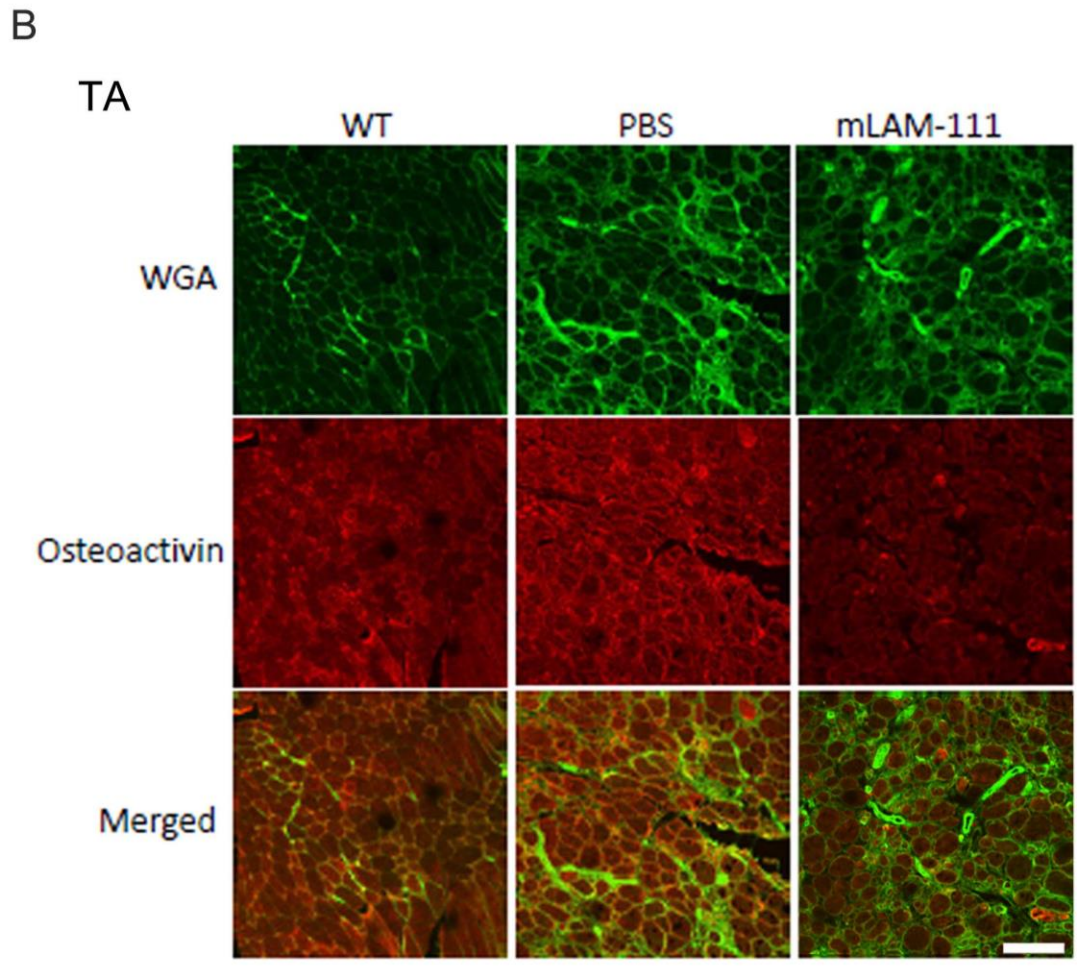

Fig 10. Immunofluorescence on critical protein changes identified from gene transcripts in TA muscle from 5 week old WT, *dy^{W}*-/- + PBS and *dy^{W}*-/- + mLAM-111 treated mice

B) Osteoactivin protein detection in 10 µm TA cryosections shown in red. Wheat-germ Agglutinin (WGA) shown in green was used to outline the myofibers. Scale bar = 200 µm and Magnification = 100 X. PBS treated *dy^{W}*-/- muscle showed elevated Osteoactivin and an increase in the localization of Osteoactivin protein within the myofibers suggesting that the Osteoactivin protein is cleaved and able to enter the ruptured myofibers. These micrographs are at a smaller

magnification of the same tissue shown at a higher magnification in Figure 10 A i).

C

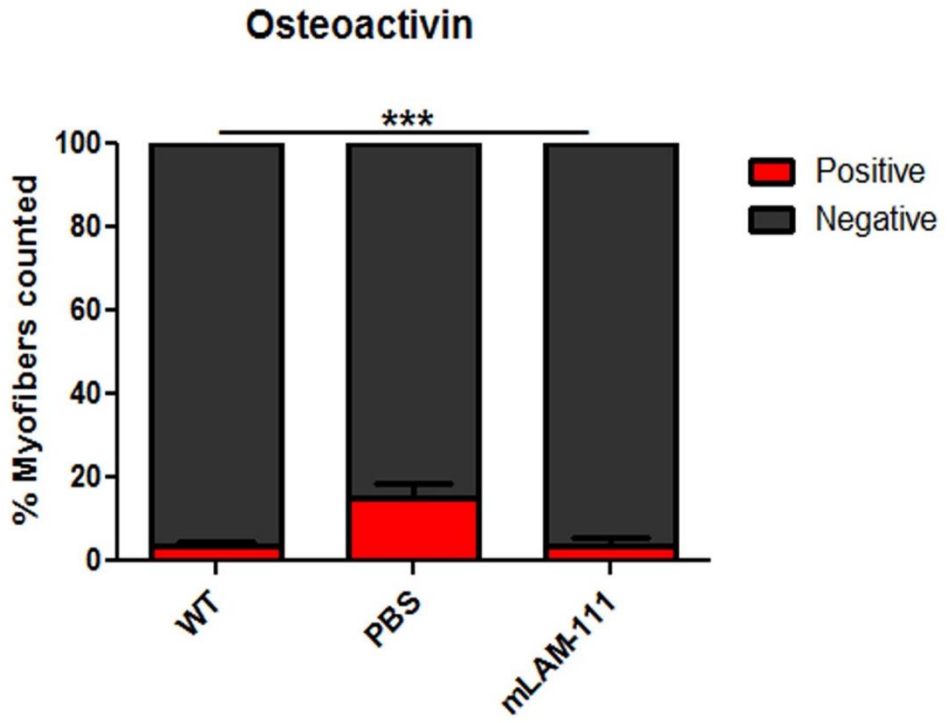

Fig 10. Immunofluorescence on critical protein changes identified from gene transcripts in TA muscle from 5 week old WT, *dy^{W}-/-* + PBS and *dy^{W}-/-* + mLAM-111 treated mice

C) Quantification of Osteoactivin positive myofibers for 5 week old TA muscle shown in Figure 10 A. WT muscle had 3.4 % osteoactivin positive myofibers ± 1.08 %, PBS muscle had 14.9 % osteoactivin positive myofibers ± 3.4 % and laminin-111 treated muscle had 3.7 % osteoactivin positive myofibers ± 1.8 %. Two-Way *ANOVA* statistical analysis of the 3 treatment groups revealed statistical significance with a *P*-value < 0.001.

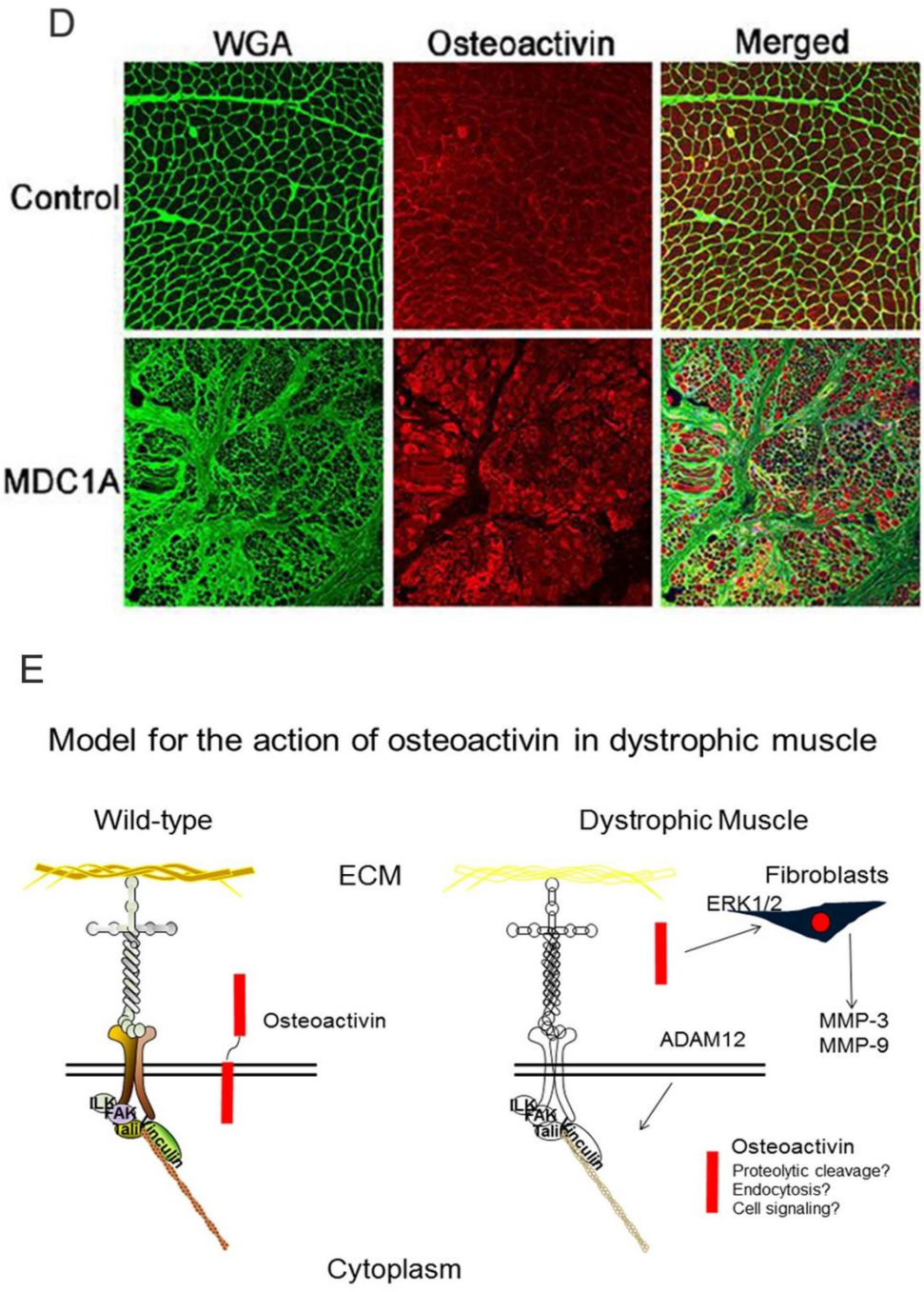

Fig 10. Immunofluorescence on critical protein changes identified from gene transcripts in TA muscle from 5 week old WT, *dy^{W}-/-* + PBS and *dy^{W}-/-* + mLAM-111 treated mice

D) Levels of Osteoactivin protein in human skeletal muscle tissue are similar to the levels of osteoactivin in *dy*^{W}*-/-* mouse tissue in Figure 10 A. Elevation of intracellular osteoactivin in diseased muscle compared to WT muscle. E) Schematic model of MDC1A disease progression showing the stage where Osteoactivin (OA) protein becomes misregulated. In WT muscle osteoactivin protein is intact and located as a transmembrane protein. However, in dystrophic muscle osteoactivin is subject to cleavage by ADAM12 and is split into two pieces. The intracellular osteoactivin component is detected by immunofluorescence in dystrophic muscle (Figure 10 A) and the extracellular component is able to participate in cell signaling and recruit fibroblasts via the ERK1/2 pathway and recruitment of matrix metalloproteinases. Figures 10 D & E were kindly provided by Dr. Dean Burkin and Dr. Ryan Wuebbles.

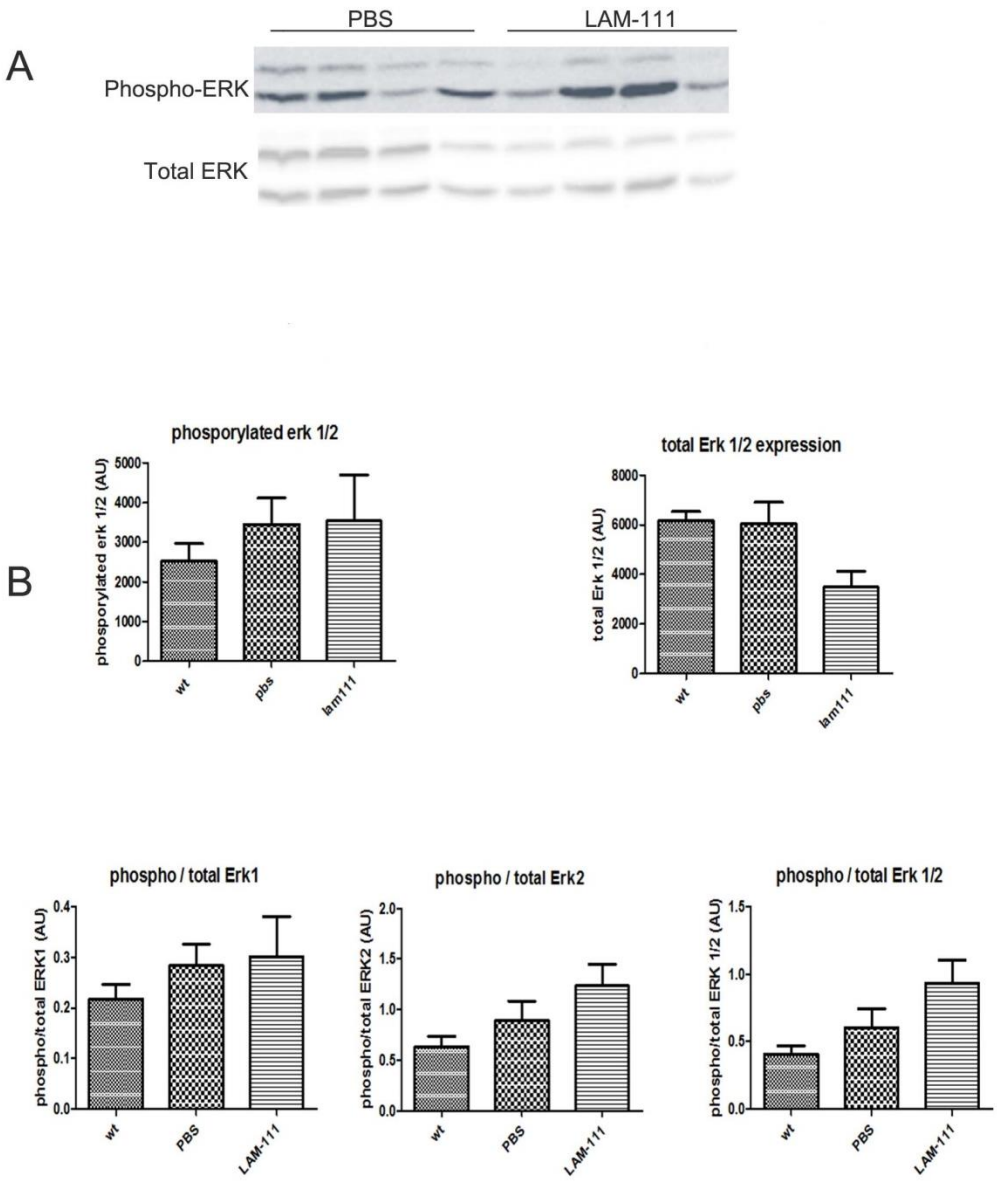

Figure 11. Immunoblotting for ERK and phospho-ERK protein

A) Immunoblots showing that laminin-111 treatment causes a decrease in total ERK protein and a corresponding elevation in phosphorylated-ERK protein when compared to PBS treated animals. B) Quantification of the immunoblots shown in Figure 11 A. The data and figure were kindly provided by Dr. Paul Brewer.

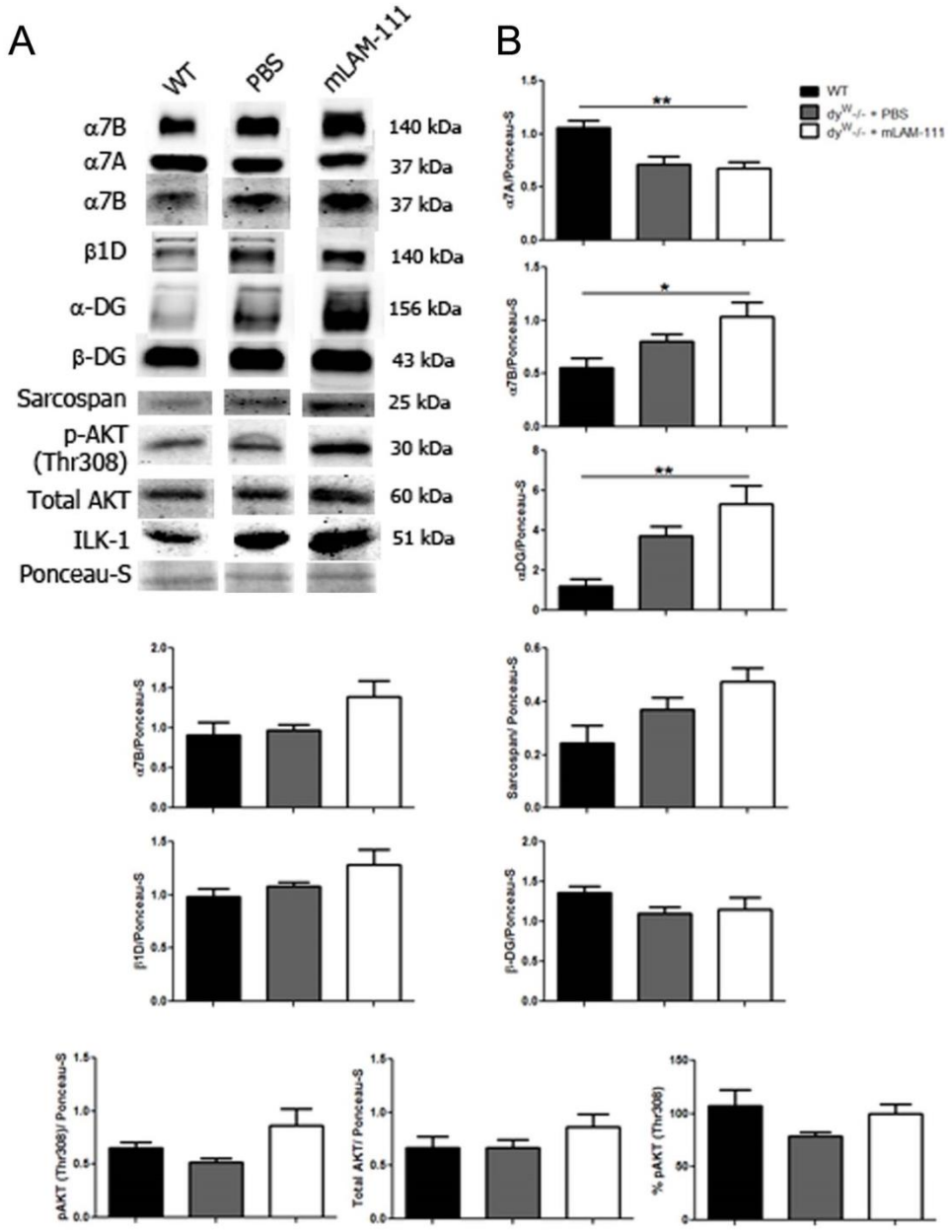

Figure 12. Immunoblots on critical protein changes identified from transcripts for 5 week old *dy^{W}-/-* mice

A) Representative immunoblots for 5 week old *dy^{W}-/-* TA muscle. B) Quantification of changes in protein expression. Statistical analysis via One-way

ANOVA showed significance in α7A, α7B and αDG expression with *p*-values (0.0032, 0.0165, 0.0016) respectively.

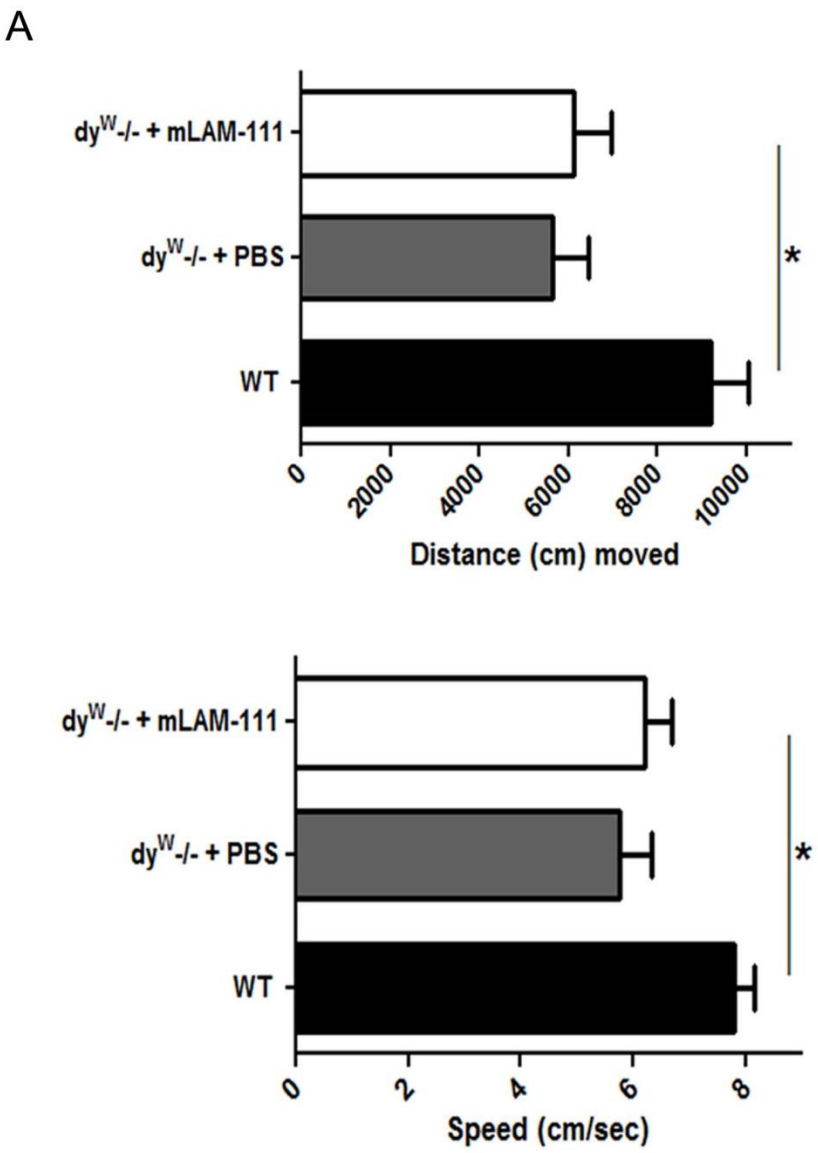

Figure 13. Histology and functional data obtained from 5 week old *dy^{W}-/-* mice

A) Activity box data was recorded for distance (cm) and speed (cm/sec) with which moved. WT animals moved an average of 9217.2 cm ± 1866.79 cm, PBS treated animals moved an average of 5631.25 cm ± 1646.27 cm and mLAM-111 treated animals moved an average of 6128.75 cm ± 1664.51 cm. Laminin-111 treatment was able to improve the speed with which moved when compared to

PBS treated animals by 7.7 %. *P*-values were (0.0221 and 0.0190) respectively with One-way *ANOVA*.

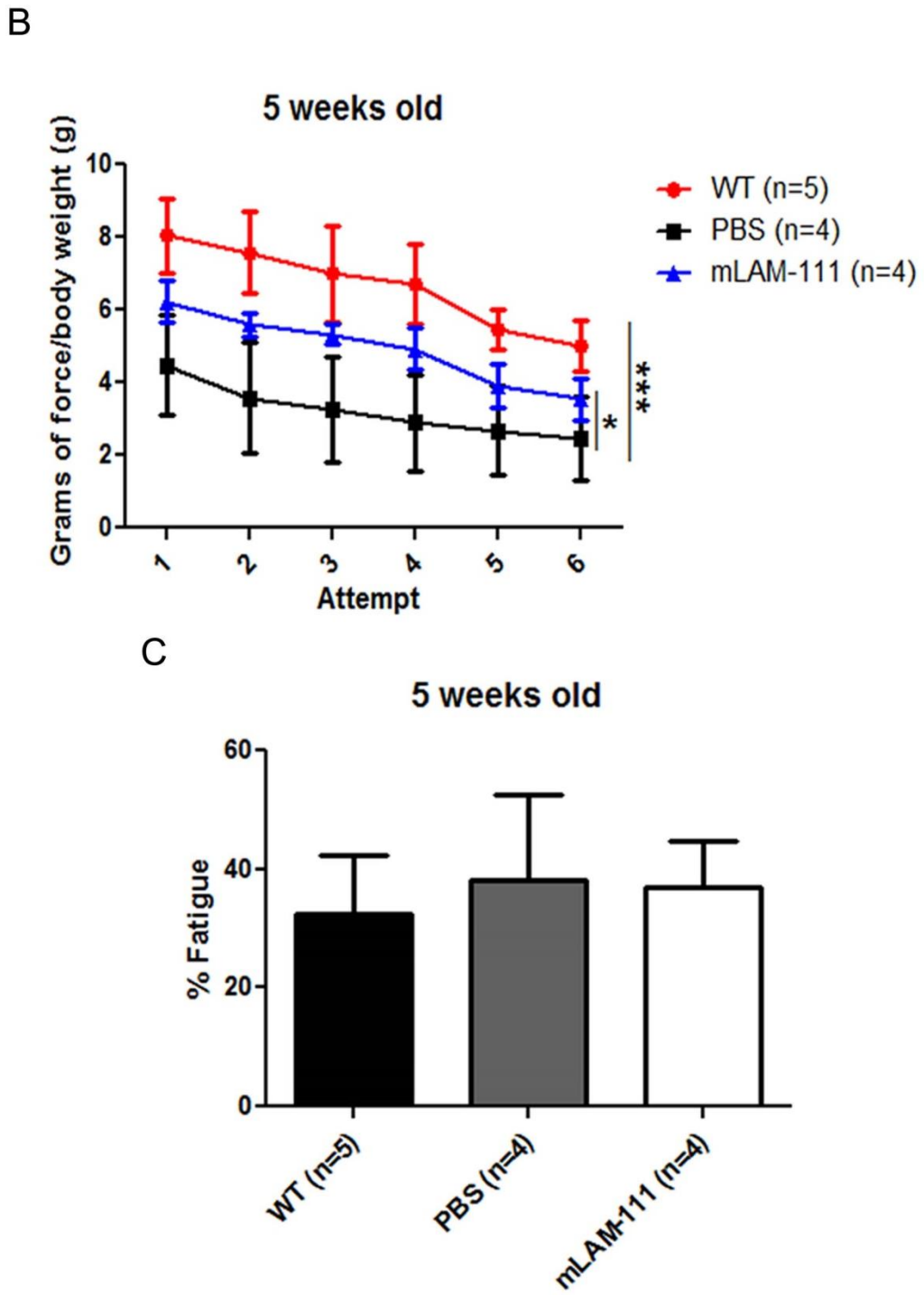

Figure 13. Histology and functional data obtained from 5 week old *dy^{W}* mice

B) Grip strength displayed as grams of force (g) normalized to body weight (g) was quantified for each treatment group. *P*-values were (< 0.0001 and 0.05)

respectively with Two-way *ANOVA*. C) Percentage (%) fatigue was quantified based on grip strength recorded in Figure 13 B and there was no statistical significance found meaning that there was no difference in how fast forelimb muscle fatigued in either PBS or laminin-111 treated animals.

A i.

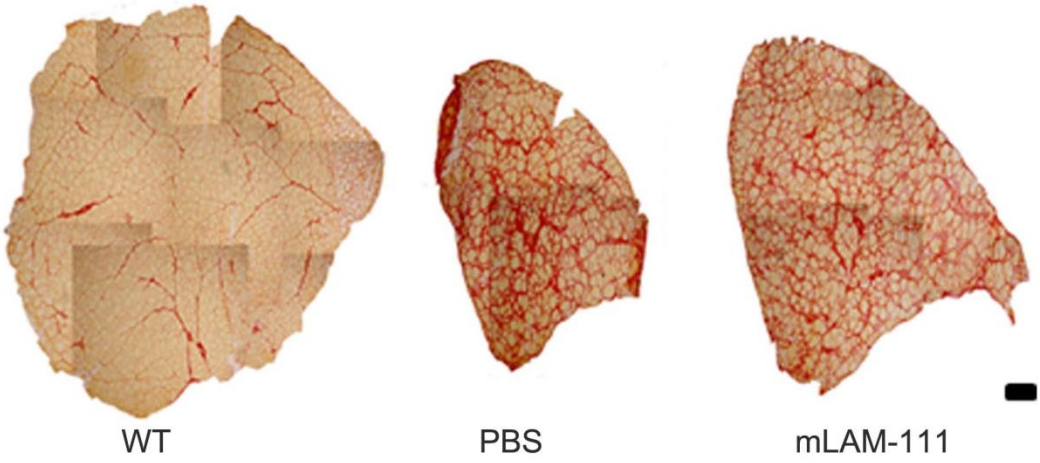
WT
PBS
mLAM-111

A ii.

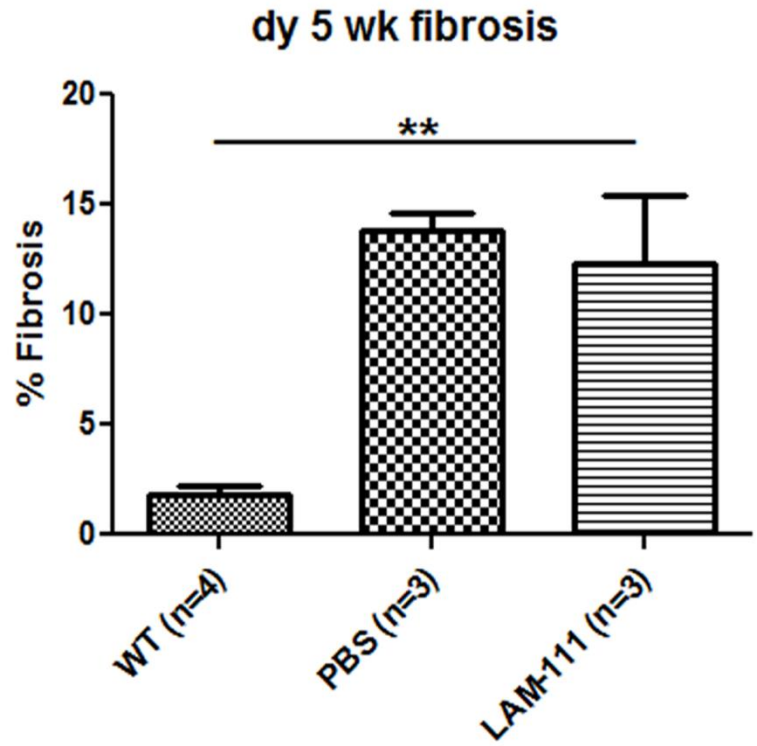
dy 5 wk fibrosis
% Fibrosis
20
15
10
5
0
**
WT (n=4)
PBS (n=3)
LAM-111 (n=3)

Figure 14. Histology and respiratory function in 5 week old WT, *dy^{W}-/-* + PBS and *dy^{W}-/-* + mLAM-111 treated mice

A) i) Representative montages of 10 µm TA cryosections stained with Sirius Red. Sirius red staining is used as a measure of fibrosis and is indicated with increased red color. Magnification = 100 X and scale bar = 200 µm. There is increased fibrotic tissue present within the PBS treatment group. Laminin-111 treatment helps to prevent this fibrotic environment. ii) Percentage (%) fibrosis for the Sirius red montages in Figure 14 A i were calculated. One-Way *ANOVA* showed statistical significance.

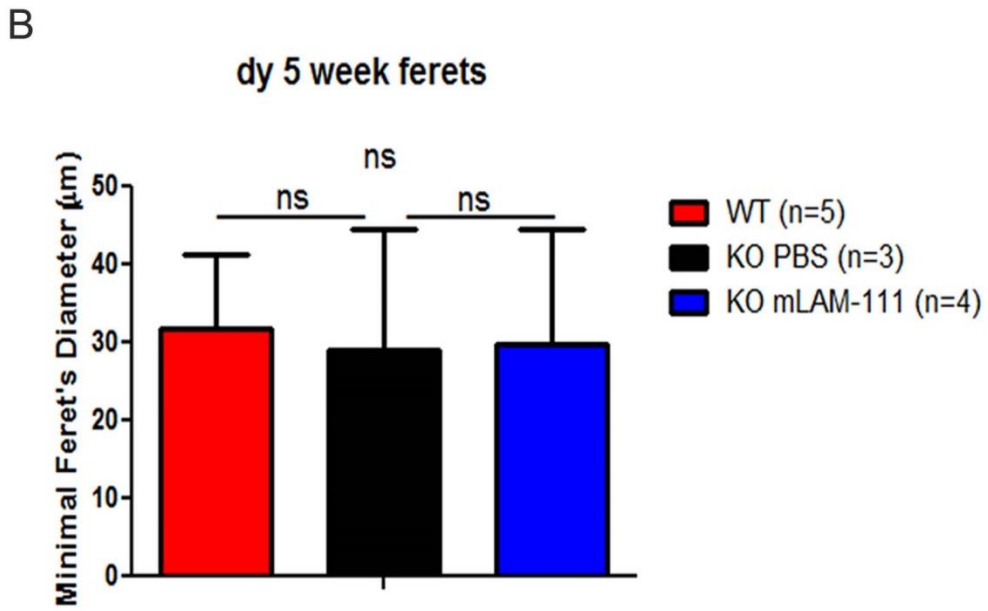

Figure 14. Histology and respiratory function in 5 week old WT, *dy^{W}-/-* + PBS and *dy^{W}-/-* + mLAM-111 treated mice

B) Minimal feret's diameter (µm) is a measure of myofiber size and was calculated for TA cryosections for each treatment group. No statistical significance was found.

C

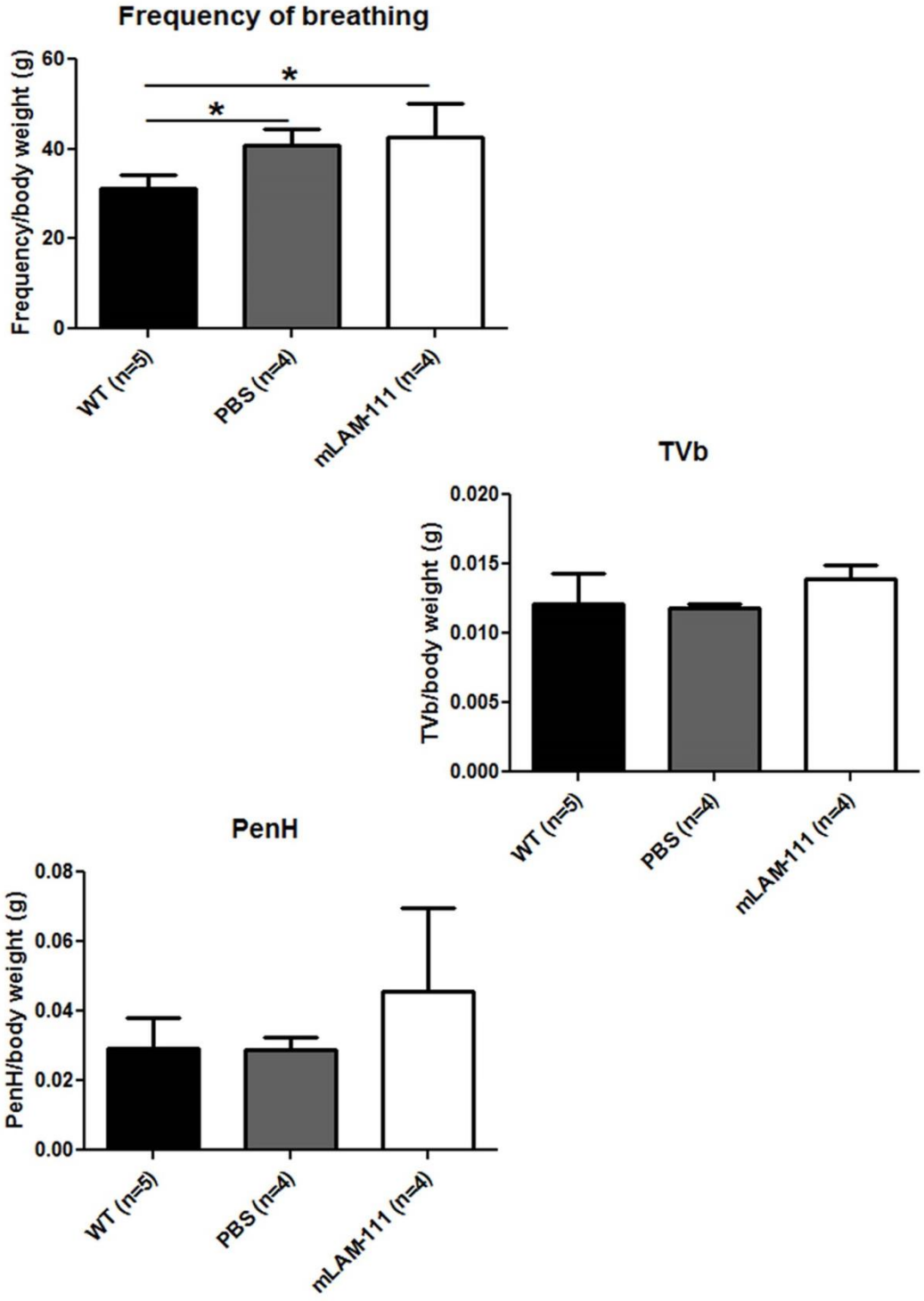
Frequency of breathing
Frequency/body weight (g)
60
40
20
0
*
*
WT (n=5)
PBS (n=4)
mLAM-111 (n=4)
TVb
TVb/body weight (g)
0.020
0.015
0.010
0.005
0.000
WT (n=5)
PBS (n=4)
mLAM-111 (n=4)
PenH
PenH/body weight (g)
0.08
0.06
0.04
0.02
0.00
WT (n=5)
PBS (n=4)
mLAM-111 (n=4)

Figure 14. Histology and respiratory function in 5 week old WT, *dy^{W}-/-* + PBS and *dy^{W}-/-* + mLAM-111 treated mice

C) Plethysmography data obtained using the Buxco Whole Body Plethysmography (WBP) system. Parameters of interest included: Frequency of breathing, Tidal Volume (TVb) and PenH. PenH (enhanced pause) is correlated to but not a direct measurement of airway resistance. Each parameter was normalized to body weight (g). *P*-value was 0.0126 with One-way *ANOVA*.

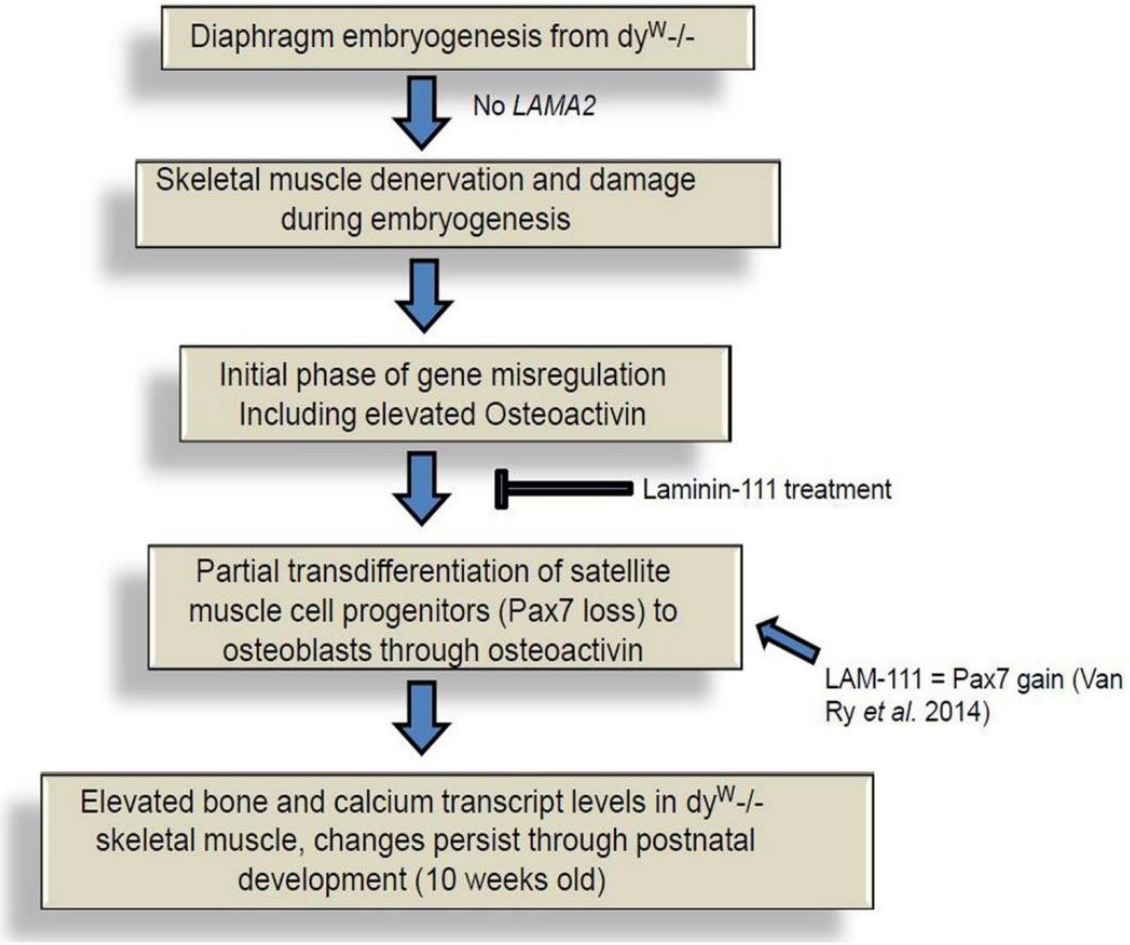

Figure 15. Model of Laminin-111 action on Osteoactivin (OA) restoration

WT muscle possesses intact osteoactivin (OA) protein. Loss of laminin-α2 in *dy*^{W}-/- muscle causes increased OA transcription but the protein is cleaved into two fragments by ADAM12. The internal fragment is visible in fibrotic patient tissue. The external fragment is free to activate myofibroblasts that secrete matrix metalloproteinases and trigger fibrotic pathways. Treatment with laminin-111 does not affect OA transcription but does however change OA protein localization. With LAM-111 treatment, OA moves back to the sarcolemma like

WT therefore suggesting that ADAM12 cleavage is prohibited and there is intact OA protein. The data and figure were kindly provided by Dr. Ryan Wuebbles.

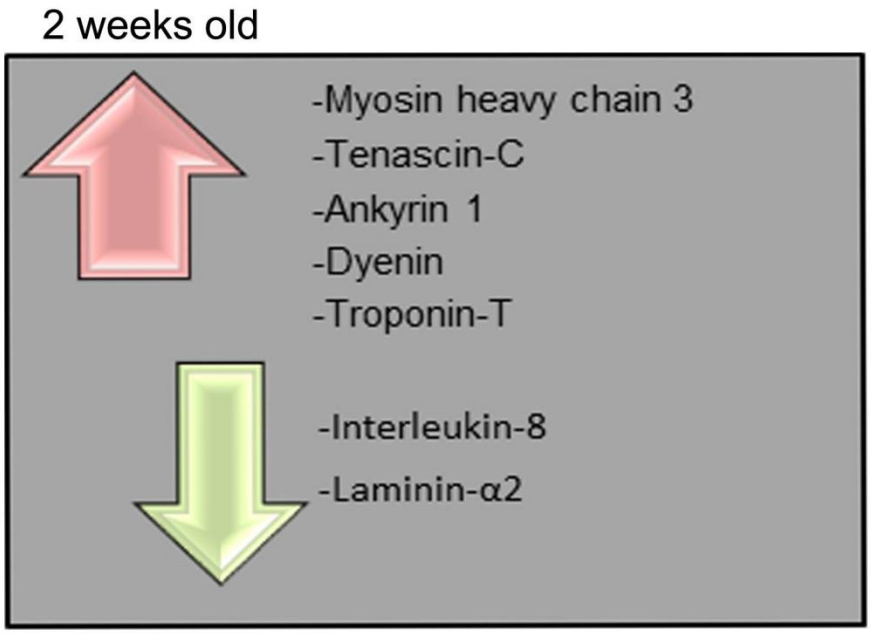

Supplemental Table 1: RNA-Seq baseline transcript summary for WT vs *dy^{W}*-/- 2 week old animals

Transcripts found to be upregulated in 2 week old *dy^{W}*-/- mice include: Ankyrin (Ankrd1), Myosin Heavy chain 3 (Myh3), Dyenin (Dnahc1), Troponin T type 2 (Tnnt2). Interleukin-8 (IL-8) was found to be down-regulated as was laminin-α2.

	2 week Down-regulated 4-fold
Il8	Interleukin-8 important mediator of the innate immune response
Lama2	Laminin-α2
	2 week up-regulated 4-fold
Stx11	Syntaxin 11 SNARE that acts to regulate protein transport between late endosomes and the trans-Golgi network
Card14	Caspase Recruitment Domain Family, Member 14 Plays a role in signaling mediated by TRAF2, TRAF3 and TRAF6 and protects cells against apoptosis. Activates NF-kappa-B via BCL10 and IKK. Stimulates the phosphorylation of BCL10
Ankrd1	Ankyrin Repeat Domain 1 (Cardiac Muscle) May play an important role in endothelial cell activation. May act as a nuclear transcription factor that negatively regulates the expression of cardiac genes. Induction seems to be correlated with apoptotic cell death in hepatoma cells
Lgals3	Lectin, Galactoside-Binding, Soluble, 3 Involved in acute inflammatory responses including neutrophil activation and adhesion, chemoattraction of monocytes macrophages, opsonization of apoptotic neutrophils, and activation of mast cells
Tnc	Tenascin C Extracellular matrix protein implicated in guidance of migrating neurons as well as axons during development, synaptic plasticity as well as neuronal regeneration. Promotes neurite outgrowth from cortical neurons grown on a monolayer of astrocytes. Ligand for integrins alpha-8/beta-1, alpha-9/beta-1, alpha-V/beta-3 and alpha-V/beta-6
Myh3	Myosin, Heavy Chain 6, Cardiac Muscle, Alpha Muscle contraction
Tlr13	Toll-Like Receptor 3 Toll-like receptors (TLRs) are single transmembrane cell-surface receptors, which have a key role in the innate immune system.
Myl7	Myosin, Light Chain 7, Regulatory mediates plus-ended movement along microfilaments. It is involved in muscle contraction through cyclic interactions with actin-rich thin filaments, creating a contractile force. It is regulated by phosphorylation via myosin light chain kinase (MLCK) and by intracellular Ca2+ concentrations.
Tnnt2	Troponin T Type 2 (Cardiac) Troponin T is the tropomyosin-binding subunit of troponin, the thin filament regulatory complex which confers calcium-sensitivity to striated muscle actomyosin ATPase activity
Timp1	Tissue inhibitor metalloproteinases
Myl4	Myosin, Light Chain 4, Alkali; Atrial, Embryonic Regulatory light chain of myosin. Does not bind calcium
Dnahc1	Dynein, Axonemal, Heavy Chain 1 Force generating protein of respiratory cilia. Produces force towards the minus ends of

	microtubules. Dynein has ATPase activity; the force-producing power stroke is thought to occur on release of ADP. Involved in sperm motility; implicated in sperm flagellar assembly (By similarity)

Supplemental Table 2: Summary of 2 week old ≥ 4–fold transcriptional changes in WT and untreated *dy^{W}*-/- mice

A total of 138 transcripts found to be up- or down- regulated ≥ 4-fold in 2 week old *dy^{W}* -/- mice were narrowed down to 14 transcripts of interest in this table.

	5 week Down-regulated 4-fold
Ibsp	integrin binding sialoprotein cell to matrix interaction espcecially bone
Bglap	Osteocalcin Bone Gamma-Carboxyglutamate (Gla) Protein bone building
Dmp1	Dentin Matrix Acidic Phosphoprotein 1
Tnn	Tenascin N neuron outgrowth and cell migration
Mmp13	Matrix metalloproteinase 8 are zinc-dependent endopeptidases that are the major proteases involved in ECM degradation.
Fam150b	cartilage oligomeric matrix protein play a role in structural integrity of cartilage via its interaction with othere extracellular matrix proteins such as collagens and fibronectin.
Galnt3	Baculoviral IAP Repeat Containing 5 dual roles in promoting cell proliferation and preventing apoptosis.
Mmp8	Matrix Metallopeptidase 3 (Stromelysin 1, Progelatinase) Can degrade fibronectin, laminin, gelatins of type I, II, IV, and V; collagens III, IV, X, and IX, and cartilage proteoglycans. Activates procollagenase
Irf4	Myosin, Heavy Chain 6, Cardiac Muscle, Alpha Muscle contraction
Pax5	Alanine--Glyoxylate Aminotransferase 2 ADMA is a potent inhibitor of nitric-oxide (NO) synthase, and this activity provides mechanism through which the kidney regulates blood pressure
	5 week up-regulated 4-fold
Adra1b	WNT Inhibitory Factor 1 Binds to WNT proteins and inhibits their activities
Mettl7b	Spectrin, Alpha, Erythrocytic 1 (Elliptocytosis 2) Spectrin is the major constituent of the cytoskeletal network underlying the erythrocyte plasma membrane. It associates with band 4.1 and actin to form the cytoskeletal superstructure of the erythrocyte plasma membrane
1810053B23Rik	Tenascin N neuron outgrowth and cell migration
Cyp4f15	Desmoglein 11 Component of intercellular desmosome junctions. Involved in the interaction of plaque proteins and intermediate filaments mediating cell-cell adhesion
Tm6sf2	carbonic anhydrase 3 slow twitch skeletal muscle and myogenesis
Aspg	WNT outsde to inside cell signaling

Pax7	PAx7 Secreted Phosphoprotein 2, 24kDa Could coordinate an aspect of bone turnover (By similarity)
Itih1	Myosin, Light Chain 7, Regulatory mediates plus-ended movement along microfilaments. It is involved in muscle contraction through cyclic interactions with actin-rich thin filaments, creating a contractile force. It is regulated by phosphorylation via myosin light chain kinase (MLCK) and by intracellular Ca2+ concentrations.
Ugt2a3	Paired Box 7 Transcription factor playing a role in myogenesis through regulation of muscle precursor cells proliferation (By similarity)
Lect2	EGF-Like Repeats And Discoidin I-Like Domains 3 Promotes adhesion of endothelial cells through interaction with the alpha-v/beta-3 integrin receptor. Inhibits formation of vascular-like structures. May be involved in regulation of vascular morphogenesis of remodeling in embryonic development
BC089597	Calcitonin acts to reduce blood calcium
Nr1i2	vitronectin Vitronectin is a cell adhesion and spreading factor found in serum and tissues. Vitronectin interact with glycosaminoglycans and proteoglycans. Is recognized by certain members of the integrin family and serves as a cell-to-substrate adhesion molecule. Inhibitor of the membrane-damaging effect of the terminal cytolytic complement pathway
Cyp3a13	claudins are found at tight junctions as a physical barrier and known for maintaining cell polarity and signal transductions
Abcg8	Osteocalcin Bone Gamma-Carboxyglutamate (Gla) Protein bone building
Fbp1	desmoglein 2 Component of intercellular desmosome junctions. Involved in the interaction of plaque proteins and intermediate filaments mediating cell-cell adhesion
Bhmt2	integrin b cell adhesion cell to matrix adhesion
0610005C13Rik	integrin binding sialoprotein cell to matrix interaction espcecially bone
Akr1b7	ficolin B marks apoptotic and necrotic cells
Etnk2	Monocyte to macrophage differentiation associated 2 key player in muscular dystrophy
Agxt	Synaptotagmin I regulatory role in the membrane interactions during trafficking of synaptic vesicles at the active zone of the synapse.
0610031O16Rik	Osteocalcin Bone Gamma-Carboxyglutamate (Gla) Protein bone building
2810459M11Rik	aggrecan proteoglycan in ECM aims to resist compression in cartilage
Ugt1a5	Vitamin D (1,25- Dihydroxyvitamin D3) Receptor Plays a

	central role in calcium homeostasis
Il8	Interleukin-8 important mediator of the innate immune response

Supplemental Table 3: Summary of 5 week old ≥ 4–fold transcriptional changes in PBS treated versus LAM-111 treated *dy^{W}-/-* mice

A total of 468 transcripts found to be up- or down- regulated ≥ 4-fold in 5 week old laminin-111 treated *dy^{W}* -/- mice were narrowed down to 34 transcripts of interest in this table.

A Overview

2 wk Gene expression changes	5 wk Gene expression changes	
KO	**KO PBS**	**KO mLAM-111**
• ↑Inflammation • ↑Apoptosis • ↑Fibrosis • ↑Demyelination • ↑Vascular Disease • ↑Infarction • ↑ROS • ↑Survival pathways • ↑GAL3 • ↑TIMPs • ↑Myosin in ILK	• ↑Inflammation • ↑Necrosis • ↑Osteomalcia • ↑Cyclins and cell cycle checkpoint regulation • ↑DNA damage checkpoints • ↑Oxidative stress • ↑Nitric Oxide • ↑ROS • ↑Mitosis of muscle cells • ↑Pulmonary hypertension • ↑Connective Tissue degradation • ↑Heart injury	• ↓Pax5 & ↑Pax7 • ↑Myosin in ILK • ↑cPLA2 in ERK/MAPK & LEF-/TCF1 in WNT/β-Catenin • ↑mTOR • ↓ROS • ↑Pulmonary surfactant

B 5 weeks old

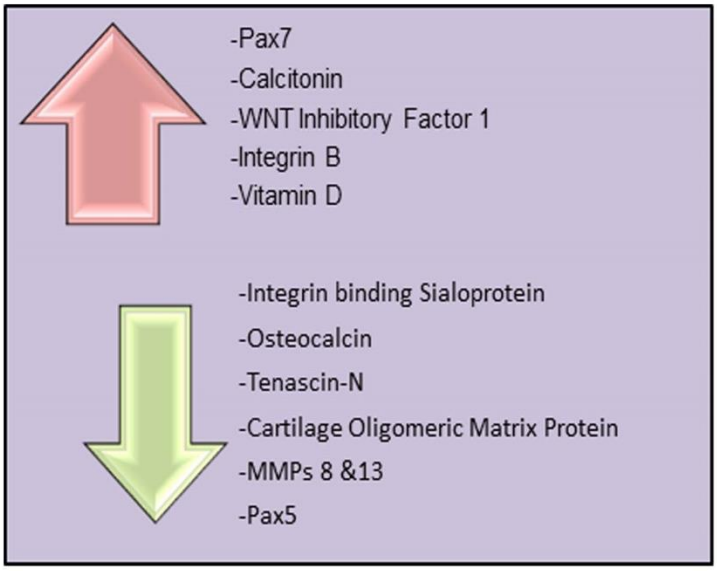

Supplemental Table 4: RNA-Seq *dy^{W}-/-* +PBS vs *dy^{W}-/-* +LAM-111

A) Overview of gene expression changes discovered for 2 week old *dy^{W}-/-* mice between WT and laminin-α2 deficient. Gene expression changes tabulated for 5 week old *dy^{W}-/-* mice between PBS treated and mLAM-111 treated groups. B) 5 week transcripts include: Integrin binding Sialoprotein (Ibsp), Osteocalcin (Bglap), MMP-13 (MMP13), Cartilage Oligomeric Matrix Protein (Fam150b),

WNT Inhibitory Factor 1 (Adra1b), Calcitonin (BC089597), Integrin B (Bhmt2), Ficolin (Akr1b7), Interleukin-8 (IL-8) and Vitamin D (Ugt1a5).

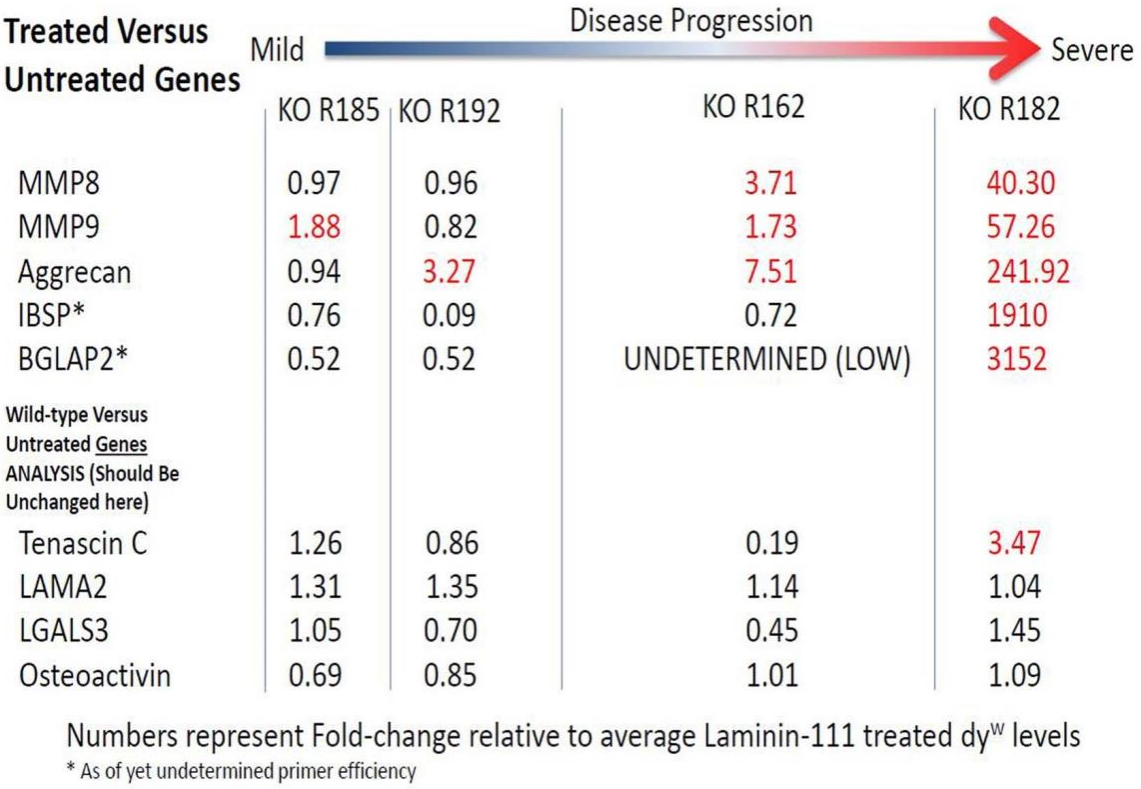

Supplemental Table 5: RT-PCR results confirming important transcript changes in 5 week old LAM-111 treated *dy^{W}-/-* mice

Comparison of expression changes (MMP8, MMP9, Aggrecan, IBSP and BGLAP2) as disease progresses in treated versus untreated genes. The data and figure were kindly provided by Dr. Ryan Wuebbles.

Chapter IV

Long term Laminin-111 protein therapy within the *mdx* mouse model for Duchenne muscular dystrophy

ABSTRACT

Duchenne Muscular Dystrophy (DMD) is the most common X-linked disease affecting 1 in 3,500 live male births. Patients with DMD suffer from severe, progressive muscle wasting and weakness with clinical symptoms first detected between 2 to 5 years of age; as the disease progresses patients are confined to a wheelchair in their teens and die in their early 20s mainly due to cardiopulmonary complications. DMD is caused by the loss of the sarcolemmal protein dystrophin (427kDa) due to mutations in the dystrophin gene. When present, dystrophin acts as a scaffold linking the cell cytoskeleton to the extracellular matrix. This loss of dystrophin in DMD results in patients experiencing greater susceptibility to muscle damage via reduced structural and functional integrity of their muscle. One potential therapeutic avenue that needs to be explored involves increasing the levels of the α7β1 integrin in order to compensate for the loss of dystrophin. To test this hypothesis, a muscle cell-based assay was developed in order to report α7 integrin promoter activity with the intent of identifying molecules that promote α7 integrin expression. Theoretically, the identification of α7 integrin enhancing compounds that help boost α7β1 integrin expression as part of drug-based therapies may lead to a novel therapeutic approach for the treatment of this disease.

INTRODUCTION

Duchenne Muscular Dystrophy is a genetic disorder that affects the skeletal and cardiac muscle. Duchenne Muscular Dystrophy (DMD) is the most common type of muscular dystrophy in boys[95]. It is an X-linked disorder that affects 1 in every 3,300 live male births [165]. This disorder results from a mutation in the DMD gene which produces three isomers of the protein Dystrophin [166]. Dystrophin is a protein that connects muscle fiber cytoskeleton to surrounding laminin in the extracellular matrix[161]. This connection provides structural integrity during muscle contractions. The failure to produce dystrophin results in the inability for the formation of the dystrophin-laminin binding complex which results in severe muscle weakness [167]. Children with DMD are not able to walk and are wheelchair-bound by their teenage years[95]. The progressive nature of DMD leads to feeding tube placement, ventilator assistance and results in the untimely death of DMD patients. Although the dystrophin gene has been known for well over 20 years there is still no effective treatment or cure for this disease [165].

Treatment with Engelbreth-Holm Swarm (EHS) laminin (found embryonically has been shown recently in the Burkin lab to reduce muscle pathology and improve viability before disease onset in the *mdx* mouse model [162]. The *mdx* mouse model has a mutation in the dystrophin gene. It is the ideal mouse model for DMD due to the absence of dystrophin in skeletal muscle and undergoes rounds of muscle degeneration and regeneration similar to that experienced by patients. Pharmacokinetic and histopathological analysis of

treated mdx tissue in these proposed experiments will help to determine whether lamininin-111 will be an effective therapy after disease onset in *mdx* mice.

The research objective for this study is to evaluate whether laminin-111 can prevent muscular dystrophy after disease onset in the *mdx* mouse model of DMD by showing that treatment reduces muscle pathology while increasing muscle strength. In addition a more complete insight into the action of laminin-111 will be achieved by investigating the pharmacokinetics and pharmacodynamics of laminin-111 administered to *mdx* mice and this data is presented in Appendix A.

MATERIALS AND METHODS

Generation of *mdx* mice

All experiments involving mice were performed under an approved protocol from the University of Nevada, Reno Institutional Animal Care and Use Committee. *Mdx* (C57BL10ScSn-Dmd strain) and wild-type (C57BL10ScSn strain) were bred separately. The wild-type control strain used in this study was C57BL10ScSn. Age-matched littermate controls were used for analysis. In order to genotype mice, genomic DNA was isolated from tail snips or ear notches using a Wizard SV DNA purification system (Promega, Madison, WI) following manufacturers instructions.

The mutation in the dystrophin gene was detected using a modified ARMS assay. The following primers were used: p259E (5’GTCACTCAGATAGTTGA

AGCCATTTAA-3'), p260E (5'-GTCACTCAGATAGTTGAAGCCATTTAG-3') and p306F (5'-CATAGTTATTAATGCATAGATATTCAG-3'). PCR conditions were as follows: 95°C for 4 minutes then 34 cycles of 95°C for 1 minute, 55°C for 1 minute and 72°C for 1 minute. Primer set p259 and p306 produced a 275bp wild-type dystrophin allele. Primer set p260 and p306 detects the *mdx* point mutation which produced a 275bp product. To genotype the dystrophin gene, separate PCR reactions were performed since the product sizes are identical in wild-type and *mdx* mice.

Experimental procedures were performed once mice were 14 days of age with fortnightly weighing until the end of study which was at 1 year of age where all mice were subject to *in vivo* experiments. To reduce experimental bias, investigators assessing and quantifying experimental outcomes were blinded to the treatment and control groups.

Laminin-111 Treatment Regime

<u>7 week</u>

Five 5 week old WT mice were treated with phosphate buffered saline (PBS) alongside five 5 week old mdx mice in each treatment group receiving either PBS or EHS mLAM-111 treatment (0.01 mg/g/week). The study ended at 7 weeks old.

10 week

In order to test the hypothesis that laminin-111 can serve as an effective treatment for DMD after disease onset, five 8 week old WT mice were treated with phosphate buffered saline (PBS) alongside five 8 week old mdx mice receiving either PBS or EHS mLAM-111 treatment (0.01 mg/g//week). The study ended at 10 weeks old.

1 year

Male *mdx* mice were treated systemically (0.01 mg/g/fortnight) from 2 weeks of age until they were 1 year old with either sterile PBS or EHS mLAM-111. Original number of mice to be treated: WT (n=5) (1 died at 10 months), PBS (n=7) (2 died between 10 and 12 months), mLAM-111 (n=5) (all survived).

Evan's Blue Dye

Mice were intraperitoneally injected with 50 µL per 10 g of body weight sterile Evan's blue dye solution (10 mg/mL). Mice were sacrificed 8 hours post-injection. Muscles were harvested and flash frozen in liquid nitrogen. 10 um cryosections were fixed with 4% paraformaldehyde and myofibers were outlined with Oregon Green 488 nm-conjugated Wheat Germ Agglutinin (Molecular Probes, Eugene, OR). Evans blue dye positive myofibers were counted per animal. Images were captured at 200 X magnification and processed using Photoshop to create the representative montages.

Survival and weights

Weights for all mice of each genotype were recorded on a fortnightly basis. Softened kibble was provided fresh daily in a petri dish on the bottom of the cage in order to ensure there was no significant weight loss within the mice.

Muscle strength

Force Gauge (San Diego Instruments Inc., San Diego, CA). A total of six measurements per mouse were recorded and all results averaged for each group. The mice were analyzed by grasping a horizontal platform with their forelimbs and pulled backwards. The peak tension (grams of force) was recorded on a digital force gauge as mice released their grip.

X-ray digital imaging

Radiographs were obtained for each mouse at the end of the 10 week study through the use of a Summit digital x-ray unit model 50-520, allowing radiographic measurement of kyphotic index. Calculations for Kyphotic Index were carried out as previously described by Hoey et al. 1985.

Activity

Opto-Varimex 4 Activity Meter (Columbus Instruments) offered unbiased data due to the machine possessing lasers that monitor and auto-track the activity of each mouse for a period of 120 minutes.

Plethysmography

Animals were subjected to plethysmography at 10 weeks of age. Animals for each genotype were used. Animals were placed in the plethysmography chamber (unrestrained) and then subjected to increasing does of aerosolized Acetyl-methacholine (6.25, 12.5, 25, 50 and 100 mg/mL), after an initial time period to acclimatize in the chamber. First mice were exposed to aerosolized PBS to gather baseline data. Experimental values were automatically generated by the pneumograph in the wall of the chamber. FinePointe software (Buxco©) was used to collect all data.

Echocardiography

In vivo echocardiography was performed on mice using a VisualSonics Vevo 2100 system with a MS 550D transducer. This allowed ultrasound imaging of the heart to take place. Mice were anesthetized with 1.5-2.0% isoflurane and placed in a supine position on a heated stage. 2-D short-axis recordings of the left ventricle at the level of the papillary muscle were obtained in M-mode. Measurements were taken to help compare the efficiency of the left ventricle during diastole and systole. Heart rate and body temperature were monitored during imaging. Left ventricle wall thickness and cavity dimensions were measured at systole and diastole for three cycles, averaged, and used with Vevo 2100 software to calculate values for fractional shortening, ejection fraction, and LV mass. Comparisons between groups of mice were made using single-factor

ANOVA in Microsoft Excel; *P* values < 0.05 were considered statistically significant.

Isolation of skeletal muscle

1 year old male wild-type and *mdx* mice were euthanized by CO2 inhalation in accordance with a protocol approved by the University of Nevada, Reno Animal Care and Use Committee. Muscles from these mice were dissected, flash-frozen in liquid nitrogen and stored at -80C.

Immunoblotting

The TA muscle from 10 week old male mice was ground in liquid nitrogen. Protein was extracted in RIPA buffer and 1:200 dilution of Protease inhibitor Cocktail Set III (Calbiochem, EMD Biosciences, San Diego, CA) for the detection of α7A and α7B integrin. Protein was quantified by BSA assay and protein was separated on 12% SDS –page gels under reduced conditions and transferred to nitrocellulose membranes. Membranes were blocked with a dilution of carnation milk buffer. The α7A integrin was detected with a 1:1000 dilution of anti-α7A (A2 345) and α7B integrin was detected by anti-α7B (B2 347) rabbit polyclonal antibodies.

Immunofluorescence

Tibialis Anterior (TA) muscles were embedded in Tissue-TEK Optimal Cutting Temperature compound (Sakura Finetek USA Inc, Torrance, CA). 10 µm sections were cut using leica CM1850 cryostat and placed onto Surgipath

microscope slides (surgipath Medical Industries, Richmond, IL). Laminin-111 was probed for by an antibody dilution of 1:50 against laminin-α1. β-dystroglycan was assessed with incubation of 1:25 dilution of β-dystroglycan antibody. It was then detected with a 1:1000 dilution of FITC anti-rabbit antibody.

Hematoxylin & Eosin staining

Tibialis Anterior muscle was cryosectioned and 10 µm sections were placed on surgipath microscope slides. Tissue sections were fixed with ice-cold 95% ethanol for 2 minutes followed by 70% ethanol for 2 minutes and then re-hydrated in running water for 5 minutes. Gill's hematoxylin (Fisher Scientific, Fair Lawn, NJ) was then used to stain the sections and rinsed in water for 5 minutes. Scott's solution (0.024 M $NaHCO_3$, 0.17 M $MgSO_4$) was then applied for 3 minutes and rinsed in water for 5 minutes. Tissue cryosections were then immersed in eosin solution (Sigma-Aldrich, St. Louis, MO) for 2 minutes. Sections were then dehydrated in ice cold 70% and 95% ethanol for 30 seconds each, followed by 100% ethanol for 2 minutes. Xylene was then used to clear the sections for 5 minutes prior to mounting with DepeX mounting medium (Electron Microscopy Services, Washington, PA). Centrally located Nuclei were counted from images composing representative montages for each mouse. Images were assessed at 200 X magnification by bright field microscopy. The number of centrally located nuclei per muscle fiber was determined by counting each image which contributed to myofibers being counted per treatment group. At least 4 animals from each treatment group were analyzed.

Sirius Red Staining

TA muscle sections were stained with Sirius Red to measure fibrosis in the skeletal muscle tissue. 10 µm cryosections on slides were fixed in 100% ethanol and then hydrated through an alcohol series (95 and 80% ethanol) and rinsed in tap water. The sections were stained with Sirius Red (0.1% in saturated aqueous picric acid solution, Rowley Biochemical Institute, Danvers, MA, USA) for 30 min followed by two washes in acidified water. The sections were dehydrated through an alcohol series, rinsed in xylene and mounted with DEPEX Mounting media (Electron Microscopy Science, Hat- field, PA, USA). Representative montages were captured and analyzed using Axiovision 4.8 software. Montages were assembled using Photoshop and Microsoft Powerpoint. Images were captured at 200 X magnification. Areas of red in the TA were considered fibrotic. Circled fibrotic areas were added together, and any non-fibrotic fibers within the fibrotic area were subtracted from the calculated area. The percentage of muscle fibrosis was quantified in treated and control muscles as a percentage of total TA muscle area. Sirius red slides were also used to measure minimal feret's diameter for mice of all 4 genotypic groups. All muscle fibers within an entire TA montage were used to determine the minimal feret's diameter.

Statistical Analysis

All averaged data are reported as the mean ± s.d. *P*-values of < 0.05 were considered to be statistically significant. GraphPad Prism Software was used to analyze and test the data.

RESULTS

Evan's Blue dye uptake within 1 year old *mdx* mice

Visibly, it is quite clear that PBS treated *mdx* mice had a higher retention of Evans blue dye within the body in Figure 16. Also, it is evident that there is Evan's blue uptake in the TA muscle in PBS treated *mdx* mice (indicated with the blue arrow in Figure 16). These results triggered the histological analysis of the TA muscle for Evan's Blue dye uptake in Figure 17.

Evan's Blue Dye Montages for 1 year old *mdx* mice

As predicted, Tibialis Anterior muscle from PBS treated *mdx* mice had a higher retention of Evan's blue dye within the muscle (Figure 17). The representative montages indicated that there was much clustering of Evan's blue dye positive myofibers to two areas of the PBS treated TA muscle. This was a drastic comparison to the more stochastic and punctate presence of Evan's blue dye positive myofibers in the TA of Laminin-111 treated *mdx* mice. This result was then verified via statistical analysis which categorically showed that this result was statistically significant. This indicated with enhanced EBD uptake that

there was indeed more damage occurring within the muscle of PBS treated animals over the course of the 1 year time frame.

Kyphosis Analysis of 1 year old *mdx* mice

The Kyphotic index calculations were carried out following a technique previously described by Hoey *et al.* 1985. Radiographs were assessed (Figure 18) in a blinded manner and visibly there is no evidence of an increase in severity of kyphosis occurring in PBS treated *mdx* mice compared to mLAM-111 treated animals. This was later quantified and indeed there was no statistical significance between wild-type, PBS treated and the laminin-111 treated mice.

Echocardiography of 1 year old *mdx* mice

Using the Vevo2100 system and Vevo 2100 software 1.4.0 we analyzed the cardiac muscle of all three treatment groups (Figure 19). Between all the 1 year old mice, there were no enhanced cardiac problems with or without treatment with laminin-111. All representative M-mode screenshots presented here, help to convey this result. There was no statistical significance with data analysis for these echocardiography results (shown in Table 2).

Respiratory function within 1 year old *mdx* mice

Plethysmography data indicates also within the 1 year old mice that there was no statistically significant difference between the three treatment groups either for Frequency of breathing, PenH or TVb which are the three main parameters to scrutinize in plethysmography data (Figure 20).

Histology of 1 year old *mdx* Tibialis Anterior muscle

TA muscle was embedded in OCT and cryosectioned for pathological assessment via Hematoxylin and Eosin (H&E) staining (Figure 21). This stain was used to quantify the number of centrally located nuclei (CLN) which is a marker for degeneration and regeneration. As expected WT data possessed very low numbers of CLN in comparison to mdx mice. Despite laminin-111 treatment for 1 year there was no difference between the number of CLN detected and the number of CLN detected in the PBS treated *mdx* muscle.

Fibrotic tissue in Tibialis Anterior muscle of 1 year old *mdx* mice

The pircrosirius red slides were used to quantify myofiber size and general pathology of LAM-111 treated versus PBS treated control tissue (Figure 22). There was no statistical significance in the quantification of minimal feret's diameter or indeed percentage fibrosis after 1 year treatment.

Activity and Function in 1 year old *mdx* mice

As above, activity box data reflected the results that indicated there was no statistically significant difference in functional activity of PBS or laminin-111 treated *mdx* mice over a 120 minute time period (Figure 23).

Myofiber sizes of Tibialis Anterior muscle in 7 weeks old and 10 weeks old *mdx* mice

Within 7 week old *mdx* TA treated with laminin-111 there was a visible increase in myofiber size whenever Minimal Feret's diameter was measured compared to WT and PBS treated animals (Figure 24). There was statistical significance within 10 week old TA muscle assessed for Minimal feret's diameter. The results indicated that laminin-111 treatment was successful in reducing the size of the myofibers. This result is promising as myofiber hypertrophy is indicative of DMD disease pathology.

Laminin-111 detection in *mdx* TA muscle after intraperitoneal treatment

Upon systemic laminin-111 treatment, laminin-111 was clearly able to travel to the target muscles as laminin-α1 was detected via immunofluorescence in Tibialis Anterior muscle (Figure 25).

Muscle strength was assessed for 10 week old *mdx* mice

In Figure 26, 10 week old grip strength assessment (Figure 26 A) indicated that there was no difference in forelimb muscle strength between PBS and laminin-111 treated *mdx* mice. Despite this result in 10 week old mice, there was reduced percentage forelimb muscle fatigue evident in laminin-111 treated mice (Figure 26 B). The percentage of Centrally located nuclei showed a statistically significant elevation in CLN within PBS treated animals. This elevation in CLN is, as mentioned previously mentioned, indicative of degeneration.

Sarcolemmal proteins after laminin treatment in 10 week old *mdx* mice

Likewise for 10 week old *mdx*, there was no difference in α7A or α7B integrin protein levels after immunoblotting upon laminin-111 treatment (Figure 27). However, there is a trend towards WT within immunofluorescent assessment of β-dystroglycan protein levels in 10 week old animals treated with laminin-111.

DISCUSSION

This study was performed in order to test how effective laminin-111 protein therapy would be as a long-term therapeutic after observing how effective this treatment had been within younger *mdx* mice[162]. There was no improvement in functional activity (Figure 23) of 1 year old treated *mdx* mice and there was absolutely no improvement in the muscle histology (Figure 21 and Figure 22). There was however reduced muscle damage indicated by a lower amount of Evan's Blue Dye uptake (Figure 17). It is important to keep in mind that these older *mdx* mice may have been very inert because of their age and size[168] (> 30 g).

It is important to keep in mind that the long-term treatment regime consisted of only one injection per fortnight so therefore laminin-111 protein could have been degraded within a short amount of time post-injection and therefore the mouse is still subject to muscle damage before the next injection is due. Repetitive treatment over a period of 1 year was expected to have a positive effect but the data was disappointing and may be explained by receptor desensitization[169–171] and tolerance[171] to the protein. Despite the presence of laminin-111 in the kidney, an immune response[172] may have been mounted to

this protein being injected repeatedly over a long time period (1 year) and therefore made the beneficial effects caused by laminin-111 in younger *mdx* mice redundant in these older *mdx* mice.

Future directions will include assessing TA muscle via immunoblotting for any change in the abundance of sarcolemmal proteins that are related to the dystrophin-glycoprotein laminin-binding complex after treatment compared to PBS controls. These proteins will include the dystroglycans, sarcoglycans and sarcospan. Immunofluorescence will also be used on the same TA muscle in order to confirm the immunoblot results. There may be a better result in delivering laminin-111 in a cocktail recipe of additional therapeutic drugs in order to have a more improved effect as delivering laminin-111 protein as part of a long-term therapy was not effective.

ACKNOWLEDGEMENTS

I would like to thank Vivian Cruz, Annmarie Vogedes and Connie Spelius for their technical assistance regards tissue collection and histological analysis. A special thanks for the immublotting results provided by Apurva Sarathy. I would also like to thank Rebecca Evans for animal breeding and Lab Animal Medicine for their continued monitoring of the mice especially for this 1 year study. Special thanks go to both Walt Mandeville and Rebecca Evans for collecting the radiography data.

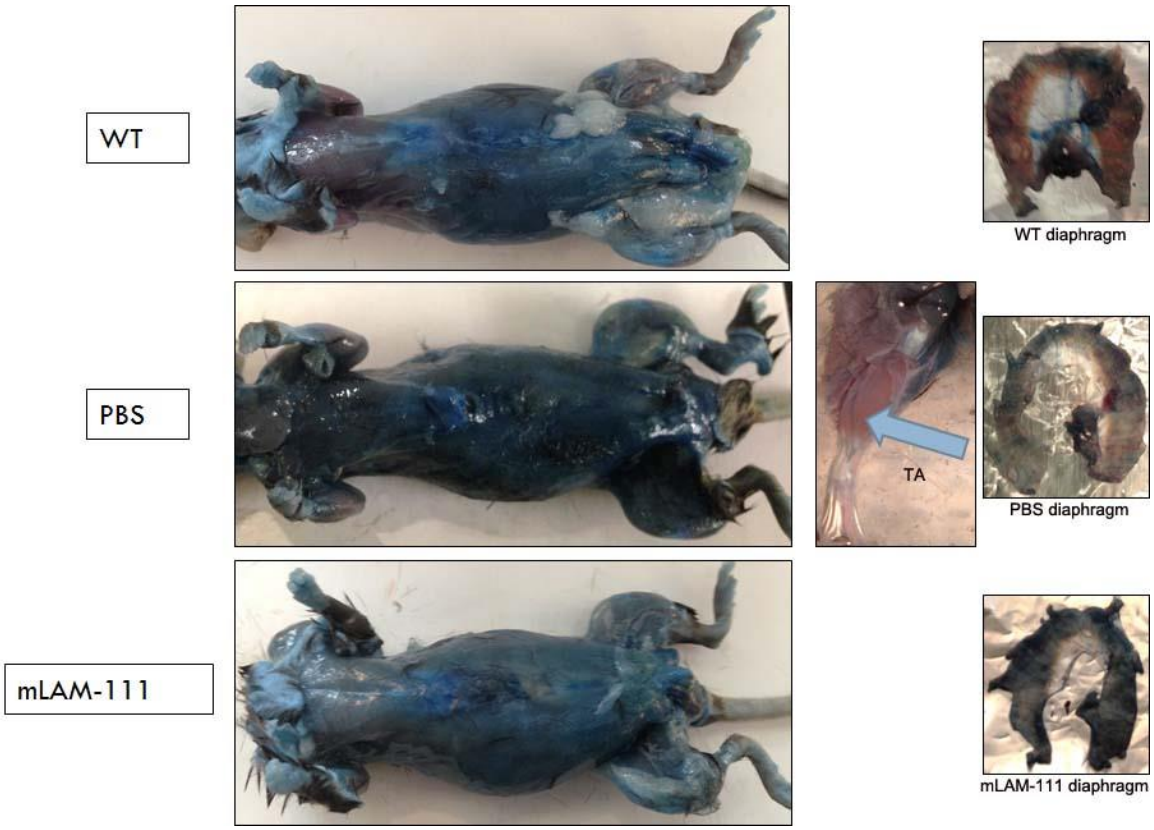

Figure 16. Evan's Blue dye uptake within 1 year old *mdx* mice

Evan's blue dye (EBD) is used as a marker for muscle damage. This blue dye is able to enter the ruptured myofiber and bind to albumin therefore resulting in red fluorescence which is then used as a marker for muscle damage. TA and diaphragm tissue uptake are also presented. PBS treated animals had distinctly increased EBD uptake within TA muscle (arrow) and less uptake within diaphragm muscle suggesting that there was more damage occurring in TA muscle. It is not clear why laminin-111 treatment caused more EBD uptake within diaphragm muscle.

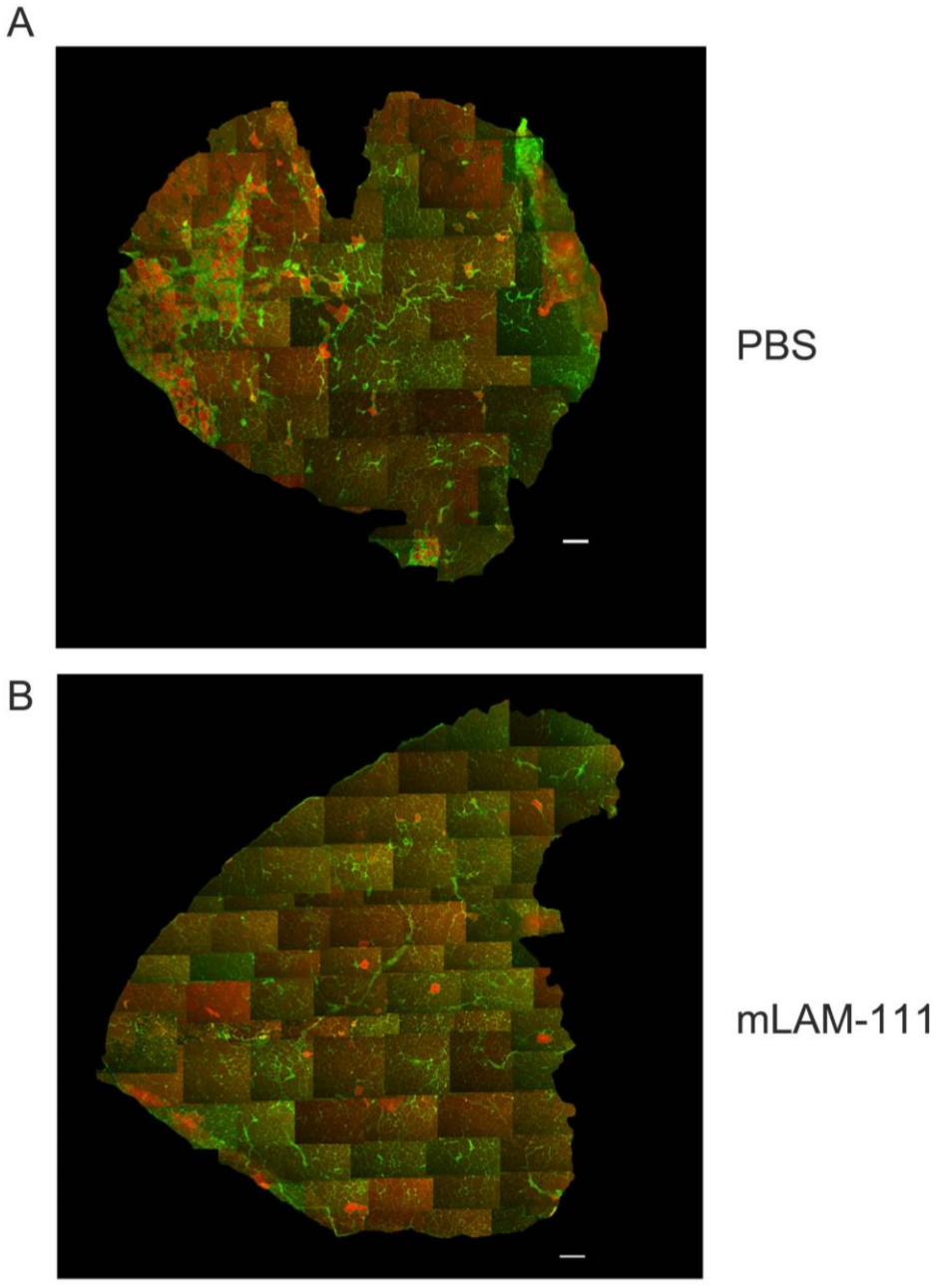

Figure 17. Evan's Blue Dye Montages for 1 year old *mdx* mice

A) and B) Representative montages for Evan's Blue Dye (EBD) uptake. PBS (n= 2) and mLAM-111 (n= 2). Images were captured at 200 X magnification. Scale

bar = 200 μm. There is increased EBD uptake in PBS treated muscle due to elevated red fluorescence indicating more muscle damage. Notice how most of the damage is occurring in one area of the muscle. However with laminin-111 treatment there was reduced EBD uptake indicated by reduced red fluorescence therefore showing that the sarcolemma was restored, preventing rupture and muscle damage after laminin-111 treatment.

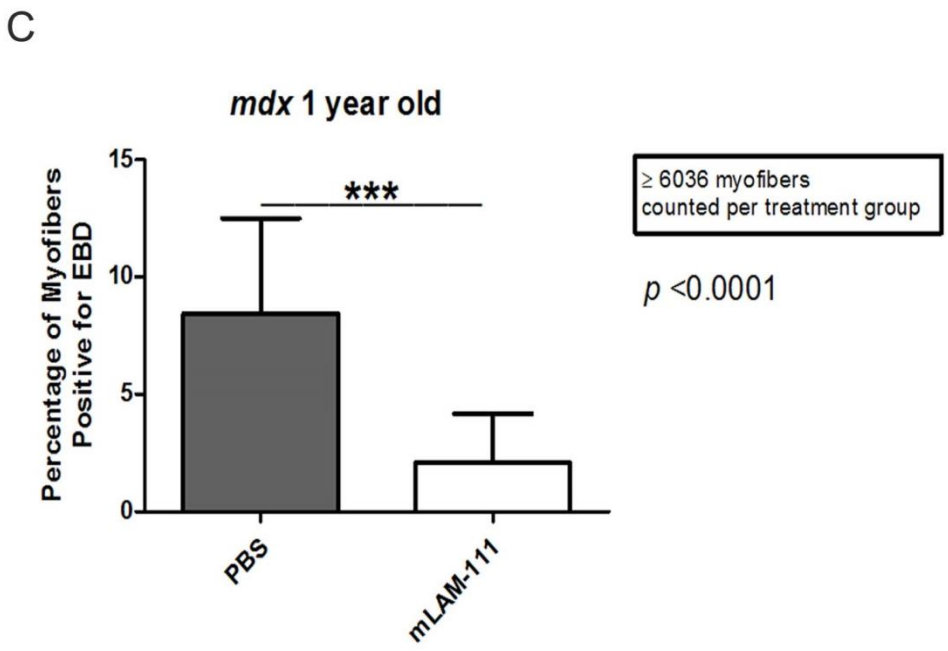

Figure 17. Evan's Blue Dye Montages for 1 year old *mdx* mice

C) Quantification of EBD positive myofibers for TA montages shown in Figure 17 A and B. PBS (n= 2) and mLAM-111 (n= 2). Captured at 200 X magnification. Scale Bar = 200 µm. The PBS treatment group had 8.4 % EBD positive myofibers ± 0.05 % while the laminin-111 treated group had 2.08 % EBD positive myofibers ± 0.02 %. A student's *t*-test revealed the *P*-value < 0.0001.

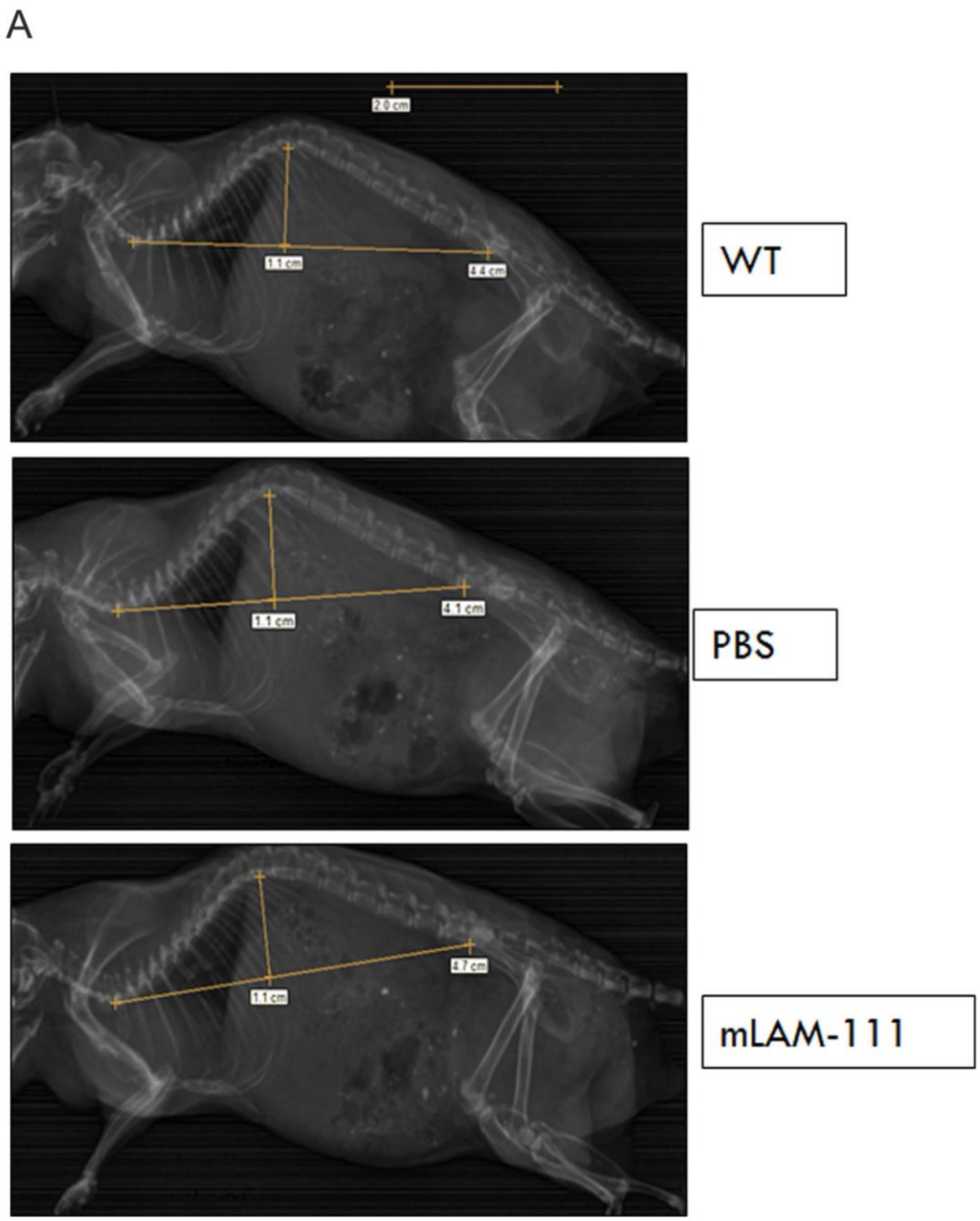

Figure 18. Kyphosis Analysis of 1 year old *mdx* mice

A) Representative radiographs for 1 year old *mdx* mice are depicted here. Kyphosis is used to describe the curvature of the spine. In muscular dystrophy there is degradation of muscles associated with the spine and therefore more

spinal curvature (kyphosis) occurs as the disease progresses. Visibly there is no difference in the degree of kyphosis regardless of treatment group.

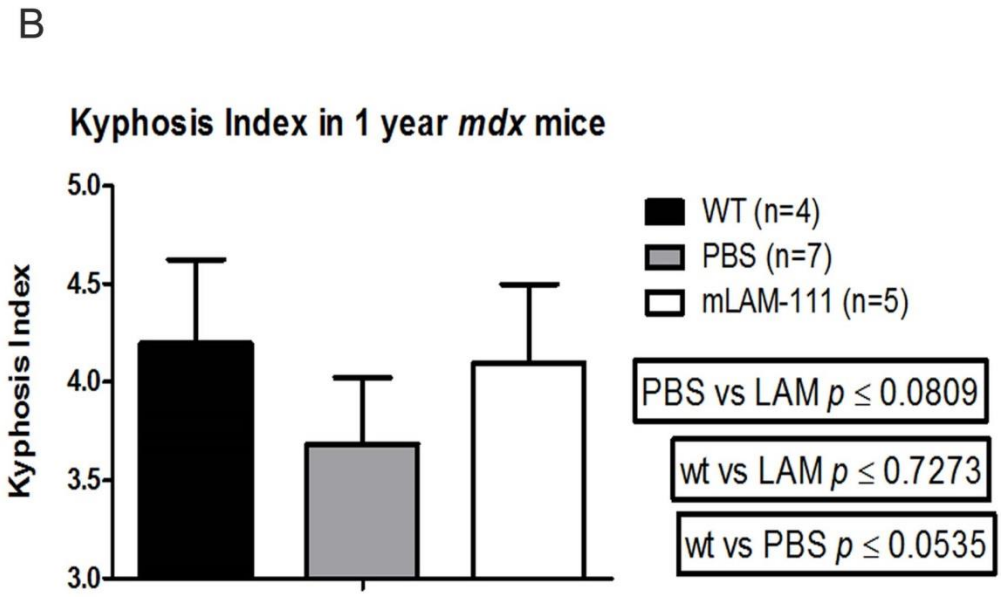

Figure 18. Kyphosis Analysis of 1 year old *mdx* mice

B) Quantification of radiographs shown in Figure 18 A, for 1 year old *mdx* mice. A lower kyphotic index indicates a higher degree of kyphosis present. In this way, WT animals had a higher kyphotic index therefore indicating less kyphosis occurring. A trend towards WT kyphotic index was evident within the EHS mLAM-111 treatment group. There was no statistical significance found when using One-Way *ANOVA*.

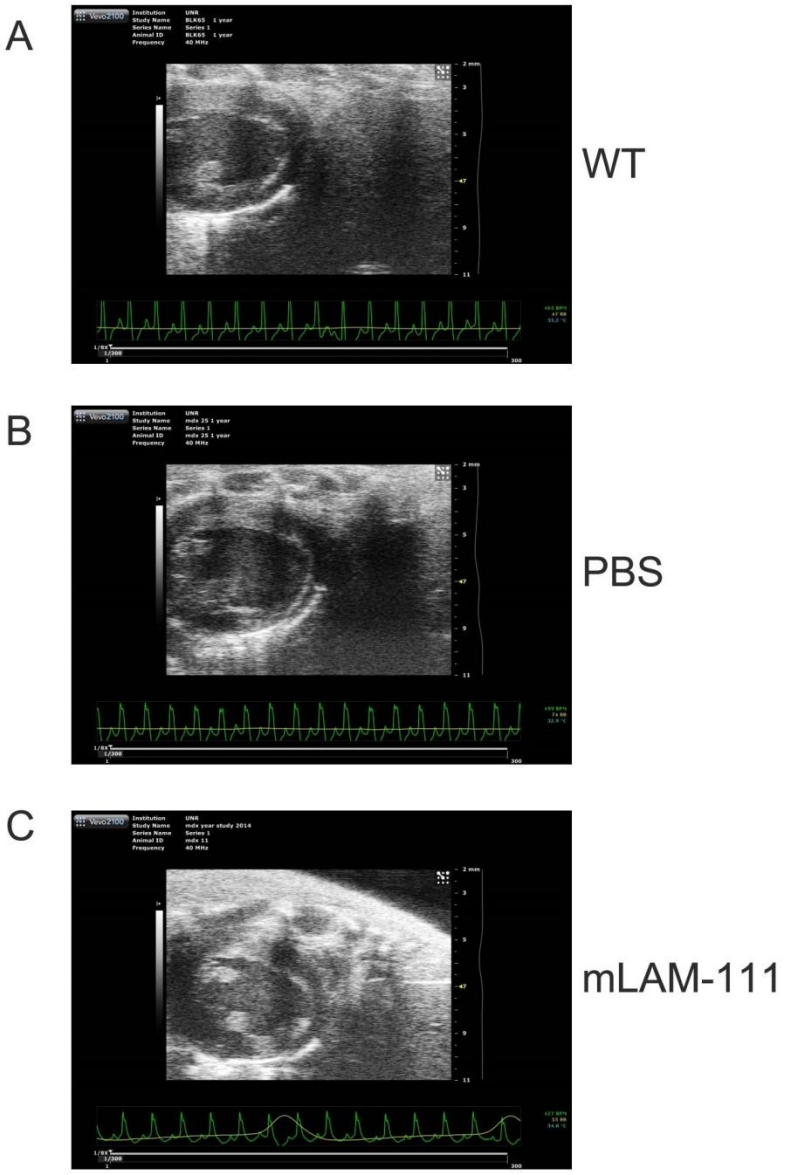

Figure 19. Echocardiography of 1 year old *mdx* mice.

A), B) & C) Representative B-mode screenshots are presented here providing a view into cardiac muscle as short-axis echoes. Papillary muscles were used as landmarks for consistency in data collection. Visibly there was no distinct

difference between the treatment groups suggesting that long-term laminin-111 treatment had no effect possibly due to receptor desensitization.

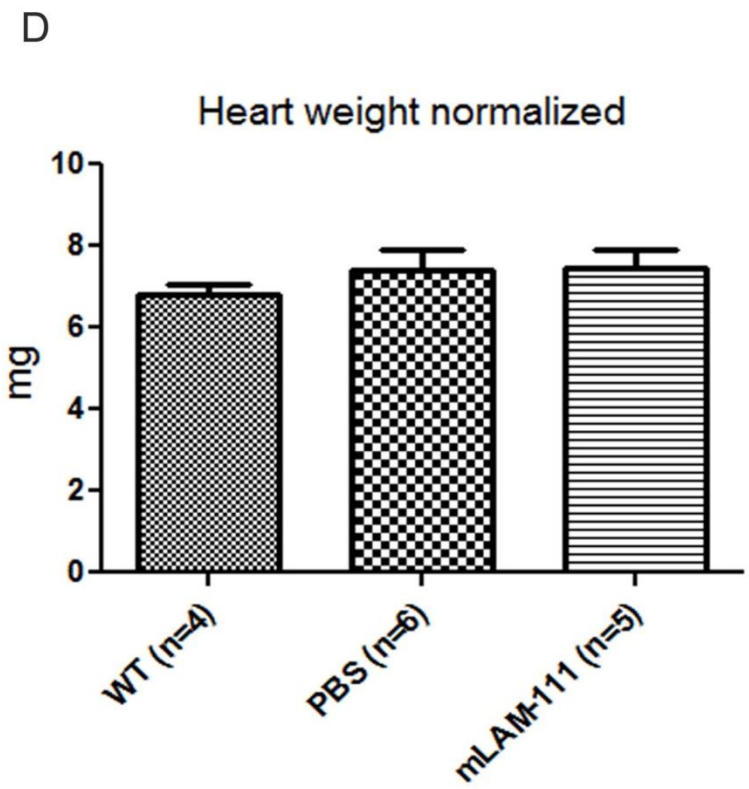

Figure 19. Echocardiography of 1 year old *mdx* mice.

D) There was no distinct difference in heart weights normalized to body weight between the treatment groups only that there was hypertrophy within cardiac muscle for *mdx* mice (PBS and mLAM-111 treatment groups).

LAM treated Compared to PBS treated	LAM/PBS	%	
			mLAM-111 treatment caused……
LVAW;d	92.30958321	%	7.7% reduction in anterior wall width during diastole
LVAW;s	94.40472446		5.6% reduction in anterior wall width during systole
LVID;d	108.2903556		8.3% increase in internal diameter during diastole
LVID;s	107.0836172		7.1% increase in internal diameter during systole
LVPW;d	72.99072708		27.1% reduction in posterior wall width during diastole
LVPW;s	83.7046185		16.3% reduction in posterior wall width during systole
EF	100.5813363	%	0.6% increase in ejection fraction
FS	101.6749811		1.7% increase fractional shortening
LV Mass AW	79.67024598		20.3% reduction anterior wall mass calculated for humans
LV Mass AW (Corrected)	79.670246		20.3% reduction anterior wall mass calculated for mice
LV Vol;d	119.6574189		19.7% increase in left ventricular volume during diastole
LV Vol;s	116.2184899		16.2% increase in left ventricular volume during systole
LAM Compared to WT	**LAM/WT**	**%**	**mLAM-111 treatment caused……**
LVAW;d	103.4533	%	3.5% increase in anterior wall width during diastole
LVAW;s	98.8507		1.1% reduction in anterior wall width during systole
LVID;d	102.3848		2.4% increase in internal diameter during diastole
LVID;s	115.5671		15.6% increase in internal diameter during systole
LVPW;d	86.59535		13.4% reduction in posterior wall width during diastole
LVPW;s	85.03325		15% reduction in posterior wall width during systole
EF	87.2611	%	12.7% reduction in ejection fraction
FS	80.64866		19.3% reduction fractional shortening
LV Mass AW	94.44645		5.6% reduction anterior wall mass calculated for humans
LV Mass AW (Corrected)	94.44645		5.6% reduction anterior wall mass calculated for mice
LV Vol;d	104.6885		4.7% increase in left ventricular volume during diastole
LV Vol;s	133.8077		33.8% increase in left ventricular volume during systole

PBS Compared to WT	PBS/WT		
LVAW;d	112.0720825	%	12.1% increase in anterior wall width during diastole
LVAW;s	104.7094843		4.7% increase in anterior wall width during systole
LVID;d	94.54651261		5.5% reduction in internal diameter during diastole
LVID;s	107.9222646		7.9% increase in internal diameter during systole
LVPW;d	118.6388411		18.6% reduction in posterior wall width during diastole
LVPW;s	101.5872861		1.6% reduction in posterior wall width during systole
EF	86.75674687		0.6% increase in ejection fraction
FS	79.32006445		1.7% increase fractional shortening
LV Mass AW	118.5467094		20.3% reduction anterior wall mass calculated for humans
LV Mass AW (Corrected)	118.5467092		20.3% reduction anterior wall mass calculated for mice
LV Vol;d	87.4902056		19.7% increase in left ventricular volume during diastole
LV Vol;s	115.1346455		16.2% increase in left ventricular volume during systole

Table 2. M-mode measurements of 1 year *mdx* echocardiography

Calculations are presented here in a tabular format for echocardiography M-mode measurements for 1 year old *mdx* mice. Most notably there was a 19.7 % increase in ventricular volume during diastole and a 16.2 % increase in ventricular volume during systole after laminin-111 treatment. Despite this there was not a change in Ejection Fraction or Fractional shortening showing that the effective pumping of the heart was not improved with laminin-111 treatment.

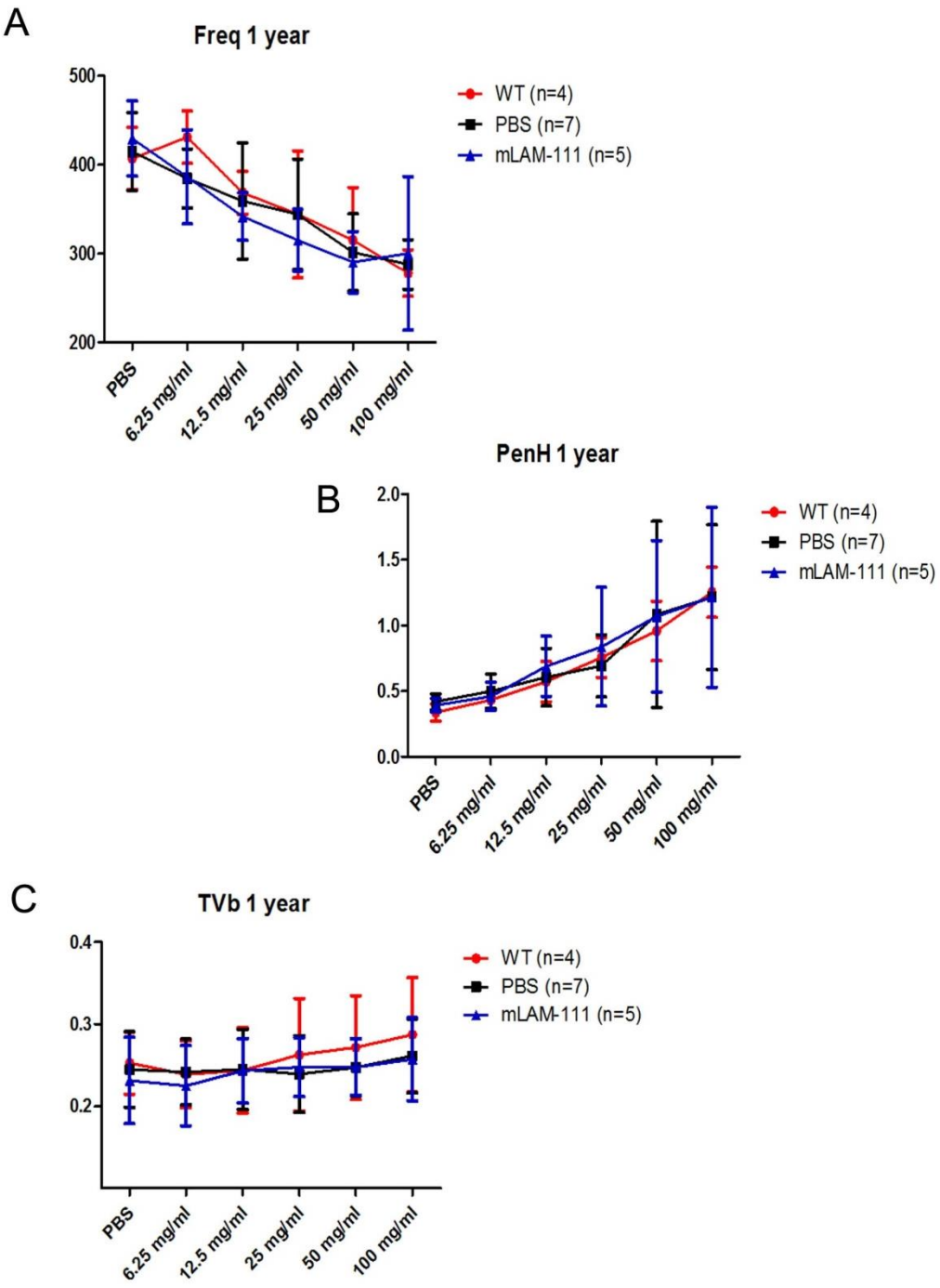

Figure 20. Respiratory function within 1 year old *mdx* mice

Plethysmography data was collected and analyzed. There was no difference between any of the treatment groups for respiratory function parameters which

included Frequency of breathing (Figure 20 A), PenH (Figure 20 B) and tidal volume (TVb) (Figure 20 C). PenH (enhanced pause) is correlated to but not a direct measurement of airway resistance. This suggests that whole body plethysmography analysis of 1 year old mice may not have been the best way to analyze the respiratory function of these larger animals.

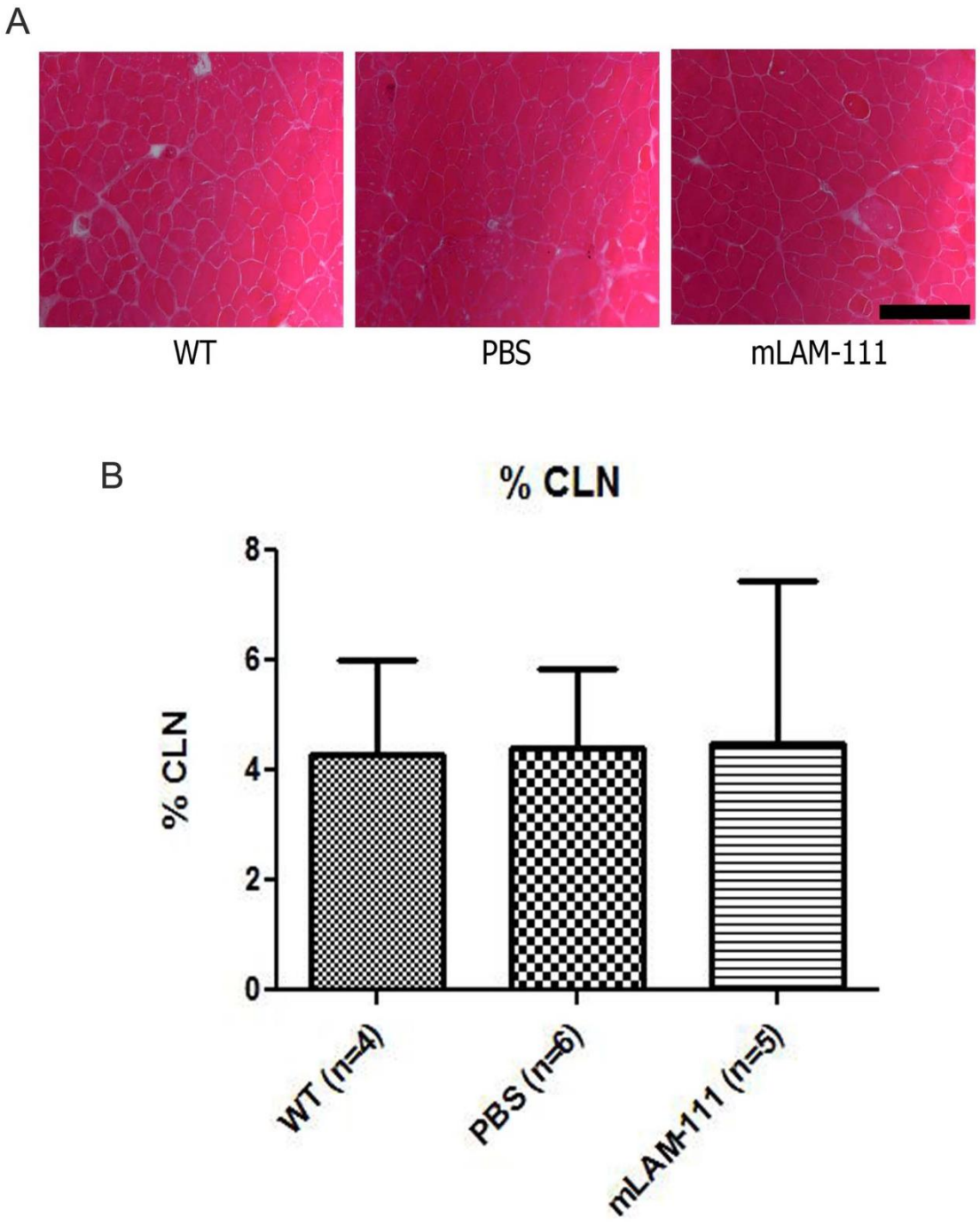

Figure 21. Histology of 1 year old *mdx* Tibialis Anterior muscle

A) Hematoxylin and Eosin staining was carried out on 10 µm TA cryosections and images were captured at a magnification of 200 X. Scale bar = 200 µm. B)

Centrally located nuclei are used as a marker of degeneration and regeneration in muscle. Percentage (%) of Centrally Located nuclei (CLN) were calculated for each treatment group. WT had 4.3 % CLN ± 1.7 %, PBS had 4.4 % CLN ± 1.4 % and mLAM-111 treated animals had 4.49 % CLN ± 2.96 %. One-Way *ANOVA* demonstrated that there was no statistical difference amongst the treatment groups with *P*-value = 0.9915. It is important to remember that within mouse muscle once damage occurs, nuclei will become centrally located and will remain their throughout the lifetime of the animal. Therefore this may help to answer why there was no difference in the percentage of CLN for the treatment groups due to the 1 year old mice enduring more damage throughout their lifetime as they are older mice. Also the treatment regime was only one injection per fortnight so therefore laminin-111 protein could have been degraded within a short amount of time post-injection and therefore the mouse is still subject to muscle damage before the next injection is due.

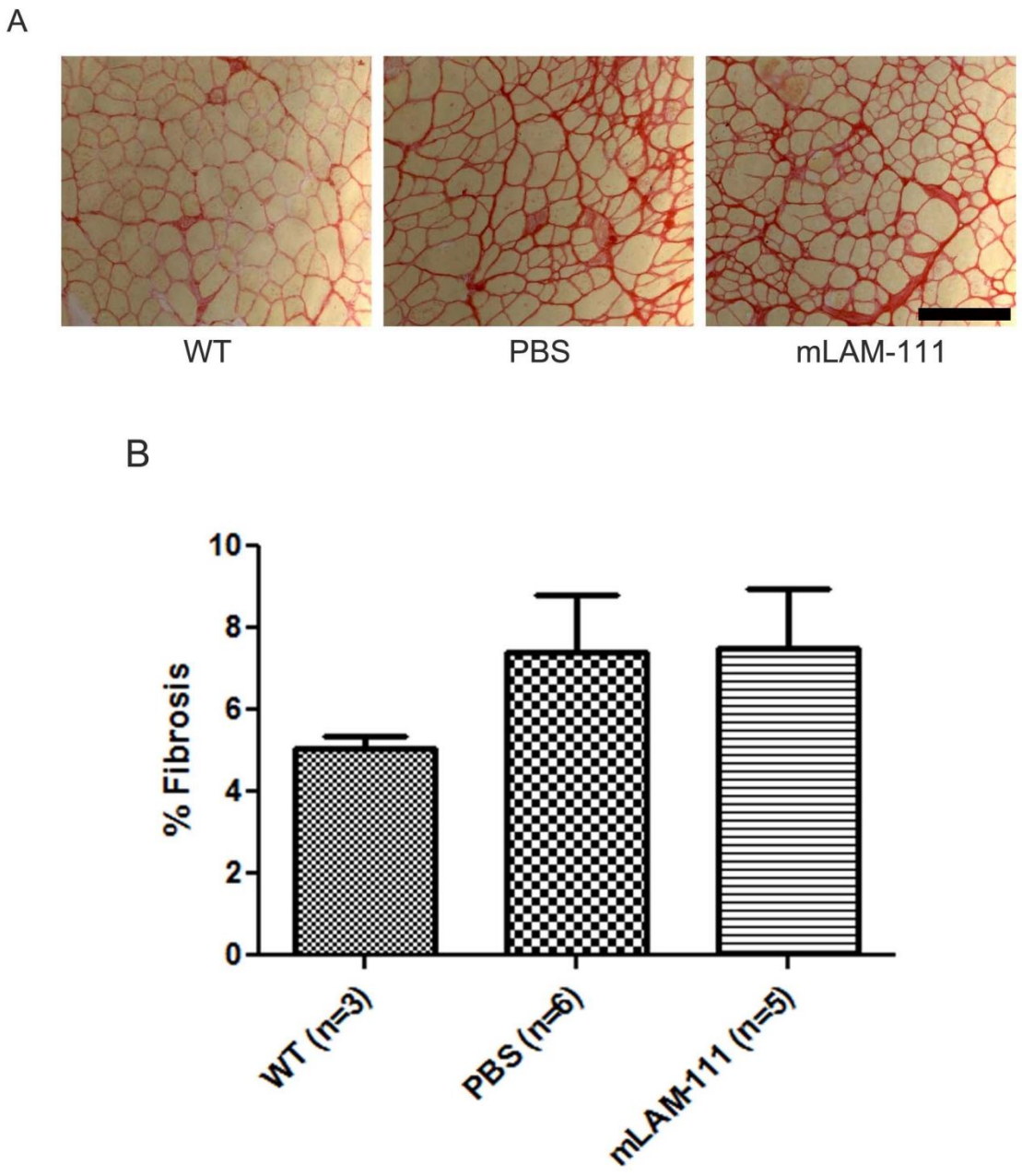

Figure 22. Fibrotic tissue in Tibialis Anterior muscle of 1 year old *mdx* mice

A) Representative TA montages stained with Sirius red presented for 1 year old *mdx* mice. Magnification = 100 X. Scale bar = 200 µm. Increased red color indicates that there is more fibrotic tissue present. B) Sirius red staining was

carried out in order to calculate the percentage (%) of fibrotic tissue within TA cryosections shown in Figure 22 A. One-Way *ANOVA* revealed no statistical significance with *P*-value = 0.4979.

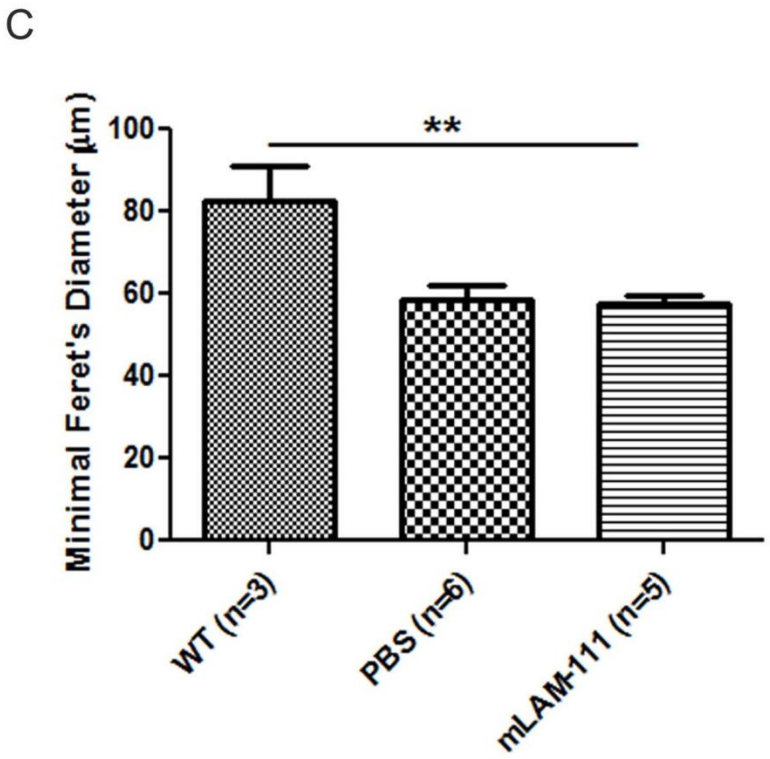

Figure 22. Fibrotic tissue in Tibialis Anterior muscle of 1 year old *mdx* mice

C) Minimal Feret's diameter was also calculated for the same 1 year old muscle groups shown in Figure 22 A. Minimal ferret's diameter is used to measure the size of myofibers. Statistical significance was recorded when *P*-values were < 0.05. One-Way *ANOVA* revealed statistical significance for comparison of the 3 treatment groups but there was no statistical significance found between PBS and laminin-111 treatment. This lack of significance shows that laminin-111 treatment had no effect on myofiber size.

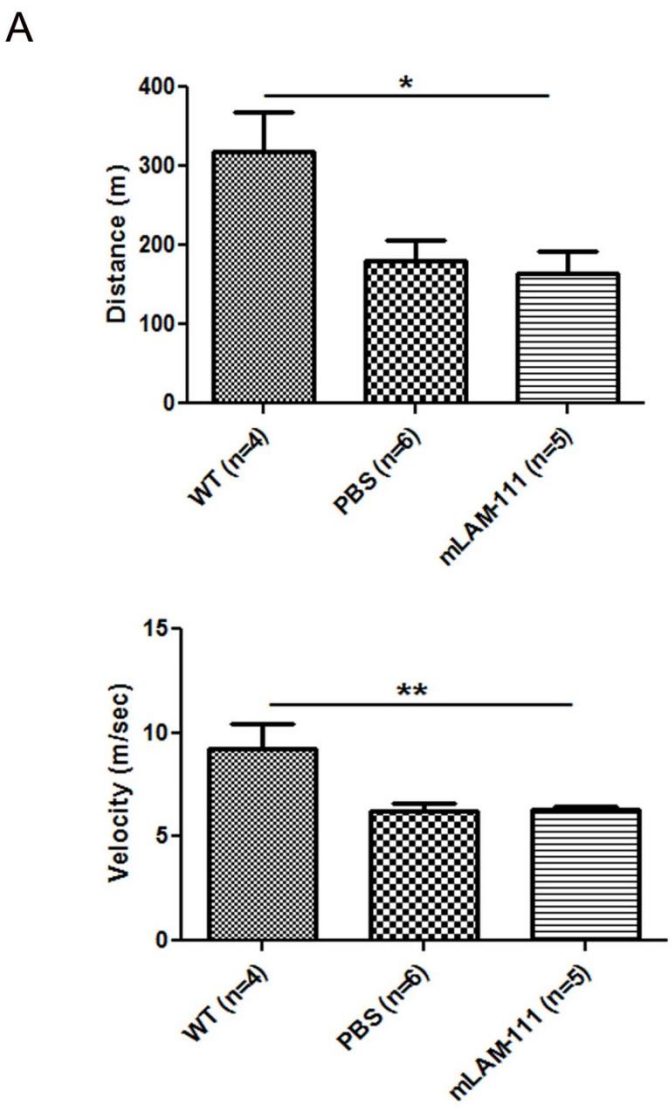

Figure 23. Activity and Function in 1 year old *mdx* mice

A) 1 year old mice were placed individually into the activity box and assessed for movability during a period of 120 minutes. Distance (m) and Velocity (m/sec) parameters were recorded. WT moved 317.6 m ± 99.9 m, PBS moved 180.7 m ± 64.6 m, mLAM-111 moved 163.7 m ± 62.8 m. Speed with which the mice moved

were for WT 9.23 m/sec ± 2.3 m/sec, PBS 6.2 m/sec ± 0.8 m/sec and mLAM-111 6.3 m/sec ± 0.3 m/sec. One-Way *ANOVA* showed statistical significance when comparing all 3 treatment groups. Statistical significance was evident when *P*-values were < 0.05. However there was no difference between PBS and laminin-111 treated animals for either distance moved or velocity.

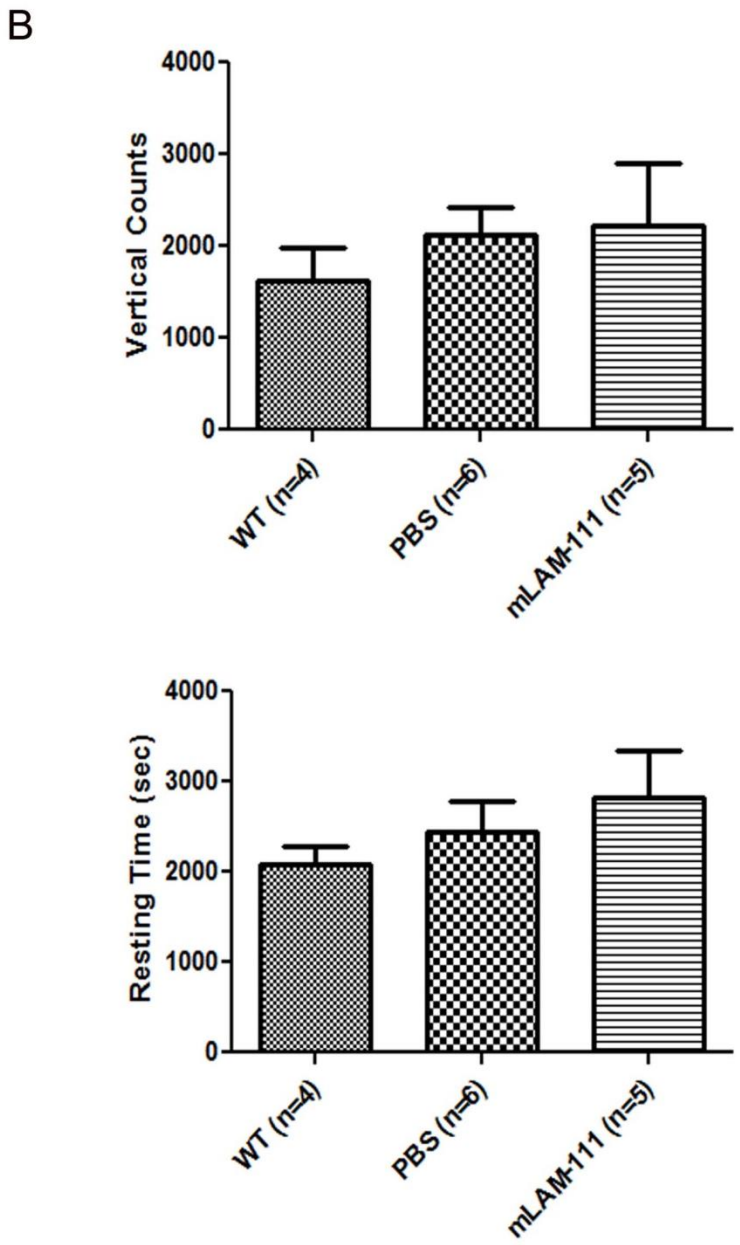

Figure 23. Activity and Function in 1 year old *mdx* mice

B) Mice were placed individually into the activity box and assessed for a period of 120 minutes. Resting time (sec) and vertical counts were recorded. One-Way

ANOVA showed no statistical significance when comparing all 3 treatment groups. Statistical significance was evident when *P* values were < 0.05.

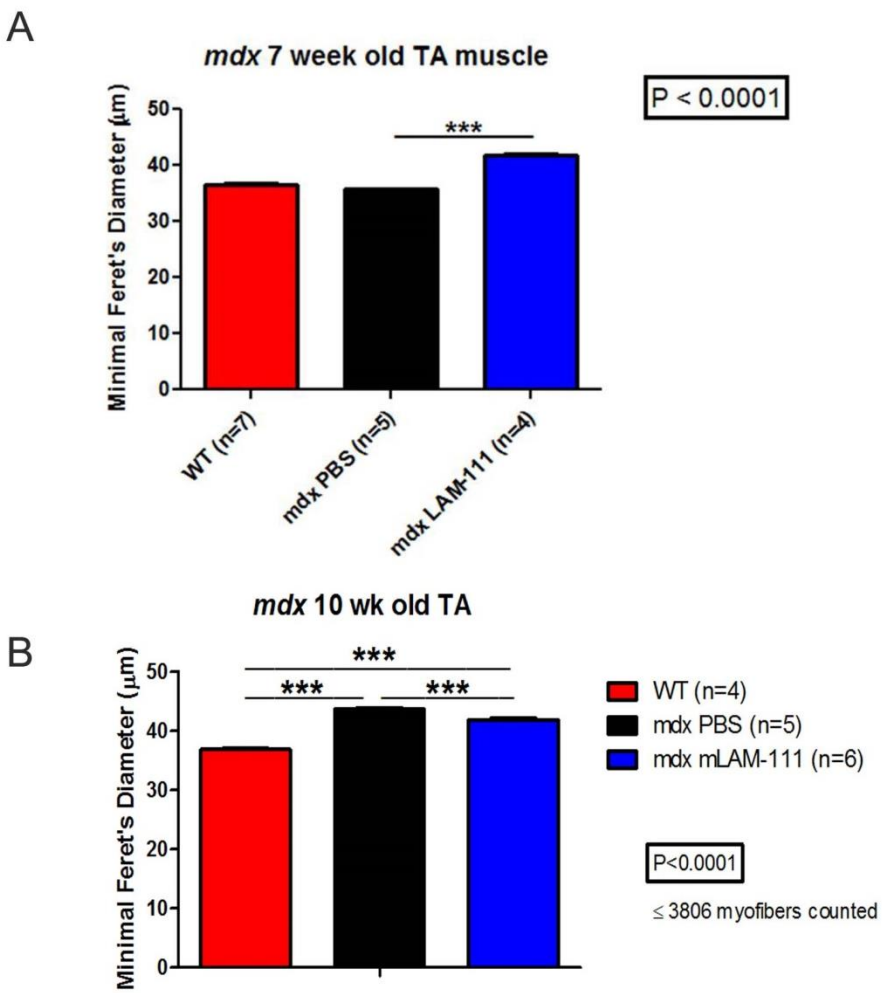

Figure 24. Myofiber sizes of Tibialis Anterior muscle in 7 weeks old and 10 weeks old *mdx* mice

Measurements for Minimal Feret's diameter were carried out on younger mice that were 7 weeks old and 10 weeks old. 7 weeks old PBS treated animals had an average myofiber diameter of 35.72 µm ± 0.1783 µm, and mLAM-111 treated animals had an average myofiber diameter of 41.88 µm ± 0.23 µm. A student's *t*-test revealed *P*-value < 0.0001. 10 week old PBS treated animals had an average myofiber diameter of 43.65 µm ± 0.2 µm and mLAM-111 treated

animals had an average myofiber diameter of 41.88 µm ± 0.20 µm. Statistical significance was when *P* values were < 0.05. One-Way *ANOVA* showed statistical analysis with *P*-value < 0.0001. There was an increase in myofiber size for 7 week old laminin-111 treated animals and a decrease in myofiber size for 10 week old laminin-111 treated animals.

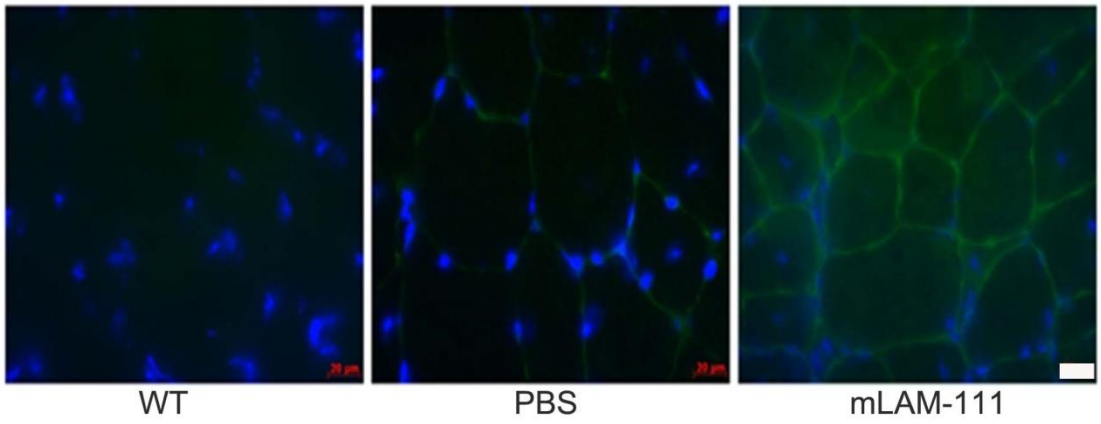

Figure 25. Laminin-111 detection in *mdx* TA muscle after intraperitoneal treatment

Immunofluorescence revealed that laminin-111 protein was able to be detected in *mdx* TA muscle after intraperitoneal injection. Scale bar = 20 µm. Magnification = 630 X. Laminin-111 is represented by green and nuclear label (DAPI) is represented by blue. WT and mutant muscle do not possess laminin-111, it is only detected after treatment.

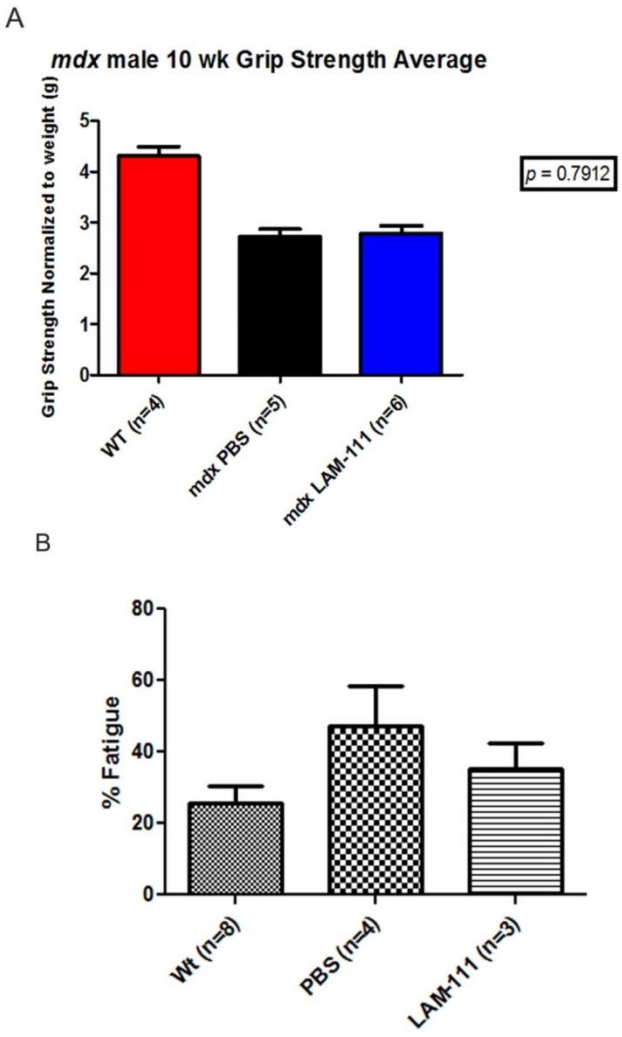

Figure 26. Muscle strength and histology was assessed for 10 week old *mdx* mice

A) Grip strength measurements for forelimb muscle strength were calculated and normalized to body weight. There was no statistical significance between the treatment groups after a *t*-test was performed the *P*-value = 0.7912. B) Percentage (%) fatigue was calculated based on grip strength shown in Figure 26 A. There was no statistical difference in forelimb muscle fatigue. Therefore laminin-111 treatment was not effective in increasing muscle strength.

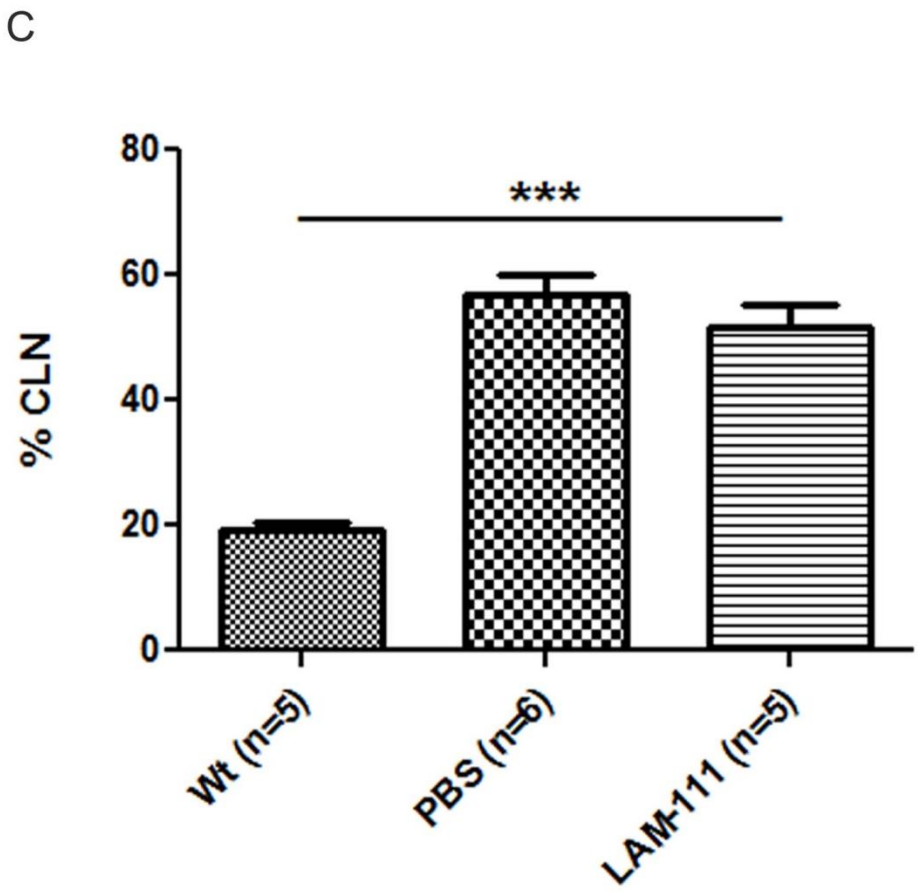

Figure 26. Muscle strength and histology was assessed for 10 week old *mdx* mice

C) Centrally located nuclei quantification is used as a marker for degeneration and regeneration. One-Way *ANOVA* statistical analysis of the 3 treatment groups showed *P*-value < 0.0001. Laminin-111 helped to prevent muscle damage as there was reduced percentage CLN when compared to PBS treated animals.

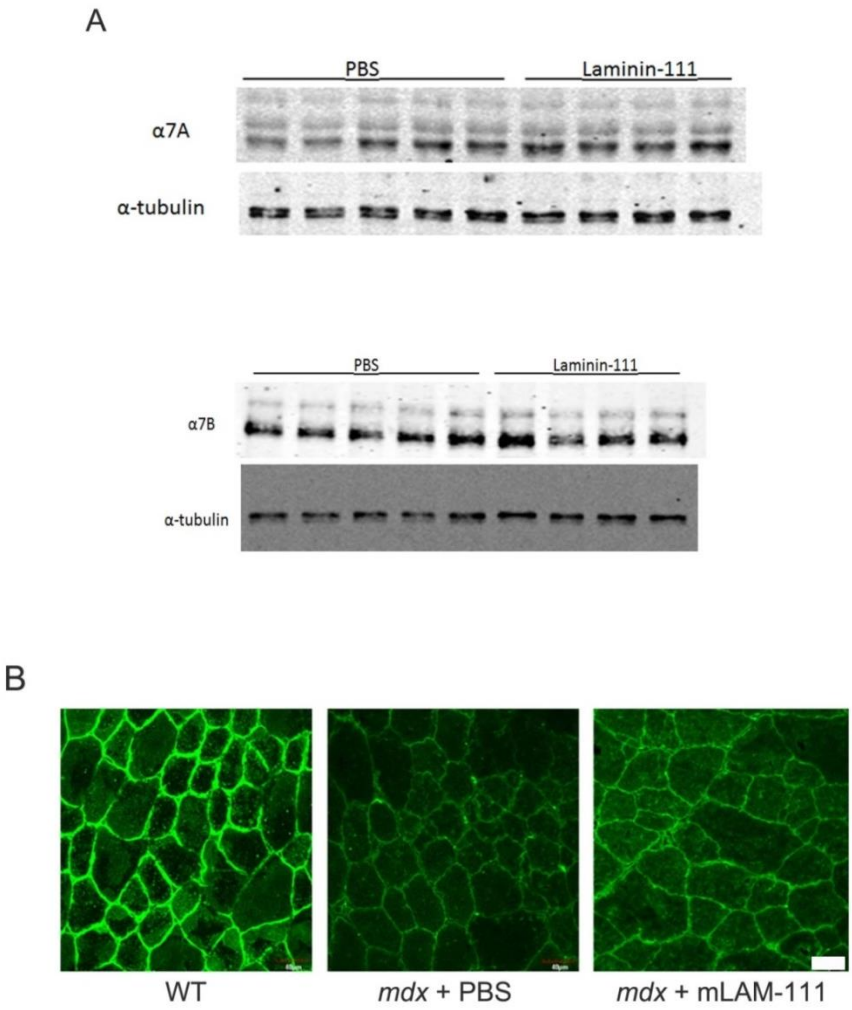

Figure 27. Sarcolemmal proteins after laminin treatment in 10 week old *mdx* mice

A) Immunoblotting shows that there is no effect on levels of α7 integrin protein after laminin-111 treatment for a two week treatment regime. B) However there is a distinct increase in β-Dystroglycan protein upon laminin treatment compared to PBS treatment visualized via confocal microscopy and this is quantified in Figure 27 B. Magnification = 400 X. Scale bar = 40 µm. Figure 27A was kindly provided by Apurva Sarathy.

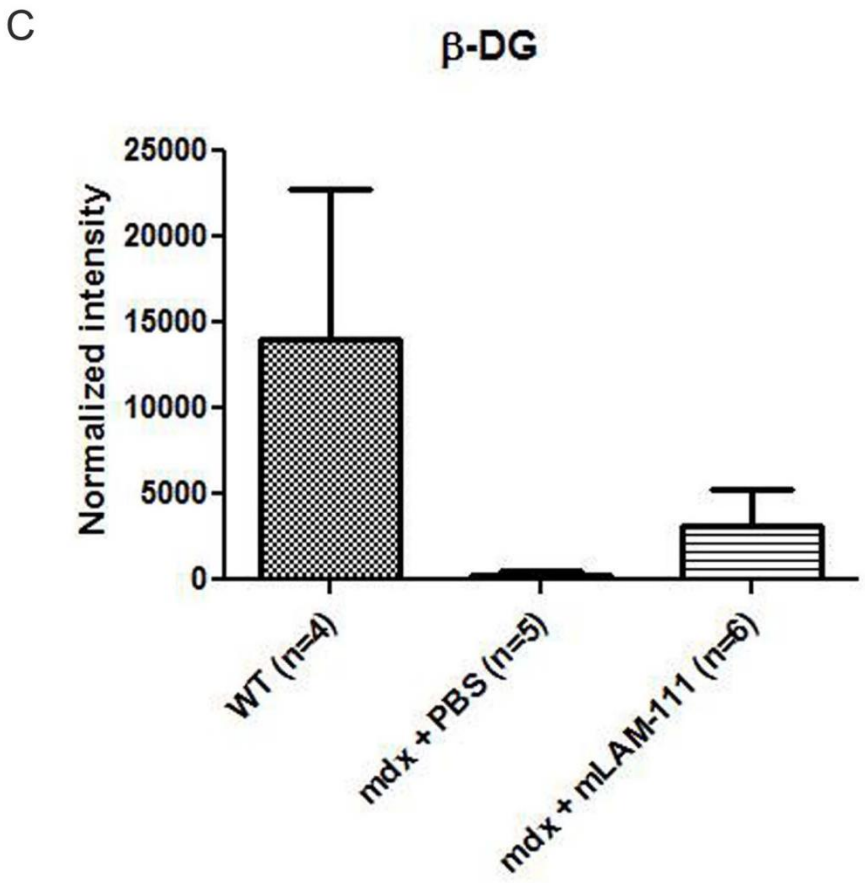

Figure 27. Sarcolemmal proteins after laminin treatment in 10 week old *mdx* mice

C) Quantification of β-DG protein levels measured from confocal images shown in Figure 27 B. Intensity was normalized by High Intensity/ Low intensity for individual images and averaged for each treatment group. PBS treatment had a normalized intensity of 274.5 ± 204.2 and laminin-111 treatment had a normalized intensity of 3128 ± 2121. Statistical *t*-testing revealed the *P*-value = 0.2561.

Chapter V

Loss of alpha7 integrin exacerbates skeletal and cardiac dysfunction in the *dy^{W}* mouse model of MDC1A

ABSTRACT

Merosin-deficient congenital muscular dystrophy type 1A (MDC1A) is caused by the loss of Laminin-211 and Laminin-221 heterotrimers which are most abundant in skeletal and cardiac muscle basal lamina; mutations in the LAMA2 gene cause the loss of these Laminin isoforms. This reduction of Laminin reduces the capacity for myofiber adhesion, loss of sarcolemmal integrity and subsequently affects the ability of the skeletal muscle syncytium to generate force in a coordinated and efficient manner. Patients experience progressive muscle wasting which confines them to a wheelchair at an early age and respiratory failure that leads to their untimely death. Currently, there is still no effective treatment or cure for this devastating disease. Recently, our lab has shown that transgenic overexpression of the α7 integrin reduces muscle pathology and improves viability in the laminin-α2 deficient mouse model of (MDC1A) [65]. However, what remains unclear is what role other significant sarcolemma related proteins play towards this rescue in MDC1A disease progression; complete ablation of both α7 integrin and laminin-α2 has never been characterized in the dy^W mouse model[173]. Thus, the overall hypothesis to be tested is that a loss of both α7 integrin and laminin-α2 will increase the overall degeneration of skeletal and cardiac muscle in this α7 integrin/ laminin-α2 double knockout (dko) mouse model[173].

INTRODUCTION

Merosin deficient congenital muscular dystrophy (MDC1A) affects approximately 0.89/100,000 individuals worldwide (1:100,000 - 1:500,000) and is thought to be the most common form of congenital muscular dystrophy affecting 30-40% of all diagnosed CMD cases[88]. Loss of merosin (Laminin-α2 protein) is caused by mutations occurring in the *LAMA2* gene which is located on chromosome 6q22-23 spanning ~260 kb with 64 exons [73,89-100]. This loss of Laminin-α2 protein in MDC1A results in the absence of Laminin-211 and Laminin-221 heterotrimers which are abundant in skeletal and cardiac muscle basal lamina. Patients, also experience demyelinating neuropathy, muscle atrophy, limited eye movement and also respiratory failure that leads to their untimely death which can be as early as the first decade of life [88,92–94]. There is an increased likelihood of seizures occurring after six months of age due to changes in white matter of the brain [97,101-102]. Symptoms depend on where the mutation occurs and a mutation which results in no laminin-α2 protein being produced will result in a more severe clinical phenotype compared to a mutation which produces a truncated form of laminin-α2. Currently, there is still no effective treatment or cure for this cruel disease [24,88].

The α7β1 integrin is a heterodimeric cell surface receptor member of the large family of integrins[60] (Figure 1). The α chain and β chain are noncovalently linked and integrins in general are evolutionarily conserved[55,61]. Integrins act as receptors for a variety of cellular components to include, leukocytes, RGD,

collagen and laminin[55]. The α7β1 integrin is prevalent within skeletal, cardiac and vascular smooth muscle. There are many splice variants of α7β1 integrin that exist. There are 3 intracellular (α7A, α7B and α7C) and 2 extracellular (X1 and X2) splice variants[28,62,63,64]. The β1 integrin possesses variants β1A and β1D, with β1D being the major isoform in mature skeletal muscle[51]. The α7β1 integrin complex is elevated in order to compensate for the instability of the dystrophin glycoprotein (DGC) laminin binding complex due to loss of dystrophin in Duchenne Muscular dystrophy (DMD)[50]. α7 integrin overexpression is able to rescue the severe dystrophic phenotype of *mdx/utr* $^{-/-}$ mice and improve the viability of these mice[51]. MDC1A patients have decreased α7β1 integrin expression[65]. This integrin is found localized at costameres, myotendinous junctions and neuromuscular junctions[59,60].

The absence of laminin-α2 in Merosin Deficient Congenital muscular dystrophy (MDC1A) has been well documented in the *dy^{W}* mouse model[124,133]. What remains unclear is the exact role of α7 integrin (laminin-α2 binding partner) and the biological effects caused by the absence of α7 integrin. Hence, we generated double knockout (dko) α7 -/-:: Laminin-α2 -/- mice and studied them alongside their littermate controls. Results from this study correlate with findings from a recent publication that suggests deletion of alpha7 integrin in laminin-α2 deficient *dy3k-/-* mice does not increase severity of the phenotype.

MATERIALS AND METHODS

Generation of α7 -/-:: Laminin-α2 -/- mice

All experiments involving mice were performed under an approved protocol from the University of Nevada, Reno Institutional Animal Care and Use Committee. *α7 +/-* mice (C57BL6-α7βgal strain) produced in the Nevada Transgenic Center were bred with Dy^{W} +/- (C57BL6 strain) mice. The dy^{W}+/- mice were a gift from Eva Engvall via Paul Martin (The Ohio State University, Columbus, OH, USA). The resulting F1 progeny generated from mating mice that were heterozygous at both the α7 locus and laminin- α2 locus were genotyped in order to detect α7 -/-:: Laminin-α2 -/- double knockouts. The wild-type control strain used in this study was C57BL6. Age-matched littermate controls were used for analysis.

In order to genotype mice, genomic DNA was isolated from tail snips or ear notches using a Wizard SV DNA purification system (Promega, Madison, WI) following manufacturers instructions. Mice were genotyped using multiplex PCR to detect the wild-type and targeted α7 integrin allele using the following primers: α7F10 (5'-TGAAGGAATGAGTGCACAGTGC-3'), α7exonR1 (5'-AGATGCCTGTGGGCAGAGTAC-3') and βgalR2 (5'-GACCTGCAGGCATGCAAG-3'). PCR conditions for α7 integrin were as follows: 94°C for 3 minutes, then 35 cycles of 94°C for 20 seconds, 62°C for 30 seconds, 72°C for 1 minute. After these cycles, then 72°C for 10 minutes. A wild-type band was 727 bp, whereas the α7 integrin targeted allele produced a 482 bp band. To genotype the α7 integrin gene, separate PCR reactions were performed since

there were two different reverse primers needed in wild-type and α7 integrin null mice.

To detect the mutation in the laminin- α2 gene, the following primers were used: DYWF (5'-ACTGCCCTTTCTCACCCACCCTT-3'), LAMA2exonR1 (5'-GTTGATGCGCTTGGGAC-3') and Lac/ZR2 (5'-GTCGACGACGACAGTATCGGCCTCAG-3'). PCR conditions were as follows: 95°C for 5 minutes then 33 cycles of 94°C for 20 seconds, 62°C for 30 seconds and 72°C for 45 seconds. After these cycles, then 72°C for 10 minutes. A wild-type band was 250 bp whereas the laminin- α2 targeted allele produced a 480 bp band.

Experimental procedures were performed once mice were 14 days of age with weekly weighing until the end of study which was at 10 weeks of age where all mice were subject to *in vivo* experiments. To reduce experimental bias, investigators assessing and quantifying experimental outcomes were blinded to the treatment and control groups.

Survival and weights

Weights for all mice of each genotype were recorded on a weekly basis. Softened kibble was provided fresh daily in a petri dish on the bottom of the cage in order to ensure there was no significant weight loss within the mice.

Muscle strength

Muscle strength assessed at 10 weeks of age using the Chatillon DFE Digital Force Gauge (San Diego Instruments Inc., San Diego, CA). A total of six measurements per mouse were recorded and all results averaged for each group. The mice were analyzed by grasping a horizontal platform with their forelimbs and pulled backwards. The peak tension (grams of force) was recorded on a digital force gauge as mice released their grip.

X-ray digital imaging

Radiographs were obtained for each mouse at the end of the 10 week study through the use of a Summit digital X-ray unit model 50-520, allowing radiographic measurement of kyphotic index. Calculations for Kyphotic Index were carried out as previously described by Hoey *et al*. 1985.

Activity

Opto-Varimex 4 Activity Meter (Columbus Instruments) offered unbiased data due to the machine possessing lasers that monitor and auto-track the activity of each mouse for a period of 30 minutes.

Plethysmography

Animals were subjected to plethysmography at 10 weeks of age. Animals for each genotype were used. Animals were placed in the plethysmography chamber (unrestrained) and then subjected to increasing does of aerosolized

Acetyl-methacholine (6.25, 12.5, 25, 50 and 100 mg/mL), after an initial time period to acclimatize in the chamber. First mice were exposed to aerosolized PBS to gather baseline data. Experimental values were automatically generated by the pneumograph in the wall of the chamber. FinePointe software (Buxco©) was used to collect all data.

Echocardiography

In vivo echocardiography was performed on mice using a VisualSonics Vevo 2100 system with a MS 550D transducer[174]. This allowed ultrasound imaging of the heart to take place. Mice were anesthetized with 1.5-2.0% isoflurane and placed in a supine position on a heated stage. 2-D short-axis recordings of the left ventricle at the level of the papillary muscle were obtained in M-mode. Measurements were taken to help compare the efficiency of the left ventricle during diastole and systole. Heart rate and body temperature were monitored during imaging. Left ventricle wall thickness and cavity dimensions were measured at systole and diastole for three cycles, averaged, and used with Vevo 2100 software to calculate values for fractional shortening, ejection fraction, and LV mass[175,176,177]. Comparisons between groups of mice were made using single-factor ANOVA in Microsoft Excel; P values < 0.05 were considered statistically significant.

Isolation of skeletal muscle

10 week old wild-type, α7WT:: laminin-α2 -/-, α7-/-:: laminin- α2WT, and α7-/-::laminin- α2-/- mice were euthanized by CO_2 inhalation in accordance with a protocol approved by the University of Nevada, Reno Animal Care and Use Committee. The Tibialis Anterior and cardiac muscles from these mice were dissected, flash-frozen in liquid nitrogen and stored at -80°C.

Immunofluorescence

Tibialis Anterior (TA) muscle were embedded in Tissue-TEK Optimal Cutting Temperature compound (Sakura Finetek USA Inc, Torrance, CA). 10 µm sections were cut using leica CM1850 cryostat and placed onto Surgipath microscope slides (surgipath Medical Industries, Richmond, IL). The α7 integrin was detected with a 1:500 dilution of CA5.5 mouse monoclonal antibody (Sierra Biosource, Morgan Hill, CA) followed by a 1:100 dilution of FITC-conjugated anti-mouse IgG. Myofibers were outlined with a 1:1000 dilution of FITC-conjugated Wheat Germ Agglutinin. Laminin- α2 was detected with a 1: 500 dilution of *LAMA2* mouse monoclonal followed by a 1: 200 dilution of Alexa Fluo 594 nm anti-mouse IgG. Myofibers were outlined with a 1:1000 dilution of TexasRed-conjugated Wheat Germ Agglutinin.

Sirius Red Staining

TA muscle sections were stained with Sirius Red to measure fibrosis in the skeletal muscle tissue. 10 µm cryosections on slides were fixed in 100%

ethanol and then hydrated through an alcohol series (95 and 80% ethanol) and rinsed in tap water. The sections were stained with Sirius Red (0.1% in saturated aqueous picric acid solution, Rowley Biochemical Institute, Danvers, MA, USA) for 30 min followed by two washes in acidified water. The sections were dehydrated through an alcohol series, rinsed in xylene and mounted with DEPEX Mounting media (Electron Microscopy Science, Hat- field, PA, USA). Representative montages were captured and analyzed using Axiovision 4.8 software. Montages were assembled using Photoshop and Microsoft Powerpoint. Images were captured at 200 X magnification. Areas of red in the TA were considered fibrotic. Circled fibrotic areas were added together, and any non-fibrotic fibers within the fibrotic area were subtracted from the calculated area. The percentage of muscle fibrosis was quantified in treated and control muscles as a percentage of total TA muscle area. Sirius red slides were also used to measure minimal feret's diameter for mice of all 4 genotypic groups. All muscle fibers within an entire TA montage were used to determine the minimal feret's diameter.

Masson's Trichrome Staining

TissueTek OCT-embedded TA muscles were cryosectioned and stained using a Masson's Trichrome Staining Kit (American Master Tech Scientific, Lodi, CA). Images were captured at 100 X magnification under bright field using a Zeiss Axioskop 2 Plus fluorescent microscope, and images were captured with Hamamatsu Color Chilled 3CCD digital camera with HPS-SCSI (C5810)

software. Images were processed and measured with the use of Axiovision 4.8 software. All muscle fibers within an entire montage were used to determine the percentage (%) of blue collagen deposition. Therefore helping to determine the extent to which fibrosis is occurring within cardiac muscle.

Statistical Analysis

All averaged data are reported as the mean ± s.d. *P*-values of < 0.05 were considered to be statistically significant.

RESULTS

Mendelian Inheritance for F1 progeny (n =341) produced from breeding parent mice that are both heterozygous for α7 integrin and laminin-α2

Categories for progeny genotypes are as described in tables 3 & 4. Chi-squared analysis was used as a statistical test for these results for Mendelian Inheritance. X^2 = 35.3546 with 3 degrees of freedom. Embryonic lethality is observed for *α7-/-:: dy-/-* with an approximate 66% deviation from the higher expected number of double knockout mice.

Immunofluorescence to show laminin-alpha2 reduction in the *α7 -/- :: dy -/-* mouse model

Laminin-α2 protein is minimally present within the laminin- α2 knockout mouse genotype as it is only a partial knockout within the Dy^W laminin- α2

deficient strain of mice (Figure 30). α7 WT :: dy WT (*n*= 12), α7 WT :: dy -/- (*n*= 11), α7 -/- :: dy WT (*n*= 5), *α7 -/- :: dy -/-* (*n*= 5).

Immunofluorescence to show both alpha7 reduction in the *α7 -/- :: dy -/-* mouse model

α7 integrin protein is reduced within *α7-/-* (α7-/-:: dyWT and α7-/-:: dy -/-) tissues (Figure 31). α7 WT :: dy WT (*n*= 12), α7 WT :: dy -/- (*n*= 11), α7 -/- :: dy WT (*n*= 5), *α7 -/- :: dy -/-* (*n*= 5).

Kyphosis analysis via digital X-rays comparing α7 WT :: dy WT, α7 WT :: dy -/-, α7 -/- :: dy WT, and *α7 -/- :: dy -/-* 10 week old mice

The kyphotic index calculations were carried out following a technique previously described[178]. Radiographs were assessed in a blinded manner and visibly there is a similar increase in the severity of kyphosis occurring in *α7-/-:: dy-/-* animals compared with a7WT::dy-/- animals(Figure 32). This result is visible in the representative radiographs presented. Statistically this result was significant.

Weights and muscle function assessment comparing α7 WT :: dy WT, α7 WT :: dy -/-, α7 -/- :: dy WT, and *α7 -/- :: dy -/-* mice

No statistical significance was observed for *α7-/-:: dy-/-* grip strength assessing forelimb muscle strength compared to the other 3 genotypes (Figure 33). Percentage of forelimb muscle fatigue was also elevated within *α7-/-:: dy-/-* compared to the other genotypes. Activity box data showed consistent statistical

significance with regards to distance moved and ambulatory time which was severely reduced in *α7-/-:: dy-/-* mice. The number of vertical stand-ups were also reduced for *α7-/-:: dy-/-* animals and this was coupled with an extension in resting time for these animals.

Heart analysis comparing α7 WT :: dy WT, α7 WT :: dy -/-, α7 -/- :: dy WT, and *α7 -/- :: dy -/-* 10 week old mice

Whenever heart weight was normalized to body weight there was an increase in mass evident for *α7-/-:: dy-/-* mice which was similar to α7WT:: dy-/-. Within *in vivo* echocardiography, the representative B-mode screenshots reflect the vast range of cardiac functions within all genotypes of this study (Figure 34). The worst phenotype was observed in *α7-/-:: dy-/-* mice with atrial flutter/fibrillation evident and increased Left Ventricular wall thickness. These *α7-/-:: dy-/-* mice had very much reduced left ventricular volume during systole.

Echocardiography data comparing α7 WT :: dy WT, α7 WT :: dy -/-, α7 -/- :: dy WT, and *α7 -/- :: dy -/-* 10 week old mice

For α7WT:: dyWT versus α7WT:: dy-/- the most significant differences are with Left ventricular Internal diameter (LVID) in both diastole and systole (Figure 35 A). There was also a huge reduction in the ability of the left ventricle to pump blood and this is indicated by the significant reduction in Left ventricular volume for both diastole and systole.

For α7WT:: dyWT versus α7-/-:: dy-/- it is a very similar situation to the one previously described, small internal diameter and therefore less efficient blood pumping due to the decreased size of the ventricle and reduced volume in both diastole and systole (Figure 35 B).

For α7-/-:: dyWT versus α7WT:: dy-/-, it is the same situation. These results indicate that α7 integrin plays a critical role in rescuing cardiac muscle whenever laminin-α2 is absent (Figure 35 C). In the absence of both α7integrin and laminin-α2 there are detrimental consequences with regards heart function due to reduced blood filling capacity with reduced ventricular volume during systole and the occurrence of atrial flutter.

Increased collagen visible within *α7 -/- :: dy -/-* cardiac muscle

Heart tissue cryosections show elevated blue fibrotic tissue deposition within the cardiac montages for *α7-/-::dy-/-* (Figure 36). Quantification of this shows that laminin-α2 deficiency has similar effects for both α7WT:: dy-/- and *α7-/-:: dy-/-.* This result therefore indicates that laminin-α2 is important for protection against collagen deposition however this result was not statistically significant and would warrant the need for more *n* numbers.

Fibrotic tissue analysis within Tibialis Anterior muscle of α7 WT :: dy WT, α7 WT :: dy -/-, α7 -/- :: dy WT, and *α7 -/- :: dy -/-* 10 week old mice

Again, as above, montages were assembled this time for TA muscle (Figure 37). Visibly laminin-α2 deficiency for both α7WT:: dy-/- and *α7-/-:: dy-/-*

mice results in a more degradative muscle pathology due to excessive scar tissue formation indicated here by red color which is labeled fibrotic tissue. There was no statistical significance but single loss of laminin-α2 seemed to have a more severe effect but very similar to double knockout of both α7 integrin and laminin-α2. Single loss of only α7 integrin resulted in the most muscle hypertrophy when assessing myofiber minimal ferret's diameter.

DISCUSSION

The α7 integrin is an important transmembrane cell surface receptor in skeletal, cardiac and vascular smooth muscle. Laminin- α2 is an important binding partner for α7 integrin[92,108,117]. It connects the extracellular matrix to the integrin on the sarcolemma. α7 integrin plays an important role in cell signaling as it binds to talin and cytoskeletal F-actin. Laminin-integrin binding complex helps to transduce external mechanical stresses involved with muscle contraction and connect them with a cellular response via signaling. It is important to remember that this laminin-integrin interaction is very much a two-way system i.e. there can be inside- outside signaling and also outside-inside signaling. The relationship between them is very much a bi-directional one. Disruption of these components causes neuromuscular disease in both humans and mice. This emphasizes the importance of this binding complex in maintaining the integrity of the sarcolemmal to withstand the mechanical forces associated with muscle contraction.

Together these results suggest that laminin- α2 plays a critical role in maintaining proper function of skeletal and cardiac muscle. Transgenic overexpression of α7 integrin in skeletal muscle in previous studies demonstrated that overexpression can help partially rescue the disease phenotype and extend the lifespan of the mice. This study helps to reiterate previous literature[173]. The severe embryonic lethality of double knockout *α7-/-:: dy-/-* mice furthers this previous knowledge and emphasizes the importance of α7 integrin in rescuing the loss of laminin-α2[65]. The duplicity of their bi-directional relationship of protecting the structural and functional integrity of muscle is very much highlighted in the generation of this double knockout mouse model.

We observed severe muscle pathology in 10 week old *α7-/-:: dy-/-* mice which is a new result for this field of study as no one has ever created this particular double knockout mouse model in the dy^{W}*-/-*[173]*.* Partial knockdown of both proteins in *α7-/-:: dy-/-* mice results in severe skeletal and cardiac muscle degeneration, reduced functional activity and fibrotic scar tissue deposition. Here, compensation by α7 integrin helps these mice to maintain functional integrity. The *α7-/-:: dy-/-* mice analyzed in this study exhibited a phenotype similar to that of single knockout of laminin-α2 in dy^{W}*-/-* mice. This phenotypic similarity between these two genotypes suggests that there is functional overlap in the role of α7 integrin in maintaining muscle structure and function. The alpha7 integrin has a redundant role as loss of laminin-α2 is detrimental to muscle pathology. Double knockout *α7-/-:: dy-/-* mice exhibit a severe cardiac phenotype similar to

that of the *dy-/-* mice suggesting that laminin-α2 is very critical to cardiac muscle function by its presence[179–185]. It also suggests there is no active sarcolemmal complex able to cope and compensate for the loss of both of them. Therefore, the heart is not able to pump efficiently in a coordinated manner and we see the atrial fibrillation occurring[175–177,186].

The *α7-/-:: dy-/-* mouse is a new mouse model for muscular dystrophy that has been identified which lacks both α7 integrin and laminin-α2. This has never been studied before in this particular dy^{W} *-/-* mouse model[173]. Further investigation will reveal the effects on pathophysiology and expression of sarcolemmal proteins. Results from characterization of this new α7 integrin / laminin-α2 double knockout mouse model will aid in understanding the exact role that α7 integrin and laminin-α2 play in MDC1A. It will also potentially help with the identification of novel therapeutic targets for this devastating neuromuscular disease.

ACKNOWLEDGEMENTS

The project described was supported by grants from the National Center for Research Resources (SP20RR016464-11), Institute of General Medical Sciences (8 P20 GM103440-11) from the National Institutes of Health, CureCMD and Struggle Against Muscular Dystrophy. I would especially like to thank Dr. Andrea Agarwal for Echocardiography training and blinded analysis.

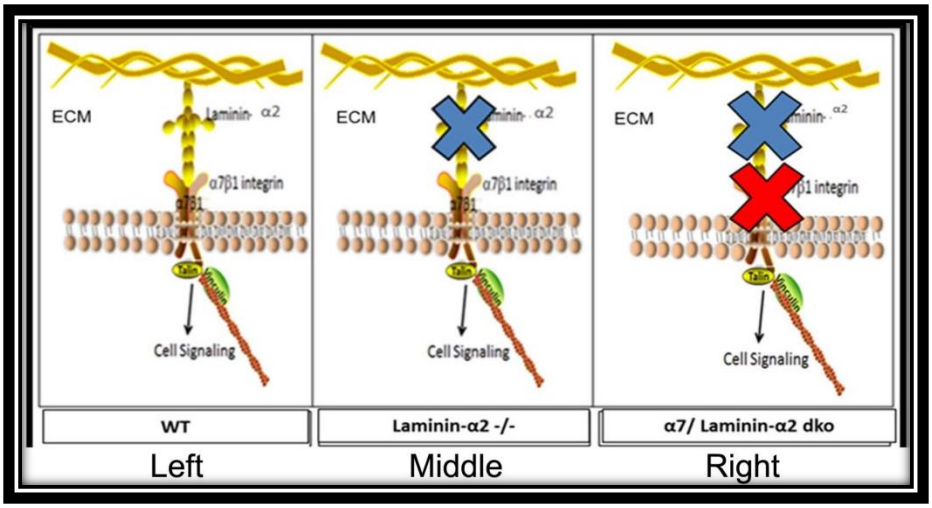

Figure 28. Schematic representation of the α7 integrin- laminin-α2 binding complex

α7 integrin binding to laminin-α2 acts as a strengthening molecular glue in the WT sarcolemma. However, this strength is lost upon the absence of laminin-α2 in muscle. We wish to investigate ablation of the α7 integrin- laminin-α2 binding complex in this α7/laminin-α2 double knockout (DKO mouse model).

Figure 29. Photographs of 10 week old *dy^{W}-/-* and *a7-/-* :: *dy-/-* mice

α7 integrin-laminin-α2 double knockout (DKO) mouse alongside its littermate control laminin-α2 knockout (*Dy^{W}*) mouse at 10 weeks of age. More advanced kyphosis is evident within the DKO mouse.

Category	Observed	Expected	Actual %	Expected %
Wild-type (WT)	240	192	70.381%	56.305%
Alpha7 KO	36	64	10.557%	18.768%
Dy^W (Lamα2 KO)	59	64	17.302%	18.768%
Double Knockout	6	21	1.760%	6.158%

Categories:	
WT:	alpha7 WT & Dy^W WT, alpha7 Het & Dy^W WT, alpha7 WT & Dy^W Het, alpha7 Het & Dy^W Het
Alpha7 KO:	alpha7 Knockout & Dy^W WT, alpha7 Knockout & Dy^W Het
Dy^W KO :	alpha7 WT & Dy^W Knockout, alpha7 Het & Dy^W Knockout
Double Knockout:	alpha7 Knockout & Dy^W Knockout

Table 3 & Table 4: Mendelian Inheritance for F1 progeny (n =341) produced from breeding parent mice that are both heterozygous for α7 integrin and laminin-α2

Categories for each genotype are labeled here in order to define how Mendelian inheritance was calculated. Chi-squared value was 35 with 3 degrees of freedom. Embryonic lethality is evident within the DKO mouse.

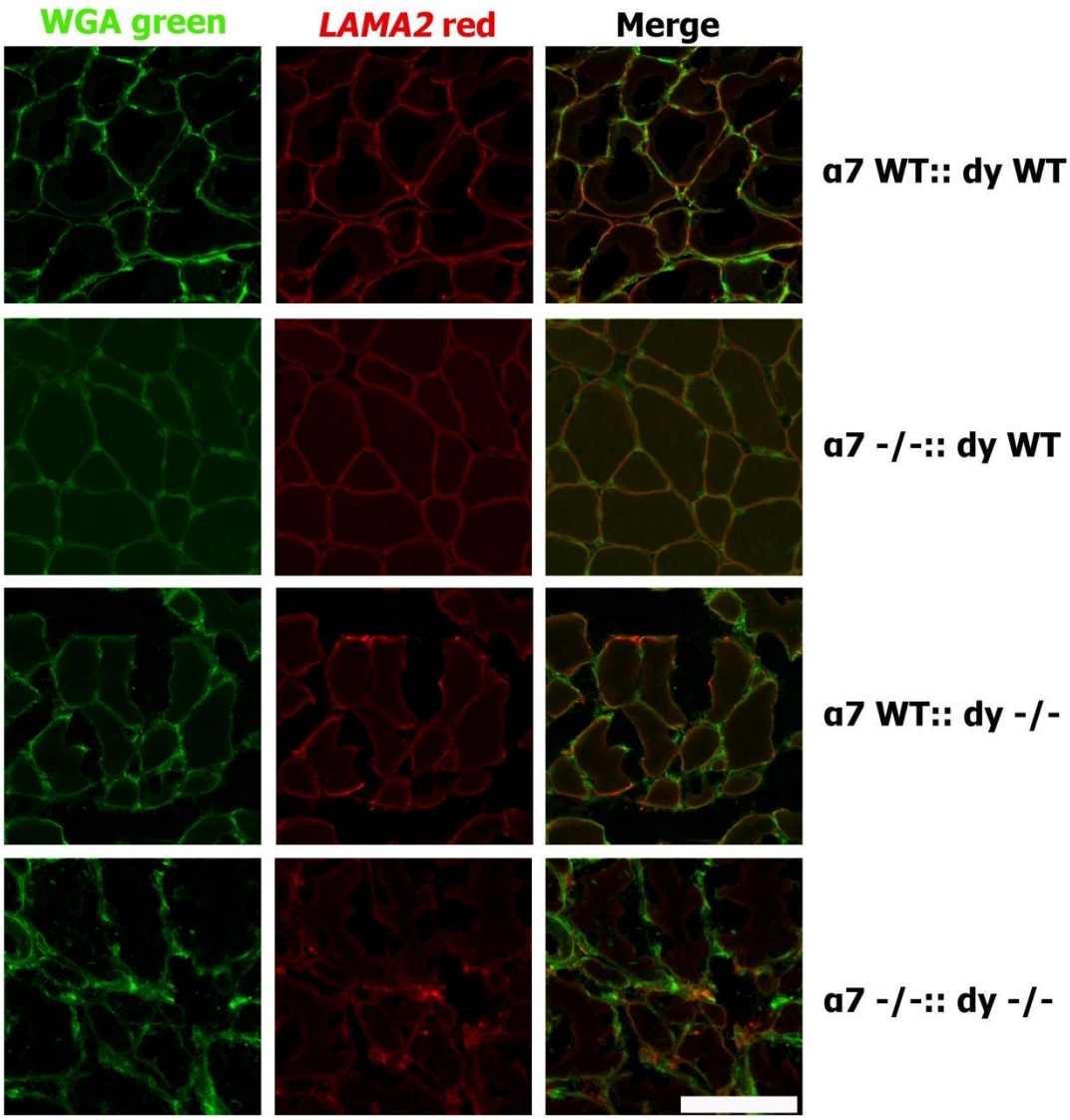

Figure 30. Immunofluorescence to show laminin-alpha2 reduction in the *α7 -/- :: dy -/-* mouse model

Confocal microscopy was employed to show presence or reduction of laminin-α2 protein in TA muscle cryosections. Wheat germ agglutinin (WGA) was used to outline the myofibers. Magnification = 400 X. Scale bar = 100 µm. Green

represents WGA and red represents laminin-α2. *α7-/- :: dy -/-* protein localization in muscle is more disorganized compared to the other 3 genotypes.

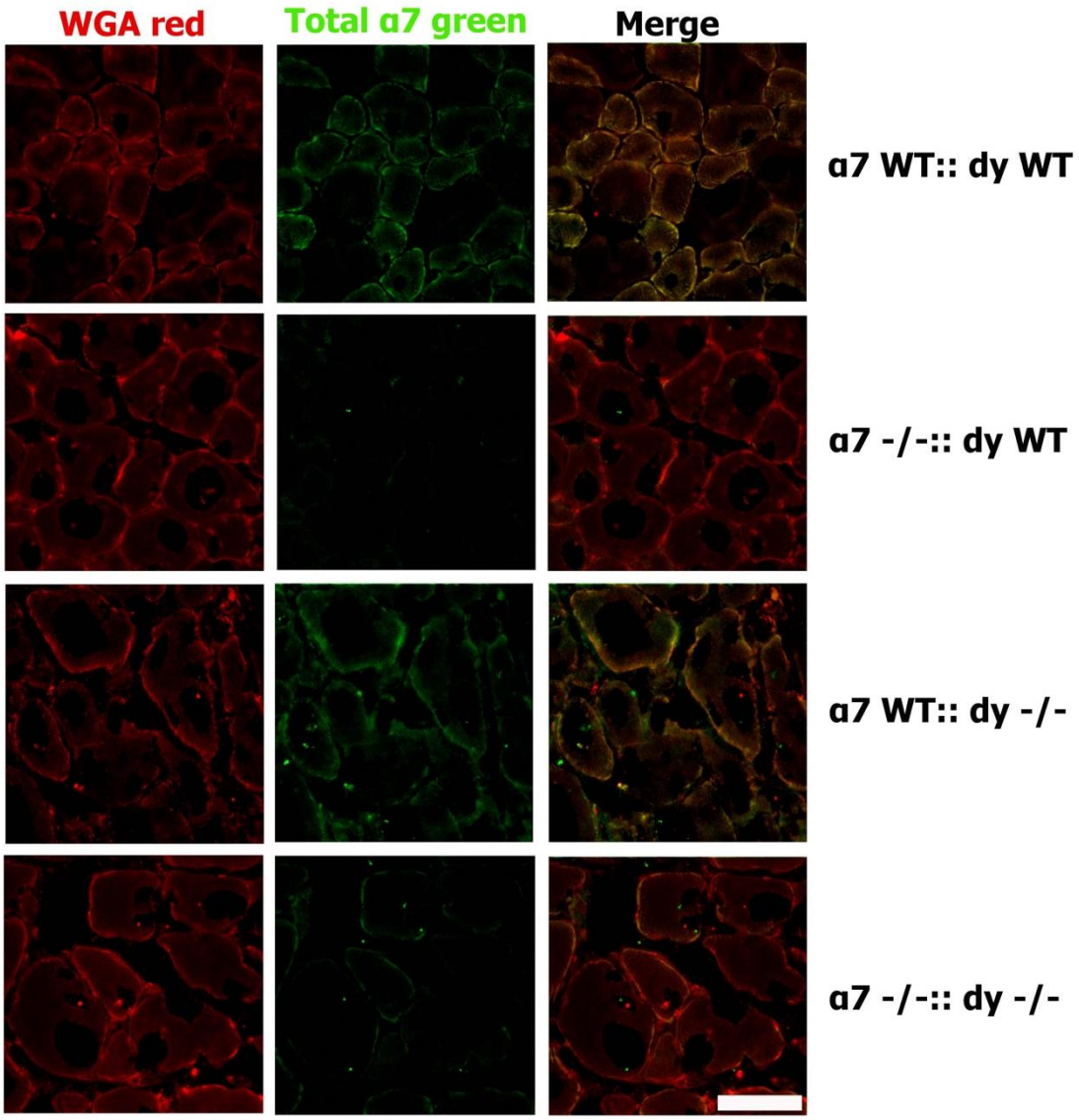

Figure 31. Immunofluorescence to show alpha7 reduction in the *α7 -/- :: dy -/-* mouse model

Confocal images were collected and analyzed for the presence of alpha7 integrin protein. Wheat germ Agglutinin (WGA) was used to outline the myofibers. Magnification = 400 X. Scale bar = 100 µm. Red represents WGA and green

represents α7 integrin presence. alpha7 integrin protein was greatly reduced in *dy-/-* animals.

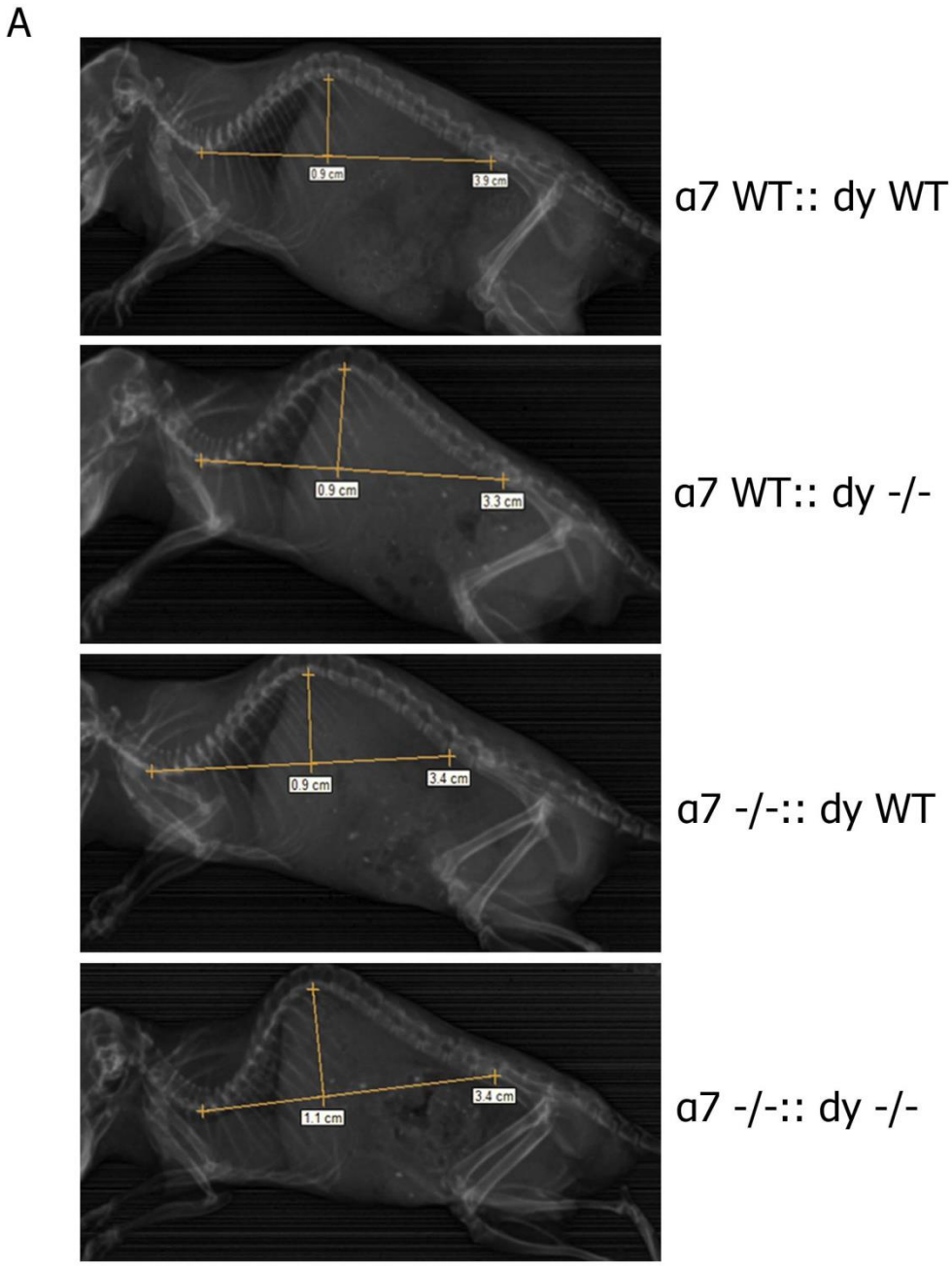

Figure 32. Kyphosis analysis via digital X-rays comparing α7 WT :: dy WT, α7 WT :: dy -/-, α7 -/- :: dy WT, and *α7 -/- :: dy -/-* 10 week old mice

(B) Kyphosis is used to describe the curvature of the spine. In muscular dystrophy there is degradation of muscles associated with the spine and

therefore more spinal curvature (kyphosis) occurs as the disease progresses. Kyphotic Index calculations for each of the genotypes: α7 WT :: dy WT (*n*= 12), α7 WT :: dy -/- (*n*= 11), α7 -/- :: dy WT (*n*= 5), *α7 -/- :: dy -/-* (*n*= 5). A lower kyphotic index indicates a higher degree of kyphosis present. In this way, WT animals had a higher kyphotic index therefore indicating less kyphosis occurring. The calculations were based on radiographs as shown in Figure 32 B. Loss of laminin-α2 protein causes severe kyphosis and whenever alpha7 integrin protein is reduced in addition, it causes slightly more kyphosis. One-Way *ANOVA* analysis produced a *P*-value = 0.0026.

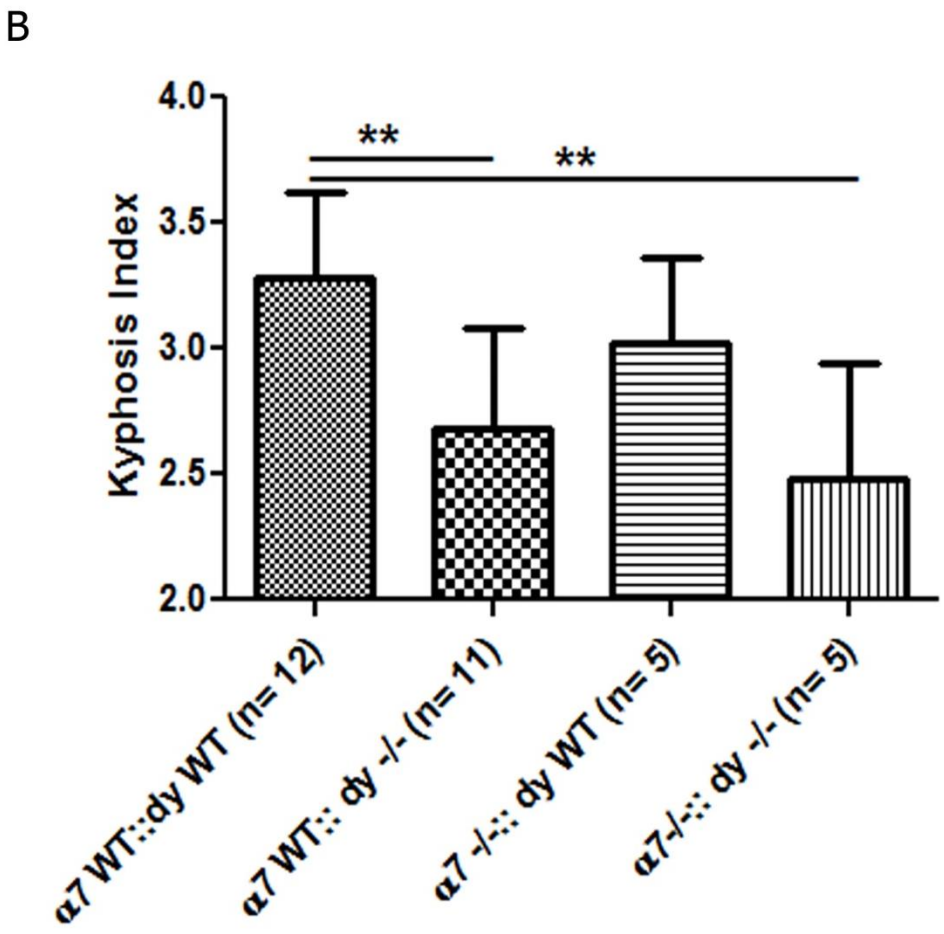

Figure 32. Kyphosis analysis via digital X-rays comparing α7 WT :: dy WT, α7 WT :: dy -/-, α7 -/- :: dy WT, and *α7 -/- :: dy -/-* 10 week old mice

(A) Representative X-ray radiographs for each of the genotypes: α7 WT :: dy WT (*n*= 12), α7 WT :: dy -/- (*n*= 11), α7 -/- :: dy WT (*n*= 5), *α7 -/- :: dy -/-* (*n*= 5). Visibly, the severity of kyphosis looks similar for both α7 WT :: dy -/- mice and *α7 -/- :: dy -/-* mice. Kyphotic index calculations are presented in Figure 32 A.

A

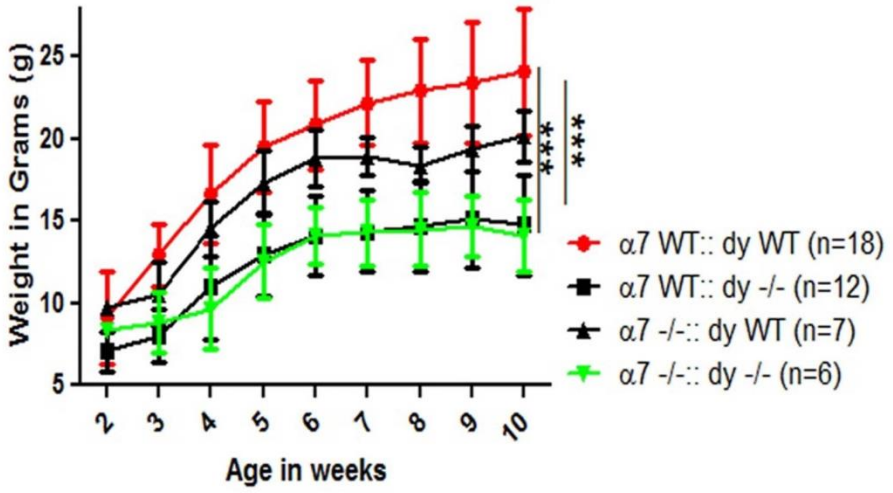

Figure 33. Weights and muscle function assessment comparing α7 WT :: dy WT, α7 WT :: dy -/-, α7 -/- :: dy WT, and *α7 -/- :: dy -/-* mice

(A) Weights (g) were recorded in a weekly manner for all mice until 10 weeks old. Each genotype weighed on average at 10 weeks old : α7 WT :: dy WT mice weighed 19.07 g ± 1.723 g, α7 WT :: dy -/- mice weighed 12.44 g ± 1.025 g, α7 -/- :: dy WT mice weighed 16.43 g ± 1.306 g, and *α7 -/- :: dy -/-* mice weighed 12.32 g ± 0.8777 g at 10 weeks old. One-Way *ANOVA* statistical analysis revealed the *P*-value = 0.0013. α7 WT :: dy -/- mice and *α7 -/- :: dy -/-* mice had very similar weight gain over the entire period of the study therefore suggesting that there was no detrimental effect by additionally reducing alpha7 integrin alongside laminin-α2.

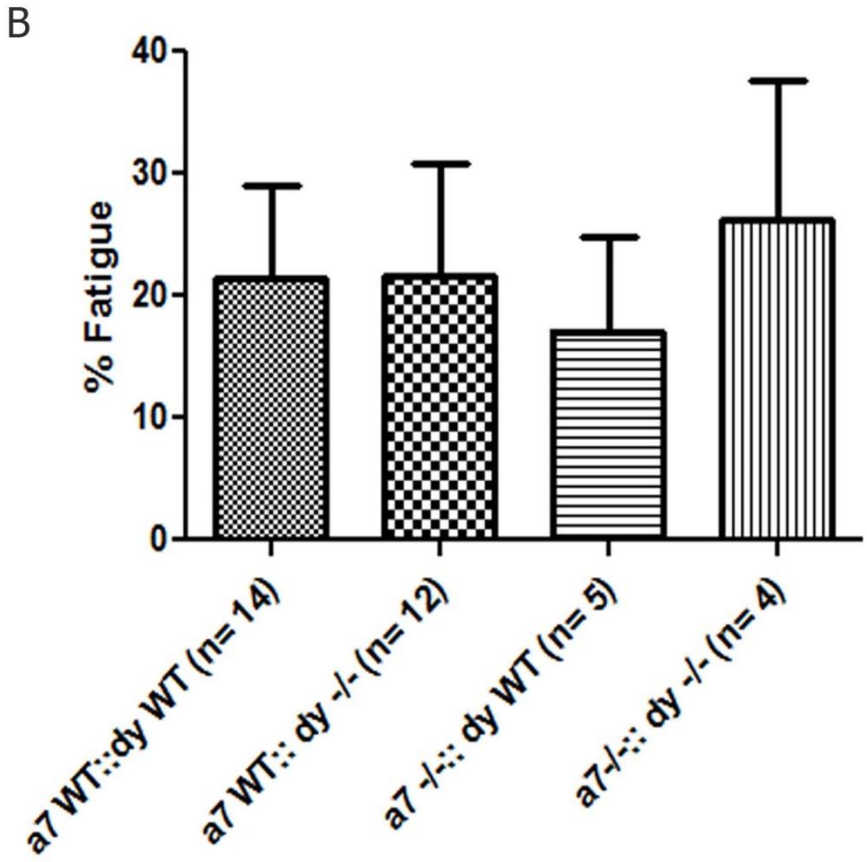

Figure 33. Weights and muscle function assessment comparing α7 WT :: dy WT, α7 WT :: dy -/-, α7 -/- :: dy WT, and *α7 -/- :: dy -/-* 10 week old mice

(B) Forelimb muscle grip strength measurements (six in total) were recorded (grams of force) and normalized to body weight. The percentage (%) fatigue for forelimb muscles was calculated. No statistical significance was found between the 4 different genotypes.

C

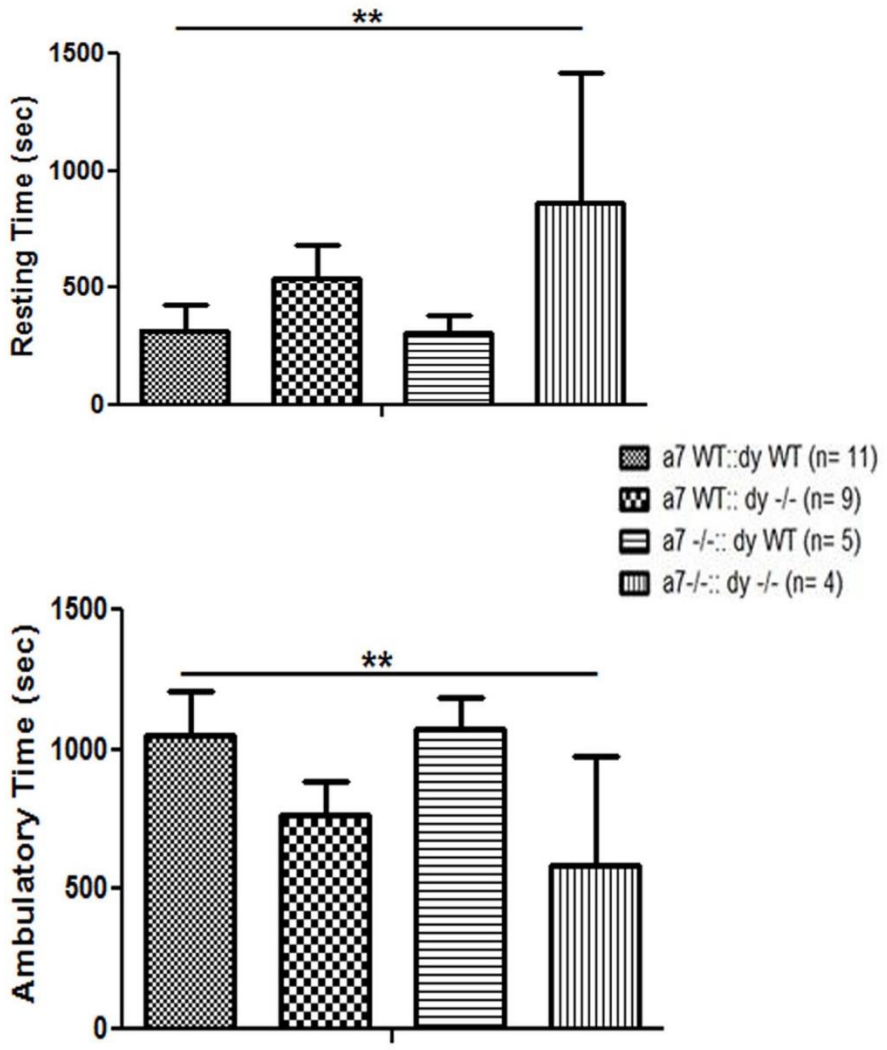

Figure 33. Weights and muscle function assessment comparing α7 WT :: dy WT, α7 WT :: dy -/-, α7 -/- :: dy WT, and *α7 -/- :: dy -/-* 10 week old mice

(C) Activity box data was collected for mice in a non-biased way for 30 minutes. The results for resting time (sec) and ambulatory time (sec) are presented. α7 WT :: dy WT mice had a resting time of 318.8 sec ± 34.03 sec and ambulatory

time of1052 sec ± 48.24 sec, α7 WT :: dy -/- mice had a resting time of 542.7 sec ± 47.88 sec and ambulatory time of 768.0 sec ± 39.67 sec, α7 -/- :: dy WT mice had a resting time of 308.0 sec ± 34.37 sec and ambulatory time of 1074 sec ± 48.75 sec, *α7 -/- :: dy -/-* mice had a resting time of 860.3 sec ± 277.9 sec and ambulatory time of 589.0 sec ± 194.5 sec. Student *t*-test's revealed a ** *P*-value = 0.0063 for resting time (sec) and ** *P*-value = 0.0048 for ambulatory time (sec).

D

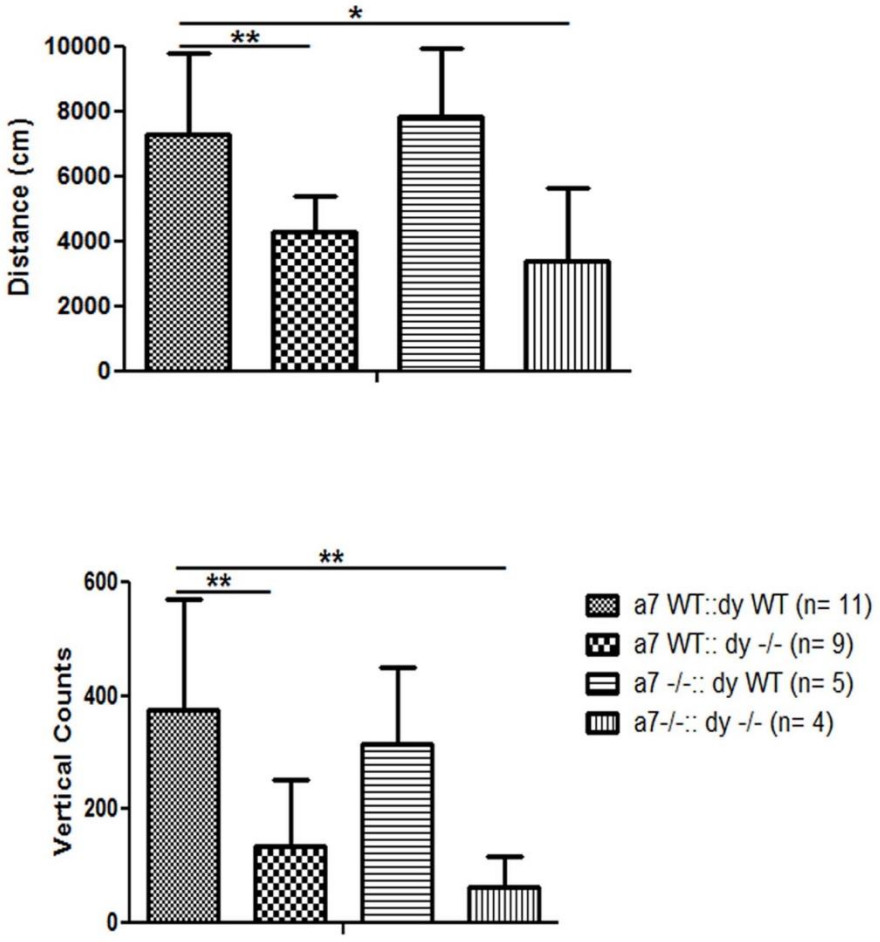

Figure 33. Weights and muscle function assessment comparing α7 WT :: dy WT, α7 WT :: dy -/-, α7 -/- :: dy WT, and *α7 -/- :: dy -/-* 10 week old mice

(D) Activity box data was collected for mice in a non-biased way for 30 minutes. The results for distance moved (cm) and vertical counts are presented. Vertical counts act as a way of measuring how many stand-ups each mouse can accomplish. α7 WT :: dy WT moved 7296 cm ± 756.4 cm and stood 374.0 times ± 59.40, α7 WT :: dy -/- moved 4319 cm ± 360.1 cm and stood 136.0 times ± 38.33, α7 -/- :: dy WT moved 7883 cm ± 939.2 cm and stood 315.0 times ±

60.37, *α7 -/- :: dy -/-* moved 3385 cm ± 1146 cm and stood 62.00 times ± 27.00. Student *t*-tests revealed for distance moved ** *P*-values = 0.0039 and * = 0.0174, for vertical counts P-values were 0.0050 and 0.0092 respectively. Therefore based on these results it looks as though *α7-/- :: dy -/-* knockdown produces no additive effects.

A

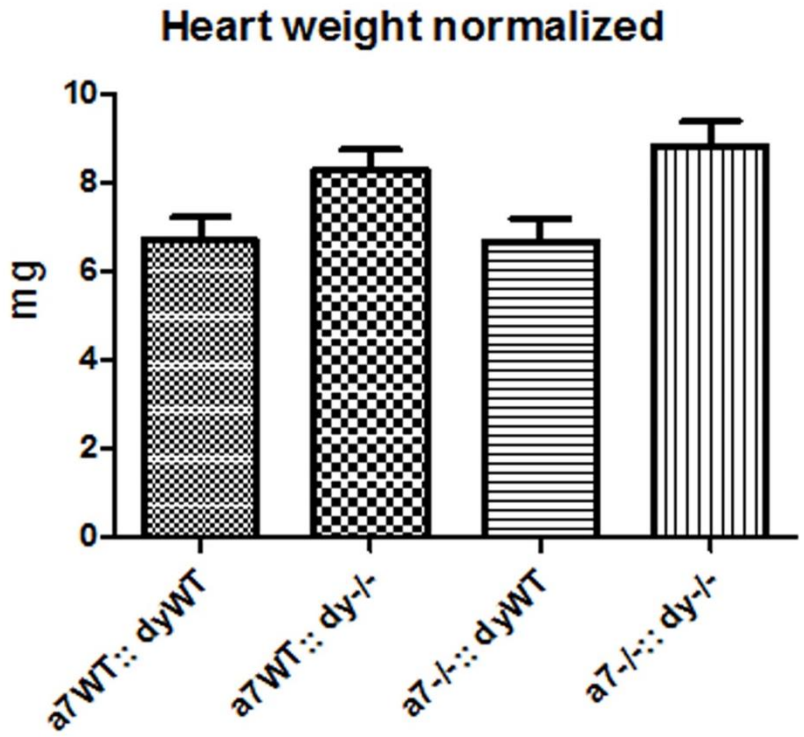

Figure 34. Heart analysis comparing α7 WT :: dy WT, α7 WT :: dy -/-, α7 -/- :: dy WT, and *α7 -/- :: dy -/-* 10 week old mice

(A) Heart weights (mg) were recorded and normalized to body weight. There was no statistical significance found between the 4 genotypes.

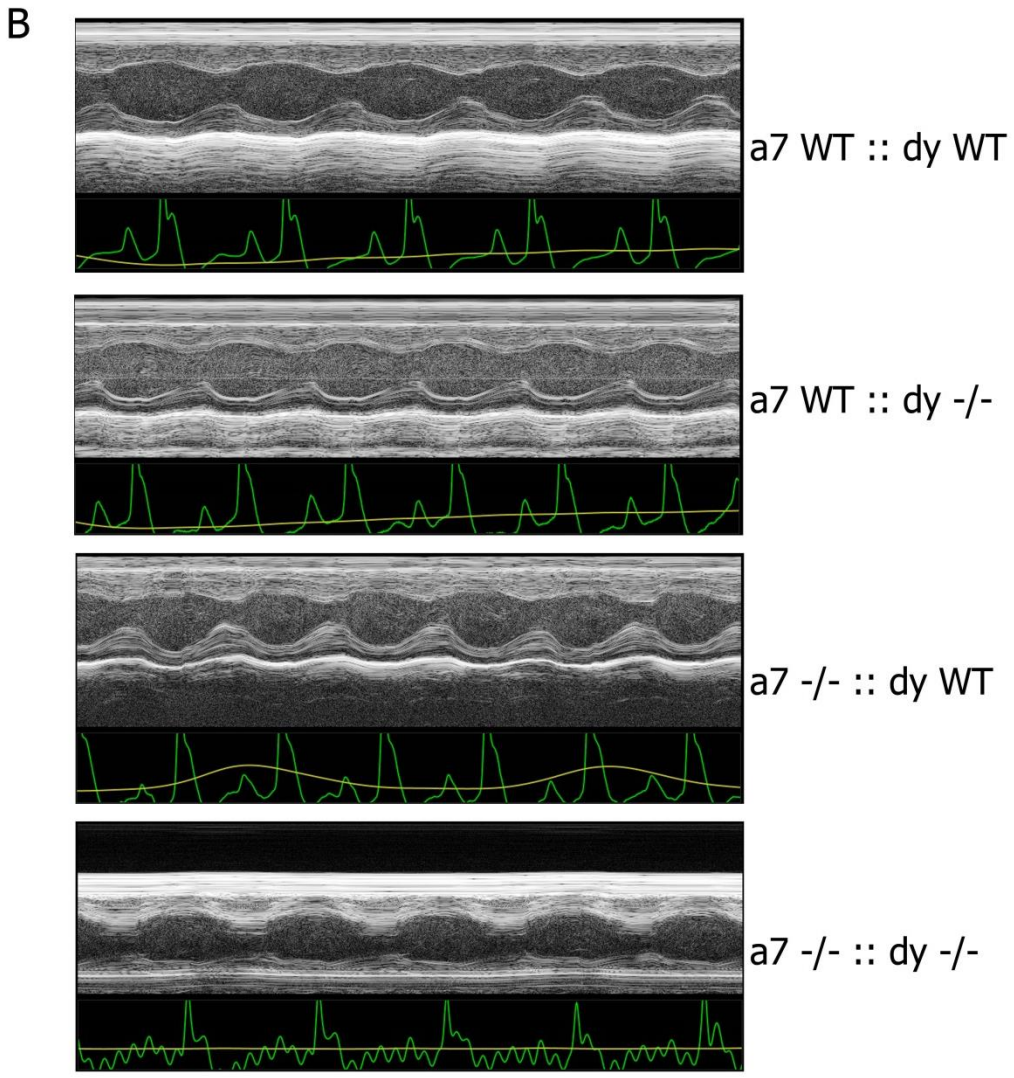

Figure 34. Heart analysis comparing α7 WT :: dy WT, α7 WT :: dy -/-, α7 -/- :: dy WT, and *α7 -/- :: dy -/-* 10 week old mice

(B) Representative M-mode frames captured during echocardiography for each genotype. Atrial flutter or fibrillation is clearly evident within *α7 -/- :: dy -/-* mice.

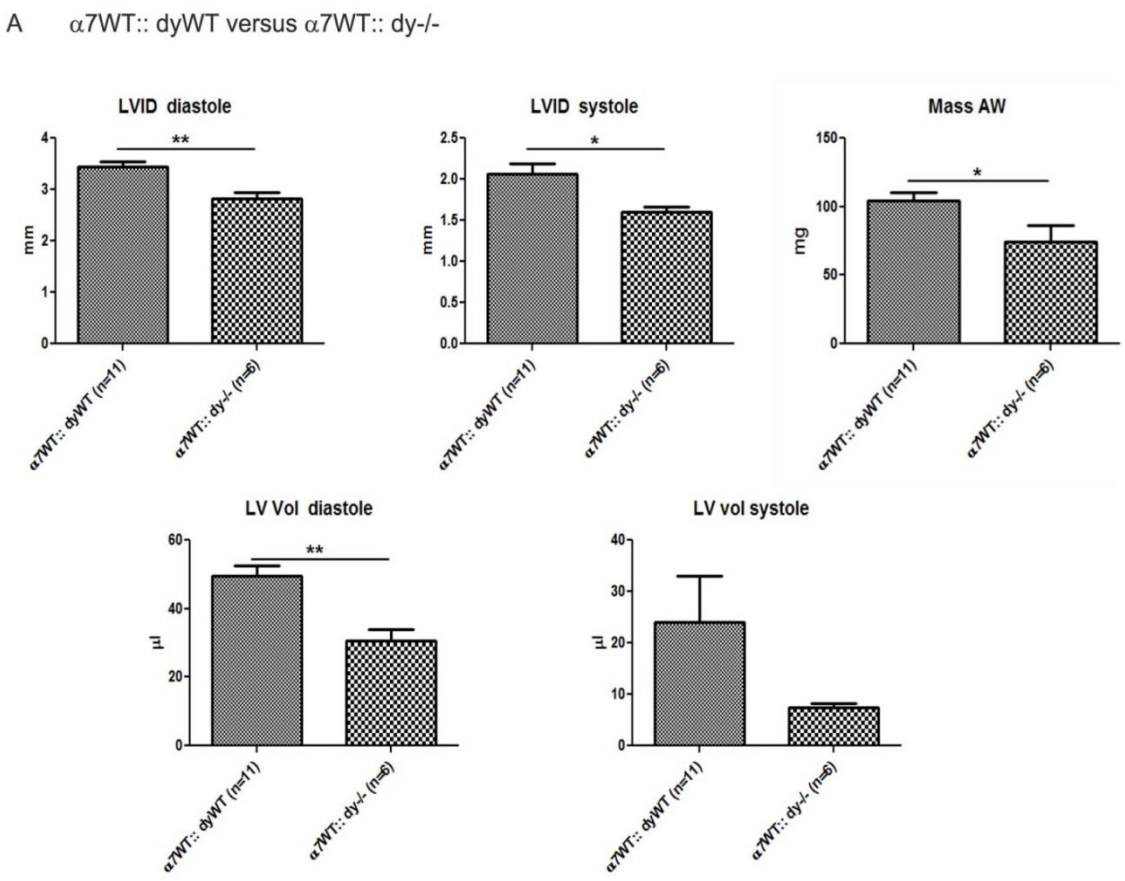

Figure 35. Echocardiography data

A, B and C) M-mode analysis provided a plethora of parameters to scrutinize. Significant values in KO WT versus KO KO: LVAW, s (mm) *P*-value = 0.0315, LVID, d (mm) *P*-value = 0.0180, Mass AW, corr. (mg) *P*-value = 0.0183, LV vol, d (µL) *P*-value = 0.0204. The data for this figure was kindly provided by Dr. Andrea Agarwal.

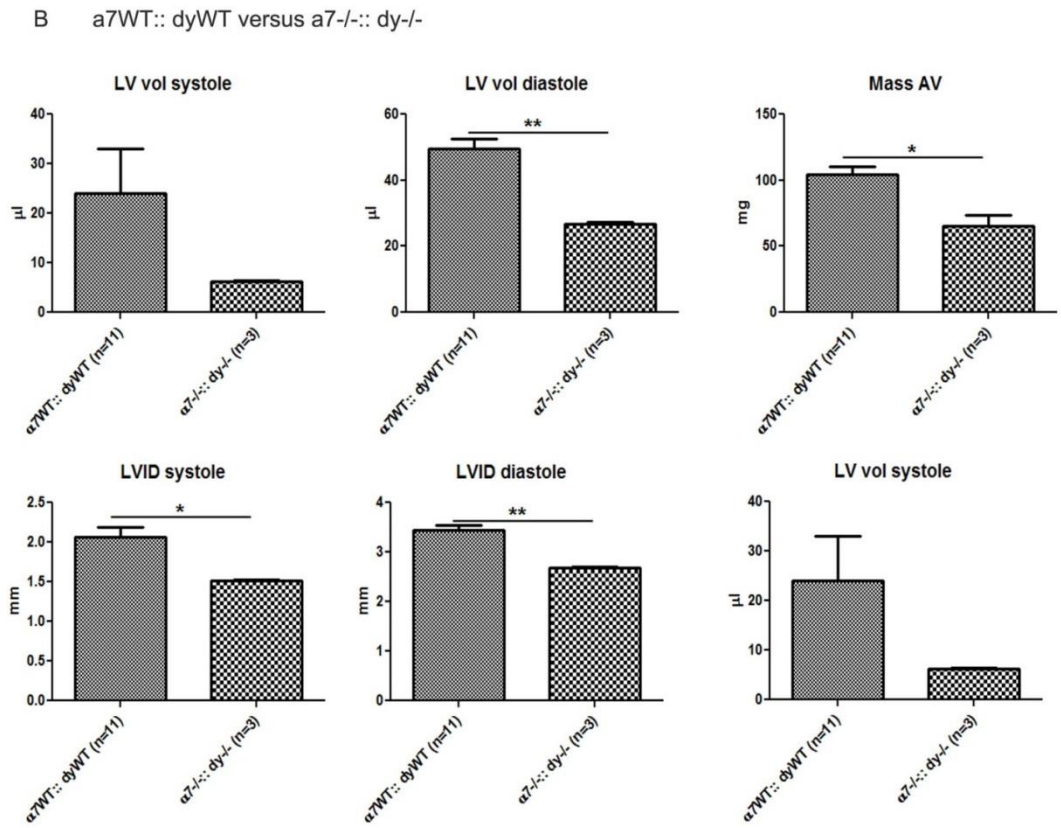

Figure 35. Echocardiography data

A, B and C) M-mode analysis provided a plethora of parameters to scrutinize. Significant values in KO WT versus KO KO: LVAW, s (mm) *P*-value = 0.0315, LVID, d (mm) *P*-value = 0.0180, Mass AW, corr. (mg) *P*-value = 0.0183, LV vol, d (µL) *P*-value = 0.0204. The data for this figure was kindly provided by Dr. Andrea Agarwal.

C a7-/-:: dyWT versus a7WT:: dy-/-

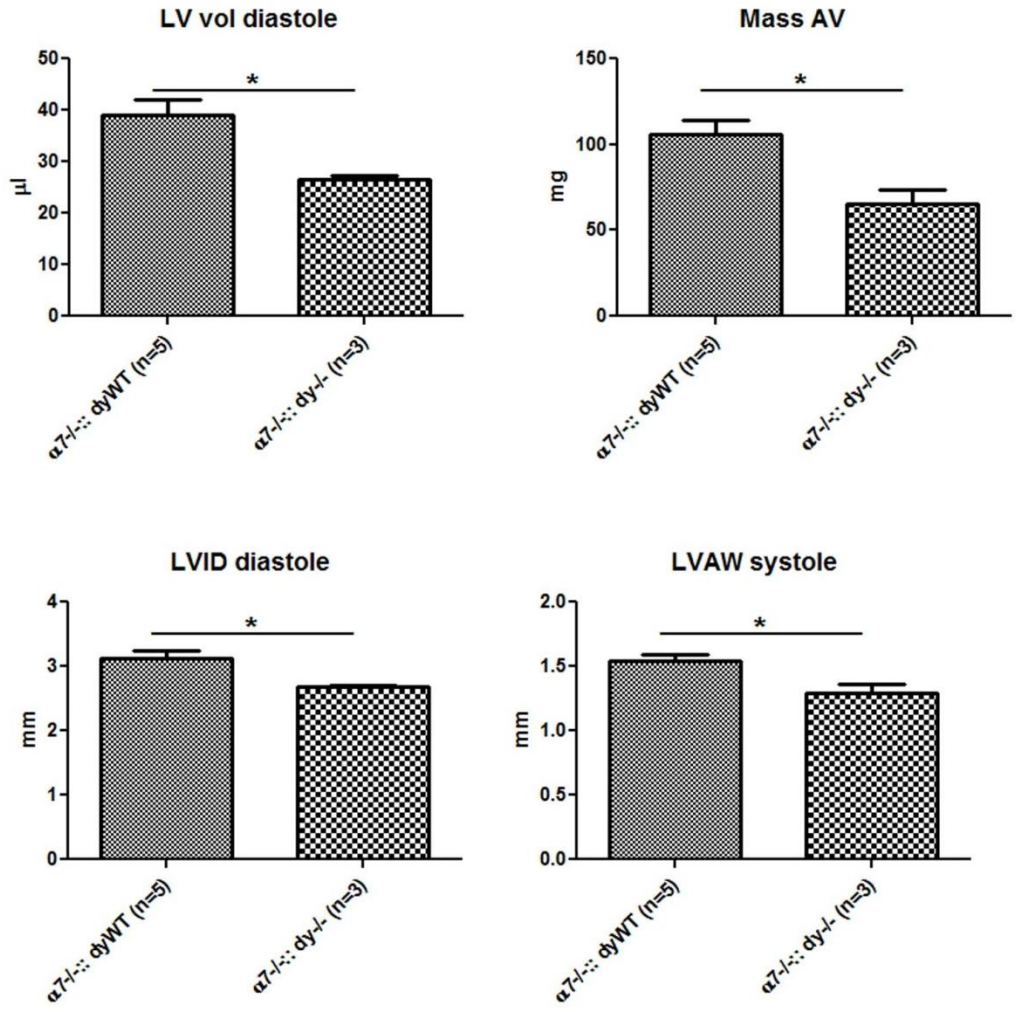

Figure 35. Echocardiography data

A, B and C) M-mode analysis provided a plethora of parameters to scrutinize. Significant values in KO WT versus KO KO: LVAW, s (mm) *P*-value = 0.0315, LVID, d (mm) *P*-value = 0.0180, Mass AW, corr. (mg) *P*-value = 0.0183, LV vol, d (µL) *P*-value = 0.0204. The data for this figure was kindly provided by Dr. Andrea Agarwal.

A

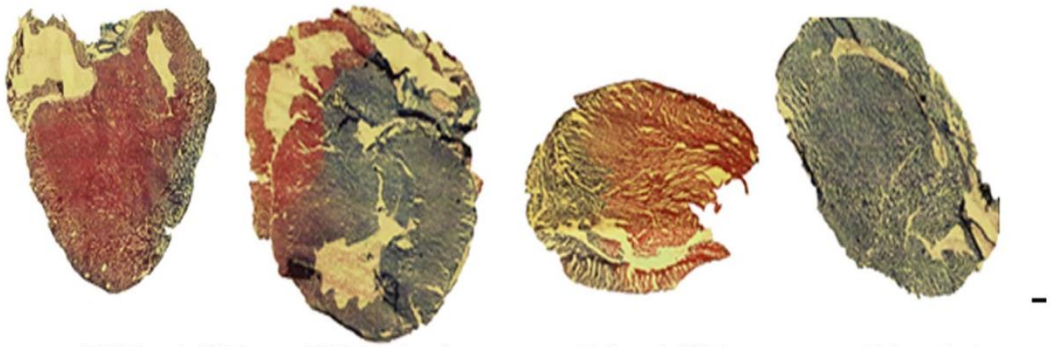
α7WT :: dyWT
α7WT :: dy -/-
α7-/- :: dyWT
α7-/- :: dy-/-

B

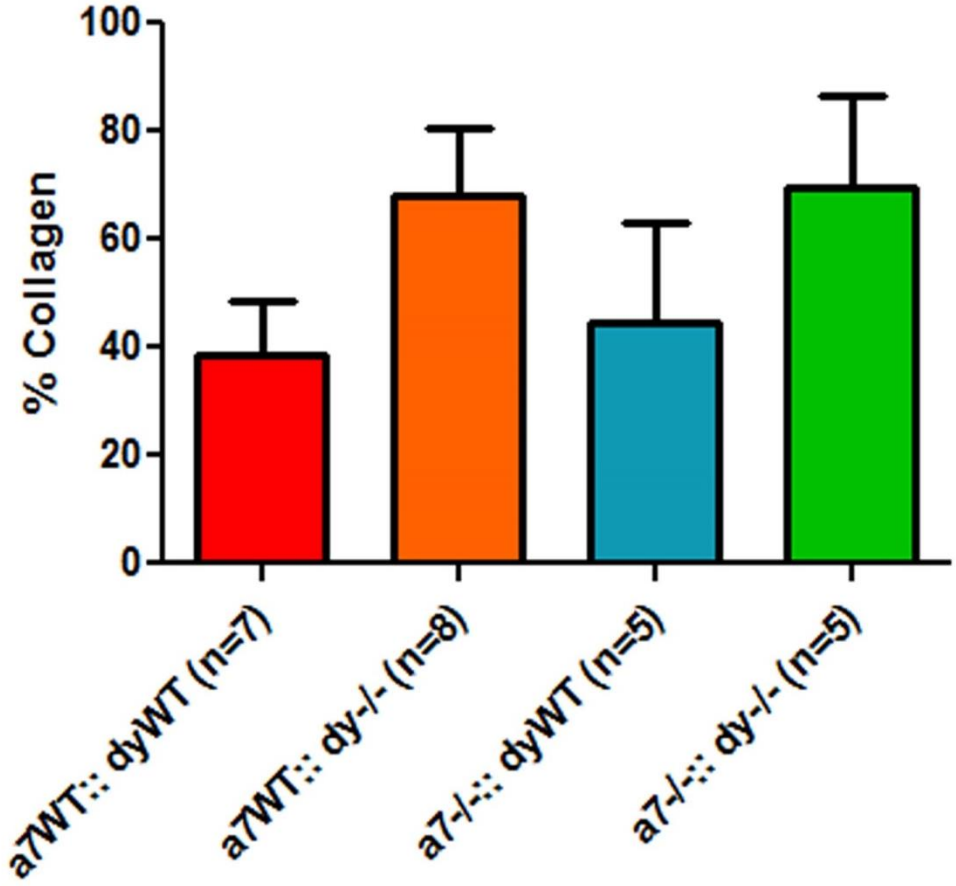
% Collagen
100
80
60
40
20
0
a7WT:: dyWT (n=7)
a7WT:: dy-/- (n=8)
a7-/-:: dyWT (n=5)
a7-/-:: dy-/- (n=5)

Figure 36. Increased collagen visible within *α7 -/- :: dy -/-* cardiac muscle

A) Masson's trichrome staining was carried out on heart cryosections to analyze the presence of collagen within cardiac muscle. Collagen is represented by blue color. Magnification = 100 X. Scale bar = 200 µm. B) The percentage of collagen present in cardiac muscle shown in Figure 36 A was quantified. No statistical significance was found and One-Way *ANOVA* analysis was performed with *P*-value = 0.3032. Surprisingly, there is a lot of fibrosis evident in WT cardiac muscle and this was consistently found. Again, α7WT:: dy-/- and *α7-/- :: dy-/-* have similar phenotypes further suggesting that the double knockout has no additive effects.

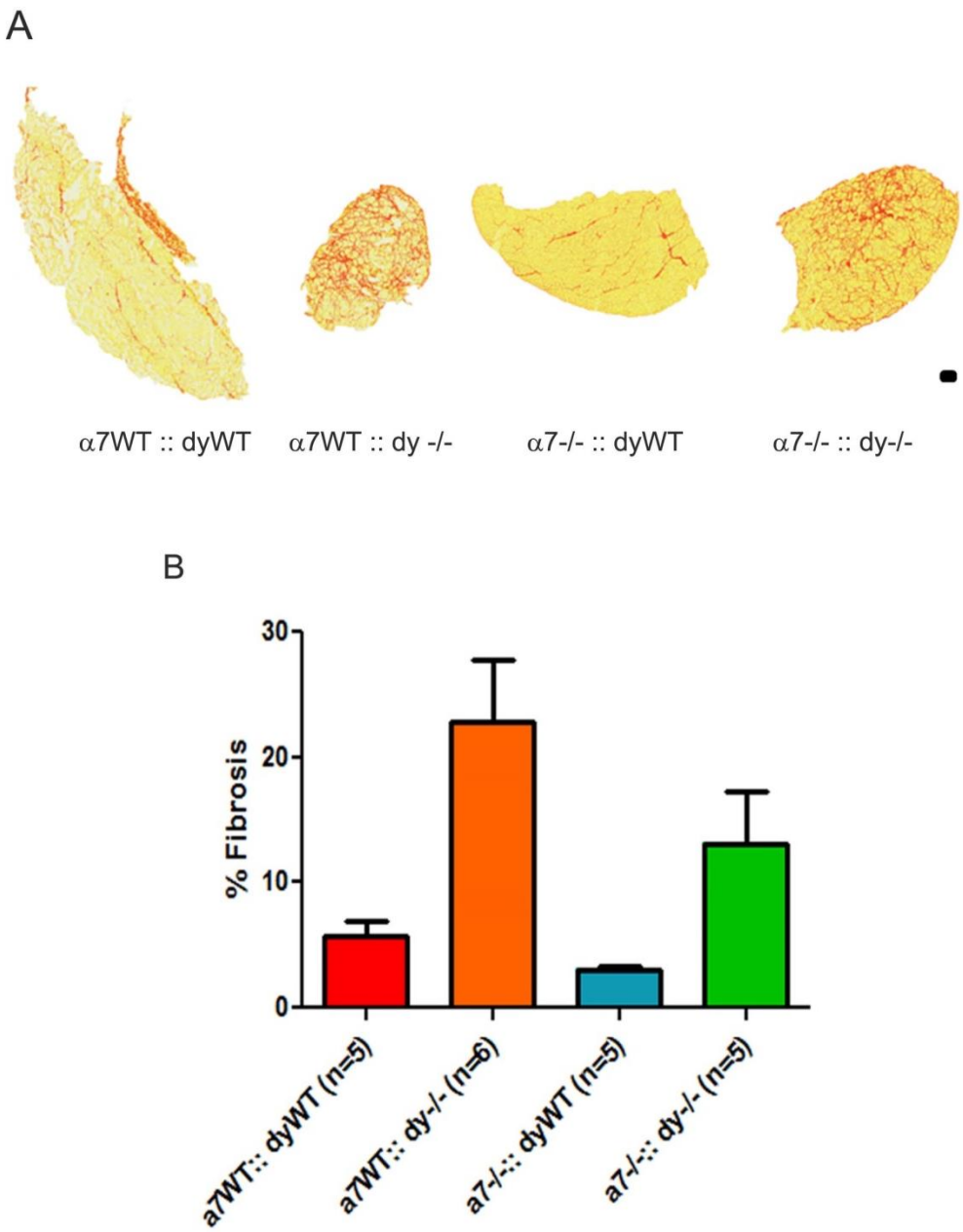

Figure 37. Fibrotic tissue analysis within Tibialis Anterior muscle of α7 WT :: dy WT, α7 WT :: dy -/-, α7 -/- :: dy WT, and *α7 -/- :: dy -/-* 10 week old mice

A) Representative TA cryosections stained with Sirius red. Increased red color indicates that there is more fibrotic tissue present. Magnification = 200 X. Scale bar = 200 µm. B) Sirius red staining was carried out in order to calculate the percentage (%) of fibrotic tissue within TA cryosections shown in Figure 37 A. One-Way *ANOVA* showed statistical significance with *P*-value = 0.0039. Elevated fibrosis is evident for both α7WT:: dy-/- and *α7-/- :: dy-/-* muscle showing that loss of laminin-α2 alone is sufficient enough to cause a fibrotic environment.

C

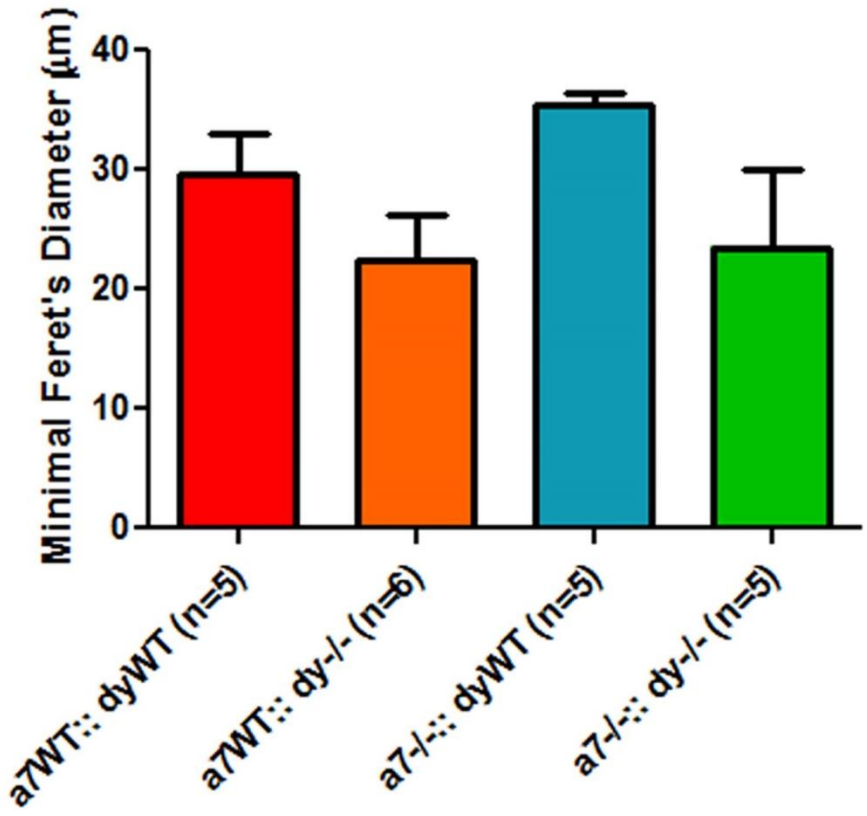

Figure 37. Fibrotic tissue analysis within Tibialis Anterior muscle of α7 WT :: dy WT, α7 WT :: dy -/-, α7 -/- :: dy WT, and *α7 -/- :: dy -/-* 10 week old mice

C) Minimal Feret's diameter was also calculated for muscle groups shown in Figure 37 A. Minimal ferret's diameter is used to measure the size of myofibers. One-way *ANOVA* resulted in *P*-value = 0.1454 and therefore no statistical significance was found. Interestingly, α7WT:: dy-/- and *α7-/- :: dy-/-* muscle showed similar myofiber sizes.

Chapter VI

Conclusions and Future Directions

The main hypothesis of this dissertation is that laminin-111 can act as an effective replacement protein therapy for the loss of laminin-α2 in *dy^{W}-/-* (MDC1A) and indeed dystrophin in *mdx* (DMD).

Patients with MDC1A are usually diagnosed after disease onset. Because systemic laminin-111 treatment was able to have many beneficial effects before disease onset (previously published), we therefore carried out this study to investigate whether laminin-111 protein would be able to have the same beneficial effects when treatment was started after disease onset in the *dy^{W} -/-* mice. Chapter 2 discusses laminin protein therapy after disease onset.

Laminin-111 treatment was effective in reducing percentage (%) muscle fatigue in 8 week old *dy^{W}-/-* mice. Our studies suggest that treatment with laminin-111 after disease onset had a minimal effect to improve the overall integrity of the muscle whilst helping to reduce scar tissue formation. This in turn helped to minimally improve activity of these animals post-treatment after disease onset. This study would be a step towards trying to link what happens at the patient bedside to one of the current mouse models used to study this disease. As with all scientific studies it is important that they correlate to what is currently experienced in the medical field. Results from this study along with an understanding of laminin-111 pharmacokinetics will help pave the way in developing this protein as an exciting potential therapeutic for MDC1A patients.

Recently we have shown that EHS derived mouse laminin-111 protein can act as a substitution therapy in laminin-α2 deficient mice [142]. Our studies showed

that *dy*^{W}*-/-* mice treated with laminin-111 showed reduced muscle pathology, maintained muscle strength and dramatically increased longevity (Rooney et al., 2012). In this study presented in Chapter 3, we investigated the transcriptional changes that occur during disease progression within diaphragm muscle of the *dy*^{W}*-/-* mouse model of MDC1A. We also examined how treatment with laminin-111 protein before disease onset altered transcriptional changes in the diaphragm muscle to identify on-target and off-target drug action.

Using RNAseq technology we were able to show that more than 800 transcripts were altered as a result of disease progression in the diaphragm muscle of 2 week old *dy*^{W} *-/-* mice. Our studies showed that at 2 weeks of age transcript variability in the diaphragm muscle between animals is low. At 5 weeks of age there is significant variability in transcript abundance in the diaphragm muscle between animals. Laminin-111 treatment reduced the number of transcripts that changed and we identified several specific transcripts that changed as a result of laminin-111 treatment.

These RNA-Seq experiments helped us to identify osteoactivin (GPNMB) as a novel biomarker of MDC1A disease progression. Given the transcript and protein level changes in Osteoactivin observed during disease progression in the *dy*^{W} *-/-* mouse model, we next wanted to confirm that this occurred on patient muscle. Immunofluorescence for Osteoactivin using muscle from an MDC1A patient and unaffected control showed that Osteoactivin is normally located in the extracellular matrix in unaffected muscle, but in the MDC1A muscle it is localized within the muscle cells. This may cause misregulation of MAPK signaling (and

potentially activation of TGF-beta and fibrotic pathways) in muscle cells. Although laminin-111 treatment did not change transcript levels, treatment in mice appears to restore normal localization of Osteoactivin in skeletal muscle and therefore would potentially restore MAPK signaling in muscle and prevent further fibrosis.

Our results also reemphasized the role of Galectin-3 as a biomarker in this disease. Laminin-111 treatment also helped to restore many sarcolemmal proteins and improved muscle function by reducing muscle fibrosis. Laminin-111 treatment is likely acting to stabilize proteins and is not altering signaling pathways in skeletal muscle to a great extent. Laminin-111 helps to strengthen and reinforce the sarcolemma in the *dy*^{W}*-/-* mouse during prolonged progressive muscle injury induced by contraction offering a protective niche against the occurrence of this degenerative scenario by reducing inflammation, fibrosis and apoptosis via improved matrix-mechanotransduction. Significant changes may be being masked by huge misregulation in individuals. This study may help to pave the way in teasing out the molecular pathways associated with MDC1A disease progression and treatment. In this study we show that loss of laminin-211/221 in the diaphragm muscle of mice results in a large number of transcript changes that may serve as markers for disease progression and to report the efficacy of potential therapies.

Future avenues of research experiments will include continued evaluation and individual mouse transcriptome confirmation of the RNA-seq data to identify a set of genes misregulated in all animals. For this analysis we will focus on the 2-week and 5-week Wild-type versus untreated *dy*^{W} *-/-* data. Genes which are

altered early in the process will be evaluated during embryogenesis (for example Osteoactivin). Immunofluorescence will be used to confirm altered protein levels in skeletal muscle of

Chapter 4 looks at long term laminin treatment of *mdx* mice. The lack of significance in the results for laminin treated animals could reflect the fact that the *mdx* mice have no overt dystrophic phenotype after 10 weeks of age. However, there was elevated EBD uptake and increased kyphosis within PBS treated animals. Laminin treatment helped to reduce muscle hypertrophy at 10 weeks old. Treatment also reduced muscle fatigue experienced and there was an increase in the sarcolemmal protein, β-DG. There may be a better result in delivering laminin-111 in a cocktail recipe of additional therapeutic drugs in order to have a more improved effect. Future directions will include assessing TA muscle via immunoblotting for any change in the abundance of sarcolemmal proteins that are related to the dystrophin-glycoprotein laminin-binding complex after treatment compared to PBS controls. These proteins will include the dystroglycans, sarcoglycans and sarcospan. Immunofluorescence will also be used on the same TA muscle in order to confirm the immunoblot results.

The rhLam-111 recombinant protein is still in the early stages of trial production and it is difficult to produce due to its large size (~900 kDa). Various avenues of human laminin-111 production were explored to date. The main method of production of human recombinant laminin (rhLAM-111) involved transient transfection with laminin- α1 into a stable CHO_S cell line that produced

the –β and –γ chains of laminin. Talon technology could be used in order to knockout hamster α-4 and α-5 produced by the CHO_S cells. However, the purification protocol may have precipitated out most of the laminin-111 with which we are interested. The exact concentration of hrLAM-111 will need to be determined. A new strategy has been devised in order to generate a huge batch of hrLAM-111 with the CHO_S system and the resulting media will be harvested and sent for FPLC purification.

The α7β1 integrin is an important transmembrane cell surface receptor in skeletal, cardiac and vascular smooth muscle. Laminin- α2 is an important binding partner for α7 integrin. It connects the extracellular matrix to the integrin on the sarcolemma. α7 integrin plays an important role in cell signaling as it binds to talin and cystoskeletal F-actin. Laminin-integrin binding complex helps to transduce external mechanical stresses involved with muscle contraction and connect them with a cellular response via signaling. Disruption of these components causes neuromuscular disease in both humans and mice. This emphasizes the importance of this binding complex in maintaining the integrity of the sarcolemmal to withstand the mechanical forces associated with muscle contraction. Transgenic overexpression of α7 integrin in skeletal muscle in previous studies demonstrated that overexpression can help partially rescue the disease phenotype and extend the lifespan of the mice.

Similar to how experimental animals were designed as double knockouts to lack both dystrophin and α7 integrin (*mdx*/*α7*$^{-/-}$) and resulted in a more severe

phenotype than single knockout animals, a double knockout of both laminin-α2 and α7 integrin was created in order to study the full extent to which α7 integrin plays in laminin-α2 deficient muscle. Chapter 5 studies the new mouse model α7 integrin -/-:: laminin-α2 -/- double knockout for muscular dystrophy. Together these results suggest that both α7 integrin and laminin- α2 play critical roles in maintaining proper function of skeletal and cardiac muscle. This study analyzes the effects on skeletal and cardiac muscle with severe kyphosis and atrial fibrillation occurring within this new double knockout mouse model. There was also elevated scar tissue deposition within cardiac muscle and embryonic lethality experienced.

The severe embryonic lethality of double knockout *α7-/-:: dy-/-* mice furthers previous knowledge and emphasizes the importance of α7 integrin in rescuing the loss of laminin-α2. The duplicity of their bi-directional relationship of protecting the structural and functional integrity of muscle is very much highlighted in the generation of this double knockout double knockout mouse model. We observed severe muscle pathology in 10 week old *α7-/-:: dy-/-* mice which is a new result for this field of study as no one has ever created this double knockout mouse model. Absence of both proteins in *α7-/-:: dy-/-* mice results in severe skeletal and cardiac muscle degeneration, reduced functional activity and fibrotic scar tissue deposition. Here, compensation by α7 integrin helps these mice to maintain functional integrity.

The *α7-/-:: dy-/-* mice analyzed in this study exhibit a phenotype similar to that of single knockout of α7 integrin. This phenotypic similarity between these two genotypes suggests that there is functional overlap in the role of α7 integrin in maintaining muscle structure and function. Double knockout *α7-/-:: dy-/-* mice exhibit a hugely severe cardiac phenotype suggesting that both α7 integrin and laminin-α2 are very critical to cardiac muscle function by their presence. It also suggests there is no active sarcolemmal complex able to cope and compensate for the loss of both of them. Therefore, the heart is not able to pump efficiently in a coordinated manner and we see the atrial fibrillation occurring.

The *α7-/-:: dy-/-* mouse is a new mouse model for muscular dystrophy that has been identified which lacks both α7 integrin and laminin-α2. This has never been studied before in the dy^W mouse model[173]. Further investigation will reveal the effects on pathophysiology and expression of sarcolemmal proteins. Future directions will include TA, heart and diaphragm tissue being assessed via immunoblotting for any changes in the abundance of proteins that are related to the dystophin-glycoprotein laminin binding complex. These proteins will include dystroglycans, sarcoglycans, sarcospan, integrin-linked kinase and AKT. Immunofluorescence will be used on the same TA, heart and diaphragm muscle in order to confirm the immunoblot results.

Results from characterization of this new α7 integrin / laminin-α2 dko mouse model will aid in understanding the exact role that α7 integrin and laminin-

α2 play in MDC1A. It will also potentially help with the identification of novel therapeutic targets for this devastating neuromuscular disease.

This dissertation provides evidence that laminin-111 is beneficial with treatment before disease onset by reducing muscle pathology and increasing functional activity within mice. It is also the first time that the α7 integrin -/-:: laminin-α2 -/- double knockout mouse model has been studied and described for this particular *dy*^{W}*-/-* mouse model.

Appendix A

Laminin-111 pharmacokinetics/ pharmacodynamics and rhLam-111 production

MATERIAL AND METHODS

EHS mLAM-111

Engelbreth-Holm Swarm mouse laminin-111 supplied at 1 mg in 50 mM Tris-HCL (pH 7.4), 0.15 M NaCl was used to treat mice. The laminin was thawed slowly overnight at 4°C.

Generation of laminin-111 DNA

DNA for rhLAM-111 transfection into the CHOs system was prepared and cleaned via illustra plasmidPrep Midi Flow kit (GE Healthcare). It had to be RNased via the RNAeasy kit following manufacturers guidelines. The α chain was on one plasmid and β & γ chains on the second plasmid. The plasmids had to be linearized before transfection into the CHOs cells. Lipofectamine transfection reagent was needed and DNA had to be purified in order to perform the transient transfections into the naïve CHO_S cell system in order to harvest a huge batch of rhLam-111 media to be sent for FPLC purification. A key note with regards to the previous attempt is that any rhLAM-111 protein that had been produced may have degraded before harvest during the seven day experiment which was at 37 °C. So far I have performed MIDI preps, extracted and purified both α and β & γ DNA in preparation for transfection. However, the DNA yield has been low due to their large size. Therefore, more reagents will be needed in order to grow and purify more DNA that is necessary for large scale rhLAM-111 production.

Purification of recombinant human laminin-111 protein

rhLam-111 protein was concentrated and then was dialyzed in Tris buffered Saline (TBS).

Silver staining

ProteoSilver Stain kit (Sigma) was used to stain after SDS-PAGE gel electrophoresis. Gels were fixed for 20 minutes then subject to a 10 minute 30% ethanol wash, 10 minute water wash. After this step, the gels were immersed in sensitizer solution for 10 minutes, the gels were then washed for 10 minutes and put into silver solution for 10 minutes. There was then a water wash and gel development before stop solution was finally added.

Coomassie Staining

Coomassie staining was performed using a Fairbanks Quick coomassie staining protocol.

Immunoblotting

Protein was harvested from CHOs cell media. Proteins were separated via 4% SDS-PAGE gel electrophoresis with no stacking gel. They were then transferred to nitrocellulose membrane and blocked with (carnation milk) for 1 hour. Proteins were incubated with primary antibody overnight before being incubated with secondary antibody (1 hour) and washed with 1X TBST buffer. Protein sizes were: α 400 kDa, β 200 kDa & γ 180 kDa. Proteins were imaged using the Licor Odyssey system after detection with Laminin α-1 (H-300): sc

5582, Laminin β-1 (H-300): sc 5583, and Laminin γ-1 (H-190): sc-5584 (Santa Cruz) antibodies.

Generation of mice

Laminin-α2 -/- mice

All experiments involving mice were performed under an approved protocol from the University of Nevada, Reno Institutional Animal Care and Use Committee. The *dy*^{W}+/- mice were a gift from Eva Engvall via Paul Martin (The Ohio State University, Columbus, OH, USA). Male and female heterozygous mice were bred. In order to genotype mice, genomic DNA was isolated from tail snips or ear notches using a Wizard SV DNA purification system (Promega, Madison, WI) following manufacturers instructions. To detect the mutation in the laminin- α2 gene, the following primers were used: DYWF (5'-ACTGCCCTTTCTCACCCACCCTT-3'), LAMA2exonR1 (5'-GTTGATGCGCTTGGGAC-3') and Lac/ZR2 (5'-GTCGACGACGACAGTATCGGCCTCAG-3'). PCR conditions were as follows: 95°C for 5 minutes then 33 cycles of 94°C for 20 seconds, 62°C for 30 seconds and 72°C for 45 seconds. After these cycles, then 72°C for 10 minutes. A wild-type band was 250 bp whereas the laminin- α2 targeted allele produced a 480 bp band.

Experimental procedures were performed once mice were 10 days and 2 weeks of age with weekly weighing until the end of study which was at 2 weeks and 5 weeks of age where all mice were subject to *in vivo* experiments. To

reduce experimental bias, investigators assessing and quantifying experimental outcomes were blinded to the treatment and control groups.

Mdx mice

The mutation in the dystrophin gene was detected using a modified ARMS assay. The following primers were used: p259E (5'GTCACTCAGATAGTTGA AGCCATTTAA-3'), p260E (5'-GTCACTCAGATAGTTGAAGCCATTTAG-3') and p306F (5'-CATAGTTATTAATGCATAGATATTCAG-3'). PCR conditions were as follows: 95°C for 4 minutes then 34 cycles of 95°C for 1 minute, 55°C for 1 minute and 72°C for 1 minute. Primer set p259 and p306 produced a 275 bp wild-type dystrophin allele. Primer set p260 and p306 detects the *mdx* point mutation which produced a 275 bp product. To genotype the dystrophin gene, separate PCR reactions were performed since the product sizes are identical in wild-type and *mdx* mice.

Husbandry

dy^{W}-/- mice and *mdx* were housed with their wild-type littermates alongside the provision of mashed kibble and access to water. Husbandry and protocols were carried out via IACUC approval. Knockout mice that lost ≥ 20% body weight (g) were euthanized. Pups were genotyped at 10 days old and at the end of each study, the female WT and dy^{W}-/- mice were euthanized by CO_2 inhalation in accordance with a protocol approved by the University of Nevada, Reno Animal Care and Use Committee. The diaphragm muscles from these mice

were dissected, flash-frozen in liquid nitrogen and stored at -80°C as previously reported by [134].

Treatment with rhLam-111 and EHS mLam-111in *dy^{W}-/-*

Female *dy^{W}-/-* mice were systemically injected at 11 days old weekly with 0.01mg/g of rhLam-111 or EHS mLam-111 until they were 5 weeks old. Control littermate *dy^{W}-/-* mice were injected with the equivalent volume of sterile Tris buffered saline (TBS). Male *dy^{W}-/-* mice were systemically injected at 2 weeks old weekly with 0.01 mg/g of rhLam-111 or EHS mLam-111 until they were 10 weeks old. Control littermate *dy^{W}-/-* mice were injected with the equivalent volume of sterile Phosphate buffered Saline (PBS).

Pharmacokinetic Intramuscular *in vivo* Imaging

Intramuscular Injection with DyLight-488nm labelled laminin-111 was at the same volume that would be administered as if giving a 0.01 mg/g systemic injection. The IVIS system (XENOGEN, VivoVision systems, CA) was employed to image the mouse post-intramuscular injection.

Muscle Strength

Muscle strength assessed at 5 weeks & 10 weeks of age for male mice using the Chatillon DFE Digital Force Gauge (San Diego Instruments Inc., San Diego, CA). A total of six measurements per mouse were recorded and all results averaged for each group. The mice were analyzed by grasping a horizontal

platform with their forelimbs and pulled backwards. The peak tension (grams of force) was recorded on a digital force gauge as mice released their grip.

ELISA

For Pharmacokinetic analysis of laminin-111, systemic injection of EHS mLAM-111 in *dy^{W} -/-* and *mdx* mice was followed by retro-orbital bleeds performed at various time points (0 min, 30 min, 1 hour, 2 hour, 4 hour, 8 hour and 24 hour). An ELISA designed to detect the laminin-α1 chain demonstrated that laminin-111 had a half-life of ~90 minutes within the serum of *dy^{W}-/-* mice. The protein was cleared from the bloodstream much more quickly than that of the WT littermate controls. This phenomenon suggests that the laminin-a2 deficient muscle is much more leaky and therefore requires laminin-111 to help stabilize the sarcolemma and provide protection against the sheer stresses of mechanotransduction. Labeled EHS mLAM-111 was detected 18 hours post-intramuscular injection.

Hematoxylin and Eosin staining

Tibialis Anterior muscle was cryosectioned and 10 µm sections were placed on surgipath microscope slides. Tissue sections were fixed with ice-cold 95 % ethanol for 2 minutes followed by 70 % ethanol for 2 minutes and then re-hydrated in running water for 5 minutes. Gill's hematoxylin (Fisher Scientific, Fair Lawn, NJ) was then used to stain the sections and rinsed in water for 5 minutes. Scott's solution (0.024 M $NaHCO_3$, 0.17 M $MgSO_4$) was then applied for 3

minutes and rinsed in water for 5 minutes. Tissue cryosections were then immersed in eosin solution (Sigma-Aldrich, St. Louis, MO) for 2 minutes. Sections were then dehydrated in ice cold 70 % and 95 % ethanol for 30 seconds each, followed by 100 % ethanol for 2 minutes. Xylene was then used to clear the sections for 5 minutes prior to mounting with DepeX mounting medium (Electron Microscopy Services, Washington, PA). Centrally located Nuclei were counted from images composing representative montages for each mouse. Images were assessed at 200 X magnification by bright field microscopy. The number of centrally located nuclei per muscle fiber was determined by counting each image which contributed to myofibers being counted per treatment group. At least 4 animals from each treatment group were analyzed.

Statistical Analysis

All averaged data are reported as the mean ± s.d. P-values of < 0.05 were considered to be statistically significant.

RESULTS

Laminin-111 half-life calculation for *dy^{W}-/-* mice

The ELISA results for the half-life of laminin-111 (Figure 38) revealed that once intraperitoneally injected laminin remains in the serum of WT mice for 120 minutes whereas *dy^{W}-/-* serum retains the laminin for 90 minutes. The protein was cleared from the bloodstream much more quickly than that of the WT littermate controls. This phenomenon suggests that the laminin-a2 deficient

muscle is much more leaky and therefore requires laminin-111 to help stabilize the sarcolemma and provide protection against the sheer stresses of mechanotransduction. One has to ponder over where the laminin is going. Pharmacodynamic studies will need to be employed to help answer these questions.

Laminin-111 Half-life calculation for *mdx* mice

The laminin-111 half-life worked out to be 140 minutes for WT mice and only 50 minutes for *mdx* mice before it was cleared out of the serum (Figure 39). The n numbers were good at n=3 each treatment group.

EHS mouse Laminin-111 detection in a WT CD1 mouse 18 hrs post-intramuscular injection

The IVIS system was utilized after EHS mLam-111 had been labelled with Dylight-488. The labelled laminin was then intramuscularly injected into the tibialis anterior muscle of a WT CD1 mouse (Figure 40). Laminin was detected up to 18 hours post-injection showing that laminin-111 had a long half-life when injected directly into target muscle.

rhLAM-111 DNA for CHOs cells

DNA for rhLAM-111 was purified in preparation for transfection into the CHOs system was cleaned (Figure 42). It had to be RNased. α was on one plasmid and β & γ chains on the second plasmid. The plasmids had to be linearized before transfection into the CHOs cells. However, the DNA yield has

been low due to the large size of each plasmid. Therefore, more reagents will be needed in order to grow and purify more DNA that is necessary for large scale rhLAM-111 production.

rhLam-111 protein production verification and quality control

Silver staining is an extremely sensitive method with which showed the purity of rhLam-111 protein produced from the CHOs system (Figure 43). Immunoblotting revealed that all three chains of laminin-111 (α, β, & γ) were able to be produced after transfection and were demonstrated via separate immunoblots. The control used was manufactured human laminin-111. Fairbanks coomassie staining was used as a second verification to look at the total number of proteins in the cell supernatant of the rhLam-111 CHOs media compared to naïve media. Controls used included supernatant from the dialysis of rhLam-111 and CHOs naïve dialyzed media.

Clustering and cell adhesion assays

rhLaminin-111 in a 100 nM concentration was able to form neuromuscular junctions (NMJs) in clustering assays of differentiated C2C12 cells (Figure 44) and rhLam-111 proved to be more adherent to *mdx* myoblasts compared to WT C2C12 myoblasts in cell adhesion assays[187].

Immunofluorescent detection of laminin-111

After systemic treatment both mouse laminin-111 and human recombinant laminin forms were able to be detected in *dy^{W}-/-* Tibialis anterior muscle (Figure

45). This showed that the rhLAM-111 was able to be delivered systemically to the target muscle of interest.

Functional assessment of *dy^{W}-/-* mice treated with laminin

There was no real significant difference in the functional activity of mice treated with EHS mLam-111 compared to mice treated with rhLam-111 (Figure 46). This could mean that this study needs more n numbers to comment further. More pure rhLam-111 needs to be produced.

Integrin immunoblotting after laminin-111 treatment

rhLam-111 was not effective in producing the same effects as EHS mLaminin-111 on α7A or α7B integrin in *dy^{W}-/-* mice treated with the recombinant protein (Figure 47).

Histological analysis of laminin treated *dy^{W}-/-* mice

There was no difference regards muscle pathology between EHS mLam-111 treated and rhLam-111 treated animals (Figure 48). However there was a trend towards WT for rhLam-111 treatment regards increased minimal feret's diameter measurements. Laminin-111 treatment, especially rhLam-111 was able to increase myofiber size.

Immunological response to laminin-111 treatment

With the rhLAM-111, we tested whether there was any immunogenicity whenever it was injected systemically into the *dy^{W}-/-* mouse every week from 2

weeks old up to 5 weeks old (Figure 49). It had already been contemplated that other contaminating proteins in the rhLAM-111 coupled with the fact that human protein injected into a mouse could elicit an immune response especially during a 3 week experiment. An ELISA was performed on the harvested serum from these mice alongside WT, PBS and EHS mLAM-111 treated littermate controls. Preliminary results showed that there was an immune response elicited towards the injected hrLAM-111 upon the detection of elevated IgG antibodies in the serum of these mice.

hLam-111 transgenic mouse production

Gawlik *et al.* 2004 demonstrated feasibility of transgenic expression in dy^{W}-/- mice by generation of Laminin-α1 dy^{W}-/- mice. Recently, the Burkin lab has been able to generate transgenic founder mouse lines positive for human Laminin-α1, β1 and γ1 chains (Figure 50). This transgenic overexpression of Laminin-111 will be included within the study in order to investigate the most exaggerated effect due to the presence of Laminin-111.

DISCUSSION

These were disappointing results for rhLam-111 *in vivo* trials but it is important to remember that this recombinant protein is still in the early stages of trial production and it is difficult to produce due to its large size (~900 kDa). Various avenues of human laminin-111 production were explored to date. The

main method of production of human recombinant laminin (hrLAM-111) involved transient transfection with laminin- α1 into a stable CHO_S cell line that produced the –β and –γ chains of laminin. This transfection proved successful in that immunblotting performed on the media harvested showed that all three chains of LAM-111 were present. Talon technology could be used in order to knockout hamster α-4 and α-5 produced by the CHO_S cells. However, the purification protocol may have precipitated out most of the laminin-111 with which we are interested. The exact concentration of hrLAM-111 will need to be determined. A new strategy has been devised in order to generate a huge batch of hrLAM-111 with the CHO_S system and the resulting media will be harvested and sent for FPLC purification.

ACKNOWLEDGEMENTS

I would like to thank Dr. Mark Hubbard, Dr. Breeana Hubbard and Dr. Ryan Wuebbles for their technical assistance in the design of the CHO_s system and ELISA experiments. I would also like to thank Apurva Sarathy for the immunofluorescent clustering assay.

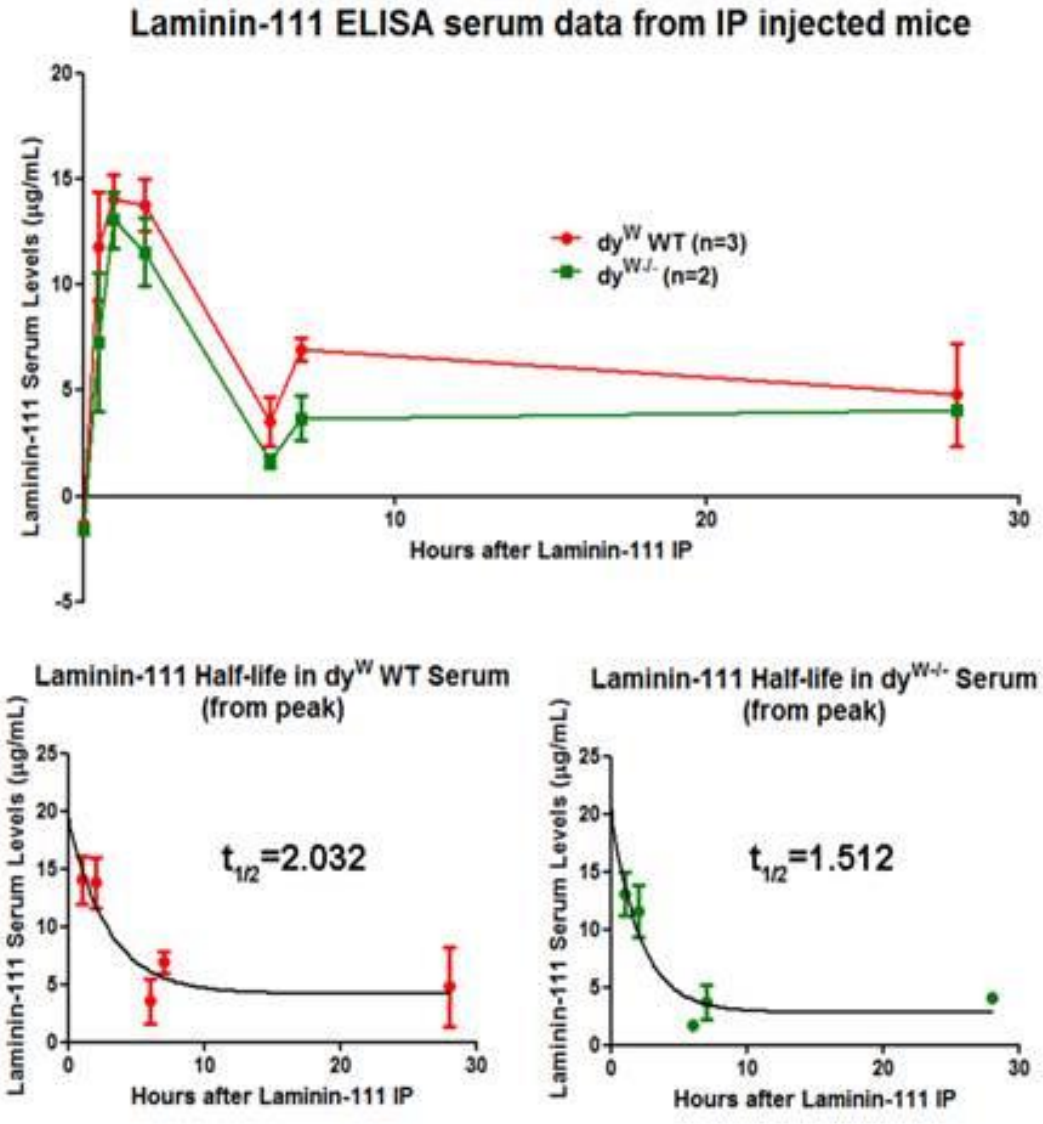

Figure 38. Laminin-111 half-life calculation for *dy^{W}-/-* mice

Half-life of EHS mouse laminin-111 (intraperitoneally injected), was calculated using an ELISA designed to detect laminin-α1 in mouse serum collected over a period of time. This figure was kindly provided by Dr. Ryan Wuebbles.

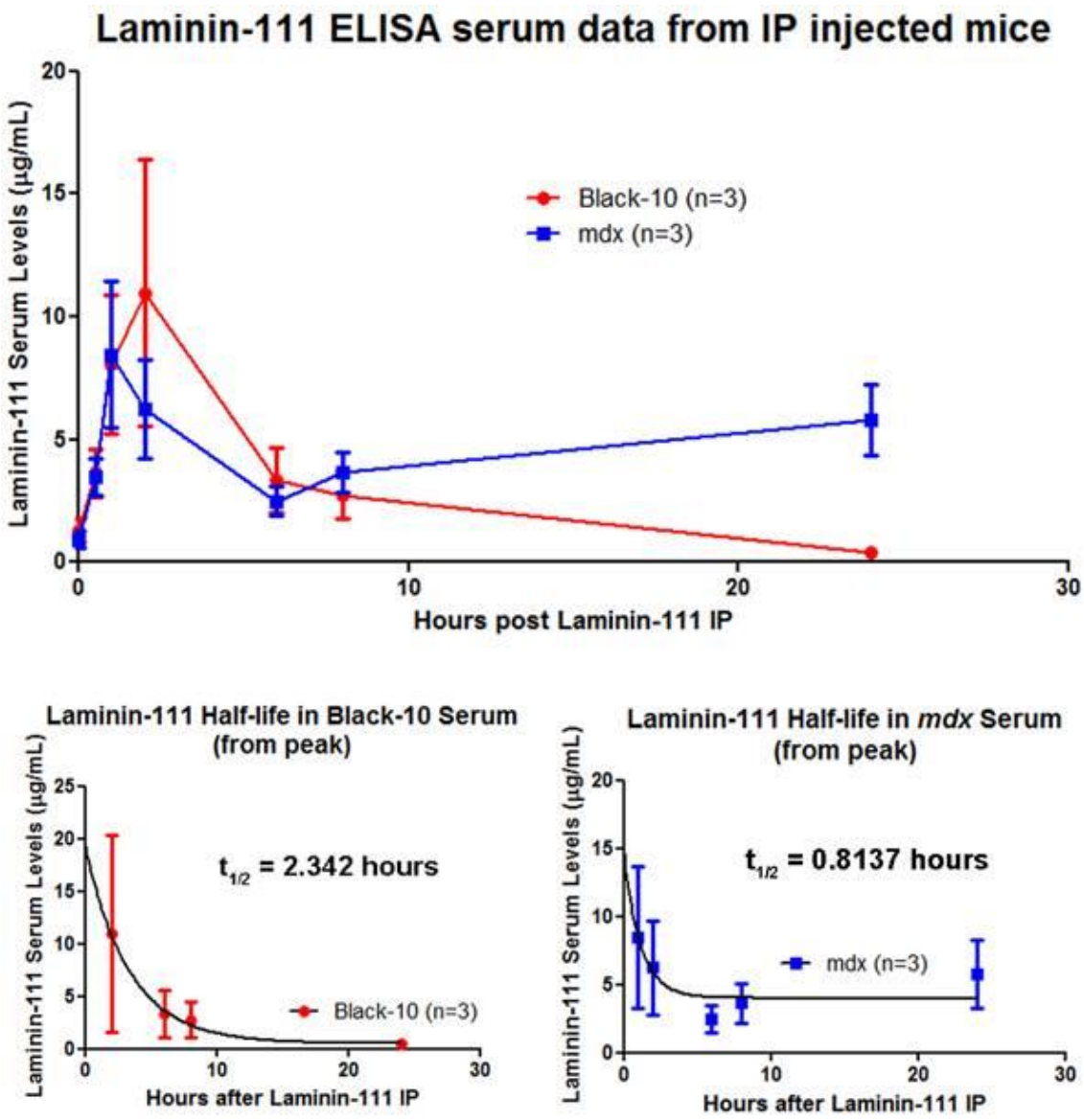

Figure 39. Laminin-111 Half-life calculation for *mdx* mice

Half-life determination performed using Graphpad Prism non-linear regression (curve fit) with exponential one-phase decay from the peak Laminin-111 concentration. A more complete insight into the action of laminin-111 will be achieved by investigating the pharmacokinetics and pharmacodynamics of laminin-111 administered to *mdx* mice. Pharmacokinetics involved collecting

serum (30 min, 1 hour, 2 hour, 4 hour, 8 hour, 24 hour, 48 hour, 72 hour) via retro-orbital bleeds from 5 WT and 5 *mdx* mice injected intraperitoneally (I.P) with 0.01 mg/g mLAM-111. Baseline serum will be collected at 0 hour prior to the initial injection. ELISA assays were carried out on the serum in order to help determine the movement of laminin-111 once it was *in vivo* and how fast laminin-111 can clear out of the lymphatic system. This information will ultimately help decide this protein's mechanism of action alongside the collection of pharmacodynamics data which will involve the collection of tissue at various time points after injection in order to discover how quickly laminin-111 can be delivered to the muscle. This figure was kindly provided by Dr. Ryan Wuebbles.

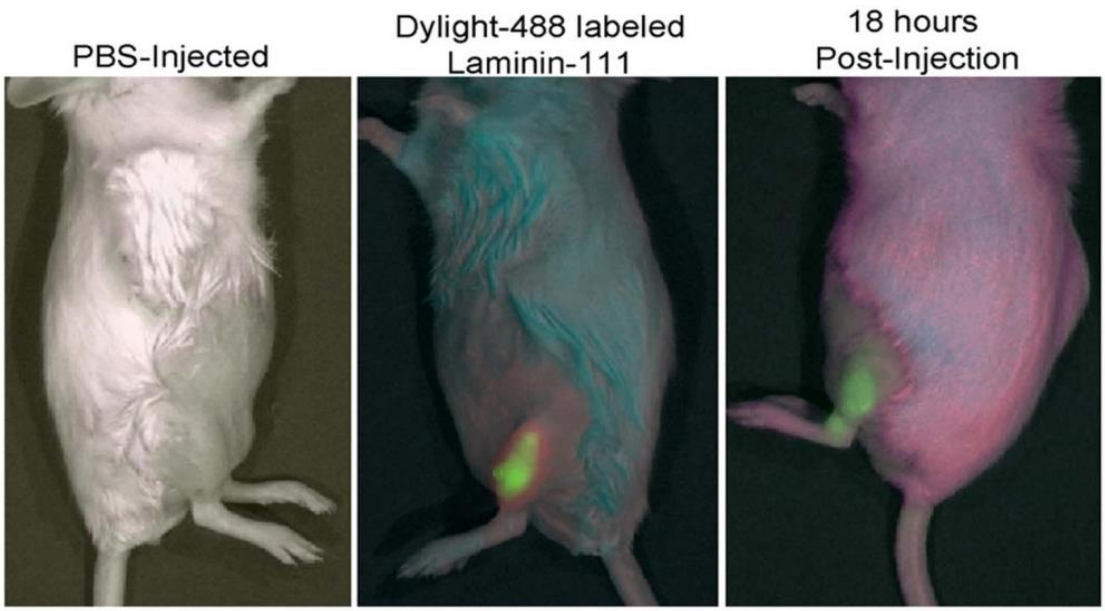

Figure 40. EHS mouse Laminin-111 detection in a WT CD1 mouse 18 hours post-intramuscular injection

Dylight-488 labelled laminin-111 was detected 18 hours post-intramuscular injection using the IVIS Lumina System. Half-life of EHS mouse laminin-111 (intraperitoneally injected), was calculated using an ELISA designed to detect laminin-α1 in mouse serum collected over a period of time. This figure was kindly provided by Dr. Ryan Wuebbles.

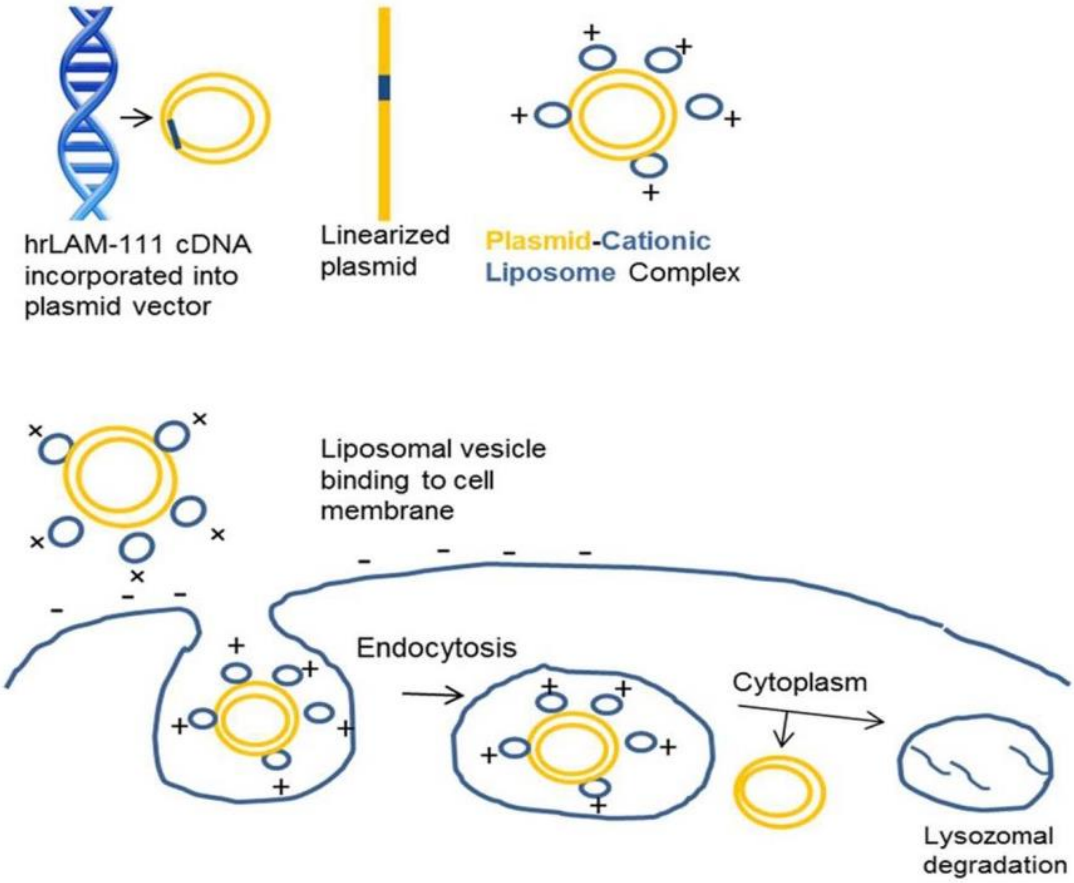

Figure 41. Diagrammatic representation of rhLam-111 production in the CHO_s system

CHOs system was utilized in order to produce rhLAM-111 after transfection with α, β & γ linearized plasmids.

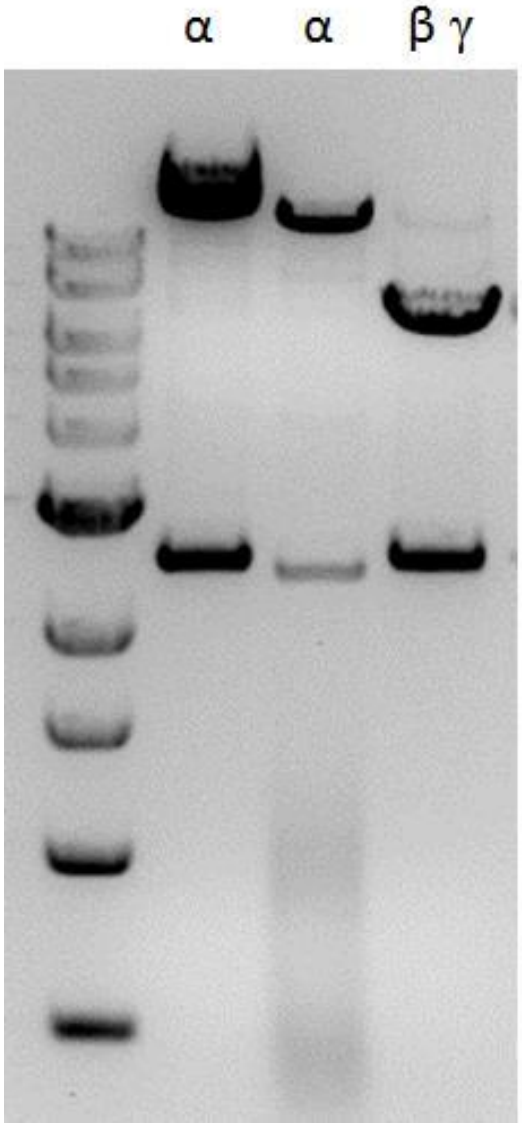

Figure 42. rhLAM-111 DNA for CHOs cells

Recombinant human laminin-111 (α, β, γ) DNA was prepared and cleaned. Confirmation was via Agarose gel electrophoresis. The process of production involved growing naïve CHO_s cells, transfecting them, harvesting the media and sending it for FPLC purification.

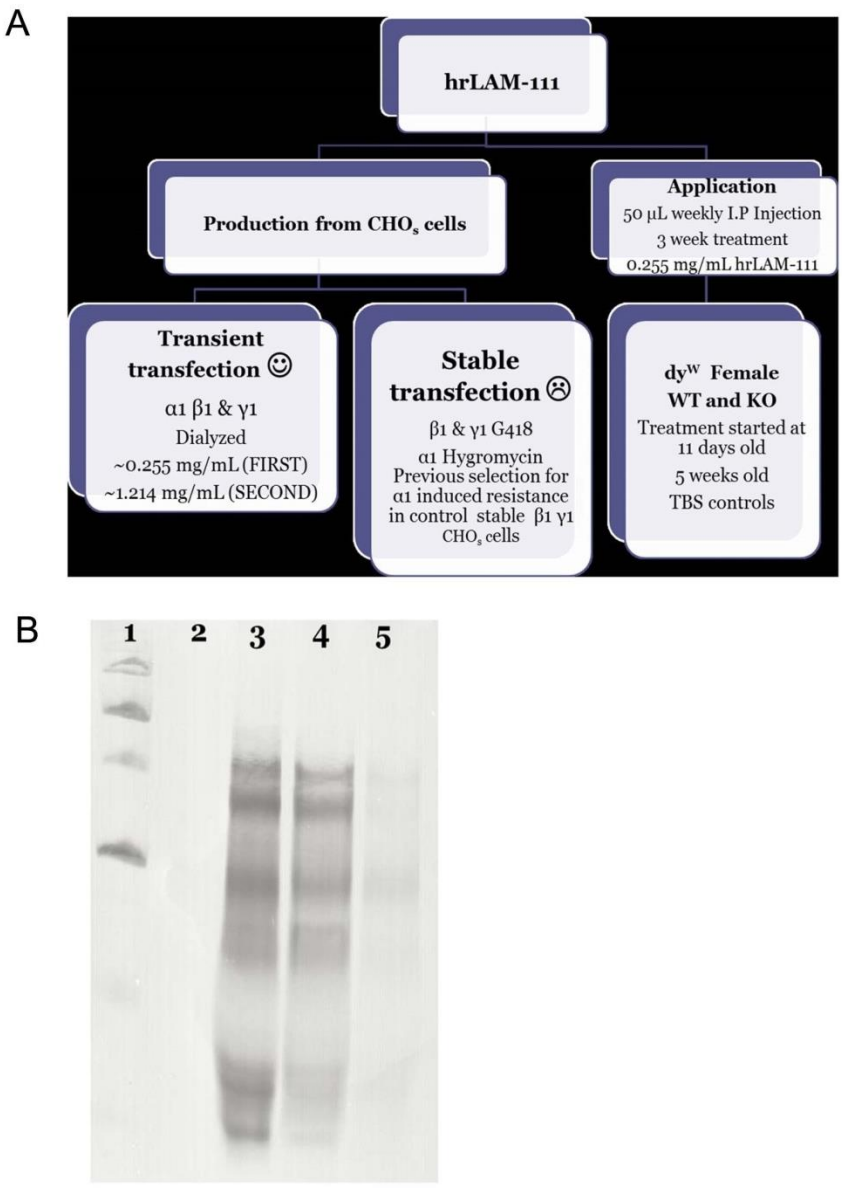

Figure 43. rhLam-111 protein production verification and quality control

A) rhLAM-111 production from CHO_s cells and application for *in vivo* studies. B) Different concentrations of rhLAM-111 protein that was subject to silver staining to help assess its purity.

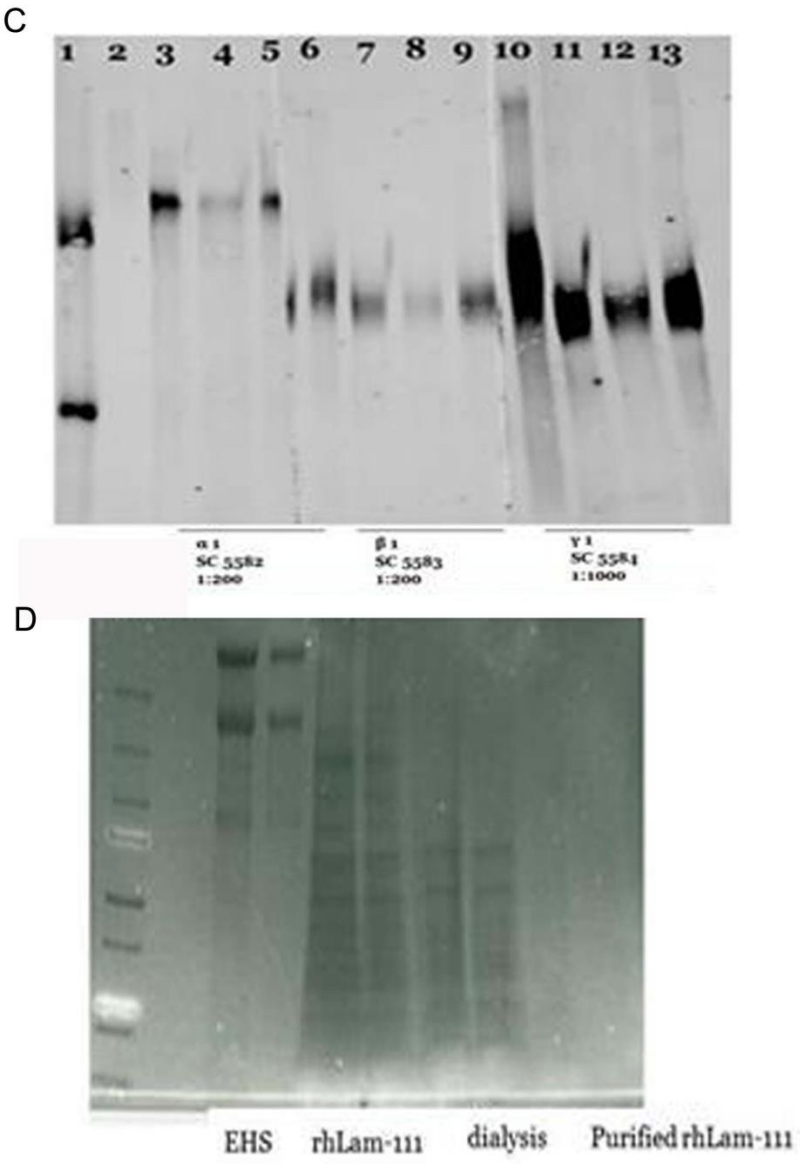

Figure 43. rhLam-111 protein production verification and quality control

C) Immunoblotting helped to confirm the presence of laminin -α1 chain (lanes 3, 4 & 5), –β1 chain (lanes 7,8 &9) and -γ1 chain (lanes 11, 12 &13) in the rhLAM-111 protein produced from the CHO_S system. D) Coomassie staining revealed that lots of the initial rhLAM-111 harvested from the CHO_S system was eventually lost through the dialysis purification process.

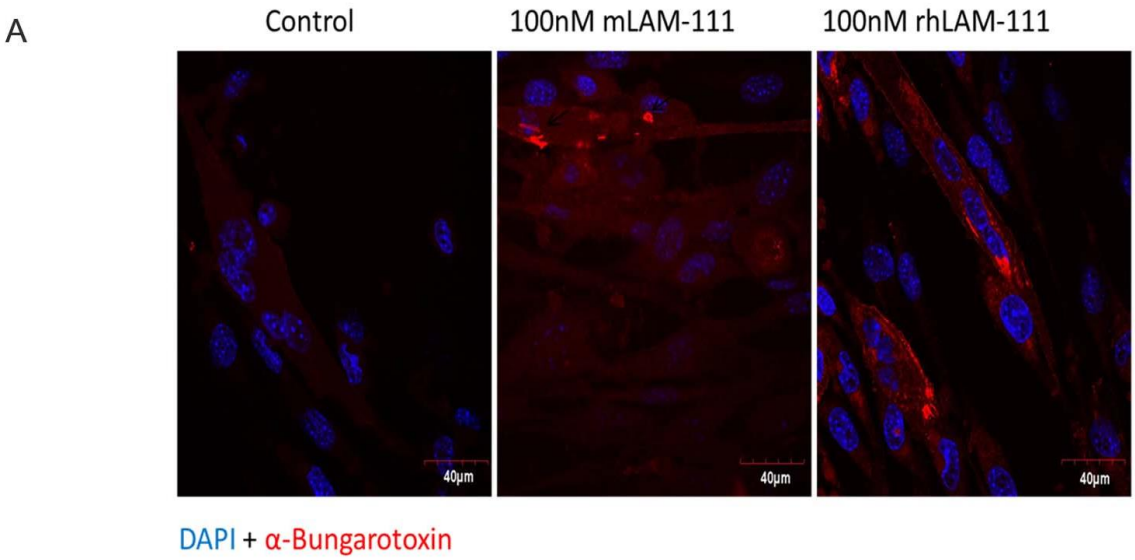

Figure 44. Clustering and cell adhesion assays

A) Clustering assay with detection of α-Bungarotoxin at neuromuscular junctions within C2C12 cells. Laminin-111 treatment aids formation of NMJs and is evident here with punctate red areas. Scale bar: 40 µm. This figure was kindly provided by Apurva Sarathy.

B

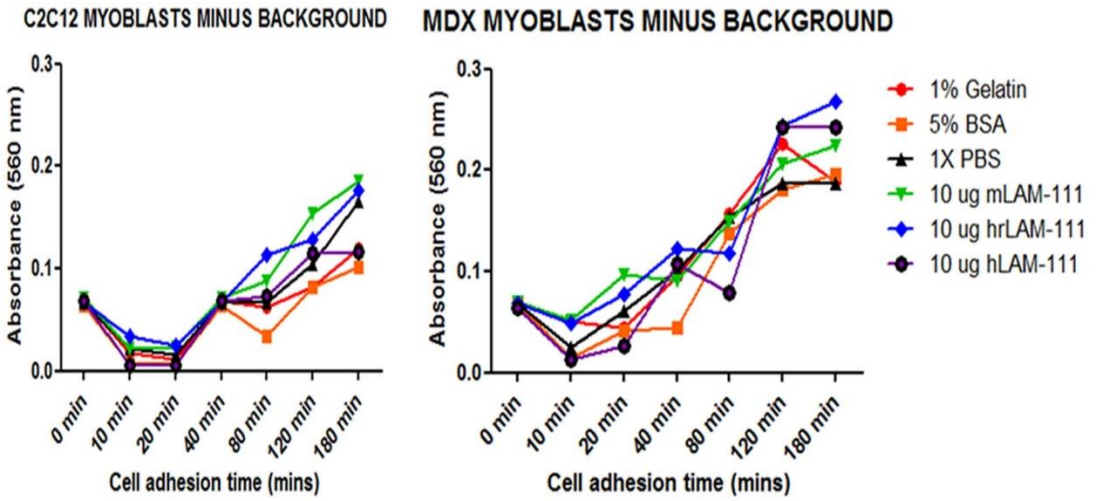

10 ug Laminin-111	C2C12 % adherence compared to 1X PBS
EHS mLAM-111	+ 13.4 %
hrLAM-111	+ 7.4 %
hLAM-111	- 32.8%

10 ug Laminin-111	MDX% adherence compared to 1X PBS
EHS mLAM-111	+ 25.5 %
hrLAM-111	+ 55.9 %
hLAM-111	+ 38.8%

Figure 5. Cell adhesion assay to compare activity of various forms of laminin-111 on C2C12 and *mdx* myoblasts.. (n=1).

Figure 44. Clustering and cell adhesion assays

B) C2C12 myoblasts and *mdx* myoblasts were used in cell adhesion assays to help test how effective the rhLAM-111 protein produced using the CHO_s system was compared to the manufactured EHS mLAM-111 protein. There was no statistical difference evident.

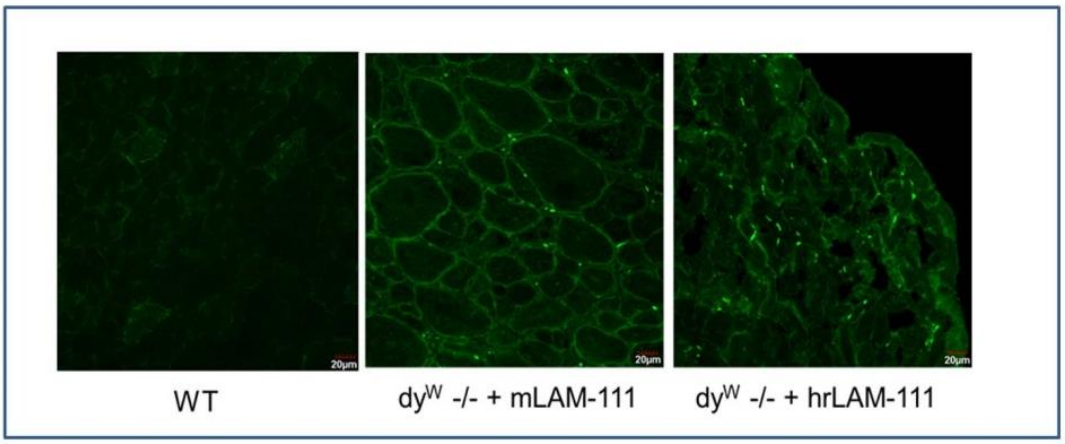

Figure 45. Immunofluorescent detection of laminin-111

Mice were intraperitoneally treated with either mouse Lam-111 or recombinant human Lam-111 produced using the CHO_s system. Laminin-1 (green) was able to be detected via immunofluorescence on the sarcolemma in TA muscle of treated animals.

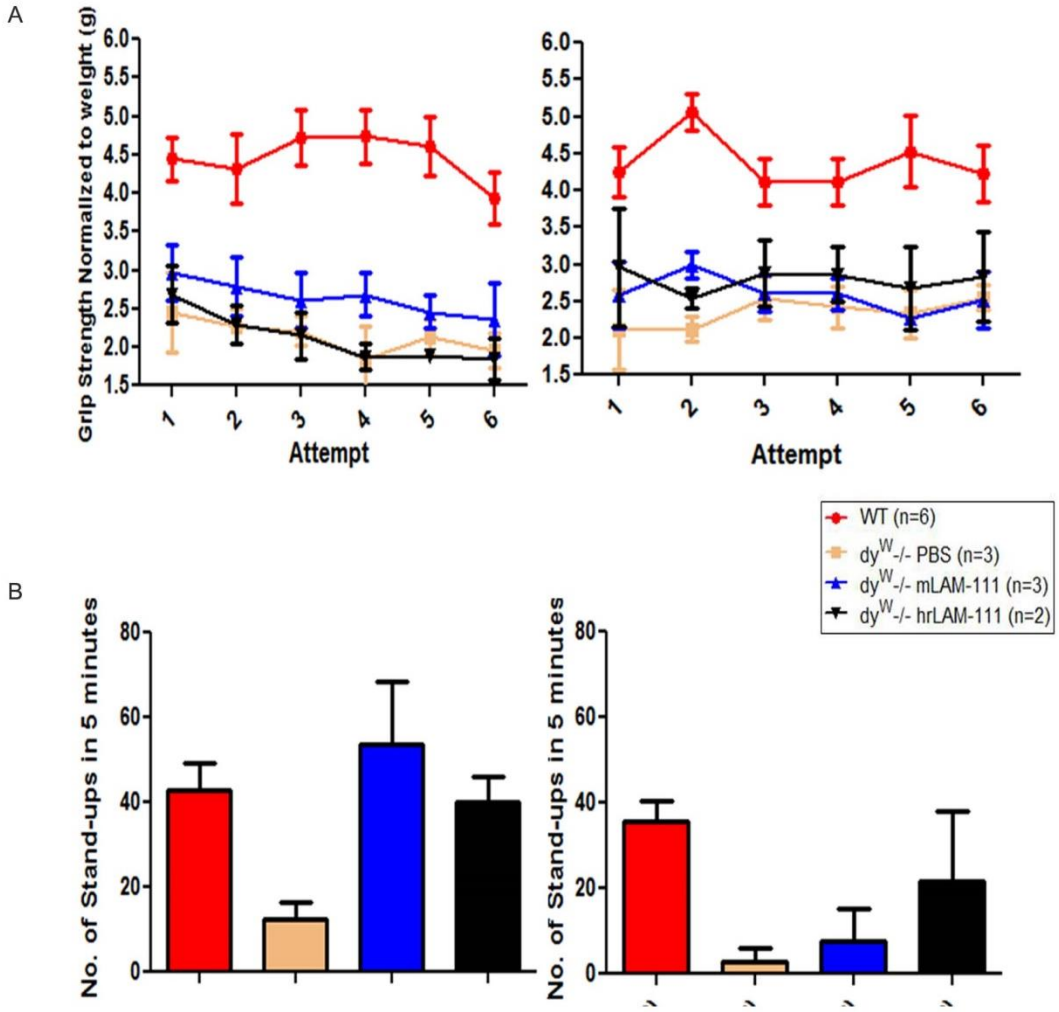

Figure 46. Functional assessment of *dy^{W}-/-* mice treated with laminin

A) *dy^{W}* -/- mice were treated with PBS, EHS m-Lam-111 or rhLam-111. Mice were assessed for function at both 5 (left) and 10 (right) weeks of age. Grip strength measurements were recorded. B) Number of stand-ups accomplished by each treatment group were averaged and shown here. rhLAM-111 was not effective in causing a beneficial effect.

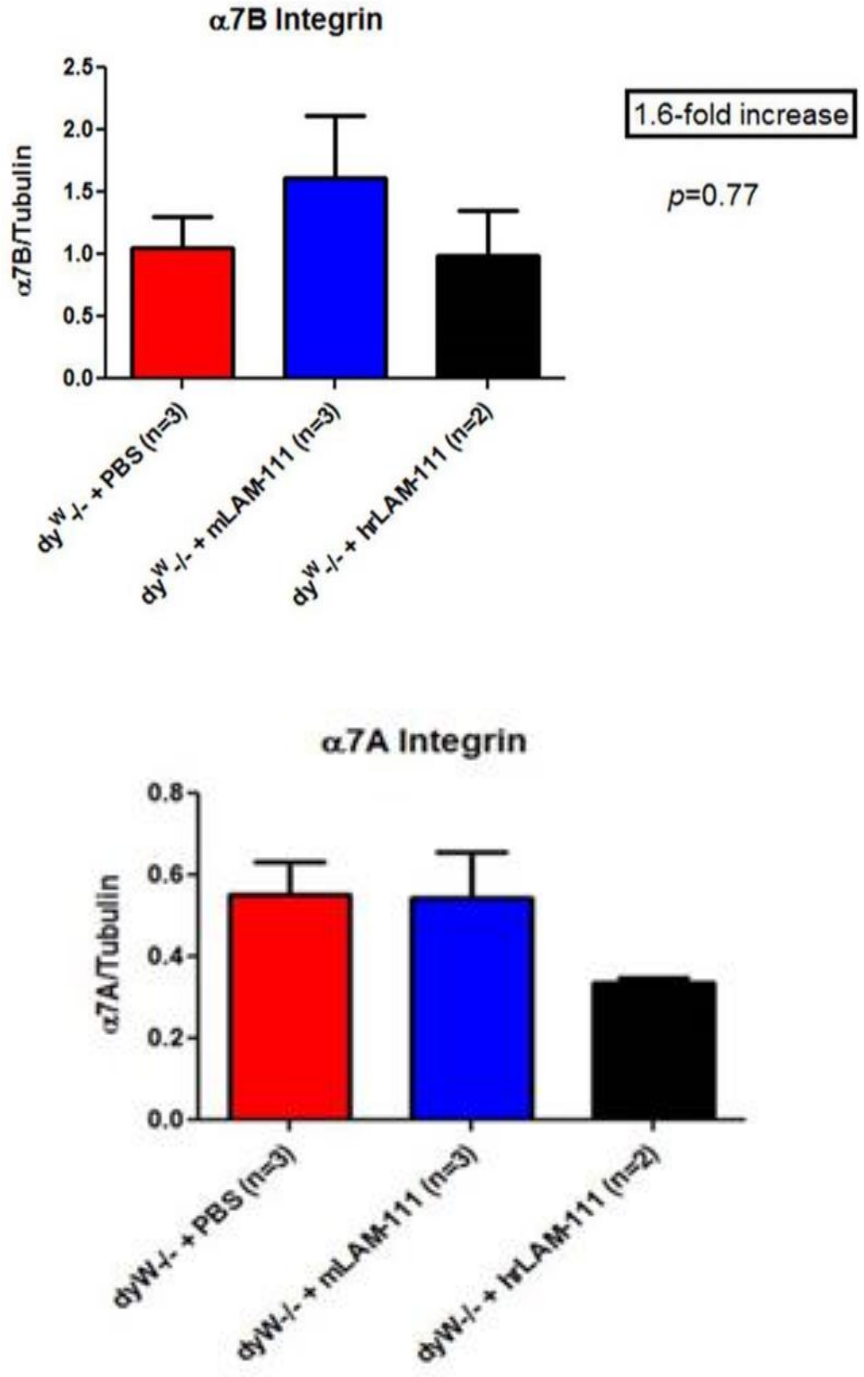

Figure 47. Integrin immunoblotting after laminin-111 treatment

Comparison of rhLam-111 effects with EHS mLam-111 effects after intraperitoneal treatment. rhLAM-111 had no beneficial effect in elevating alpha7 integrin protein.

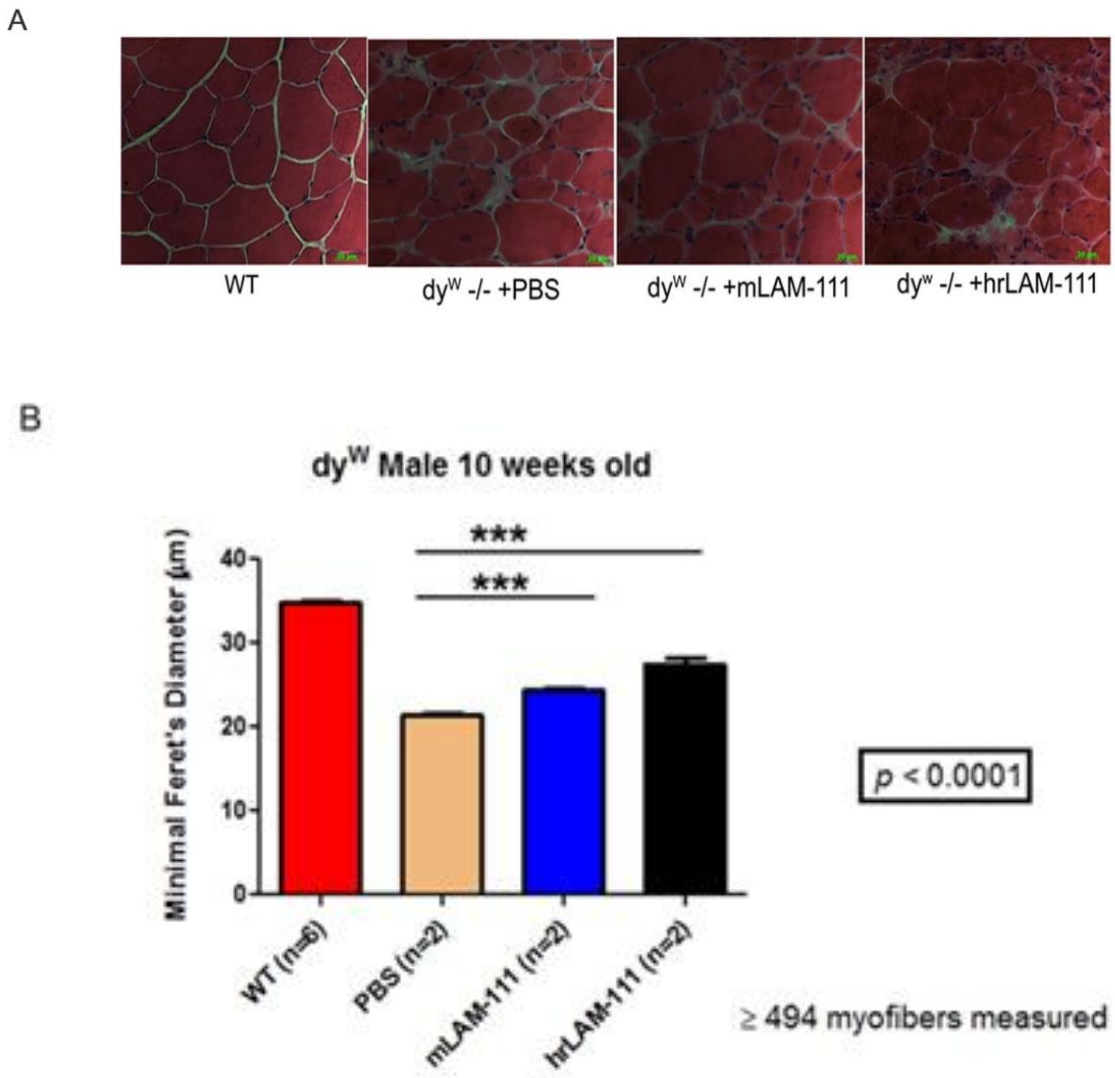

Figure 48. Histological analysis of laminin treated *dy^{W}-/-* mice

A) Hematoxylin and Eosin staining of 10 week old *dy^{W}* TA muscle. B) Minimal feret's diameter was measured for these mice and results were considered statistically significant with *P* values < 0.05. Average myofiber size increased towards WT upon treatment with rhLAM-111 protein.

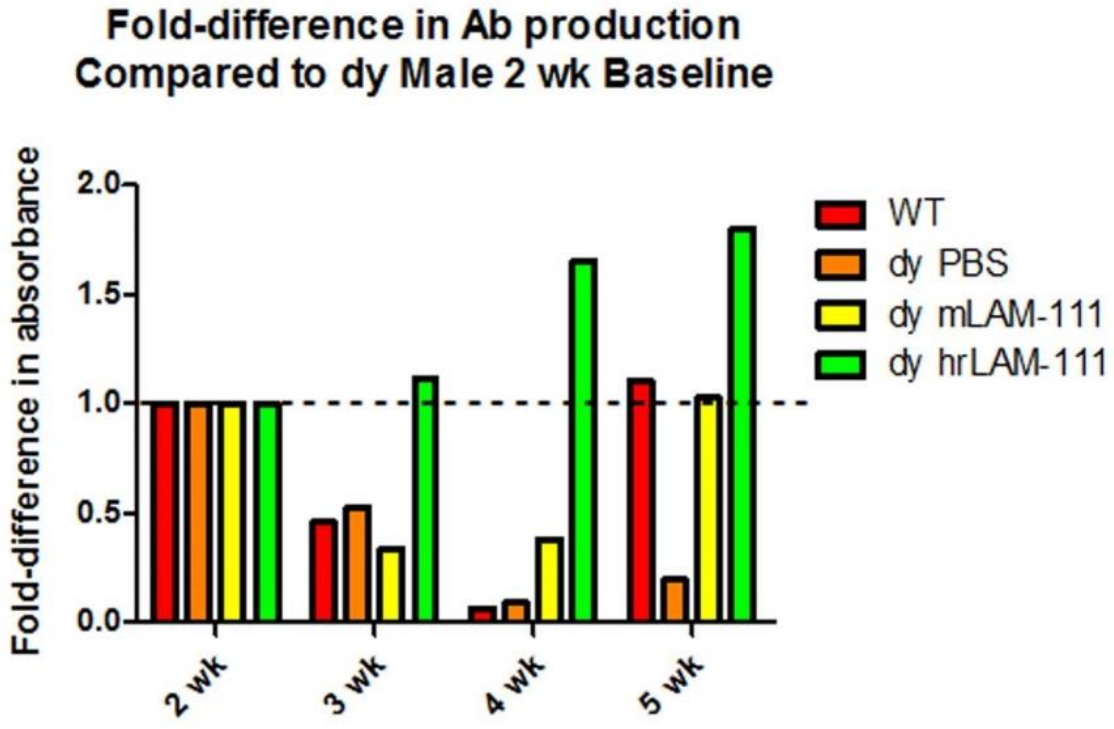

Figure 49. Immunological response to laminin-111 treatment

Intraperitoneal treatment with rhLAM-111 in *dy*^{W} mice amounted to an immune response to the human laminin-111 protein injected into the mouse species.

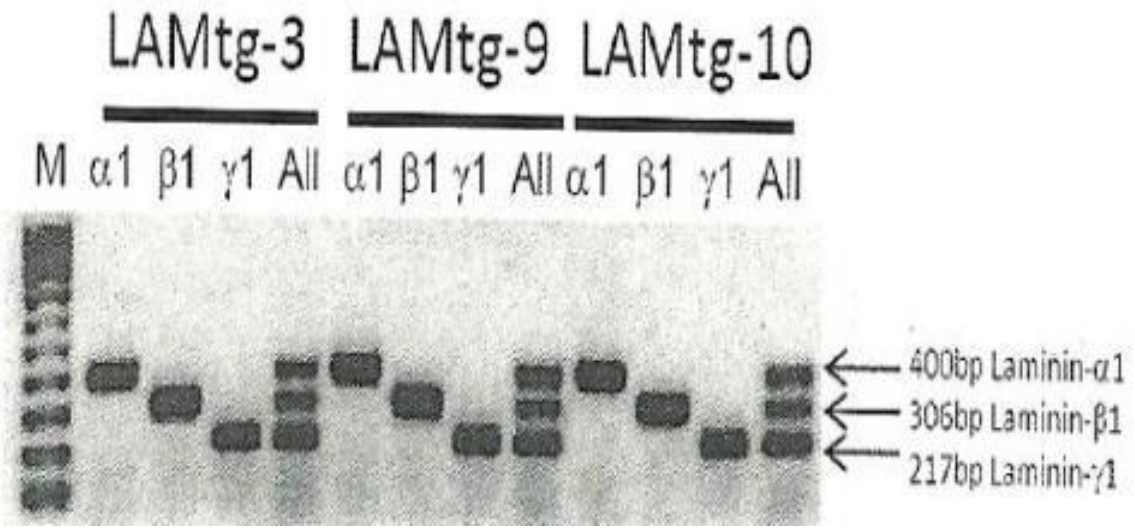

Figure 50. hLam-111 transgenic mouse production

Mice expressing all three chains of human laminin-111 have been generated.

The Burkin lab has been able to generate transgenic founder mouse lines positive for human Laminin-α1, β1 and γ1 chains (Figure 50). This transgenic overexpression of Laminin-111 will be used in order to investigate the most exaggerated effect due to the presence of Laminin-111. This figure was kindly provided by Dr. Dean Burkin and Rebecca Evans.

Appendix B

Transcriptome Data

ABSTRACT

Merosin deficient congenital muscular dystrophy type 1A (MDC1A) is caused by loss of laminin-211 and laminin-221 within the basal lamina of skeletal and cardiac muscle. This absence of laminin-211/221 reduces the capacity for myofiber adhesion, loss of sarcolemmal integrity and subsequently the ability of the skeletal muscle syncytium to generate force in a coordinated and efficient manner. Patients experience progressive muscle wasting which confines them to a wheelchair at an early age and respiratory failure that leads to their untimely death. Currently, there is no effective treatment or cure for this devastating disease. This study set out to determine the transcriptional changes that occur within the diaphragm muscle during MDC1A disease progression using RNA-Seq technology. Our results show major transcriptional changes with age in pathways associated with immune response, cell growth and survival and muscle repair. Galectin-3 is known to help stabilize myofibers and these transcripts were found to be upregulated (six-fold) in diseased muscle compared to wild-type muscle. Together, this study will help to identify novel therapeutic targets that may be useful in the treatment of MDC1A.

INTRODUCTION

Merosin deficient congenital muscular dystrophy (MDC1A) is caused by the loss of Laminin-211 and Laminin-221 heterotrimers which are most abundant in skeletal and cardiac muscle basal lamina; mutations in the *LAMA2* gene cause the loss of these Laminin isoforms. This reduction of Laminin reduces the capacity for myofiber adhesion, loss of sarcolemmal integrity and subsequently affects the ability of the skeletal muscle syncytium to generate force in a coordinated and efficient manner. Patients, from birth, experience progressive muscle wasting which confines them to a wheelchair at an early age and respiratory failure that leads to their untimely death. Currently, there is still no effective treatment or cure for this devastating disease.

Merosin deficient congenital muscular dystrophy (MDC1A) affects approximately 0.89/100,000 individuals worldwide (1:100,000 - 1:500,000) and is deemed to be the most common form of congenital muscular dystrophy. Loss of merosin (Laminin-α2 protein) is caused by mutations occurring in the *LAMA2* gene which is located on chromosome 6q22-23 [90,91]. This loss of Laminin-α2 protein in MDC1A results in the absence of Laminin-211 and Laminin-221 heterotrimers which are abundant in skeletal and cardiac muscle basal lamina. Patients, also experience demyelinating neuropathy, muscle atrophy, limited eye movement and also respiratory failure that leads to their untimely death which can be as early as the first decade of life (Jones *et al.*, 2001; Muntoni *et al.*,

2004; Philpot *et al*., 1999). There is an increased likelihood of seizures occurring after six months of age due to changes in white matter of the brain (Jones *et al.*, 2001; Muntoni *et al.*, 2004; Philpot *et al.*, 1999). Currently, there is still no effective treatment or cure for this cruel disease (Mendell, *et al.*, 2006; Muntoni *et al.*, 2004).

MATERIALS AND METHODS

Generation of Laminin-α2 *-/-* mice

All experiments involving mice were performed under an approved protocol from the University of Nevada, Reno Institutional Animal Care and Use Committee. The *dyW+/-* mice were a gift from Eva Engvall via Paul Martin (The Ohio State University, Columbus, OH, USA). Male and female heterozygous mice were bred together. In order to genotype mice, genomic DNA was isolated from tail snips or ear notches using a Wizard SV DNA purification system (Promega, Madison, WI) following manufacturers instructions. To detect the mutation in the laminin- α2 gene, the following primers were used: DYWF (5'-ACTGCCCTTTCTCACCCACCCTT-3'), LAMA2exonR1 (5'-GTTGATGCGCTTGGGAC-3') and Lac/ZR2 (5'-GTCGACGACGACAGTATCGGCCTCAG-3'). PCR conditions were as follows: 95°C for 5 minutes then 33 cycles of 94°C for 20 seconds, 62°C for 30 seconds and 72°C for 45 seconds. After these cycles, then 72°C for 10 minutes. A wild-type band was 250 bp whereas the laminin- α2 targeted allele produced a 480 bp band.

Experimental procedures were performed once mice were 10 days old and 2 weeks of age with weekly weighing until the end of study which was at 2 weeks and 5 weeks of age where all mice were subject to *in vivo* experiments. To reduce experimental bias, investigators assessing and quantifying experimental outcomes were blinded to the treatment and control groups.

Husbandry

dy^{W}-/- mice were housed with their wild-type littermates alongside the provision of mashed kibble and access to water. Husbandry and protocols were carried out via IACUC approval. Knockout mice that lost ≥ 20% body weight (g) were euthanized. Pups were genotyped at 10 days old and at the end of each study, the female WT and *dy^{W}-/-* mice were euthanized by CO_2 inhalation in accordance with a protocol approved by the University of Nevada, Reno Animal Care and Use Committee. The diaphragm muscles from these mice were dissected, flash-frozen in liquid nitrogen and stored at -80°C as previously reported by [134].

Laminin-111 protein treatments

dy^{W}-/- mice were systemically injected with 0.01 mg/g/week of laminin-111 protein (Invitrogen). Laminin-111 was stored at -80°C and thawed slowly at 4°C overnight before use. *dy^{W} -/-* mice were systemically injected (weekly) from 10 days old until 5 weeks old.

Experimental Design

Female Wild-type (n=5) and *dy*^{W} -/- (n=5) mice were sacrificed at 2 weeks old untreated. Another treatment group within this study incorporated female *dy*^{W} -/- (n=4) systemically treated from 10 days old to 5 weeks old with 0.01 mg/g/week laminin-111. Alongside this treatment group *dy*^{W} -/- control mice (n=4) were systemically injected with a volume of sterile Phosphate buffered saline (PBS) that equated to such in the laminin-111 treatment group. At 5 weeks of age, PBS and laminin-111 treated *dy*^{W} -/- mice were sacrificed following a protocol approved by the Animal Care and Use Committee at the University of Nevada, Reno. Temporal analysis of WT, PBS and Laminin-111 treatment groups at 5 weeks of age was planned with the hope of identifying what changes occur within the transcriptome of these animals.

Muscle transcripts

The muscle transcript ontology groups of interest included: Integrin signaling, Inflammation, Fibrosis, Apoptosis (ILK, AKT), Extracellular Matrix signaling, Cell surface receptors and signaling (integrins and dystrophin and utrophin glycoproteins) and Cell Survival pathways (AKT).

RNA-Sequencing

Diaphragm tissue was homogenized and suspended in TRIzol reagent (GibcoBRL, Life Technologies). Total RNA was isolated following the manufacturer's instructions (GibcoBRL, Life Technologies). The pooled samples were DNased and cleaned before being sent to the UC Davis genome center for

RNA-Sequencing. The RNA samples were measured after cleaning and were then pooled in order to reduce cost. Aliquots of individual mouse RNA samples were stored at -80°C and then used for qRT-PCR in order to confirm the results received from the RNA-Seq data generated. TRIzol was added to individual samples, RNA was extracted, DNased, RNA samples were pooled, cleaned and eluted using RNeasy Mini Spin Columns (Qiagen) according to the manufacturer's instructions (double sample pool for cleaning), RNA was measured for content using the nanodrop.

Data Analysis

Microsoft Excel and Ingenuity Pathway Analysis (IPA) software were employed in order to visualize the signaling pathways affected within the treatment groups. Protein expression levels were analyzed and processed using GraphPad Prism software. Fold-changes in protein were calculated using changes in intensity within ImageJ software.

Statistical Analysis of RNA-Seq data

Each sample was subjected to alignment and counting of mapped reads. For this, TopHat was used for alignment to the genome, then reads were counted per locus (all isoforms counted together for one gene) using htseq-counts. In order to adjust for large differences in the number of mapped reads in each sample (with the sample with the most reads having more than 6 times as many

reads as the sample with the fewest reads), prior to analysis, counts were down-sampled using binomial sampling as described by[143]. Genes with less than 1 count per million reads in all 8 samples were filtered from the counts table, leaving 15,026 genes in the analysis. Differential expression analysis was conducted using the Bioconductor package edgeR, version 3.4.2[144–147]. Analysis was conducted using a multifactorial GLM with factors for time, group (WT, PBS treated *dy^{W}-/-* and LAM-111 treated *dy^{W}-/-*), and their interaction. This multifactorial method was chosen during analysis as it is considered to be more powerful than running each discrete comparison. Due to the lack of replication, tagwise dispersion parameters were estimated from a multifactorial GLM with factors for time and group but no interaction effect. *P*-values were adjusted for multiple testing using the false-discovery rate (FDR) method of Benjamini and Hochberg (1995)[148]. Log2-fold changes and FDR-adjusted p-values less than 0.1 for all 15,026 genes included in the analysis.

RESULTS

Transcriptome data analysis encompassed changes in 5 week old diaphragm tissue harvested from PBS treated *dy^{W} -/-* versus LN-111 Treated-*dy^{W} -/-* mice. Relatively few significant changes (~275 total genes), most genes have apparently little to do with muscle or ECM, many genes associated with bone growth and maintenance, muscle and ECM associated genes which were found to be significantly

altered were tenascin N, elane (elastase), aggrecan, MMP8, MMP9, MMP13, proteinase-3. Several genes associated with neuronal signaling. Our results at this age may represent individual disease state changes and not changes specifically associated with Laminin-111 treatment. 5 week old diaphragm from Wild-type versus Untreated *dy^{W}* -/- changes: Over 1,000 genes were significantly altered, current analysis is continuing on the known functions for all genes on the list, one interesting gene upregulated in the *dy^{W}* -/- diaphragm is osteoactivin (GPNMB).

Heat map for 2 week old *dy^{W}*-/- mouse signaling networks misregulated by loss of laminin-α2

Signaling networks upregulated include immune cell trafficking, cellular movement and inflammatory response. Signaling networks down-regulated include cell death and cellular maintenance. It is important to remember that this is before disease onset (Figure 51). A main overview of pathways affected include: Inflammatory Response, Cellular movement, Immune cell trafficking, Apoptosis, Fibrosis, Scar tissue formation and ROS.

Heat map for 5 week old *dy^{W}*-/- mouse signaling networks that were misregulated upon laminin-111 treatment

Networks upregulated include vitamin and mineral metabolism alongside lipid metabolism. Networks down-regulated include inflammatory response and

immune cell trafficking (Figure 52). A main overview of pathways affected include Inflammatory response, Cellular movement, Immune cell trafficking, Necrosis, and Repair pathways upregulated with laminin treatment.

2 week old *dy^{W} -/-* Integrin involvement in extracellular matrix interactions, cellular movement and survival signaling pathways

Integrin is consistently involved in the alteration of signaling pathways (Figure 53) and there is also involvement in initiating ERK/MAPK downstream signaling pathways (Figure 54) in 2 week old *Dy^{W}-/-.*

Comprehensive summary of ≥4-fold changes in 2 week old *dy^{W}-/-* mice

138 transcripts misregulated ≥4–fold between WT and *dy^{W}-/-* at 2 weeks old.

Comprehensive summary of ≥4-fold changes in 5 week old *dy^{W}-/-* mice

468 transcripts misregulated ≥4–fold between *dy^{W} -/-* PBS treated and Dy^{W}-/- Laminin treated at 5 weeks old.

DISCUSSION

The aim of this study was to identify transcriptional changes within diaphragm muscle for the MDC1A mouse model compared to wild type controls. Muscle contraction causes acute damage to the integrity of the sarcolemma within healthy skeletal muscle resulting in myofiber rupture that releases many susceptible candidates for immune targeting. This process may be aberrantly

activated in the progressive disease state of Laminin-α2 deficient skeletal muscle resulting in chronic injury with the prolonged release of many intracellular molecules including proinflammatory cytokines, growth factors and cytosolic calcium which is directly involved in the activation and recruitment of t-lymphocytes facilitating a positive feedback mechanism for further myofiber contraction, rupture, apoptosis and fibrotic scar tissue formation. It is unclear from past and current studies what exact role or what key immune players have in the pathophysiology of MDC1A. Treatment with Laminin-111 (found embryonically) reduces muscle pathology and improves viability in the *dy^{W}-/-* MDC1A mouse model. Laminin-111 helps to strengthen and reinforce the sarcolemma in the *dy^{W}-/-* mouse during prolonged progressive muscle injury induced by contraction offering a protective niche against the occurrence of this degenerative scenario by reducing inflammation, fibrosis and apoptosis via improved matrix-mechanotransduction.

At 2 weeks of age the variability between animals is low and the RNA-Seq data appears solid. At 5 weeks of age there is significant variability between mice and the RNA-Seq data requires more interpretation. The changes observed in some of the transcripts were the result of only one mouse in the 5 week study. RT-PCR data analysis confirms this result. Osteoactivin is involved in differentiation of skeletal and muscle tissue and may serve as a novel biomarker for disease progression. RT-PCR confirmed that it is increased in mice and also now in an MDC1A patient muscle that we have in our tissue archive.

Osteoactivin (OA) is a (*Dchil*) dendritic-cell associated heparin sulphate proteoglycan- dependent integrin ligand [155,156]. In humans, OA is known as the *GPNMB* gene. The osteoactivin gene encodes a protein of 572 amino acids and is localized to the membrane as a Type-1 transmembrane glycoprotein [151,156]. OA is expressed in osteoblasts actively involved in bone matrix production and mineralization. OA is also necessary for osteoblast differentiation *in vitro* [150]. Syndecan-4 is a receptor on T-cells for OA which therefore initiates an inhibitory function on T cell activation[157]. OA is upregulated in muscle denervation and unloading stress. The regulatory mechanisms of OA in muscle and bone have not yet been determined, however the role of OA in transdifferentiation of myoblasts into osteoblasts has been eluded to in a published study by [149]. Interestingly, osteoblast differentiation is characteristically identified by expression of markers which include Osteoactivin (*Gpnmb*) and Osteocalcin (*Bglap*) [158]. Transdifferentiation is the manner in which a somatic cell retains plasticity and can be transformed into another somatic cell. This process can also described as lineage reprogramming. It was first demonstrated whenever mouse embryonic fibroblasts became myoblasts by forced expression of MyoD[159].

Laminin-111 is the predominant Laminin isoform found in the basal lamina of developing embryonic skeletal muscle[115]. However in adult skeletal and cardiac muscle Laminin-111 is replaced by Laminin-211 and Laminin-221 isoforms which help to anchor myofibers to the basement membrane and form neuromuscular junctions[116,188]. Laminin-α2 protein is an essential component of the basal lamina that surrounds muscle fibers and is composed of α, β, and γ

heterotrimers[161]. MDC1A is caused by the loss of Laminin-α2 protein. Regeneration of Laminin-α2 deficient muscle is also dependent on the presence of Laminin[124,162]. Molecules that reinforce muscle-basal lamina interactions and restore normal survival signaling pathways are likely candidates for drug-based therapeutics for MDC1A.

Laminin-111 can be systemically delivered to all major muscles affected in MDC1A patients helping to enhance muscle integrity and addresses the primary defect of cellular adhesion in MDC1A. Laminin-111 is unlikely to elicit and immune response since it is naturally expressed during embryonic development and in the adult kidney basement membrane[142]. Treatment with Laminin-111 has been shown recently to reduce muscle pathology and improve viability in the (*dy^{W}-/-)* MDC1A mouse model [131]. In one such study, Evan's Blue Dye uptake was used to examine the integrity of the sarcolemma and Laminin-111 treatment had beneficial effects in Laminin-α2 deficient muscle by causing a 7.3-fold reduction in sarcolemmal rupture. The α7β1 integrin is the major Laminin-binding integrin in cardiac and skeletal muscle[163]. MDC1A patients and *dy^{W}-/-* mice have reduced levels of α7 integrin contributing to severe muscle pathology [188] Laminin-111 has been shown to increase α7 integrin expression in mouse and human muscle cells [164].

Laminin-111 treatment in mice appears to block Osteoactivin expression and therefore would potentially restore MAPK signaling in muscle and prevent further fibrosis. The immunofluorescence data confirms in patients the mouse RNA-Seq data and RT-PCR studies.

ACKNOWLEDGEMENTS

Dr. Ryan Wuebbles for assistance with RNA-Seq and qRT-PCR studies. I would like to thank Dr. Joseph Fass and Dr. Ryan Kim for generating and processing the RNA-Seq data at the UC Davis Genome center. I would also like to thank Dr. Paul Brewer for kindly performing the ERK immunoblots and Rebecca Evans for genotyping the *dy*^{W}-/- mice.

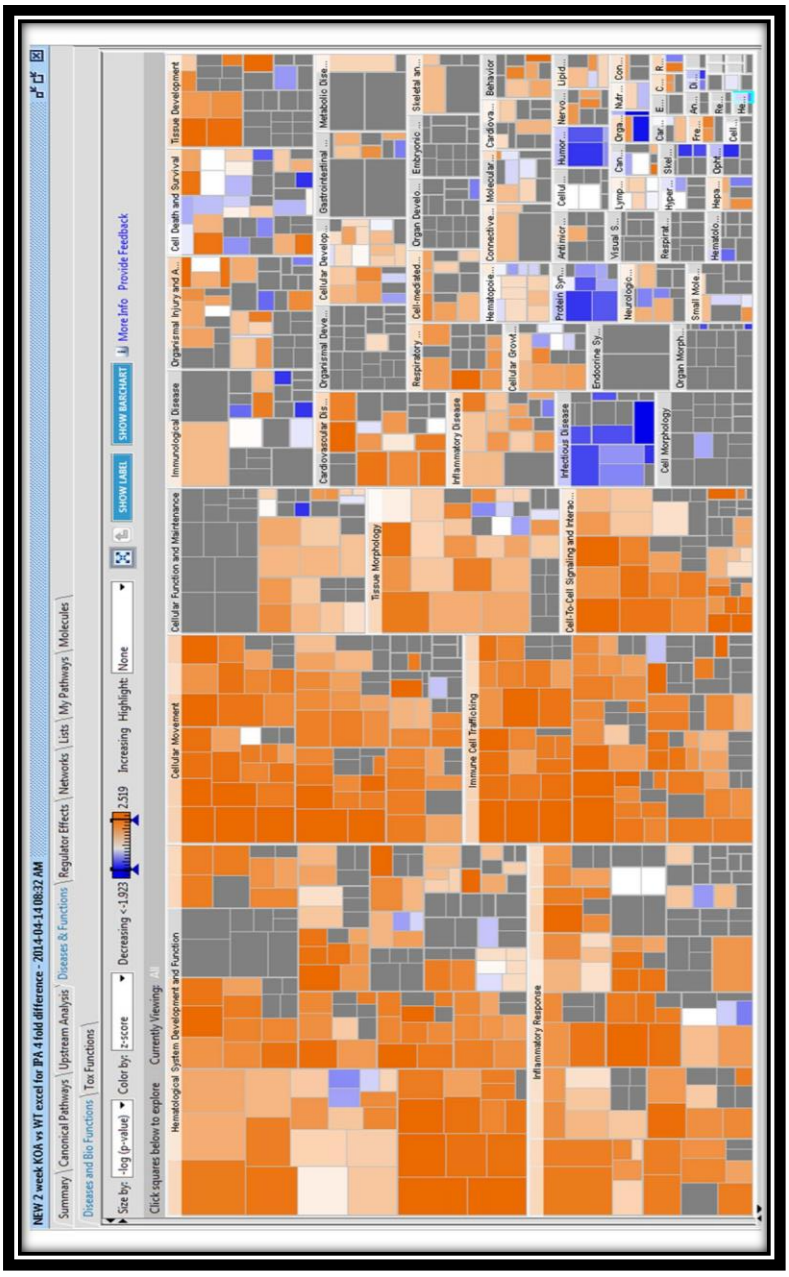

Figure 51 Heat map for 2 week old *dy^{W}-/-* mouse signaling networks misregulated by loss of laminin-α2

Upregulated genes represented by orange. Downregulated genes represented by blue.

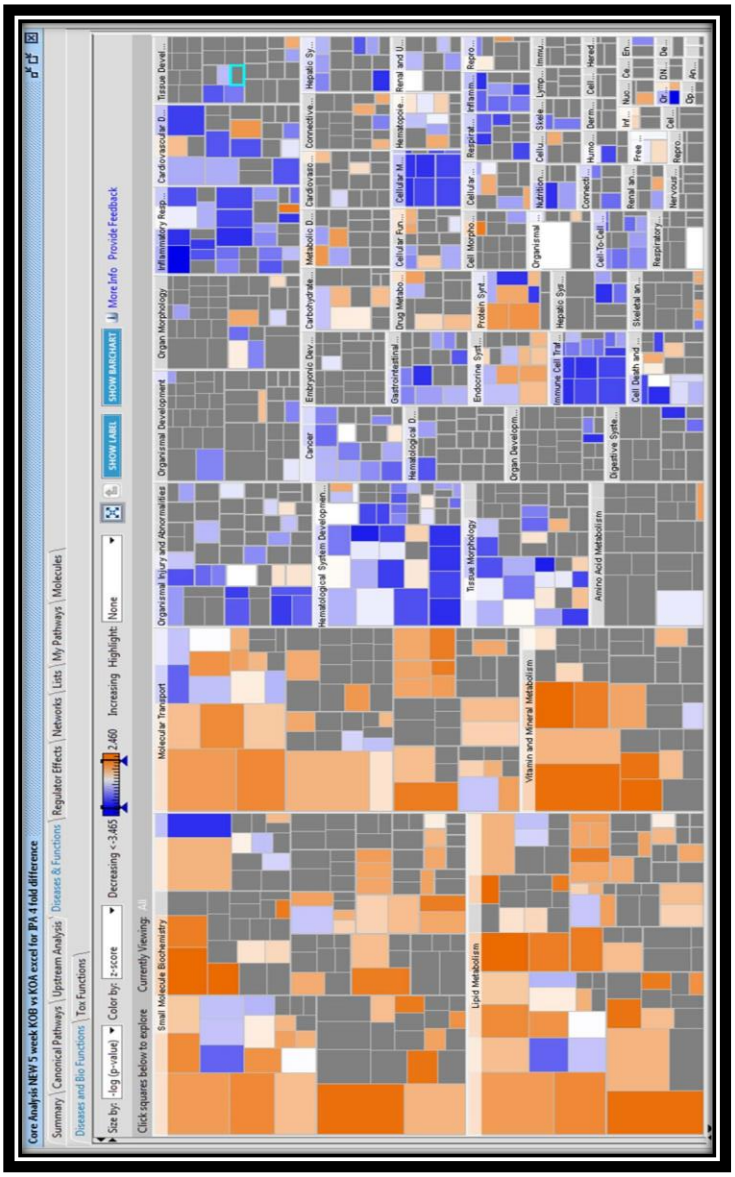

Figure 52. Heat map for 5 week old *dy^{W}-/-* mouse signaling networks that were misregulated upon laminin-111 treatment

Upregulated genes represented by orange. Down regulated genes represented by blue.

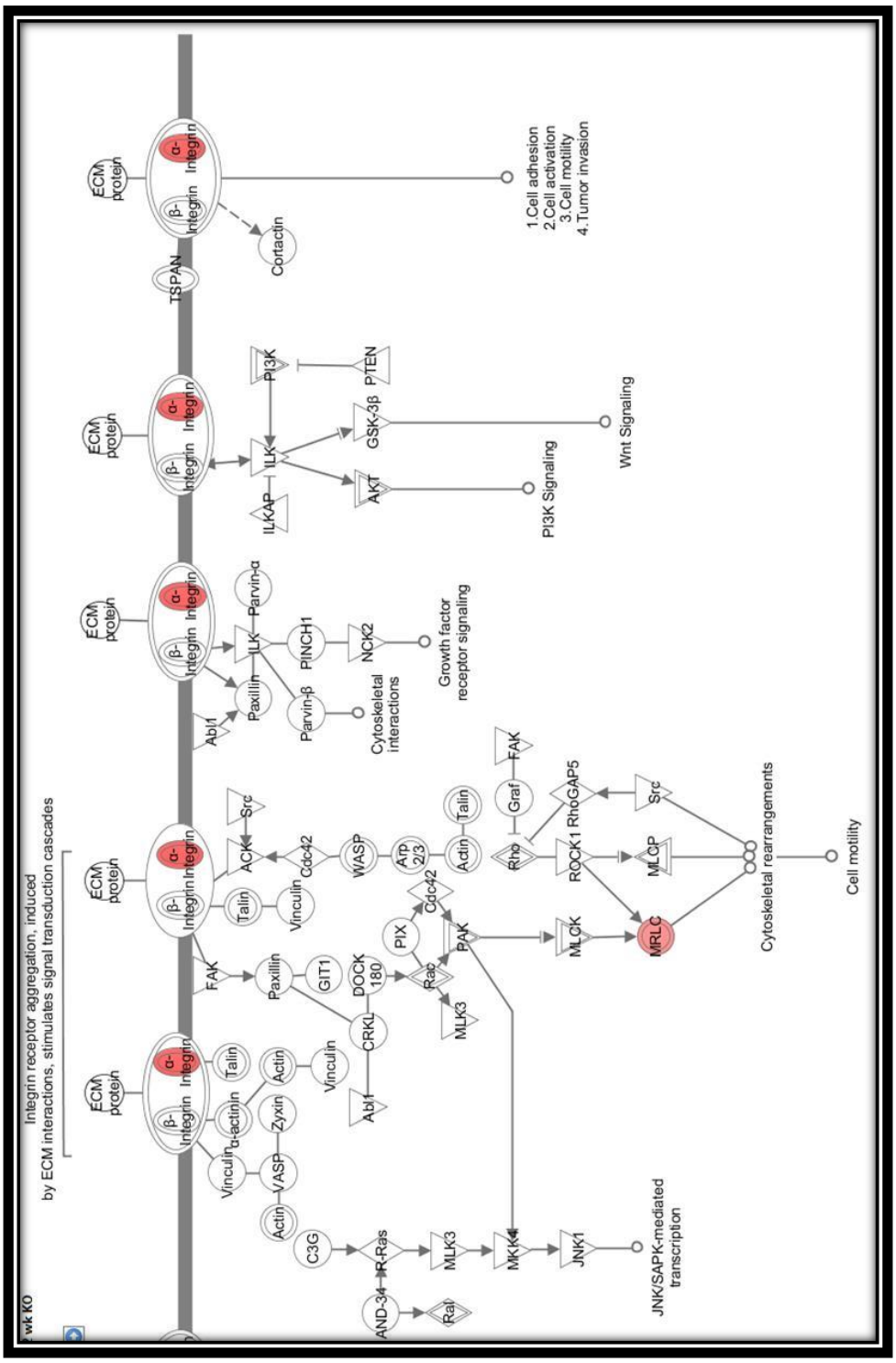

Figure 53. 2 week old *dy^{W} -/-* Integrin involvement in extracellular matrix interactions, cellular movement and survival signaling pathways

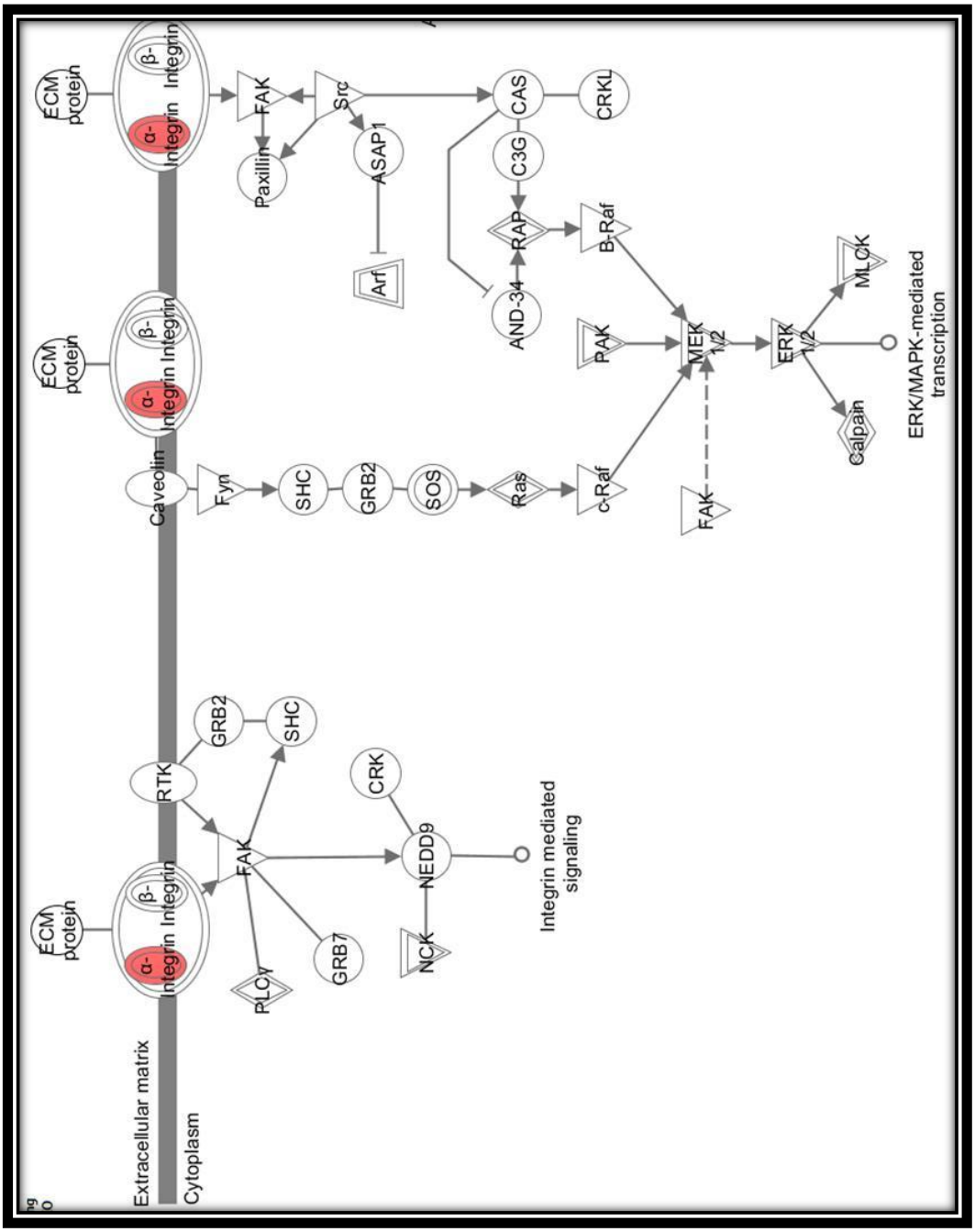

Figure 54. 2 week old *dy^{W} -/-* Integrin involvement in initiating ERK/MAPK downstream signaling pathways

2 week ≥ 4-fold difference

GENE	logFC_KO_over_WT	FDR	Function
Scgb1a1	-13.2038	2.89E-39	Secretoglobin, Family 1A, Member 1 Binds phosphatidylcholine, phosphatidylinositol, polychlorinated biphenyls (PCB) and weakly progesterone
Sec14l3	-10.5178	1.23E-18	Selenocysteine involved in antioxidant behavior
Sftpb	-10.4183	1.23E-18	Surfactant, Pulmonary-Associated Protein C for alveolar stability
Sftpd	-10.3659	5.46E-18	Surfactant, Pulmonary-Associated Protein C for alveolar stability
Cldn18	-9.87196	3.72E-15	Claudins are found at tight junctions as a physical barrier and known for maintaining cell polarity and signal transductions
Chia	-8.03046	4.59E-06	Chitinase, Acidic Its function is in the inflammatory response and in protecting cells against apoptosis is inhibited by allosamidin, suggesting that the function of this protein depends on carbohydrate binding
Scnn1g	-7.98484	9.80E-06	Sodium Channel, Non-Voltage-Gated 1, Gamma Subunit
Scgb3a2	-7.61726	0.000146	Secretoglobin, Family 1A, Member 1 Binds phosphatidylcholine, phosphatidylinositol, polychlorinated biphenyls (PCB) and weakly progesterone
Sftpc	-7.29131	3.17E-20	Surfactant, Pulmonary-Associated Protein C for

			alveolar stability
Sftpa1	-6.96979	6.44E-23	Surfactant, Pulmonary-Associated Protein C for alveolar stability
E030019B13Rik	-6.94359	0.003973	RIKEN cDNA E030019B13 gene
Sfta2	-6.94359	0.003973	Surfactant, Pulmonary-Associated Protein C for alveolar stability
S100g	-6.94359	0.004956	S100 Calcium Binding Protein G This cytosolic protein belongs to a family of calcium-binding proteins that includes calmodulin, parvalbumin, troponin C, and S100 protein.
Slc34a2	-6.77686	1.30E-18	Solute Carrier Family 23 (Ascorbic Acid Transporter), Member 1 Sodium/ascorbate cotransporter. Mediates lectrogenic uptake of vitamin C, with a stoichiometry of 2 Na(+) for each ascorbate
Rhbg	-6.50039	0.023785	Rh Family, B Glycoprotein (Gene/Pseudogene) Functions as a specific ammonium transporter
Mlc1	-6.50039	0.023785	Megalencephalic Leukoencephalopathy With Subcortical Cysts 1 Regulates the response of astrocytes to hypo-osmosis by promoting calcium influx
Pnliprp1	-6.36448	0.036951	Pancreatic Lipase-Related Protein 1 May function as inhibitor of dietary triglyceride digestion. Lacks detectable lipase activity towards triglycerides, diglycerides, phosphatidylcholine, galactolipids or cholesterol esters (in vitro) (By similarity)
Slc25a21	-6.36448	0.036951	Solute Carrier Family 23 (Ascorbic Acid Transporter), Member 1 Sodium/ascorbate cotransporter. Mediates

			lectrogenic uptake of vitamin C, with a stoichiometry of 2 Na(+) for each ascorbate
Il8	-6.22697	1.36E-10	Interleukin-8 important mediator of the innate immune response
Lamp3	-6.01392	1.69E-09	Lysosome associated membrane protein
Ager	-4.38287	0.012432	Advanced Glycosylation End Product-Specific Receptor The advanced glycosylation end product (AGE) receptor encoded by this gene is a member of the immunoglobulin superfamily of cell surface receptors. It is a multi-ligand receptor, and besides AGE, interacts with other molecules implicated in homeostasis, development, and inflammation, and certain diseases, such as diabetes and Alzheimer's disease.
Irx1	-4.2336	0.010733	Iroquois Homeobox 1 role in many developmental processes
Car5a	-3.82149	0.065864	Carbonic anhydrase 5a, mitochondrial
Nkx2-1	-3.61684	0.089384	NK2 Homeobox 11 Transcription factor that binds and activates the promoter of thyroid specific genes such as thyroglobulin, thyroperoxidase, and thyrotropin receptor. Crucial in the maintenance of the thyroid differentiation phenotype. May play a role in lung development and surfactant homeostasis
Gm4956	-3.02513	0.035316	Predicted gene
Lama2	-3.0068	8.05E-11	Laminin-α2
Wfdc2	-2.45846	0.041273	WAP Four-Disulfide Core Domain 2 Broad range protease inhibitor

Plek	2.010477	0.036951	Pleckstrin Major protein kinase C substrate of platelets
Cyp4f18	2.010628	0.05633	Mucosa-specific cytochrome P450 enzyme active in the metabolism of sex steroids and xenobiotic substrates
Ms4a6b	2.015674	0.005589	Membrane-spanning 4-domains, subfamily A, member 6B immune?
Plac8	2.042618	0.000878	Placenta-Specific 8 brown fat cell differentiation, defense response to bacterium, nucleus chromatin binding, protein binding
Cd52	2.048367	0.01817	CD52 Molecule May play a role in carrying and orienting carbohydrate, as well as having a more specific role
Dio2	2.070554	0.002823	Deiodinase, Iodothyronine, Type II1 Responsible for the deiodination of T4 (3,5,3',5'-tetraiodothyronine) into T3 (3,5,3'-triiodothyronine). Essential for providing the brain with appropriate levels of T3 during the critical period of development
Stx11	2.079843	0.04176	Syntaxin 11 SNARE that acts to regulate protein transport between late endosomes and the trans-Golgi network
Lat2	2.111883	0.008663	Linker For Activation Of T Cells Family, Member 2 Involved in FCER1 (high affinity immunoglobulin epsilon receptor)-mediated signaling in mast cells. May also be involved in BCR (B-cell antigen receptor)-mediated signaling in B-cells and FCGR1 (high affinity immunoglobulin gamma Fc receptor I)-mediated signaling in myeloid cells. Couples activation of these receptors

			and their associated kinases with distal intracellular events through the recruitment of GRB2
Emr1	2.116129	0.024873	Egf-Like Module Containing, Mucin-Like, Hormone Receptor-Like 1 Could be involved in cell-cell interactions
Cybb	2.136779	0.027832	Cytochrome B-245, Beta Polypeptide Critical component of the membrane-bound oxidase of phagocytes that generates superoxide. It is the terminal component of a respiratory chain that transfers single electrons from cytoplasmic NADPH across the plasma membrane to molecular oxygen on the exterior
Slamf7	2.140173	0.088282	Isoform 1 mediates NK cell activation
Clec4a2	2.142002	0.002082	C-type lectin domain family 4, member α2 immune system process, innate immune response integral component of membrane, membrane carbohydrate binding
Runx1	2.14289	0.00018	Runt-Related Transcription Factor 1 The protein encoded by this gene represents the alpha subunit of CBF and is thought to be involved in the development of normal hematopoiesis. Chromosomal translocations involving this gene are well-documented and have been associated with several types of leukemia.
Gpr34	2.146967	0.003833	G Protein-Coupled Receptor 34 G protein-coupled receptors (GPCRs), such as GPR34, are integral

			membrane proteins containing 7 putative transmembrane domains (TMs). These proteins mediate signals to the interior of the cell via activation of heterotrimeric G proteins that in turn activate various effector proteins, ultimately resulting in a physiologic response.
Itgam	2.178598	0.039179	Macrophage antigen-1
Atp8b4	2.189358	0.049184	ATPase, Class I, Type 8B, Member 4 This gene encodes a member of the cation transport ATPase (P-type) family and type IV subfamily. The encoded protein is involved in phospholipid transport in the cell membrane
Ly9	2.200132	0.062293	Lymphocyte Antigen 9 May participate in adhesion reactions between T lymphocytes and accessory cells by homophilic interaction
Msr1	2.223096	0.054442	Macrophage Scavenger Receptor 1 Membrane glycoproteins implicated in the pathologic deposition of cholesterol in arterial walls during atherogenesis. Two types of receptor subunits exist. These receptors mediate the endocytosis of a diverse group of macromolecules, including modified low density lipoproteins (LDL). Isoform III does not internalize actetylated LDL
Lst1	2.229202	0.019488	Leukocyte Specific Transcript 1 Possible role in modulating immune responses. Induces morphological changes including production of filopodia and microspikes

			when overexpressed in a variety of cell types and may be involved in dendritic cell maturation. Isoform 1 and isoform 2 have an inhibitory effect on lymphocyte proliferation
Cxcl10	2.232386	0.023785	Chemokine (C-X-C Motif) Ligand 10 Chemotactic for monocytes and T-lymphocytes. Binds to CXCR3
Evi2b	2.233146	0.055725	Ecotropic Viral Integration Site 2B
Card14	2.257698	0.057749	Caspase Recruitment Domain Family, Member 14 Plays a role in signaling mediated by TRAF2, TRAF3 and TRAF6 and protects cells against apoptosis. Activates NF-kappa-B via BCL10 and IKK. Stimulates the phosphorylation of BCL10
Egr1	2.280286	0.009349	Early Growth Response 1 Transcriptional regulator. Recognizes and binds to the DNA sequence 5'-CGCCCCCGC-3'(EGR-site). Activates the transcription of target genes whose products are required for mitogenesis and differentiation
Arl11	2.281866	0.023785	ADP-Ribosylation Factor-Like 11 May play a role in apoptosis. May act as a tumor suppressor
Thbs4	2.292313	6.20E-06	Thrombospondin 4 Acts as an extracellular mitogen and stimulates early erythroid progenitors proliferation in presence of EPO. Adhesive glycoprotein that mediates cell-to-cell and cell-to-matrix interactions. Can bind to fibrinogen, fibronectin, laminin and type V collagen

Slc2a6	2.326007	0.086347	Solute Carrier Family 23 (Ascorbic Acid Transporter), Member 1 Sodium/ascorbate cotransporter. Mediates lectrogenic uptake of vitamin C, with a stoichiometry of 2 Na(+) for each ascorbate
Ifi44l	2.329776	0.022705	Interferon-Induced Protein 44-Like Exhibits a low antiviral activity against hepatitis C virus
Ccr2	2.330837	0.001005	Chemokine (C-C Motif) Receptor 2 migration of immune cells. Other functions include angiogenic activity, apoptosis, T-cell differentiation and phagocyte activation. Inadvertent activation of chemokine receptors leads to autoimmunity by inappropriately targeting self-antigens for destruction by cytotoxic T-cells and macrophages.
Lilrb3	2.333939	0.002031	Leukocyte Immunoglobulin-Like Receptor, Subfamily B (With TM And ITIM Domains), Member 3 May act as receptor for class I MHC antigens. Becomes activated upon colligation of LILRB3 and immune receptors, such as FCGR2B and the B-cell receptor. Down-regulates antigen-induced B-cell activation by recruiting phosphatases to its immunoreceptor tyrosine-based inhibitor motifs (ITIM) (By similarity)
Pmaip1	2.339957	0.021507	Phorbol-12-Myristate-13-Acetate-Induced Protein 1 Promotes activation of caspases and apoptosis.

			Promotes mitochondrial membrane changes and efflux of apoptogenic proteins from the mitochondria. Contributes to p53/TP53-dependent apoptosis after radiation exposure. Promotes proteasomal degradation of MCL1.
Wfdc17	2.352242	0.031692	WAP four-disulfide core domain 17 ?
S100a4	2.354645	0.0002	S100 Calcium Binding Protein A4 S100 proteins are localized in the cytoplasm and/or nucleus of a wide range of cells, and involved in the regulation of a number of cellular processes such as cell cycle progression and differentiation.
Clec7a	2.35468	0.012432	C-Type Lectin Domain Family 7, Member A1 innate immune response The encoded glycoprotein is a small type II membrane receptor with an extracellular C-type lectin-like domain fold and a cytoplasmic domain with an immunoreceptor tyrosine-based activation motif.
Gm6377	2.378228	0.0912	Predicted gene
Socs3	2.394801	0.013639	Suppressor Of Cytokine Signaling 3 SSI family members are cytokine-inducible negative regulators of cytokine signaling. The expression of this gene is induced by various cytokines, including IL6, IL10, and interferon (IFN)-gamma.
Ly86	2.396271	0.002823	Lymphocyte Antigen 86 May cooperate with CD180 and TLR4 to mediate the innate immune response to bacterial lipopolysaccharide (LPS) and

			cytokine production. Important for efficient CD180 cell surface expression (By similarity)
Adam8	2.425141	0.00152	ADAM Metallopeptidase With Thrombospondin Type 1 Motif, 15
Ankrd1	2.47285	0.007531	Ankyrin Repeat Domain 1 (Cardiac Muscle) May play an important role in endothelial cell activation. May act as a nuclear transcription factor that negatively regulates the expression of cardiac genes. Induction seems to be correlated with apoptotic cell death in hepatoma cells
Clec4a3	2.481941	0.003883	C-type lectin domain family 4, member a3 C-type lectins are an important group of proteins found in the immune system of animals.
Milr1	2.485463	0.026871	Mast Cell Immunoglobulin-Like Receptor 1 Immunoglobulin-like receptor which plays an inhibitory role in degranulation of mast cells. Negatively regulates IgE-mediated mast cell activation and suppresses the type I immediate hypersensitivity reaction (By similarity)
Lilrb4	2.490647	0.00152	Leukocyte Immunoglobulin-Like Receptor, Subfamily B (With TM And ITIM Domains), Member 4 Inhibits receptor-mediated phosphorylation of cellular proteins and mobilization of intracellular calcium ions
Ccr5	2.534424	0.020598	Chemokine (C-C Motif) Receptor 5 (Gene/Pseudogene) Receptor for a number of inflammatory CC-chemokines including

			MIP-1-alpha, MIP-1-beta and RANTES and subsequently transduces a signal by increasing the intracellular calcium ion level.
Evi2a	2.563247	0.002919	Ecotropic Viral Integration Site 2A May complex with itself or/and other proteins within the membrane, to function as part of a cell-surface receptor
Mx1	2.570041	0.069429	Myxovirus (Influenza Virus) Resistance 1, Interferon-Inducible Protein P78 (Mouse) Enhances ER stress-mediated cell death after influenza virus infection. May regulate the calcium channel activity of TRPCs
Sox11	2.584335	4.99E-05	SRY (Sex Determining Region Y)-Box 17
Tlr1	2.584702	0.030108	Toll-Like Receptor 1 Participates in the innate immune response to microbial agents. Specifically recognizes diacylated and triacylated lipopeptides. Cooperates with TLR2 to mediate the innate immune response to bacterial lipoproteins or lipopeptides. Acts via MYD88 and TRAF6, leading to NF-kappa-B activation, cytokine secretion and the inflammatory response (By similarity)
Cd72	2.59714	0.018697	Cluster of differentiation Plays a role in B-cell proliferation and differentiation
Nlrc5	2.616321	0.078665	NLR Family, CARD Domain Containing 5 Probable regulator of the NF-kappa-B and type I interferon signaling pathways. May also regulate the type II interferon signaling pathway. Plays a role in

			homeostatic control of innate immunity and in antiviral defense mechanisms
Cd200r1	2.647261	0.012242	CD200 Receptor 1 Both the receptor and substrate are cell surface glycoproteins containing two immunoglobulin-like domains.
C3ar1	2.653413	0.000146	Complement Component 3a Receptor 1 Receptor for the chemotactic and inflammatory peptide anaphylatoxin C3a. This receptor stimulates chemotaxis, granule enzyme release and superoxide anion production
Ms4a6d	2.665341	4.59E-06	Membrane-Spanning 4-Domains, Subfamily A, Member 3 (Hematopoietic Cell-Specific) Hematopoietic modulator for the G1-S cell cycle transition.
Gpr141	2.669057	0.008658	G Protein-Coupled Receptor 34 G protein-coupled receptors (GPCRs), such as GPR34, are integral membrane proteins containing 7 putative transmembrane domains (TMs). These proteins mediate signals to the interior of the cell via activation of heterotrimeric G proteins that in turn activate various effector proteins, ultimately resulting in a physiologic response.
Igfn1	2.679489	0.093525	Immunoglobulin-Like And Fibronectin Type III Domain Containing 1
Clec12a	2.688102	0.000152	C-Type Lectin Domain Family 12, Member A Cell surface receptor that modulates signaling cascades and mediates tyrosine phosphorylation of target MAP

			kinases
Lgals3	2.699016	4.20E-05	Lectin, Galactoside-Binding, Soluble, 3 Involved in acute inflammatory responses including neutrophil activation and adhesion, chemoattraction of monocytes macrophages, opsonization of apoptotic neutrophils, and activation of mast cells
Clec4n	2.720614	0.000662	C-type lectin domain family 4, member n defense response to fungus, immune system process, ...integral component of membrane, membrane carbohydrate binding, protein binding
Ccr1	2.738489	0.016852	Chemokine (C-C Motif) Receptor 1 Receptor for a C-C type chemokine. Binds to MIP-1-alpha, MIP-1-delta, RANTES, and MCP-3 and, less efficiently, to MIP-1-beta or MCP-1 and subsequently transduces a signal by increasing the intracellular calcium ions level. Responsible for affecting stem cell proliferation
Gm7325	2.749498	0.000134	predicted gene
Saa1	2.788181	0.052635	Serum Amyloid A1 Major acute phase reactant. Apolipoprotein of the HDL complex
Fcgr4	2.793587	0.012277	Fc receptor, IgG, low affinity IV cellular response to lipopolysaccharide, NK T cell proliferation cell surface, external side of plasma membrane
Mcoln2	2.854397	0.007715	Mucolipin 2 cation channel proteins
Oas1a	2.890803	0.011099	2'-5'-Oligoadenylate Synthetase 1, 40/46kDa critical role in cellular innate

			antiviral response. In addition, it may also play a role in other cellular processes such as apoptosis, cell growth, differentiation and gene regulation.
Rrad	2.893496	6.90E-11	Ras-Related Associated With Diabetes1 May play an important role in cardiac antiarrhythmia via the strong suppression of voltage-gated L-type Ca(2+) currents. Regulates voltage-dependent L-type calcium channel subunit alpha-1C trafficking to the cell membrane (By similarity). Inhibits cardiac hypertrophy through the calmodulin-dependent kinase II (CaMKII) pathway. Inhibits phosphorylation and activation of CAMK2D
Havcr2	2.899389	0.000878	Hepatitis A Virus Cellular Receptor 2 Regulates macrophage activation. Inhibits T-helper type 1 lymphocyte (Th1)-mediated auto- and alloimmune responses and promotes immunological tolerance. May be also involved in T-cell homing. Receptor for LGALS9
Tnc	2.946252	1.59E-09	Tenascin C Extracellular matrix protein implicated in guidance of migrating neurons as well as axons during development, synaptic plasticity as well as neuronal regeneration. Promotes neurite outgrowth from cortical neurons grown on a monolayer of astrocytes. Ligand for integrins alpha-8/beta-1, alpha-9/beta-1, alpha-V/beta-3 and alpha-

			V/beta-6
Myh3	2.948189	2.06E-05	Myosin, Heavy Chain 6, Cardiac Muscle, Alpha Muscle contraction
Cx3cr1	3.009414	3.78E-06	Chemokine (c-x-c motif) ligand 13 chemotactic for b lymphocytes
Tac1	3.015431	0.083316	Tachykinin, Precursor 1 Tachykinins are active peptides which excite neurons, evoke behavioral responses, are potent vasodilators and secretagogues, and contract (directly or indirectly) many smooth muscles
Ctss	3.048477	0.00151	Cathepsin S Thiol protease. Key protease responsible for the removal of the invariant chain from MHC class II molecules. The bond-specificity of this proteinase is in part similar to the specificities of cathepsin L and cathepsin N
Mpeg1	3.084788	0.001367	Macrophage Expressed 1 Cell cycle.
Chrng	3.107202	1.37E-05	Cholinergic Receptor, Nicotinic, Gamma (Muscle) After binding acetylcholine, the AChR responds by an extensive change in conformation that affects all subunits and leads to opening of an ion-conducting channel across the plasma membrane
Bcl2a1b	3.15306	0.00136	B cell leukemia/lymphoma 2 related protein A1b extrinsic apoptotic signaling pathway in absence of ligand, intrinsic apoptotic signaling pathway in response to DNA damage,mitochondrial outer membrane
Slfn1	3.166401	0.042972	Schlafen 1 cell cycle arrest,

			negative regulation of cell proliferation, ... Component cytoplasm, nucleus Function protein binding
Rgs1	3.167701	0.003181	Regulator Of G-Protein Signaling 1 Inhibits signal transduction by increasing the GTPase activity of G protein alpha subunits thereby driving them into their inactive GDP-bound form. This protein may be involved in the regulation of B-cell activation and proliferation
Tlr13	3.197299	0.002081	Toll-Like Receptor 3 Toll-like receptors (TLRs) are single transmembrane cell-surface receptors, which have a key role in the innate immune system.
Slfn4	3.274274	0.002823	Schlafen 4 ????? Macrophage activition
Clec4e	3.303059	0.040944	C-Type Lectin Domain Family 4, Member E Induces secretion of inflammatory cytokines through a pathway that depends on SYK, CARD9 and NF-kappa-B
Clec4d	3.320008	0.018258	C-Type Lectin Domain Family 4, Member D Functions as an endocytic receptor. May be involved in antigen uptake at the site of infection, either for clearance of the antigen, or for processing and further presentation to T cells
AF251705	3.338226	4.59E-06	Cd300C antigen
Gp49a	3.354174	0.000132	Glycoprotein 49 A integral component of membrane, membrane
Lair1	3.393095	4.20E-05	Leukocyte-Associated Immunoglobulin-Like Receptor 1 Leukocyte-Associated Immunoglobulin-Like Receptor 1

Myl7	3.427885	0.05736	Myosin, Light Chain 7, Regulatory mediates plus-ended movement along microfilaments. It is involved in muscle contraction through cyclic interactions with actin-rich thin filaments, creating a contractile force. It is regulated by phosphorylation via myosin light chain kinase (MLCK) and by intracellular Ca2+ concentrations.
Gpnmb	3.513174	1.71E-06	Glycoprotein (Transmembrane) Nmb GPNMB may be involved in growth delay and reduction of metastatic potential.
Tnnt2	3.528144	5.39E-06	Troponin T Type 2 (Cardiac) Troponin T is the tropomyosin-binding subunit of troponin, the thin filament regulatory complex which confers calcium-sensitivity to striated muscle actomyosin ATPase activity
B3gnt5	3.568479	0.00959	UDP-GlcNAc:BetaGal Beta-1,3-N-Acetylglucosaminyltransferase 5 Probably plays a central role in regulating neolacto-series glycolipid synthesis during embryonic development
Trem2	3.62577	5.62E-09	Triggering Receptor Expressed On Myeloid Cells 2 May have a role in chronic inflammations and may stimulate production of constitutive rather than inflammatory chemokines and cytokines.
Cd300lb	3.713677	0.000585	CD300 Molecule-Like Family Member B Acts as an activating immune receptor through its interaction with

			ITAM-bearing adapter TYROBP, and also independently by recruitment of GRB2
Timp1	3.741032	2.32E-11	Tissue inhibitor metalloproteinases
Dcx	3.765629	0.046214	Doublecortin Microtubule-associated protein required for initial steps of neuronal dispersion and cortex lamination during cerebral cortex development
4930433N12Rik	3.765629	0.056142	RIKEN cDNA 4930433N12 gene unclassified gene
AI747448	3.795366	0.002081	Expressed sequence AI747448 calcium-activated chloride channel
Myl4	3.800622	1.24E-12	Myosin, Light Chain 4, Alkali; Atrial, Embryonic Regulatory light chain of myosin. Does not bind calcium
Ms4a7	3.80414	1.77E-11	Membrane-Spanning 4-Domains, Subfamily A, Member 7 May be involved in signal transduction as a component of a multimeric receptor complex
Ccl8	3.867142	0.003541	Chemokine (C-C Motif) Ligand 8 Chemotactic factor that attracts monocytes, lymphocytes, basophils and eosinophils. May play a role in neoplasia and inflammatory host responses. This protein can bind heparin. The processed form MCP-2(6-76) does not show monocyte chemotactic activity, but inhibits the chemotactic effect most predominantly of CCL7, and also of CCL2 and CCL5 and CCL8
Il1rn	3.946387	0.056142	Interleukin 1 Receptor Antagonist This protein inhibits the activities of

			interleukin 1, alpha (IL1A) and interleukin 1, beta (IL1B), and modulates a variety of interleukin 1 related immune and inflammatory responses
Ccl7	3.96701	0.000472	Chemokine (C-C Motif) Ligand 7 Chemotactic factor that attracts monocytes and eosinophils, but not neutrophils. Augments monocyte anti-tumor activity. Also induces the release of gelatinase B. This protein can bind heparin. Binds to CCR1, CCR2 and CCR3
Ccl2	3.998562	0.001005	Chemokine (C-C Motif) Ligand 2 Chemotactic factor that attracts monocytes and basophils but not neutrophils or eosinophils. Augments monocyte anti-tumor activity. Has been implicated in the pathogenesis of diseases characterized by monocytic infiltrates, like psoriasis, rheumatoid arthritis or atherosclerosis. May be involved in the recruitment of monocytes into the arterial wall during the disease process of atherosclerosis
Dio3	4.085234	0.016763	Deiodinase, Iodothyronine, Type III May play a role in preventing premature exposure of developing fetal tissues to adult levels of thyroid hormones. Can regulate circulating fetal thyroid hormone concentrations throughout gestation. Essential role for regulation of thyroid hormone inactivation during embryological development
Ms4a4c	4.164097	2.26E-05	Membrane-Spanning 4-

			Domains, Subfamily A, Member 3 (Hematopoietic Cell-Specific) Hematopoietic modulator for the G1-S cell cycle transition.
Fgr	4.197254	0.002033	Feline Gardner-Rasheed Sarcoma Viral Oncogene Homolog Non-receptor tyrosine-protein kinase that transmits signals from cell surface receptors devoid of kinase activity and contributes to the regulation of immune responses, including neutrophil, monocyte, macrophage and mast cell functions, cytoskeleton remodeling in response to extracellular stimuli, phagocytosis, cell adhesion and migration.
Ccr7	4.285654	0.007423	Chemokine (C-C Motif) Receptor 7 Receptor for the MIP-3-beta chemokine. Probable mediator of EBV effects on B-lymphocytes or of normal lymphocyte functions
Fcgr1	4.308408	6.39E-06	Fc Fragment Of IgG, High Affinity Ia, Receptor (CD64) Functions in both innate and adaptive immune responses
Spp1	4.54767	4.59E-06	Secreted Phosphoprotein 1 Binds tightly to hydroxyapatite. Appears to form an integral part of the mineralized matrix. Probably important to cell-matrix interaction Function: Acts as a cytokine involved in enhancing production of interferon-gamma and interleukin-12 and reducing production of interleukin-10 and is essential in the pathway that leads to type I

			immunity (By similarity)
Gm14635	6.136662	0.078665	Predicted gene
Slurp1	6.286614	0.055416	Secreted LY6/PLAUR Domain Containing 1 Has an antitumor activity. Was found to be a marker of late differentiation of the skin. Implicated in maintaining the physiological and structural integrity of the keratinocyte layers of the skin
Ccl3	6.422436	0.034844	Chemokine (C-C Motif) Ligand 3 Monokine with inflammatory and chemokinetic properties. Binds to CCR1, CCR4 and CCR5. One of the major HIV-suppressive factors produced by CD8+ T-cells.
Gal	6.546565	0.023785	Galanin/GMAP Prepropeptide Contracts smooth muscle of the gastrointestinal and genitourinary tract, regulates growth hormone release, modulates insulin release, and may be involved in the control of adrenal secretion
Alpi	6.546565	0.023785	Alkaline Phosphatase, Intestinal The intestinal alkaline phosphatase gene encodes a digestive brush-border enzyme. This enzyme is upregulated during small intestinal epithelial cell differentiation.
LOC100038947	6.766751	0.011099	Signal-regulatory protein beta 1-like macrophages immune?
Dnahc1	6.766751	0.019805	Dynein, Axonemal, Heavy Chain 1 Force generating protein of respiratory cilia. Produces force towards the minus ends of microtubules. Dynein has ATPase activity; the force-producing power stroke is thought to occur on release of ADP. Involved in

			sperm motility; implicated in sperm flagellar assembly (By similarity)
R3hdml	7.277344	0.001005	R3H Domain Containing-Like Putative serine protease inhibitor (By similarity)

Table 5: Comprehensive summary of ≥4-fold transcript changes in 2 week old *dy^{W}* -/- mice

Upregulated genes in 2 week old *dy^{W}*-/- versus WT mice are represented by red. Downregulated genes in 2 week old *dy^{W}*-/- versus WT mice are represented by green. There were 138 transcripts affected ≥ 4-fold (up- or down- regulated) in total.

Gene	logFC_KOB_over_KOA	FDR	Function
Ibsp	-10.95044485	4.05E-22	Integrin binding sialoprotein cell to matrix interaction especially bone
Gypa	-9.606432069	0.000878	Glycophorins A (GYPA), major sialoglycoproteins of the human erythrocyte membrane
Bglap	-9.526367475	7.13E-13	Osteocalcin Bone Gamma-Carboxyglutamate (Gla) Protein bone building
Dmp1	-9.397267856	9.18E-10	Dentin Matrix Acidic Phosphoprotein 1
Hemgn	-9.170222597	1.25E-10	proliferation and differentiation of hematopoetic cells /may prevent apoptosis through activation of NFkB
Tnn	-8.767674471	8.23E-07	Tenascin N neuron outgrowth and cell migration
Rhag	-8.621187693	3.41E-08	RHAG (Rh-Associated Glycoprotein) is a Protein Coding gene. Associated with rhesus blood group antigen expression.
Cldn13	-7.624846904	0.000111	This gene encodes a member of the claudin family. Plays a major role in tight junction-specific obliteration of the intercellular space, through calcium-independent cell-adhesion activity.
Bglap2	-7.403672161	0.000418	Osteocalcin Bone Gamma-Carboxyglutamate (Gla) Protein bone building
Tspo2	-7.27891563	0.000762	TSPO2 (Translocator Protein 2), binds cholesterol and mediates its redistribution during erythropoiesis
Ms4a3	-6.991471919	0.003859	Membrane-Spanning 4-Domains, Subfamily A,

			Member 3 (Hematopoietic Cell-Specific)
Rep15	-6.991471919	0.008997	RAB15 Effector Protein Regulates transferrin receptor recycling from the endocytic recycling compartment
Fcnb	-6.909676539	0.004621	Ficolin B marks apoptotic and necrotic cells
Pif1	-6.730703309	0.00977	PIF1 5'-To-3' DNA Helicase
Nphs2	-6.526340781	0.018413	Nephrosis 2, Idiopathic, Steroid-Resistant (Podocin)
Parpbp	-6.526340781	0.019033	PARP1 Binding Protein
4833427F10Rik	-6.412167249	0.035432	Unclassified gene
Mpo	-6.207865915	4.41E-14	Myeloperoxidase polymorphonuclear leukocytes
Gm694	-6.152516921	0.043782	Unclassified gene
Mmp13	-6.016864393	0.041989	Matrix metalloproteinase 8 are zinc-dependent endopeptidases that are the major proteases involved in ECM degradation.
Ngp	-5.823936637	0.021428	Neutrophilic granule protein neutrophils immune
Ltf	-5.588858274	0.000523	Lactotransferrin
Camp	-5.545496993	0.053769	Cathelicidin Antimicrobial Peptide
Slc4a1	-5.463455071	0.02011	Solute Carrier Family 4 (Anion Exchanger), Member 1 (Diego Blood Group)
Kel	-5.342640808	4.75E-06	Kell Blood Group, Metallo-Endopeptidase
Acan	-5.283918037	5.01E-06	Aggrecan proteoglycan in ECM aims to resist compression in cartilage
Rhd	-5.283918037	6.97E-06	Rh Blood Group, D Antigen
Neil3	-4.745290481	0.000588	Nei Endonuclease VIII-Like 3 (E. Coli)
S100a9	-4.408537824	0.050901	S100 Calcium Binding Protein A9 S100A9 is a calcium- and zinc-binding

			protein which plays a prominent role in the regulation of inflammatory processes and immune response.
Elane	-4.294346398	3.26E-06	Elastase, Neutrophil Expressed
Hoxc8	-4.111315601	0.003463	Homeobox protein hox-3a housekeeping gene developmental regulatory system that provides cells with specific positional identities
Ctsg	-4.033736233	0.000457	Cathepsin G
Myb	-3.944059969	0.00977	Nuclear Receptor Subfamily 0, Group B, Member 2 The protein has been shown to interact with retinoid and thyroid hormone receptors,
Calca	-3.929580387	0.000145	Calcitonin-Related Polypeptide Alpha
Prss34	-3.794188791	0.030307	Protease, Serine, 34 (Trypsin 34)
Mmp9	-3.749450484	0.023531	Matrix Metallopeptidase 9
Vpreb3	-3.6941367	0.011112	Histidine Decarboxylase Histamine regulates several physiologic processes, including neurotransmission, gastric acid secretion, inflamation, and smooth muscle tone
Nnat	-3.685327935	0.024241	Sp7 Transcription Factor Transcriptional activator essential for osteoblast differentiation. Binds to SP1 and EKLF consensus sequences and to other G/C-rich sequences (By similarity)
Ctse	-3.591608703	0.000792	Claudins are found at tight junctions as a physical barrier and known for maintaining cell polarity and signal transductions

Gfi1b	-3.516649854	0.057457	Growth Factor Independent 1B Transcription Repressor
Igll1	-3.516649854	0.05866	Asialoglycoprotein Receptor 2 Mediates the endocytosis of plasma glycoproteins to which the terminal sialic acid residue on their complex carbohydrate moieties has been removed.
Sp7	-3.516649854	0.059139	Sp7 Transcription Factor
F2rl2	-3.516649854	0.0597	Coagulation Factor II (Thrombin) Receptor-Like 2
Cdca2	-3.488735315	0.023702	Cell Division Cycle Associated 2
Rag1	-3.488735315	0.045873	Cadherin-Related Family Member 3 Cadherins are calcium-dependent cell adhesion proteins. They preferentially interact with themselves in a homophilic manner in connecting cells; cadherins may thus contribute to the sorting of heterogeneous cell types
Ermap	-3.448203348	0.009765	Erythroblast Membrane-Associated Protein (Scianna Blood Group)
Phex	-3.432466485	0.017168	T-Cell Activation RhoGTPase Activating Protein May function as a GTPase-activating protein and may play important roles during T-cell activation
Epb4.2	-3.432466485	0.018413	Secreted Phosphoprotein 1 Binds tightly to hydroxyapatite. Appears to form an integral part of the mineralized matrix. Probably important to cell-matrix interaction Function: Acts as a cytokine involved in enhancing production of interferon-gamma and

			interleukin-12 and reducing production of interleukin-10 and is essential in the pathway that leads to type I immunity (By similarity)
Retnlg	-3.38541844	0.062538	Resistin Like Beta
Itgb2l	-3.373913642	0.018413	Mucosa-specific cytochrome P450 enzyme active in the metabolism of sex steroids and xenobiotic substrates
Gata1	-3.318690488	0.006966	GATA Binding Protein 1 (Globin Transcription Factor 1)
Dcstamp	-3.296679501	0.097338	Dendrocyte Expressed Seven Transmembrane Protein
Fam150b	-3.275804321	0.028438	Cartilage oligomeric matrix protein play a role in structural integrity of cartilage via its interaction with other extracellular matrix proteins such as collagens and fibronectin.
Trim10	-3.256300142	0.029912	Kynurenine 3-Monooxygenase (Kynurenine 3-Hydroxylase) gene encodes a mitochondrion outer membrane protein that catalyzes the hydroxylation of L-tryptophan metabolite, L-kynurenine, to form L-3-hydroxykynurenine. Required for synthesis of quinolinic acid, a neurotoxic NMDA receptor antagonist and potential endogenous inhibitor of NMDA receptor signaling in axonal targeting, synaptogenesis and apoptosis during brain development. Quinolinic acid may also affect NMDA

			receptor signaling in pancreatic beta cells, osteoblasts, myocardial cells, and the gastrointestinal tract
Gfi1	-3.182485215	0.051525	Growth Factor Independent 1 Transcription Repressor
Cd177	-3.160436406	0.001573	CD177 Molecule
S100a8	-3.080480416	0.070974	S100 Calcium Binding Protein A8
Rprml	-3.039119059	0.080927	Reprimo-Like
Wnt9b	-2.963297833	0.01551	Solute Carrier Family 23 (Ascorbic Acid Transporter), Member 1 Sodium/ascorbate cotransporter. Mediates lectrogenic uptake of vitamin C, with a stoichiometry of 2 Na(+) for each ascorbate
Dntt	-2.9617134	0.056854	Aldolase B, Fructose-Bisphosphate The developing embryo produces aldolase A, which is produced in even greater amounts in adult muscle where it can be as much as 5% of total cellular protein. key role in carbohydrate metabolism as it catalyzes one of the major steps of the glycolytic-gluconeogenic pathway
Mtfr2	-2.9617134	0.057284	Mitochondrial Fission Regulator 2
Galnt3	-2.9617134	0.058369	Baculoviral IAP Repeat Containing 5 dual roles in promoting cell proliferation and preventing apoptosis.
Mogat1	-2.877251095	0.029946	Monoacylglycerol O-Acyltransferase 1
Mki67	-2.859186566	0.008055	Marker Of Proliferation Ki-67
Prtn3	-2.788143116	0.001812	Proteinase 3

Wif1	-2.729034071	0.001573	Activin A Receptor, Type IC Plays a role in cell differentiation, growth arrest and apoptosis
Sez6l	-2.656107386	0.006878	Seizure Related 6 Homolog (Mouse)-Like
1700023L04Rik	-2.647620278	0.019397	Unclassified gene
Spta1	-2.607594526	0.056854	Spectrin, Alpha, Erythrocytic 1
Car1	-2.552610624	0.006966	Unclassified gene
Nr4a3	-2.546230669	0.029946	Nucleolar And Spindle Associated Protein 1 Microtubule-associated protein with the capacity to bundle and stabilize microtubules (By similarity). May associate with chromosomes and promote the organization of mitotic spindle microtubules around them
Mmp8	-2.534225828	0.001111	Matrix Metallopeptidase 3 (Stromelysin 1, Progelatinase) Can degrade fibronectin, laminin, gelatins of type I, II, IV, and V; collagens III, IV, X, and IX, and cartilage proteoglycans. Activates procollagenase
Depdc1a	-2.533589198	0.047483	DEP Domain Containing 1
Cenpe	-2.508894249	0.029946	Centromere Protein E, 312kDa
Siglecg	-2.496124962	0.002128	Sialic Acid Binding Ig-Like Lectin
Niacr1	-2.467122255	0.038728	Niacin Receptor
Espl1	-2.464271043	0.004251	Extra Spindle Pole Bodies Homolog 1 (S. Cerevisiae
Kif11	-2.442622389	0.018205	Kinesin Family Member 11
Spp1	-2.44185001	0.038728	Secreted Phosphoprotein 1
Hapln1	-2.431191311	0.028791	Hyaluronan And Proteoglycan Link Protein 1
Dtl	-2.407179369	0.03852	Denticleless E3 Ubiquitin Protein Ligase Homolog

			(Drosophila)
2810417H13Rik	-2.397477367	0.008967	Unclassified gene
Fignl1	-2.377528766	0.045873	Fidgetin-Like 1
Ankef1	-2.377528766	0.047668	Ankyrin Repeat And EF-Hand Domain Containing 1
Faim3	-2.327154754	0.05713	Fas Apoptotic Inhibitory Molecule 3
Lep	-2.322644249	0.029946	Leptin
Calcb	-2.28962057	0.017078	Calcitonin-Related Polypeptide Beta
Kif14	-2.274958018	0.0597	Plasminogen acts as a proteolytic factor in a variety of other processes including embryonic development, tissue remodeling, tumor invasion, and inflammation.
Edil3	-2.261977547	0.055502	EGF-Like Repeats And Discoidin I-Like Domains 3
Tpx2	-2.254603707	0.027915	Glutamine-Fructose-6-Phosphate Transaminase 2 Most likely involved in regulating the availability of precursors for N- and O-linked glycosylation of proteins
Ptprr	-2.245188104	0.037086	Protein Tyrosine Phosphatase, Receptor Type, R
Arhgef39	-2.220801683	0.070974	Rho Guanine Nucleotide Exchange Factor (GEF) 39
Clspn	-2.220801683	0.079844	Claspin
Nsl1	-2.220801683	0.084671	NSL1, MIS12 Kinetochore Complex Component
Inhba	-2.205099173	0.013598	Inhibin, Beta A
Spib	-2.200493208	0.014836	Spi-B Transcription Factor (Spi-1/PU.1 Related)
Aurkb	-2.175281992	0.042606	Aurora Kinase B
Map7d2	-2.164532854	0.087416	Ubiquitin-Conjugating Enzyme E2C Accepts ubiquitin from the E1 complex and catalyzes its covalent attachment to other proteins. In vitro

			catalyzes 'Lys-11'- and 'Lys-48'-linked polyubiquitination. Acts as an essential factor of the anaphase promoting complex/cyclosome (APC/C), a cell cycle-regulated ubiquitin ligase that controls progression through mitosis. Acts by initiating 'Lys-11'-linked polyubiquitin chains on APC/C substrates, leading to the degradation of APC/C substrates by the proteasome and promoting mitotic exit
Ccna2	-2.160383935	0.021508	Cyclin A2
Aspm	-2.144968526	0.038978	Asp (Abnormal Spindle) Homolog, Microcephaly Associated (Drosophila)
Irf4	-2.13431486	0.018205	Myosin, Heavy Chain 6, Cardiac Muscle, Alpha Muscle contraction
Pax5	-2.120620413	0.090294	Alanine--Glyoxylate Aminotransferase 2 ADMA is a potent inhibitor of nitric-oxide (NO) synthase, and this activity provides mechanism through which the kidney regulates blood pressure
Cidec	-2.10808921	0.051139	Cell Death-Inducing DFFA-Like Effector C
Mis18bp1	-2.063222678	0.055502	MIS18 Binding Protein 1
Ccnb1	-2.058955602	0.038978	Cyclin B1
Pdcd1	-2.056088511	0.051361	Serine protease which hydrolyzes a range of proteins including type I collagen, fibronectin and fibrinogen. Remodeling
Slc7a10	-2.044090126	0.099946	Solute Carrier Family 7 (Neutral Amino Acid Transporter Light Chain,

			Asc System), Member 10
Ccnb2	-2.043079292	0.055502	Cyclin B2
Angptl7	-2.035644481	0.014339	Angiopoietin-Like 7
Aldh3b2	-2.016879317	0.079989	Antigen Identified By Monoclonal Antibody Ki-67 Thought to be required for maintaining cell proliferation
Cxcl13	-2.011669224	0.041525	Chemokine (C-X-C Motif) Ligand 13
Slc36a2	-2.007439944	0.053918	Solute Carrier Family 36 (Proton/Amino Acid Symporter), Member 2
Adra1b	2.014180343	0.02392	WNT Inhibitory Factor 1 Binds to WNT proteins and inhibits their activities
Gm20752	2.016110787	0.062065	Unclassified gene
Mfsd2a	2.028565728	0.043719	Olfactory receptor 1033 sensory perception of smell
Igsf5	2.037940342	0.026037	Immunoglobulin Superfamily, Member 5
Myl7	2.041020676	0.053648	UDP-N-Acetyl-Alpha-D-Galactosamine:Polypeptide N-Acetylgalactosaminyltransferase 3 (GalNAc-T3) Individual GalNAc-transferases have distinct activities and initiation of O-glycosylation is regulated by a repertoire of GalNAc-transferases.
Esrp2	2.041074169	0.021267	Cyclin B1 essential for cell cycle control at G2/M mitosis transmission
Akr1c19	2.043224705	0.080648	Interleukin-8 important mediator of the innate immune response
Acnat2	2.047226654	0.093949	Unclassified gene
Serpina3m	2.065105674	0.056854	Serpin Peptidase Inhibitor, Clade A (Alpha-1 Antiproteinase, Antitrypsin), Member 3
Gpld1	2.077970089	0.089321	Glycosylphosphatidylinosito

			l Specific Phospholipase D1
C730036E19Rik	2.08107011	0.083775	Nephrosis 1, Congenital, Finnish Type (Nephrin) Regulates glomerular vascular permeability. Plays a role in skeletal muscle formation through regulation of myoblast fusion (By similarity)
Kmo	2.081921044	0.093015	Kynurenine 3-Monooxygenase (Kynurenine 3-Hydroxylase)
Cyp3a44	2.084205029	0.050901	Occludin May play a role in the formation and regulation of the tight junction (TJ) paracellular permeability barrier. It is able to induce adhesion when expressed in cells lacking tight junctions
Soat2	2.092703909	0.030307	Sterol O-Acyltransferase 2
Khk	2.107269661	0.051139	Leucine Rich Repeat Neuronal 1 associated with LRRN1 include atrioventricular septal defect, and neuronitis.
Ugt1a6b	2.108829803	0.079989	UDP Glucuronosyltransferase 1 Family, Polypeptide A6
Gm16157	2.112719281	0.045873	Unclassified gene
Dhtkd1	2.118052723	0.059139	Dehydrogenase E1 And Transketolase Domain Containing 1
Cyp2d40	2.119675634	0.085216	Quinolinate Phosphoribosyltransferase Involved in the catabolism of quinolinic acid (QA) elevated levels causes neurodegenerative diseases
Serpina3k	2.119804566	0.05713	Serpin Peptidase Inhibitor, Clade A (Alpha-1 Antiproteinase, Antitrypsin),

			Member 3
Creb3l3	2.120047828	0.057457	CAMP Responsive Element Binding Protein 3-Like 3
Gjb2	2.12240577	0.093015	Gap Junction Protein, Beta 2, 26kDa
Dak	2.125577296	0.028536	Dihydroxyacetone Kinase 2 Homolog (S. Cerevisiae)
Pecr	2.148211567	0.043782	Insulin-Like Growth Factor Binding Protein, Acid Labile Subunit Involved in protein-protein interactions that result in protein complexes, receptor-ligand binding or cell adhesion
Arhgef26	2.150760081	0.045159	Rho Guanine Nucleotide Exchange Factor (GEF) 26
Aldh1l1	2.164342275	0.047668	Aldehyde Dehydrogenase 1 Family, Member L1
BC021614	2.170638621	0.02715	Unclassified gene
Aass	2.208291588	0.080927	Aminoadipate-Semialdehyde Synthase
Cblc	2.217261709	0.094626	Proprotein Convertase Subtilisin/Kexin Type 9 Crucial player in the regulation of plasma cholesterol homeostasis. Binds to low-density lipid receptor family members Regulates neuronal apoptosis via modulation of LRP8/APOER2 levels and related anti-apoptotic signaling pathways
Ahcy	2.242676451	0.053918	Adenosylhomocysteinase
Mettl7b	2.257747786	0.08564	Spectrin, Alpha, Erythrocytic 1 (Elliptocytosis 2) Spectrin is the major constituent of the cytoskeletal network underlying the erythrocyte plasma membrane. It associates with band 4.1 and actin to form the

			cytoskeletal superstructure of the erythrocyte plasma membrane
Masp1	2.265019615	0.043782	Adiponectin, C1Q And Collagen Domain Containing Important adipokine involved in the control of fat metabolism and insulin sensitivity, with direct anti-diabetic, anti-atherogenic and anti-inflammatory activities.
Tat	2.274794699	0.081026	Tyrosine Aminotransferase
Hs3st3b1	2.290471061	0.084768	Heparan Sulfate (Glucosamine) 3-O-Sulfotransferase 3B1
Slc38a4	2.293220337	0.082763	Adenosine Kinase Inhibition of this enzyme has been implicated in tissue-protective mechanisms against various physiological stresses, including ischemia, seizures, inflammation and pain, thus there is much interest in developing pharmacological ADK inhibitors
Slc17a8	2.297675402	0.070399	Solute Carrier Family 17 (Vesicular Glutamate Transporter), Member 8
0610012H03Rik	2.297675402	0.083435	Myeloperoxidase polymorphonuclear leukocytes
Adh1	2.303294478	0.080858	Acid-Sensing (Proton-Gated) Ion Channel Functions as a postsynaptic proton receptor that influences intracellular Ca(2+) concentration and calmodulin-dependent protein kinase II phosphorylation and

			thereby the density of dendritic spines.
Tmem86b	2.303561966	0.083775	Chloride Channel, Voltage-Sensitive 1 The protein encoded by this gene regulates the electric excitability of the skeletal muscle membrane.
1810053B23Rik	2.309411016	0.01551	Tenascin N neuron outgrowth and cell migration
Gldc	2.314854863	0.03852	Glycine Dehydrogenase (Decarboxylating)
Sptbn2	2.317483531	0.056854	Spectrin, Beta, Non-Erythrocytic 2
1300002K09Rik	2.338665347	0.05713	Proliferation and differentiation of hematopoetic cells /may prevent apoptosis through activation of NFkB
6430571L13Rik	2.346608392	0.043782	Unclassified gene
Cth	2.347820083	0.08208	Cystathionine Gamma-Lyase
Cyp2f2	2.351470422	0.057284	Monoacylglycerol O-Acyltransferase 1 Catalyzes the formation of diacylglycerol from 2-monoacylglycerol and fatty acyl-CoA. Probably not involved in absorption of dietary fat in the small intestine (By similarity)
Nipsnap1	2.357817549	0.079844	Nipsnap Homolog 1 (C. Elegans)
Slc17a3	2.36367621	0.050957	Protein Z, Vitamin K-Dependent Plasma Glycoprotein Appears to assist hemostasis by binding thrombin and promoting its association with phospholipid vesicles. Inhibits activity of the coagulation protease factor Xa in the presence of SERPINA10, calcium and

			phospholipids
Ttpa	2.364675089	0.089321	Phosphatidylethanolamine N-Methyltransferase The protein isoforms encoded by this gene localize to the endoplasmic reticulum and mitochondria-associated membranes.
Onecut2	2.369478936	0.060404	One Cut Homeobox 2
Mchr1	2.376066417	0.08208	Melanin-Concentrating Hormone Receptor 1
Cyp4f15	2.381345281	0.060404	Desmoglein 11 Component of intercellular desmosome junctions. Involved in the interaction of plaque proteins and intermediate filaments mediating cell-cell adhesion
Acot12	2.387267722	0.052273	Acyl-CoA Thioesterase 12
Ocln	2.404639508	0.030487	Kruppel-Like Factor 4 (Gut) Plays an important role in maintaining embryonic stem cells, and in preventing their differentiation. Required for establishing the barrier function of the skin and for postnatal maturation and maintenance of the ocular surface. Involved in the differentiation of epithelial cells and may also function in skeletal and kidney development.
Tm4sf4	2.407955293	0.057284	Transmembrane 4 L Six Family Member 4
Agxt2l1	2.412592903	0.02392	Alanine--Glyoxylate Aminotransferase 2-Like 1
Tm6sf2	2.412899312	0.029181	Carbonic anhydrase 3 slow twitch skeletal muscle and myogenesis
Cpsf4l	2.426651453	0.022987	Cleavage And Polyadenylation Specific Factor 4-Like

Leap2	2.428615595	0.006796	Liver Expressed Antimicrobial Peptide 2
Tymp	2.430509087	0.00213	Fibrinogen Alpha Chain
Slc38a3	2.434089028	0.055502	Solute Carrier Family 38, Member 3
Aspg	2.437864099	0.045057	WNT outside to inside cell signaling
Shmt1	2.442176393	0.019397	Glutamic-Pyruvate Transaminase (Alanine Aminotransferase) Participates in cellular nitrogen metabolism and also in liver gluconeogenesis starting with precursors transported from skeletal muscles (By similarity)
Myh6	2.446107263	0.053402	Myosin, Heavy Chain 6, Cardiac Muscle, Alpha
Sec14l2	2.447268731	0.029181	SEC14-Like 2 (S. Cerevisiae)
Hsd17b13	2.453927186	0.086342	Programmed Cell Death 1 Inhibitory cell surface receptor involved in the regulation of T-cell function during immunity and tolerance. Upon ligand binding, inhibits T-cell effector functions in an antigen-specific manner. Possible cell death inducer, in association with other factors
Slc10a5	2.460263008	0.051139	Solute Carrier Family 10, Member 5
Mat1a	2.465772512	0.047483	Golgi Transport 1A May be involved in fusion of ER-derived transport vesicles with the Golgi complex
Aldh1b1	2.468548321	0.046008	Carbonic anhydrase 5a, mitochondrial for proton transfer
Pemt	2.468976542	0.094665	Phosphatidylethanolamine N-Methyltransferase

Saa4	2.47040722	0.051323	Serum Amyloid A4, Constitutive
Gm4952	2.475492914	0.050901	Coagulation factor 11
Nr1i3	2.478338137	0.045057	Nuclear Receptor Subfamily 1, Group I, Member 3
Hrsp12	2.485437319	0.055502	Heat-Responsive Protein 12
Pax7	2.488211312	0.096583	PAx7 Secreted Phosphoprotein 2, 24kDa Could coordinate an aspect of bone turnover (By similarity)
Pklr	2.499710313	0.066993	Cell Death-Inducing DFFA-Like Effector B Activates apoptosis
Sardh	2.509430038	0.038728	Sarcosine Dehydrogenase
Apoc1	2.510518264	0.045534	Apolipoprotein C-I
Hsd17b2	2.512555427	0.08208	Apolipoprotein F Minor apolipoprotein that associates with LDL. Inhibits cholesteryl ester transfer protein (CETP) activity and appears to be an important regulator of cholesterol transport. Also associates to a lesser degree with VLDL, Apo-AI and Apo-AII
Cldn14	2.515471094	0.030307	Claudin 14
Apon	2.517351953	0.052927	Unclassified gene
2810007J24Rik	2.518769834	0.099946	Unclassified gene
Slc22a18	2.520164954	0.045159	Solute Carrier Family 22, Member 18
Hamp	2.521360194	0.012396	Hepcidin Antimicrobial Peptide
Sec14l4	2.526325679	0.025271	Inter-Alpha-Trypsin Inhibitor Heavy Chain 1 binding protein between hyaluronan and other matrix protein, including those on cell surfaces in tissues to regulate the localization, synthesis and

			degradation of hyaluronan which are essential to cells undergoing biological processes Function: Contains a potential peptide which could stimulate a broad spectrum of phagocytotic cells
1700001C19Rik	2.527795195	0.035907	Surfactant, Pulmonary-Associated Protein C for alveolar stability
Asl	2.528828883	0.019341	Argininosuccinate Lyase
Bhmt	2.536332732	0.012396	Kinesin Family Member 11 Kinesin superfamily proteins (KIFs) are motor proteins that convert chemical energy, typically in the form of ATP, into mechanical force. They act upon microtubules to move vesicles and organelles within cells, cause the beating of flagella and cilia, and act within the mitotic and meiotic spindles to segregate replicated chromosomes to progeny cells.
Dhcr24	2.536747411	0.074172	24-Dehydrocholesterol Reductase
Dnase2b	2.544462481	0.019397	Deoxyribonuclease II Beta
Marc1	2.548646948	0.054751	Mitochondrial Amidoxime Reducing Component 1
Cdhr5	2.550079346	0.07193	Cadherin-Related Family Member 5
Mup6	2.559687729	0.021428	Neuronal Growth Regulator 1 May be involved in cell-adhesion. May function as a trans-neural growth-promoting factor in regenerative axon sprouting in the mammalian brain (By similarity)
Cml2	2.560778952	0.047668	Camello-Like Protein 2

Itih1	2.565300495	0.079844	Myosin, Light Chain 7, Regulatory mediates plus-ended movement along microfilaments. It is involved in muscle contraction through cyclic interactions with actin-rich thin filaments, creating a contractile force. It is regulated by phosphorylation via myosin light chain kinase (MLCK) and by intracellular Ca2+ concentrations.
Ugt2a3	2.573838614	0.070974	Paired Box 7 Transcription factor playing a role in myogenesis through regulation of muscle precursor cells proliferation (By similarity)
Lect2	2.583375823	0.080359	EGF-Like Repeats And Discoidin I-Like Domains 3 Promotes adhesion of endothelial cells through interaction with the alpha-v/beta-3 integrin receptor. Inhibits formation of vascular-like structures. May be involved in regulation of vascular morphogenesis of remodeling in embryonic development
BC089597	2.589805289	0.061603	Calcitonin acts to reduce blood calcium
Gcgr	2.590829792	0.056854	Glucagon Receptor
Cyp2b13	2.590888717	0.004327	Cytochrome P450, Family 2, Subfamily B, Polypeptide 6
Glyat	2.5909104	0.069401	Mitochondrial matrix enzyme
Serpina1a	2.595254805	0.056854	Serpin Peptidase Inhibitor, Clade A (Alpha-1 Antiproteinase, Antitrypsin), Member 1

Fga	2.600257257	0.09491	Fibrinogen Alpha Chain
Igsf11	2.612634517	0.00977	Immunoglobulin Superfamily, Member 11
Fgg	2.615663211	0.099946	Fibrinogen Gamma Chain
Slc25a13	2.620476414	0.074259	Solute Carrier Family 25 (Aspartate/Glutamate Carrier), Member 13
Prhoxnb	2.624264625	0.028045	Glutathione S-Transferase Alpha 2 Conjugation of reduced glutathione protect against ROS
Cyp2d13	2.627458051	0.082465	Nuclear Receptor Subfamily 4, Group A, Member 3 steroid-thyroid hormone-retinoid receptor superfamily. The encoded protein may act as a transcriptional activator. The protein can efficiently bind the NGFI-B Response Element (NBRE). Three different versions of extraskeletal myxoid chondrosarcomas (EMCs) are the result of reciprocal translocations between this gene and other genes.
Gstm6	2.633668681	0.070974	Glutathione S-Transferase Mu 6
Reep6	2.635844406	0.043782	Hyaluronan Binding Protein 2 Activates coagulation factor VII
Cideb	2.645563552	0.069948	Cell Death-Inducing DFFA-Like Effector B
Cpn2	2.650154062	0.032905	Immunoglobulin Superfamily, Member 5 Provides, together with MAGI1, adhesion machinery at tight junctions, which may regulate the permeability of kidney glomerulus and small intestinal epithelial cells. Mediates calcium-independent homophilic

			cell adhesion.
Slc2a9	2.650190179	0.043782	Solute Carrier Family 2 (Facilitated Glucose Transporter), Member 9
Cyp3a41a	2.656839519	0.060404	Cytochrome P450, Family 3, Subfamily A, Polypeptide 41
Gcnt4	2.656839519	0.075718	Rho Guanine Nucleotide Exchange Factor (GEF) 26 Activates RhoG GTPase by promoting the exchange of GDP by GTP. Required for the formation of membrane ruffles during macropinocytosis. Required for the formation of cup-like structures during trans-endothelial migration of leukocytes. In case of Salmonella enterica infection, activated by SopB, which induces cytoskeleton rearrangements and promotes bacterial entry
F12	2.658890268	0.040904	Coagulation Factor XII (Hageman Factor)
Marcksl1-ps4	2.670699756	0.037689	Inter-Alpha-Trypsin Inhibitor Heavy Chain 3 May act as a carrier of hyaluronan in serum or as a binding protein between hyaluronan and other matrix protein, including those on cell surfaces in tissues to regulate the localization, synthesis and degradation of hyaluronan which are essential to cells undergoing biological processes
Mmd2	2.670699756	0.038978	Glucagon Receptor important in controlling blood glucose levels.
F7	2.673319736	0.050901	Coagulation Factor VII

			(Serum Prothrombin Conversion Accelerator)
Ces1g	2.674186169	0.027783	Cadherin-Related Family Member 3 Cadherins are calcium-dependent cell adhesion proteins. They preferentially interact with themselves in a homophilic manner in connecting cells; cadherins may thus contribute to the sorting of heterogeneous cell types
Afm	2.674359521	0.080056	Afamin
Gm10319	2.679104524	0.02715	Fidgetin-Like 1 May regulate osteoblast proliferation and differentiation (By similarity)
C8g	2.67916316	0.067583	PARP1 Binding Protein playing a central role DNA repair and in the maintenance of genomic stability.
Aadac	2.679392746	0.083536	Claudins are found at tight junctions as a physical barrier and known for maintaining cell polarity and signal transductions
Cyp2j5	2.687014429	0.051361	Cytochrome P450, Family 2, Subfamily J, Polypeptide 5
Spp2	2.687788106	0.064504	Secreted Phosphoprotein 2, 24kDa
Pcbd1	2.688475977	0.074172	Pterin-4 Alpha-Carbinolamine Dehydratase/Dimerization Cofactor Of Hepatocyte Nuclear Factor 1 Alpha
Afmid	2.689746558	0.055656	Arylformamidase
Pglyrp2	2.693866628	0.051312	Sushi Domain Containing 1 related to calcium ion binding
Ttr	2.695657868	0.095069	Transthyretin
Nr1i2	2.69777719	0.034475	Vitronectin. Vitronectin is a cell adhesion and

			spreading factor found in serum and tissues. Vitronectin interact with glycosaminoglycans and proteoglycans. Is recognized by certain members of the integrin family and serves as a cell-to-substrate adhesion molecule. Inhibitor of the membrane-damaging effect of the terminal cytolytic complement pathway
Sult1d1	2.702094544	0.051361	Heparan Sulfate (Glucosamine) 3-O-Sulfotransferase 3B1
Cyp3a25	2.705934786	0.085328	Protease, serine 34 peptide cross-linking via chondroitin 4-sulfate glycosaminoglycan, proteolysis Component extracellular matrix, extracellular space Function glycosaminoglycan binding, heparin binding,
F13b	2.721750009	0.083353	Mannan-binding lectin serine peptidase 2 important role in the activation of the complement system
Apof	2.721775643	0.051361	Apolipoprotein F
Mafa	2.722636289	0.019397	C-Reactive Protein, Pentraxin-Related Displays several functions associated with host defense: it promotes agglutination, bacterial capsular swelling, phagocytosis and complement fixation through its calcium-dependent binding to phosphorylcholine. Can interact with DNA and

			histones and may scavenge nuclear material released from damaged circulating cells
Vtn	2.724939798	0.060404	Vitronectin
9030619P08Rik	2.725088771	0.01421	Unclassified gene
Cyp3a13	2.730187574	0.02715	Claudins are found at tight junctions as a physical barrier and known for maintaining cell polarity and signal transductions
Itih3	2.730197604	0.055656	Inter-Alpha-Trypsin Inhibitor Heavy Chain 3
Gc	2.731122478	0.084768	Group-Specific Component (Vitamin D Binding Protein)
Alb	2.740710898	0.079844	Albumin
Hpn	2.742282429	0.047668	Transcription Factor 23 Lacks DNA binding activity. Seems to play a role in the inhibition of myogenesis (By similarity)
Cyp2a12	2.745035777	0.053402	Cytochrome P450, Family 2, Subfamily A, Polypeptide 13
Prodh2	2.745077892	0.022186	Carboxylesterase 1 Involved in the detoxification of xenobiotics and in the activation of ester and amide prodrugs.
Cps1	2.752975783	0.079989	Carbamoyl-Phosphate Synthase 1, Mitochondrial
F9	2.757502507	0.045806	Coagulation Factor IX
Aldob	2.75783464	0.037759	Ankyrin Repeat And Sterile Alpha Motif Domain Containing 4B
Asgr1	2.760542813	0.052953	Asialoglycoprotein Receptor 1
Kng1	2.760911134	0.098386	Kininogen 1
F2	2.761612741	0.070974	Potassium Intermediate/Small Conductance Calcium-Activated Channel, Subfamily N, Member 2 Forms a voltage-

			independent potassium channel activated by intracellular calcium. Activation is followed by membrane hyperpolarization.
Hal	2.770854795	0.000457	Gap Junction Protein, Beta 1, 32kDa One gap junction consists of a cluster of closely packed pairs of transmembrane channels, the connexons, through which materials of low MW diffuse from one cell to a neighboring cell
Baat	2.778243606	0.019594	Von Willebrand Factor C And EGF Domains May be a regulatory element in the beta-catenin signaling pathway and a target for chemoprevention of hapatocellular carcinoma
Abcg8	2.780288082	0.085798	Osteocalcin Bone Gamma-Carboxyglutamate (Gla) Protein bone building
Cpb2	2.783670735	0.067583	Carboxypeptidase B2 (Plasma)
Fmo5	2.785606334	0.046008	Mannan-binding lectin serine peptidase 2 important role in the activation of the complement system
Hnf4a	2.793002523	0.057284	Hepatocyte Nuclear Factor 4, Alpha
AI182371	2.802086494	0.083435	Unclassified gene
Cyp17a1	2.803365334	0.038728	Cystathionine-beta-synthase Important regulator of hydrogen sulfide, especially in the brain, utilizing cysteine instead of serine to catalyze the formation of hydrogen sulfide. Hydrogen sulfide is a gastratransmitter with

			signaling and cytoprotective effects such as acting as a neuromodulator in the brain to protect neurons against hypoxic injury (By similarity)
Zfp750	2.807804337	0.045159	Zinc Finger Protein 750
Dpys	2.816179157	0.043853	Dihydropyrimidinase
Slc6a13	2.821275805	0.08208	Anillin, Actin Binding Protein Required for cytokinesis. Essential for the structural integrity of the cleavage furrow and for completion of cleavage furrow ingression
Apoa2	2.822861971	0.055656	Apolipoprotein A-II
Crp	2.838365226	0.055656	C-Reactive Protein, Pentraxin-Related
Asgr2	2.839350371	0.037086	Asialoglycoprotein Receptor 2
Cpn1	2.842127601	0.08377	Selenocysteine involved in antioxidant behavior
Rhbg	2.849832393	0.081594	Rh Family, B Glycoprotein (Gene/Pseudogene)
Gm20337	2.849832393	0.082841	Unclassified gene
Hgfac	2.852604219	0.058987	HGF Activator
Fgb	2.852860973	0.065778	Fibrinogen Beta Chain
Masp2	2.854041271	0.040635	Mannan-Binding Lectin Serine Peptidase 2
Tfr2	2.854891105	0.05808	Transferrin Receptor 2
Glyctk	2.855620374	0.047668	Glycerate Kinase
Lcat	2.863591498	0.069948	Lecithin-Cholesterol Acyltransferase
Apoc3	2.867709671	0.023702	Apolipoprotein C-III
Ces1e	2.869353896	0.070974	Carboxylesterase 1
Hrg	2.871702688	0.051139	Histidine-Rich Glycoprotein
Cfhr2	2.87267761	0.064749	Complement Factor H-Related 2
Cyp2c50	2.872843692	0.084085	Melanoma Inhibitory Activity Elicits growth inhibition on melanoma cells in vitro as well as

			some other neuroectodermal tumors, including gliomas
Tmprss6	2.877900189	0.066993	Transmembrane Protease, Serine 6
1300017J02Rik	2.887647252	0.058369	Dentin Matrix Acidic Phosphoprotein 1
Ces1b	2.892194086	0.019397	Unclassified gene
Slc26a1	2.899427534	0.029464	Solute Carrier Family 26 (Anion Exchanger), Member 1
Apoc4	2.90323266	0.03157	Apolipoprotein C-IV
Azgp1	2.905867778	0.055656	Alpha-2-Glycoprotein 1, Zinc-Binding
Plg	2.905893263	0.054751	Plasminogen
Cyp2c68	2.92894573	0.045873	Cytochrome P450, Family 2, Subfamily C, Polypeptide 68
Slc23a1	2.936737923	0.011953	Solute Carrier Family 23 (Ascorbic Acid Transporter), Member 1
Cyp2d10	2.937540789	0.047483	Cytochrome P450, Family 2, Subfamily D, Polypeptide 10
Slc22a27	2.93760266	0.055656	Solute Carrier Family 22 (Organic Anion Transporter), Member 27
Proz	2.938711184	0.08155	Protein Z, Vitamin K-Dependent Plasma Glycoprotein
Aadat	2.942427808	0.015937	Aminoadipate Aminotransferase
Agxt2	2.949410529	0.064327	Homeobox protein hox-3a housekeeping gene developmental regulatory system that provides cells with specific positional identities
Rdh7	2.950113823	0.065051	Retinol Dehydrogenase 7 (All-Trans)
Apoh	2.952108441	0.056854	Apolipoprotein H (Beta-2-Glycoprotein I)
Sult2a5	2.95345137	4.69E-05	Sulfotransferase Family, Cytosolic, 2A,

			Dehydroepiandrosterone (DHEA)-Preferring, Member 5
Adh4	2.95345137	0.056854	Alcohol Dehydrogenase 4 (Class II), Pi Polypeptide
Kcnn2	2.954895302	0.013598	Potassium Channel, Calcium Activated Intermediate/Small Conductance Subfamily N Alpha, Member 2
1190003J15Rik	2.957167744	0.01551	Unclassified gene
Cyp3a59	2.957457234	0.086107	Cytochrome P450, Family 3, Subfamily A, Polypeptide 59
Hamp2	2.959202867	0.000115	Hepcidin Antimicrobial Peptide 2
Acox2	2.966017249	0.023531	Acyl-CoA Oxidase 2, Branched Chain
Nr0b2	2.968112329	0.05832	Nuclear Receptor Subfamily 0, Group B, Member 2
Cbs	2.9753635	0.028399	Cystathionine-Beta-Synthase
Dmgdh	2.976881529	0.050901	Dimethylglycine Dehydrogenase
Pipox	2.977336073	0.046442	Pipecolic Acid Oxidase
Akr1c12	2.977476853	0.025271	Aldo-Keto Reductase Family 1, Member C12
Proc	2.981340483	0.046794	S100 Calcium Binding Protein A9 S100A9 is a calcium- and zinc-binding protein which plays a prominent role in the regulation of inflammatory processes and immune response.
Ambp	2.982403628	0.081594	Alpha-1-Microglobulin/Bikunin Precursor
Pah	2.984956402	0.053402	Phenylalanine Hydroxylase
Fbp1	2.9854912	0.044152	Desmoglein 2 Component of intercellular desmosome junctions. Involved in the interaction of plaque

			proteins and intermediate filaments mediating cell-cell adhesion
Cml1	2.987594259	0.032759	Neuronatin May participate in the maintenance of segment identity in the hindbrain and pituitary development, and maturation or maintenance of the overall structure of the nervous system. May function as a regulatory subunit of ion channels
Rgn	2.99199617	0.070974	Regucalcin
Iyd	2.99628826	0.050901	Iodotyrosine Deiodinase
Akr1c20	3.003607499	0.07171	Aldo-Keto Reductase Family 1, Member C20
Serpinc1	3.004517545	0.043782	Serpin Peptidase Inhibitor, Clade C (Antithrombin), Member 1
Sult2a3	3.0082184	0.022331	Sulfotransferase Family, Cytosolic, 2A, Dehydroepiandrosterone (DHEA)-Preferring, Member 3
Hoga1	3.012196349	0.067585	4-Hydroxy-2-Oxoglutarate Aldolase 1
Cyp2c70	3.019497052	0.060664	Unclassified gene
Habp2	3.019922607	0.074172	Hyaluronan Binding Protein 2
Mug1	3.035155395	0.099636	Unclassified gene
Abcg5	3.035645753	0.08155	ATP-Binding Cassette, Sub-Family G (WHITE), Member 5
A930016O22Rik	3.038171586	0.043782	Unclassified gene
Slc6a12	3.038799244	0.028791	Solute Carrier Family 6 (Neurotransmitter Transporter), Member 12
C8b	3.0404134	0.083536	Complement Component 8, Beta Polypeptide
Serpina1b	3.047712744	0.047483	Serpin Peptidase Inhibitor, Clade A (Alpha-1 Antiproteinase, Antitrypsin),

			Member 1
Agmat	3.05216902	0.019341	Agmatine Ureohydrolase (Agmatinase)
Pbld2	3.052728089	0.040833	Phenazine Biosynthesis-Like Protein Domain Containing
Ces2a	3.052989003	0.080927	Forkhead Box A3 Transcription factor that is thought to act as a 'pioneer' factor opening the compacted chromatin for other proteins through interactions with nucleosomal core histones and thereby replacing linker histones at target enhancer and/or promoter sites Involved in regulation of neuronal-specific transcription. May be involved in regulation of spermatogenesis
Serpind1	3.059090798	0.078095	Serpin Peptidase Inhibitor, Clade D (Heparin Cofactor), Member 1
Timd2	3.064278526	0.039953	Paired box 5 differentiation of b cells, neural regulation
Bhmt2	3.071062126	0.016586	Integrin b cell adhesion cell to matrix adhesion
Cyp2d26	3.086998721	0.051361	Leptin May function as part of a signaling pathway that acts to regulate the size of the body fat depot. An increase in the level of LEP may act directly or indirectly on the CNS to inhibit food intake and/or regulate energy expenditure as part of a homeostatic mechanism to maintain constancy of the adipose mass
Mia2	3.095540611	0.029464	Spectrin, Beta, Non-Erythrocytic 2 Probably plays an important role in

			neuronal membrane skeleton
0610005C13Rik	3.101945733	0.047668	Integrin binding sialoprotein cell to matrix interaction especially bone
Abcc6	3.105270819	0.097388	ATP-Binding Cassette, Sub-Family C (CFTR/MRP), Member 6
Tdo2	3.119418527	0.029946	Glycosylphosphatidylinositol Specific Phospholipase D1 This protein hydrolyzes the inositol phosphate linkage in proteins anchored by phosphatidylinositol glycans (GPI-anchor) thus releasing these proteins from the membrane
Mir133a-2	3.127588324	0.080858	MicroRNA 133a-2
Arg1	3.127932184	0.012396	Inhibin, Beta A Inhibins/activins are involved in regulating a number of diverse functions such as hypothalamic and pituitary hormone secretion, gonadal hormone secretion, germ cell development and maturation, erythroid differentiation, insulin secretion, nerve cell survival, embryonic axial development or bone growth, depending on their subunit composition.
Akr1b7	3.128003	0.005831	Ficolin B marks apoptotic and necrotic cells
1810008I18Rik	3.128147614	0.008883	Unclassified gene
Slc17a4	3.128221182	0.014339	Solute Carrier Family 17, Member 4
Hpd	3.134423723	0.04116	Cell death-inducing DNA fragmentation factor-like effector involved in apoptosis

Grb7	3.13455911	0.01683	Growth Factor Receptor-Bound Protein 7
Cfhr1	3.135059509	0.055656	Complement Factor H-Related 1
Serpina1c	3.145614427	0.053918	Serpin Peptidase Inhibitor, Clade A (Alpha-1 Antiproteinase, Antitrypsin), Member 1
Serpinf2	3.146203902	0.051525	Serpin Peptidase Inhibitor, Clade F (Alpha-2 Antiplasmin, Pigment Epithelium Derived Factor), Member 2
Dct	3.170904657	0.008883	Formimidoyltransferase Cyclodeaminase Binds and promotes bundling of vimentin filaments originating from the Golgi (By similarity)
Foxa2	3.170904657	0.061603	Forkhead Box A2
Qprt	3.171064893	0.029946	Quinolinate Phosphoribosyltransferase
Aspdh	3.175473602	0.021193	Aspartate Dehydrogenase Domain Containing
Slc27a5	3.178800433	0.057457	Pyrimidinergic Receptor P2Y, G-Protein Coupled, 4 They have diverse physiological roles including regulation of platelet aggregation, muscle contraction, neurotransmission, and epithelial cell communication and migration.
Hnf1a	3.196589308	0.012396	HNF1 Homeobox A
Mst1	3.201750618	0.028399	Macrophage Stimulating 1
Atp7b	3.209440083	0.031839	ATPase, Cu++ Transporting, Beta Polypeptide
Hnf1b	3.209440083	0.035907	Nuclear Receptor Subfamily 5, Group A, Member 2 Key regulator of cholesterol 7-alpha-

			hydroxylase gene (CYP7A) expression in liver. May also contribute to the regulation of pancreas-specific genes and play important roles in embryonic development
Ryr2	3.209440083	0.037086	Nicotinamide Riboside Kinase 2 Reduces laminin matrix deposition and cell adhesion to laminin, but not to fibronectin. Involved in the regulation of PXN at the protein level and of PXN tyrosine phosphorylation. May play a role in the regulation of terminal myogenesis
Cyp2c40	3.209440083	0.088358	Selenocysteine involved in antioxidant behavior
Hgd	3.213909162	0.047933	Dimethylglycine Dehydrogenase This gene encodes an enzyme involved in the catabolism of choline, catalyzing the oxidative demethylation of dimethylglycine to form sarcosine. The enzyme is found as a monomer in the mitochondrial matrix, and uses flavin adenine dinucleotide and folate as cofactors. Mutation in this gene causes dimethylglycine dehydrogenase deficiency, characterized by a fishlike body odor, chronic muscle fatigue, and elevated levels of the muscle form of creatine kinase in serum.
Cyp2c54	3.219868673	0.092399	Cytochrome P450, Family 2, Subfamily C, Polypeptide 54
Angptl3	3.227835555	0.030307	RAB15 Effector Protein

			Regulates transferrin receptor recycling from the endocytic recycling compartment
Upb1	3.230544405	0.055502	HOP Homeobox Overexpression causes cardiac hypertrophy (By similarity). May act as a tumor suppressor
Ftcd	3.23266034	0.034048	Formimidoyltransferase Cyclodeaminase
Cyp4f14	3.233146992	0.053402	Cytochrome P450, Family 4, Subfamily F, Polypeptide 14
Gm10768	3.23340507	0.080858	Unclassified gene
Etnk2	3.236611161	0.032905	Monocyte to macrophage differentiation associated 2 key player in muscular dystrophy
Sema4g	3.241139985	0.045159	Sema Domain, Immunoglobulin Domain (Ig), Transmembrane Domain (TM) And Short Cytoplasmic Domain, (Semaphorin) 4G
Abcb11	3.248935938	0.055502	Selenocysteine involved in antioxidant behavior
Mug-ps1	3.249230191	0.029912	CAMP Responsive Element Binding Protein 3-Like 3 Transcription factor that may act during endoplasmic reticulum stress by activating unfolded protein response target genes. Activated in response to cAMP stimulation. In acute inflammatory response, may activate expression of acute phase response (APR) genes. May be involved in growth suppression
Slc10a1	3.25230001	0.038507	Solute Carrier Family 10 (Sodium/Bile Acid

			Cotransporter), Member 1
Slc22a30	3.255356308	0.079989	Solute Carrier Family 22 (Organic Anion Transporter), Member 30
Car5a	3.263940659	0.00044	Carbonic Anhydrase VA, Mitochondria
Rgs16	3.266306131	0.018413	Regulator Of G-Protein Signaling 16
Slc2a2	3.277581446	0.046008	Solute Carrier Family 2 (Facilitated Glucose Transporter), Member 2
Aldh8a1	3.281164141	0.045057	Aldehyde Dehydrogenase 8 Family, Member A1
Sall1	3.281691929	0.03852	Spalt-Like Transcription Factor 1
Gstm3	3.295955467	0.059895	Type II transmembrane serine protease involved in blood coagulation and cell growth and morphology maintenance
Cyp2a5	3.296794317	0.069401	Cytochrome P450, Family 2, Subfamily A, Polypeptide 5
Uox	3.328465674	0.058382	Urate Oxidase, Pseudogene
Gnmt	3.336355746	0.013882	Glycine N-Methyltransferase
Gjb1	3.34218346	0.048648	Zinc Finger Protein 750 Transcription factor involved in epidermis differentiation. Required for terminal epidermal differentiation:
Hsd3b3	3.345704209	0.022829	Hydroxy-Delta-5-Steroid Dehydrogenase, 3 Beta- And Steroid Delta-Isomerase 3
Otc	3.351946566	0.045806	Ornithine Carbamoyltransferase
Sult2a7	3.360404901	0.035475	Sulfotransferase Family, Cytosolic, 2A, Dehydroepiandrosterone (DHEA)-Preferring, Member 7

Keg1	3.380950701	0.000601	Unclassified gene
Serpina1d	3.383334435	0.044152	Serpin Peptidase Inhibitor, Clade A (Alpha-1 Antiproteinase, Antitrypsin), Member 1
Agxt	3.385754357	0.07193	Synaptotagmin I regulatory role in the membrane interactions during trafficking of synaptic vesicles at the active zone of the synapse.
Acsm1	3.397470054	0.041922	Acyl-CoA Synthetase Medium-Chain Family Member 1
Adamts13	3.4125908	0.08155	ADAM Metallopeptidase With Thrombospondin Type 1 Motif, 13
P2ry4	3.4125908	0.082319	Pyrimidinergic Receptor P2Y, G-Protein Coupled, 4
Ccdc151	3.4125908	0.082763	Coiled-Coil Domain Containing 151
Acat3	3.420619147	0.004491	Acetyl-CoA Acetyltransferase 2
0610031O16Rik	3.430349025	0.018942	Osteocalcin Bone Gamma-Carboxyglutamate (Gla) Protein bone building
Gckr	3.442102174	0.044684	Glucokinase (Hexokinase 4) Regulator
Akr1d1	3.444713939	0.024084	Seizure Related 6 Homolog (Mouse)-Like ontribute to specialized endoplasmic reticulum functions in neurons
Haao	3.457567573	0.022112	3-Hydroxyanthranilate 3,4-Dioxygenase
Slc22a7	3.466830764	0.076594	Solute Carrier Family 22 (Organic Anion Transporter), Member 7
BC024386	3.478587777	0.039803	Growth Factor Receptor-Bound Protein 7 Adapter protein that interacts with the cytoplasmic domain of numerous receptor kinases and modulates down-stream signaling. Promotes

			activation of down-stream protein kinases, including STAT3, AKT1, MAPK1 and/or MAPK3. Promotes activation of HRAS. Plays a role in signal transduction in response to EGF. Plays a role in the regulation of cell proliferation and cell migration. Plays a role in the assembly and stability of RNA stress granules.
2810459M11Rik	3.492435219	0.024241	Aggrecan proteoglycan in ECM aims to resist compression in cartilage
Gls2	3.49290308	0.02466	Glutaminase 2 (Liver, Mitochondrial)
Mup9	3.497058371	0.096948	Unclassified gene
Uroc1	3.520338054	0.019218	Urocanate Hydratase 1
Pbld1	3.526080021	0.032905	Phenazine Biosynthesis-Like Protein Domain Containing
Cyp26a1	3.531412444	0.015937	Cytochrome P450, Family 26, Subfamily A, Polypeptide 1
Mup4	3.536712123	0.05866	Growth Factor Independent 1 Transcription Repressor Transcription repressor essential for hematopoiesis. Functions in a cell-context and development-specific manner. Regulates neutrophil differentiation, promotes proliferation of lymphoid cells, and is required for granulocyte development. Mediates, together with U2AF1L4, the alternative splicing of CD45 and controls T-cell receptor signaling. Regulates the endotoxin-mediated Toll-like receptor (TLR) inflammatory response by

			antagonizing RELA
Ttc36	3.553368363	0.012381	Cbl Proto-Oncogene C, E3 Ubiquitin Protein Ligase Regulator of EGFR mediated signal transduction
Hao2	3.56948483	0.021428	Hydroxyacid Oxidase 2 (Long Chain)
Foxa3	3.570853365	0.02217	Forkhead Box A3
Cyp7a1	3.591204075	0.019065	Chemokine-Like Receptor 1 Receptor for the chemoattractant adipokine chemerin/RARRES2 and for the omega-3 fatty acid derived molecule resolvin E1. Interaction with RARRES2 induces activation of intracellular signaling molecules, such as SKY, MAPK1/3 (ERK1/2), MAPK14/P38MAPK and PI3K leading to multifunctional effects, like, reduction of immune responses, enhancing of adipogenesis and angionesis.
Nags	3.603383439	0.047668	N-Acetylglutamate Synthase
Aqp8	3.620851616	0.000325	Aquaporin 8
Upp2	3.642869945	0.056526	Dendrocyte Expressed Seven Transmembrane Protein Probable cell surface receptor that plays several roles in cellular fusion, cell differentiation, bone and immune homeostasis.
Amdhd1	3.661765286	0.015975	RIKEN cDNA 2810417H13 gene chromatin binding cellular response to DNA damage
Nr5a2	3.703605046	0.051043	Carbohydrate (Chondroitin

			6) Sulfotransferase 3 Chondroitin sulfate constitutes the predominant proteoglycan present in cartilage and is distributed on the surfaces of many cells and extracellular matrices. May play a role in the maintenance of naive T-lymphocytes in the spleen
Sult2a2	3.742921638	4.51E-12	Unclassified gene
Cux2	3.748697977	0.014695	Cut-Like Homeobox 2
2610528J11Rik	3.756886737	0.03852	Unclassified gene
Lrit2	3.756886737	0.043177	Leucine-Rich Repeat, Immunoglobulin-Like And Transmembrane Domains 2
Cdhr3	3.790938756	0.02217	Neutrophilic granule protein neutrophils immune
Ugt1a5	3.791214918	0.047483	Vitamin D (1,25-Dihydroxyvitamin D3) Receptor Plays a central role in calcium homeostasis
Sds	3.887522026	0.007376	Serine Dehydratase
F11	3.891558943	0.046511	Coagulation Factor XI
Syt1	3.942248085	0.002959	PDZ Domain Containing 1 encodes a PDZ domain-containing scaffolding protein. PDZ domain-containing molecules bind to and mediate the subcellular localization of target proteins.
Cyp2d9	3.946254616	0.080927	Cytochrome P450, Family 2, Subfamily D, Polypeptide 6
Pkhd1	4.034642668	0.026111	Polycystic Kidney And Hepatic Disease 1 (Autosomal Recessive)
Dsg1c	4.034642668	0.032318	Desmoglein 11 Component of intercellular desmosome junctions. Involved in the interaction of plaque

			proteins and intermediate filaments mediating cell-cell adhesion
Lrit1	4.034967101	0.00979	Leucine-Rich Repeat, Immunoglobulin-Like And Transmembrane Domains 1
Xkr9	4.034967101	0.045873	XK, Kell Blood Group Complex Subunit-Related Family, Member 9
Gsta2	4.103177744	6.20E-06	Glutathione S-Transferase Alpha 2 Conjugation of reduced glutathione protect against ROS
5033403H07Rik	4.122085393	0.014761	Unclassified gene
Pcsk9	4.127105554	0.019397	Proprotein Convertase Subtilisin/Kexin Type 9 Crucial player in the regulation of plasma cholesterol homeostasis. Binds to low-density lipid receptor family members Regulates neuronal apoptosis via modulation of LRP8/APOER2 levels and related anti-apoptotic signaling pathways
Sult1e1	4.149450823	6.56E-06	Sulfotransferase Family 1E, Estrogen-Preferring, Member 1
Ido2	4.165918534	0.001065	Indoleamine 2,3-Dioxygenase 2
Sftpa1	4.23486603	8.31E-06	Surfactant, Pulmonary-Associated Protein A for alveolar stability
Gm8883	4.281969586	0.000203	Unclassified gene
Pnpla1	4.337403369	0.026621	Patatin-Like Phospholipase Domain Containing 1
Hsd3b2	4.337403369	0.053402	Hydroxy-Delta-5-Steroid Dehydrogenase, 3 Beta-And Steroid Delta-Isomerase 2
Sult3a1	4.355723394	0.000133	Unclassified gene
Fam47e	4.525127289	0.000325	Family With Sequence

			Similarity 47, Member E
Adh6-ps1	4.528934836	0.001411	Unclassified gene
Vwce	4.617976069	0.016182	Von Willebrand Factor C And EGF Domains
Sftpc	4.686973256	1.68E-08	Surfactant, Pulmonary-Associated Protein C for alveolar stability
Cyp2g1	4.697993101	0.000517	Cytochrome P450, Family 2, Subfamily G, Polypeptide 1 Pseudogene
Asic5	4.697993101	0.000792	Acid-Sensing (Proton-Gated) Ion Channel Functions as a postsynaptic proton receptor that influences intracellular Ca(2+) concentration and calmodulin-dependent protein kinase II phosphorylation and thereby the density of dendritic spines.
Sec14l3	4.896406666	0.000169	Selenocysteine involved in antioxidant behavior
Sult1b1	5.122234712	0.021428	Sulfotransferase Family, Cytosolic, 1B, Member 1
Sftpb	5.262777738	6.56E-06	Surfactant, Pulmonary-Associated Protein B for alveolar stability
Meiob	5.366787213	4.75E-06	Meiosis Specific With OB Domains
Anks4b	5.538959579	0.008883	Ankyrin Repeat And Sterile Alpha Motif Domain Containing 4B
Cldn18	6.279235395	0.027649	Claudins are found at tight junctions as a physical barrier and known for maintaining cell polarity and signal transductions
Nppa	6.313457728	5.01E-06	Natriuretic Peptide A
Clec2h	6.415049264	0.023444	C-Type Lectin Domain Family 2, Member H
Lamp3	6.539170587	0.014339	Lysosome associated membrane protein

Il8	6.759345201	0.006796	Interleukin-8 important mediator of the innate immune response
Sftpd	6.950324684	0.002876	Surfactant, Pulmonary-Associated Protein D for alveolar stability
Slc34a2	8.191482395	6.93E-07	Solute Carrier Family 34 (Type II Sodium/Phosphate Cotransporter), Member 2

5 weeks old

Table 6: Comprehensive summary of ≥4-fold transcript changes in 5 week old *dy^{W} -/-* mice

Upregulated genes in 5 week old LAM-111 treated versus untreated *dy^{W} -/-* mice are represented by red. Downregulated genes in 5 week old LAM-111 treated versus untreated *dy^{W} -/-* mice are represented by green. There were 468 transcripts affected ≥ 4-fold (up- or down- regulated) in total.

Bibliography

1. Meinen, S. *et al.* Apoptosis inhibitors and mini-agrin have additive benefits in congenital muscular dystrophy mice. *EMBO Mol. Med.* **3,** 465–79 (2011).

2. Kinnett, K. *et al.* Imperatives for DUCHENNE MD: a Simplified Guide to Comprehensive Care for Duchenne Muscular Dystrophy. *PLoS Curr.* **7,** (2015).

3. Jungbluth, H. & Gautel, M. Pathogenic Mechanisms in Centronuclear Myopathies. *Front. Aging Neurosci.* **6,** 339 (2014).

4. Ramspacher, C. *et al.* Developmental Alterations in Heart Biomechanics and Skeletal Muscle Function in Desmin Mutants Suggest an Early Pathological Root for Desminopathies. *Cell Rep.* **11,** 1564–1576 (2015).

5. Smith, L. L., Gupta, V. A. & Beggs, A. H. Bridging integrator 1 (Bin1) deficiency in zebrafish results in centronuclear myopathy. *Hum. Mol. Genet.* **23,** 3566–3578 (2014).

6. Gregor, M. *et al.* Mechanosensing through focal adhesion-anchored intermediate filaments. *FASEB J.* **28,** 715–29 (2014).

7. Nelson, B. R. *et al.* Skeletal muscle-specific T-tubule protein STAC3 mediates voltage-induced Ca2+ release and contractility. *Proc. Natl. Acad. Sci.* **110,** 11881–11886 (2013).

8. Sandonà, D. & Betto, R. Sarcoglycanopathies: molecular pathogenesis and therapeutic prospects. *Expert Rev. Mol. Med.* **11,** e28 (2009).

9. Sztal, T. E., Sonntag, C., Hall, T. E. & Currie, P. D. Epistatic dissection of laminin-receptor interactions in dystrophic zebrafish muscle. *Hum. Mol. Genet.* **21,** 4718–31 (2012).

10. Adams, J. C. & Brancaccio, A. The evolution of the dystroglycan complex, a major mediator of muscle integrity. *Biol. Open* **4,** 1163–79 (2015).

11. Peters, M. F., Adams, M. E. & Froehner, S. C. Differential association of syntrophin pairs with the dystrophin complex. *J. Cell Biol.* **138,** 81–93 (1997).

12. Le Rumeur, E. Dystrophin and the two related genetic diseases, Duchenne and Becker muscular dystrophies. *Bosn. J. Basic Med. Sci.* **15,** 14–20 (2015).

13. Roberts, T. C. *et al.* Multi-level omics analysis in a murine model of dystrophin loss and therapeutic restoration. *Hum. Mol. Genet.* (2015). doi:10.1093/hmg/ddv381

14. Taniguchi, K. *et al.* Mammalian formin fhod3 regulates actin assembly and sarcomere organization in striated muscles. *J. Biol. Chem.* **284,** 29873–81 (2009).

15. Razzaq, A. *et al.* Amphiphysin is necessary for organization of the excitation-contraction coupling machinery of muscles, but not for synaptic vesicle endocytosis in Drosophila. *Genes Dev.* **15,** 2967–79 (2001).

16. Petersen, J. A. *et al.* Dysferlinopathy in Switzerland: clinical phenotypes and potential founder effects. *BMC Neurol.* **15,** 182 (2015).

17. Zhong, M., Pan, S.-Y. & Li, W. [Identification of Duchenne muscular dystrophy carrier by detecting junction fragments between the breakpoints of introns]. *Nan Fang Yi Ke Da Xue Xue Bao* **35,** 1308–11 (2015).

18. Jenkins, C. A. & Forman, O. P. Identification of a novel frameshift mutation in the DMD gene as the cause of muscular dystrophy in a Norfolk terrier dog. *Canine Genet. Epidemiol.* **2,** 7 (2015).

19. Sciandra, F., Bigotti, M. G., Giardina, B., Bozzi, M. & Brancaccio, A. Genetic Engineering of Dystroglycan in Animal Models of Muscular Dystrophy. *Biomed Res. Int.* **2015,** 635792 (2015).

20. Timpani, C. A., Hayes, A. & Rybalka, E. Revisiting the dystrophin-ATP connection: How half a century of research still implicates mitochondrial dysfunction in Duchenne Muscular Dystrophy aetiology. *Med. Hypotheses* (2015). doi:10.1016/j.mehy.2015.08.015

21. Pandey, S. N., Kesari, A., Yokota, T. & Pandey, G. S. Muscular Dystrophy: Disease Mechanisms and Therapies. *Biomed Res. Int.* **2015,** 1–2 (2015).

22. Suneja, B., Suneja, E. S., Adlakha, V. K. & Chandna, P. A Rare Case Report of Neurodegenerative Disease: Duchenne Muscular Dystrophy in Two Male Siblings. *Int. J. Clin. Pediatr. Dent.* **8,** 163–5

23. Orengo, J. P., Ward, A. J. & Cooper, T. A. Alternative splicing dysregulation secondary to skeletal muscle regeneration. *Ann. Neurol.* **69,** 681–90 (2011).

24. Mendell, J. R., Boué, D. R. & Martin, P. T. The congenital muscular dystrophies: recent advances and molecular insights. *Pediatr. Dev. Pathol. Off. J. Soc. Pediatr. Pathol. Paediatr. Pathol. Soc.* **9,** 427–443 (2006).

25. Taratuto, A. L. *et al.* Merosin-deficient congenital muscular dystrophy associated with abnormal cerebral cortical gyration: an autopsy study. *Neuromuscul. Disord.* **9,** 86–94 (1999).

26. Wang, M., Wu, B., Tucker, J. D., Lu, P. & Lu, Q. Cationic polyelectrolyte-mediated delivery of antisense morpholino oligonucleotides for exon-skipping in vitro and in mdx mice. *Int. J. Nanomedicine* **10,** 5635–46 (2015).

27. Foster, R. F., Thompson, J. M. & Kaufman, S. J. A laminin substrate promotes myogenesis in rat skeletal muscle cultures: analysis of replication and development using antidesmin and anti-BrdUrd monoclonal antibodies. *Dev. Biol.* **122,** 11–20 (1987).

28. Burkin, D. J. & Kaufman, S. J. The alpha7beta1 integrin in muscle development and disease. *Cell Tissue Res.* **296,** 183–90 (1999).

29. Kaufman, S. J. & Foster, R. F. Replicating myoblasts express a muscle-specific phenotype. *Proc. Natl. Acad. Sci. U. S. A.* **85,** 9606–10 (1988).

30. Velling, T. *et al.* Distinct alpha 7A beta 1 and alpha 7B beta 1 integrin expression patterns during mouse development: alpha 7A is restricted to skeletal muscle but alpha 7B is expressed in striated muscle, vasculature, and nervous system. *Dev. Dyn.* **207,** 355–71 (1996).

31. Brancaccio, M. *et al.* Differential onset of expression of alpha 7 and beta 1D integrins during mouse heart and skeletal muscle development. *Cell Adhes. Commun.* **5,** 193–205 (1998).

32. Gu, M., Wang, W., Song, W. K., Cooper, D. N. & Kaufman, S. J. Selective modulation of the interaction of alpha 7 beta 1 integrin with fibronectin and laminin by L-14 lectin during skeletal muscle differentiation. *J. Cell Sci.* **107 (Pt 1,** 175–81 (1994).

33. Ross, J. J., Duxson, M. J. & Harris, A. J. Formation of primary and secondary myotubes in rat lumbrical muscles. *Development* **100,** 383–94 (1987).

34. Sanes, J. R., Engvall, E., Butkowski, R. & Hunter, D. D. Molecular heterogeneity of basal laminae: Isoforms of laminin and collagen IV at the

neuromuscular junction and elsewhere. *J. Cell Biol.* **111,** 1685–1699 (1990).

35. Harris, A. J., Duxson, M. J., Fitzsimons, R. B. & Rieger, F. Myonuclear birthdates distinguish the origins of primary and secondary myotubes in embryonic mammalian skeletal muscles. *Development* **107,** 771–84 (1989).

36. George-Weinstein, M., Foster, R. F., Gerhart, J. V & Kaufman, S. J. In vitro and in vivo expression of alpha 7 integrin and desmin define the primary and secondary myogenic lineages. *Dev. Biol.* **156,** 209–29 (1993).

37. Echtermeyer, F., Schöber, S., Pöschl, E., von der Mark, H. & von der Mark, K. Specific induction of cell motility on laminin by alpha 7 integrin. *J. Biol. Chem.* **271,** 2071–5 (1996).

38. Yao, C. C., Ziober, B. L., Sutherland, A. E., Mendrick, D. L. & Kramer, R. H. Laminins promote the locomotion of skeletal myoblasts via the alpha 7 integrin receptor. *J. Cell Sci.* **109 (Pt 1,** 3139–50 (1996).

39. Song, W. K., Wang, W., Foster, R. F., Bielser, D. A. & Kaufman, S. J. H36-alpha 7 is a novel integrin alpha chain that is developmentally regulated during skeletal myogenesis. *J. Cell Biol.* **117,** 643–57 (1992).

40. Kaufman, S. J., Foster, R. F., Haye, K. R. & Faiman, L. E. Expression of a developmentally regulated antigen on the surface of skeletal and cardiac muscle cells. *J. Cell Biol.* **100,** 1977–87 (1985).

41. Alberts, B. *et al. Molecular Biology of the Cell, Fifth Edition*. *Molecular Biology* (2008).

42. Garland Science - Molecular Biology of the Cell, Fifth Edition Resources. at <http://www.garlandscience.com/garlandscience_resources/book_resources.jsf?isbn=9780815341055&landing=student>

43. Pisciotta, A. *et al.* Stem cells isolated from human dental pulp and amniotic fluid improve skeletal muscle histopathology in mdx/SCID mice. *Stem Cell Res. Ther.* **6,** 156 (2015).

44. Shoji, E. *et al.* Early pathogenesis of Duchenne muscular dystrophy modelled in patient-derived human induced pluripotent stem cells. *Sci. Rep.* **5,** 12831 (2015).

45. Hagiwara, H. *et al.* Bone marrow transplantation improves outcome in a mouse model of congenital muscular dystrophy. *FEBS Lett.* **580,** 4463–8 (2006).

46. Gao, Y., Li, Y., Guo, X., Wu, Z. & Zhang, W. Loss of STAT1 in bone marrow-derived cells accelerates skeletal muscle regeneration. *PLoS One* **7,** e37656 (2012).

47. Zhang, Y. *et al.* Long-term engraftment of myogenic progenitors from adipose-derived stem cells and muscle regeneration in dystrophic mice. *Hum. Mol. Genet.* **24,** 6029–6040 (2015).

48. Yoshida, T., Pan, Y., Hanada, H., Iwata, Y. & Shigekawa, M. Bidirectional signaling between sarcoglycans and the integrin adhesion system in cultured L6 myocytes. *J. Biol. Chem.* **273,** 1583–90 (1998).

49. Yoshida, M. & Ozawa, E. Glycoprotein complex anchoring dystrophin to sarcolemma. *J. Biochem.* **108,** 748–52 (1990).

50. Hodges, B. L. *et al.* Altered expression of the alpha7beta1 integrin in human and murine muscular dystrophies. *J. Cell Sci.* **110 (Pt 2,** 2873–81 (1997).

51. Burkin, D. J., Wallace, G. Q., Nicol, K. J., Kaufman, D. J. & Kaufman, S. J. Enhanced expression of the alpha 7 beta 1 integrin reduces muscular dystrophy and restores viability in dystrophic mice. *J. Cell Biol.* **152,** 1207–18 (2001).

52. Burkin, D. J. *et al.* Transgenic expression of {alpha}7{beta}1 integrin maintains muscle integrity, increases regenerative capacity, promotes hypertrophy, and reduces cardiomyopathy in dystrophic mice. *Am. J. Pathol.* **166,** 253–63 (2005).

53. Capetanaki, Y., Bloch, R. J., Kouloumenta, A., Mavroidis, M. & Psarras, S. Muscle intermediate filaments and their links to membranes and membranous organelles. *Exp. Cell Res.* **313,** 2063–2076 (2007).

54. Hynes, R. O. & Zhao, Q. The evolution of cell adhesion. *J. Cell Biol.* **150,** F89–96 (2000).

55. Hynes, R. O. Integrins: versatility, modulation, and signaling in cell adhesion. *Cell* **69,** 11–25 (1992).

56. Senter, L. *et al.* Interaction of dystrophin with cytoskeletal proteins: binding to talin and actin. *Biochem. Biophys. Res. Commun.* **192,** 899–904 (1993).

57. Samarel, A. M. Costameres, focal adhesions, and cardiomyocyte mechanotransduction. *Am. J. Physiol. Heart Circ. Physiol.* **289,** H2291–301 (2005).

58. Ervasti, J. M. Costameres: the Achilles' heel of Herculean muscle. *J. Biol. Chem.* **278,** 13591–4 (2003).

59. Bao, Z. Z., Lakonishok, M., Kaufman, S. & Horwitz, A. F. Alpha 7 beta 1 integrin is a component of the myotendinous junction on skeletal muscle. *J. Cell Sci.* **106 (Pt 2,** 579–89 (1993).

60. Belkin, A. M. *et al.* Beta 1D integrin displaces the beta 1A isoform in striated muscles: localization at junctional structures and signaling potential in nonmuscle cells. *J. Cell Biol.* **132,** 211–26 (1996).

61. Hynes, R. O. Integrins: bidirectional, allosteric signaling machines. *Cell* **110,** 673–87 (2002).

62. Song, W. K., Wang, W., Sato, H., Bielser, D. A. & Kaufman, S. J. Expression of alpha 7 integrin cytoplasmic domains during skeletal muscle development: alternate forms, conformational change, and homologies with serine/threonine kinases and tyrosine phosphatases. *J. Cell Sci.* **106 (Pt 4,** 1139–52 (1993).

63. Ziober, B. L. *et al.* Alternative extracellular and cytoplasmic domains of the integrin alpha 7 subunit are differentially expressed during development. *J. Biol. Chem.* **268,** 26773–83 (1993).

64. Collo, G., Starr, L. & Quaranta, V. A new isoform of the laminin receptor integrin alpha 7 beta 1 is developmentally regulated in skeletal muscle. *J. Biol. Chem.* **268,** 19019–24 (1993).

65. Doe, J. A. *et al.* Transgenic overexpression of the α7 integrin reduces muscle pathology and improves viability in the dy(W) mouse model of merosin-deficient congenital muscular dystrophy type 1A. *J. Cell Sci.* **124,** 2287–97 (2011).

66. Lidov, H. G. & Kunkel, L. M. Dystrophin and Dp140 in the adult rodent kidney. *Lab. Invest.* **78,** 1543–51 (1998).

67. Cohn, R. D. & Campbell, K. P. Molecular basis of muscular dystrophies. *Muscle Nerve* **23,** 1456–71 (2000).

68. Porter, G. A., Dmytrenko, G. M., Winkelmann, J. C. & Bloch, R. J. Dystrophin colocalizes with beta-spectrin in distinct subsarcolemmal

domains in mammalian skeletal muscle. *J. Cell Biol.* **117,** 997–1005 (1992).

69. Straub, V., Bittner, R. E., Léger, J. J. & Voit, T. Direct visualization of the dystrophin network on skeletal muscle fiber membrane. *J. Cell Biol.* **119,** 1183–91 (1992).

70. Miyagoe-Suzuki, Y., Nakagawa, M. & Takeda, S. Merosin and congenital muscular dystrophy. *Microsc. Res. Tech.* **48,** 181–91

71. Colognato, H. & Yurchenco, P. D. Form and function: the laminin family of heterotrimers. *Dev. Dyn.* **218,** 213–34 (2000).

72. Colognato, H., Winkelmann, D. A. & Yurchenco, P. D. Laminin polymerization induces a receptor-cytoskeleton network. *J. Cell Biol.* **145,** 619–31 (1999).

73. Helbling-Leclerc, A. *et al.* Mutations in the laminin α2–chain gene (LAMA2) cause merosin–deficient congenital muscular dystrophy. *Nat. Genet.* **11,** 216–218 (1995).

74. Koeppen, B. & Stanton, B. *Berne & Levy Physiology*. (elsevier, 2015).

75. Berne & Levy Physiology, Updated Edition | 978-0-323-07362-2 | Elsevier. at <https://www.elsevier.com/books/berne-and-levy-physiology-updated-edition/koeppen/978-0-323-07362-2>

76. Severs, N. J., Bruce, A. F., Dupont, E. & Rothery, S. Remodelling of gap junctions and connexin expression in diseased myocardium. *Cardiovasc. Res.* **80,** 9–19 (2008).

77. Pyle, W. G. & Solaro, R. J. At the crossroads of myocardial signaling: the role of Z-discs in intracellular signaling and cardiac function. *Circ. Res.* **94,** 296–305 (2004).

78. Granzier, H. L. The Giant Protein Titin: A Major Player in Myocardial Mechanics, Signaling, and Disease. *Circ. Res.* **94,** 284–295 (2004).

79. Tzu, J. & Marinkovich, M. P. Bridging structure with function: Structural, regulatory, and developmental role of laminins. *Int. J. Biochem. Cell Biol.* **40,** 199–214 (2008).

80. Aumailley, M. *et al.* A simplified laminin nomenclature. *Matrix Biology* **24,** 326–332 (2005).

81. Ekblom, P., Lonai, P. & Talts, J. F. Expression and biological role of laminin-1. *Matrix Biol.* **22,** 35–47 (2003).

82. Miner, J. H. & Yurchenco, P. D. LAMININ FUNCTIONS IN TISSUE MORPHOGENESIS. *Annu. Rev. Cell Dev. Biol.* **20,** 255–284 (2004).

83. Yamauchi, J., Kumar, A., Duarte, L., Mehuron, T. & Girgenrath, M. Triggering regeneration and tackling apoptosis: a combinatorial approach to treating congenital muscular dystrophy type 1 A. *Hum. Mol. Genet.* **22,** 4306–17 (2013).

84. Gupta, V. A. *et al.* A splice site mutation in laminin-α2 results in a severe muscular dystrophy and growth abnormalities in zebrafish. *PLoS One* **7,** e43794 (2012).

85. Kim, H. J. *et al.* Congenital muscular dystrophy type 1A with residual merosin expression. *Korean J. Pediatr.* **57,** 149–52 (2014).

86. Gawlik, K. I., Akerlund, M., Carmignac, V., Elamaa, H. & Durbeej, M. Distinct roles for laminin globular domains in laminin alpha1 chain mediated rescue of murine laminin alpha2 chain deficiency. *PLoS One* **5,** e11549 (2010).

87. Vohra, R., Accorsi, A., Kumar, A., Walter, G. & Girgenrath, M. Magnetic Resonance Imaging Is Sensitive to Pathological Amelioration in a Model for Laminin-Deficient Congenital Muscular Dystrophy (MDC1A). *PLoS One* **10,** e0138254 (2015).

88. Muntoni, F. & Voit, T. The congenital muscular dystrophies in 2004: a century of exciting progress. *Neuromuscul. Disord.* **14,** 635–49 (2004).

89. Naom, I. *et al.* The role of immunocytochemistry and linkage analysis in the prenatal diagnosis of merosin-deficient congenital muscular dystrophy. *Hum. Genet.* **99,** 535–40 (1997).

90. Helbling-Leclerc, A. *et al.* Readjusting the localization of merosin (laminin alpha 2-chain) deficient congenital muscular dystrophy locus on chromosome 6q2. *C. R. Acad. Sci. III.* **318,** 1245–52 (1995).

91. Naom, I. S. *et al.* Refinement of the laminin alpha2 chain locus to human chromosome 6q2 in severe and mild merosin deficient congenital muscular dystrophy. *J. Med. Genet.* **34,** 99–104 (1997).

92. Jones, K. J. *et al.* The expanding phenotype of laminin alpha2 chain (merosin) abnormalities: case series and review. *J. Med. Genet.* **38,** 649–57 (2001).

93. Philpot, J. *et al.* Merosin-deficient congenital muscular dystrophy: the spectrum of brain involvement on magnetic resonance imaging. *Neuromuscul. Disord.* **9,** 81–5 (1999).

94. Philpot, J. & Muntoni, F. Limitation of eye movement in merosin-deficient congenital muscular dystrophy. *Lancet (London, England)* **353,** 297–8 (1999).

95. Yiu, E. M. & Kornberg, A. J. Duchenne muscular dystrophy. *Neurol. India* **56,** 236–47

96. Teijeira, S. & Navarro, C. [Dystrophinopathies: concept and diagnostic methodology]. *Neurologia* **9,** 191–7 (1994).

97. Jennekens, F. G., ten Kate, L. P., de Visser, M. & Wintzen, A. R. Diagnostic criteria for Duchenne and Becker muscular dystrophy and myotonic dystrophy. *Neuromuscul. Disord.* **1,** 389–91 (1991).

98. Nigro, G., Comi, L. I., Politano, L. & Bain, R. J. The incidence and evolution of cardiomyopathy in Duchenne muscular dystrophy. *Int. J. Cardiol.* **26,** 271–7 (1990).

99. Bulfield, G., Siller, W. G., Wight, P. A. & Moore, K. J. X chromosome-linked muscular dystrophy (mdx) in the mouse. *Proc. Natl. Acad. Sci. U. S. A.* **81,** 1189–92 (1984).

100. Sicinski, P. *et al.* The molecular basis of muscular dystrophy in the mdx mouse: a point mutation. *Science* **244,** 1578–80 (1989).

101. Tanabe, Y., Esaki, K. & Nomura, T. Skeletal muscle pathology in X chromosome-linked muscular dystrophy (mdx) mouse. *Acta Neuropathol.* **69,** 91–5 (1986).

102. DiMario, J. X., Uzman, A. & Strohman, R. C. Fiber regeneration is not persistent in dystrophic (MDX) mouse skeletal muscle. *Dev. Biol.* **148,** 314–21 (1991).

103. Stedman, H. H. *et al.* The mdx mouse diaphragm reproduces the degenerative changes of Duchenne muscular dystrophy. *Nature* **352,** 536–539 (1991).

104. Cox, G. A. *et al.* Overexpression of dystrophin in transgenic mdx mice eliminates dystrophic symptoms without toxicity. *Nature* **364,** 725–9 (1993).

105. Yu, X., Bao, B., Echigoya, Y. & Yokota, T. Dystrophin-deficient large animal models: translational research and exon skipping. *Am. J. Transl. Res.* **7,** 1314–31 (2015).

106. Miyagoe, Y. *et al.* Laminin alpha2 chain-null mutant mice by targeted disruption of the Lama2 gene: a new model of merosin (laminin 2)-deficient congenital muscular dystrophy. *FEBS Lett.* **415,** 33–9 (1997).

107. Kuang, W. *et al.* Merosin-deficient congenital muscular dystrophy: Partial genetic correction in two mouse models. *J. Clin. Invest.* **102,** 844–852 (1998).

108. Guo, L. T. *et al.* Laminin alpha2 deficiency and muscular dystrophy; genotype-phenotype correlation in mutant mice. *Neuromuscul. Disord.* **13,** 207–15 (2003).

109. Sunada, Y., Bernier, S. M., Kozak, C. A., Yamada, Y. & Campbell, K. P. Deficiency of merosin in dystrophic dy mice and genetic linkage of laminin M chain gene to dy locus. *J. Biol. Chem.* **269,** 13729–32 (1994).

110. Xu, H., Christmas, P., Wu, X. R., Wewer, U. M. & Engvall, E. Defective muscle basement membrane and lack of M-laminin in the dystrophic dy/dy mouse. *Proc. Natl. Acad. Sci. U. S. A.* **91,** 5572–5576 (1994).

111. Besse, S. *et al.* Spontaneous muscular dystrophy caused by a retrotransposal insertion in the mouse laminin alpha2 chain gene. *Neuromuscul. Disord.* **13,** 216–22 (2003).

112. Allamand, V. *et al.* Mild congenital muscular dystrophy in two patients with an internally deleted laminin alpha2-chain. *Hum. Mol. Genet.* **6,** 747–52 (1997).

113. Timpl, R. *et al.* Laminin--a glycoprotein from basement membranes. *J. Biol. Chem.* **254,** 9933–7 (1979).

114. Aumailley, M. & Smyth, N. The role of laminins in basement membrane function. *J. Anat.* **193 (Pt 1,** 1–21 (1998).

115. Gullberg, D., Tiger, C. F. & Velling, T. Laminins during muscle development and in muscular dystrophies. *Cell. Mol. life Sci. C.* **56,** 442–460 (1999).

116. Sasaki, T., Giltay, R., Talts, U., Timpl, R. & Talts, J. F. Expression and distribution of laminin alpha1 and alpha2 chains in embryonic and adult mouse tissues: an immunochemical approach. *Exp. Cell Res.* **275,** 185–99 (2002).

117. Gawlik, K. I. & Durbeej, M. Skeletal muscle laminin and MDC1A: pathogenesis and treatment strategies. *Skelet. Muscle* **1,** 9 (2011).

118. Sewry, C. A., Chevallay, M. & Tomé, F. M. Expression of laminin subunits in human fetal skeletal muscle. *Histochem. J.* **27,** 497–504 (1995).

119. Pedrosa-Domellöf, F., Tiger, C. F., Virtanen, I., Thornell, L. E. & Gullberg, D. Laminin chains in developing and adult human myotendinous junctions. *J. Histochem. Cytochem.* **48,** 201–10 (2000).

120. Patton, B. L. *et al.* Distribution of ten laminin chains in dystrophic and regenerating muscles. *Neuromuscul. Disord.* **9,** 423–33 (1999).

121. Vachon, P. H., Loechel, F., Xu, H., Wewer, U. M. & Engvall, E. Merosin and laminin in myogenesis; specific requirement for merosin in myotube stability and survival. *J. Cell Biol.* **134,** 1483–1497 (1996).

122. Kuang, W., Xu, H., Vachon, P. H. & Engvall, E. Disruption of the lama2 gene in embryonic stem cells: laminin alpha 2 is necessary for sustenance of mature muscle cells. *Exp. Cell Res.* **241,** 117–125 (1998).

123. Smolina, N. *et al.* Primary Murine Myotubes as a Model for Investigating Muscular Dystrophy. *Biomed Res. Int.* **2015,** 594751 (2015).

124. Kuang, W., Xu, H., Vilquin, J. T. & Engvall, E. Activation of the lama2 gene in muscle regeneration: abortive regeneration in laminin alpha2-deficiency. *Lab. Invest.* **79,** 1601–13 (1999).

125. Marks, A. R. Calcium cycling proteins and heart failure: mechanisms and therapeutics. *J. Clin. Invest.* **123,** 46–52 (2013).

126. George, C. H., Parthimos, D. & Silvester, N. C. A network-oriented perspective on cardiac calcium signaling. *Am. J. Physiol. Cell Physiol.* **303,** C897–910 (2012).

127. Marian, A. J., Salek, L. & Lutucuta, S. Molecular genetics and pathogenesis of hypertrophic cardiomyopathy. *Minerva Med.* **92,** 435–51 (2001).

128. Sabri, A., Pak, E., Alcott, S. A., Wilson, B. A. & Steinberg, S. F. Coupling function of endogenous alpha(1)- and beta-adrenergic receptors in mouse cardiomyocytes. *Circ. Res.* **86,** 1047–53 (2000).

129. Townsend, D. Diastolic dysfunction precedes hypoxia-induced mortality in dystrophic mice. *Physiol. Rep.* **3,** e12513 (2015).

130. Kono, T. *et al.* Cardiac resynchronization therapy in a young patient with Duchenne muscular dystrophy. *Int. Med. Case Rep. J.* **8,** 173–5 (2015).

131. Rooney, J. E., Knapp, J. R., Hodges, B. L., Wuebbles, R. D. & Burkin, D. J. Laminin-111 protein therapy reduces muscle pathology and improves viability of a mouse model of merosin-deficient congenital muscular dystrophy. *Am. J. Pathol.* **180,** 1593–602 (2012).

132. Van Ry, P. M., Minogue, P., Hodges, B. L. & Burkin, D. J. Laminin-111 improves muscle repair in a mouse model of merosin-deficient congenital muscular dystrophy. *Hum. Mol. Genet.* **23,** 383–396 (2013).

133. Guo, L. T. *et al.* Laminin α2 deficiency and muscular dystrophy; genotype-phenotype correlation in mutant mice. *Neuromuscul. Disord.* **13,** 207–215 (2003).

134. Rooney, J. E. *et al.* Severe muscular dystrophy in mice that lack dystrophin and alpha7 integrin. *J. Cell Sci.* **119,** 2185–95 (2006).

135. Verheijden, K. A. T., Henricks, P. A. J., Redegeld, F. A., Garssen, J. & Folkerts, G. Measurement of airway function using invasive and non-invasive methods in mild and severe models for allergic airway inflammation in mice. *Front. Pharmacol.* **5,** 190 (2014).

136. Berndt, A. *et al.* Comparison of unrestrained plethysmography and forced oscillation for identifying genetic variability of airway responsiveness in inbred mice. *Physiol. Genomics* **43,** 1–11 (2011).

137. LoMauro, A., D'Angelo, M. G. & Aliverti, A. Assessment and management of respiratory function in patients with Duchenne muscular dystrophy: current and emerging options. *Ther. Clin. Risk Manag.* **11,** 1475–88 (2015).

138. Van Ry, P. M., Wuebbles, R. D., Key, M. & Burkin, D. J. Galectin-1 Protein Therapy Prevents Pathology and Improves Muscle Function in the mdx Mouse Model of Duchenne Muscular Dystrophy. *Mol. Ther.* **23,** 1285–97 (2015).

139. Yu, Q. *et al.* Omigapil Treatment Decreases Fibrosis and Improves Respiratory Rate in dy2J Mouse Model of Congenital Muscular Dystrophy. *PLoS One* **8,** e65468 (2013).

140. Erb, M. *et al.* Omigapil ameliorates the pathology of muscle dystrophy caused by laminin-alpha2 deficiency. *J. Pharmacol. Exp. Ther.* **331,** 787–95 (2009).

141. Erb, M. *et al.* Omigapil ameliorates the pathology of muscle dystrophy caused by laminin-alpha2 deficiency. *J. Pharmacol. Exp. Ther.* **331,** 787–95 (2009).

142. Rooney, J. E., Knapp, J. R., Hodges, B. L., Wuebbles, R. D. & Burkin, D. J. Laminin-111 protein therapy reduces muscle pathology and improves viability of a mouse model of merosin-deficient congenital muscular dystrophy. *Am. J. Pathol.* **180,** 1593–602 (2012).

143. Li, J. & Tibshirani, R. Finding consistent patterns: a nonparametric approach for identifying differential expression in RNA-Seq data. *Stat. Methods Med. Res.* **22,** 519–36 (2013).

144. McCarthy, D. J., Chen, Y. & Smyth, G. K. Differential expression analysis of multifactor RNA-Seq experiments with respect to biological variation. *Nucleic Acids Res.* **40,** 4288–97 (2012).

145. Robinson, M. D., McCarthy, D. J. & Smyth, G. K. edgeR: a Bioconductor package for differential expression analysis of digital gene expression data. *Bioinformatics* **26,** 139–40 (2010).

146. Robinson, M. D. & Smyth, G. K. Small-sample estimation of negative binomial dispersion, with applications to SAGE data. *Biostatistics* **9,** 321–32 (2008).

147. Robinson, M. D. & Smyth, G. K. Moderated statistical tests for assessing differences in tag abundance. *Bioinformatics* **23,** 2881–7 (2007).

148. Controlling the False discovery rate: A practical and powerful approach to multiple testing. at <http://www.math.tau.ac.il/~ybenja/MyPapers/benjamini_hochberg1995.pdf>

149. Sondag, G. R. *et al.* Osteoactivin induces transdifferentiation of C2C12 myoblasts into osteoblasts. *J. Cell. Physiol.* **229,** 955–66 (2014).

150. Selim, A. A. *et al.* Anti-osteoactivin antibody inhibits osteoblast differentiation and function in vitro. *Crit. Rev. Eukaryot. Gene Expr.* **13,** 265–75 (2003).

151. Safadi, F. F. *et al.* Cloning and characterization of osteoactivin, a novel cDNA expressed in osteoblasts. *J. Cell. Biochem.* **84,** 12–26 (2001).

152. Moghadaszadeh, B. *et al.* Compensation for dystrophin-deficiency: ADAM12 overexpression in skeletal muscle results in increased α7 integrin, utrophin and associated glycoproteins. *Hum. Mol. Genet.* **12,** 2467–2479 (2003).

153. Kronqvist, P. *et al.* ADAM12 alleviates the skeletal muscle pathology in mdx dystrophic mice. *Am. J. Pathol.* **161,** 1535–1540 (2002).

154. Engvall, E. & Wewer, U. M. The new frontier in muscular dystrophy research: booster genes. *FASEB J.* **17,** 1579–1584 (2003).

155. Sheng, M. H.-C. *et al.* Targeted overexpression of osteoactivin in cells of osteoclastic lineage promotes osteoclastic resorption and bone loss in mice. *PLoS One* **7,** e35280 (2012).

156. Shikano, S., Bonkobara, M., Zukas, P. K. & Ariizumi, K. Molecular cloning of a dendritic cell-associated transmembrane protein, DC-HIL, that promotes RGD-dependent adhesion of endothelial cells through recognition of heparan sulfate proteoglycans. *J. Biol. Chem.* **276,** 8125–34 (2001).

157. Chung, J.-S., Dougherty, I., Cruz, P. D. & Ariizumi, K. Syndecan-4 mediates the coinhibitory function of DC-HIL on T cell activation. *J. Immunol.* **179,** 5778–84 (2007).

158. Xian, L. *et al.* Matrix IGF-1 maintains bone mass by activation of mTOR in mesenchymal stem cells. *Nat. Med.* **18,** 1095–101 (2012).

159. Davis, R. L., Weintraub, H. & Lassar, A. B. Expression of a single transfected cDNA converts fibroblasts to myoblasts. *Cell* **51,** 987–1000 (1987).

160. Liu, L. *et al.* Mouse adhalin: primary structure and expression during late stages of muscle differentiation in vitro. *Biochem. Biophys. Res. Commun.* **235,** 227–235 (1997).

161. Patton, B. L., Miner, J. H., Chiu, A. Y. & Sanes, J. R. Distribution and function of laminins in the neuromuscular system of developing, adult, and mutant mice. *J. Cell Biol.* **139,** 1507–21 (1997).

162. Rooney, J. E., Gurpur, P. B. & Burkin, D. J. Laminin-111 protein therapy prevents muscle disease in the mdx mouse model for Duchenne muscular dystrophy. *Proc. Natl. Acad. Sci. U. S. A.* **106,** 7991–7996 (2009).

163. Burkin, D. J. & Kaufman, S. J. The alpha7beta1 integrin in muscle development and disease. *Cell Tissue Res.* **296,** 183–190 (1999).

164. Rooney, J. E., Gurpur, P. B., Yablonka-Reuveni, Z. & Burkin, D. J. Laminin-111 restores regenerative capacity in a mouse model for alpha7 integrin congenital myopathy. *Am. J. Pathol.* **174,** 256–64 (2009).

165. Deconinck, N. & Dan, B. Pathophysiology of duchenne muscular dystrophy: current hypotheses. *Pediatr. Neurol.* **36,** 1–7 (2007).

166. Campbell, K. P. Three muscular dystrophies: loss of cytoskeleton-extracellular matrix linkage. *Cell* **80,** 675–9 (1995).

167. Haslett, J. N. *et al.* Gene expression comparison of biopsies from Duchenne muscular dystrophy (DMD) and normal skeletal muscle. *Proc. Natl. Acad. Sci. U. S. A.* **99,** 15000–5 (2002).

168. Radley-Crabb, H. G., Fiorotto, M. L. & Grounds, M. D. The different impact of a high fat diet on dystrophic mdx and control C57Bl/10 mice. *PLoS Curr.* **3,** RRN1276 (2011).

169. Yamamoto, H. *et al.* Desensitization by different strategies of epidermal growth factor receptor and ErbB4. *J. Pharmacol. Sci.* **124,** 287–93 (2014).

170. Allouche, S., Noble, F. & Marie, N. Opioid receptor desensitization: mechanisms and its link to tolerance. *Front. Pharmacol.* **5,** 280 (2014).

171. Franck, E. *et al.* Immunological tolerance to muscle autoantigens involves peripheral deletion of autoreactive CD8+ T cells. *PLoS One* **7,** e36444 (2012).

172. Dolgikh, M. S. [Role of innate immunity in tolerance induction]. *Biomed. Khim.* **61,** 560–578 (2015).

173. Gawlik, K. I. & Durbeej, M. Deletion of integrin α7 subunit does not aggravate the phenotype of laminin α2 chain-deficient mice. *Sci. Rep.* **5,** 13916 (2015).

174. Visual Sonics Vevo 2100 Imaging System. at <http://www.uib.no/filearchive/vevo2100-manual.pdf>

175. Moran, C. M., Thomson, A. J. W., Rog-Zielinska, E. & Gray, G. A. High-resolution echocardiography in the assessment of cardiac physiology and disease in preclinical models. *Exp. Physiol.* **98,** 629–644 (2013).

176. Liu, X., Tobita, K., Francis, R. J. B. & Lo, C. W. Imaging techniques for visualizing and phenotyping congenital heart defects in murine models. *Birth Defects Res. C. Embryo Today* **99,** 93–105 (2013).

177. Ram, R., Mickelsen, D. M., Theodoropoulos, C. & Blaxall, B. C. New approaches in small animal echocardiography: imaging the sounds of silence. *Am. J. Physiol. Heart Circ. Physiol.* **301,** H1765–80 (2011).

178. Laws, N. Progression of kyphosis in mdx mice. *J. Appl. Physiol.* **97,** 1970–1977 (2004).

179. Wu, J. *et al.* Effects of heart rate and anesthetic timing on high-resolution echocardiographic assessment under isoflurane anesthesia in mice. *J. Ultrasound Med.* **29,** 1771–8 (2010).

180. Tournoux, F. *et al.* Validation of Noninvasive Measurements of Cardiac Output in Mice Using Echocardiography. *J. Am. Soc. Echocardiogr.* **24,** 465–470 (2011).

181. ZHAO, J. *et al.* [Echocardiographic evaluation of pressure overload-induced cardiac remodeling in mice using different ultrasound machines]. *Nan Fang Yi Ke Da Xue Xue Bao* **31,** 443–7 (2011).

182. Kim, G. H. Murine Fetal Echocardiography. *J. Vis. Exp.* (2013). doi:10.3791/4416

183. Franchi, F. *et al.* Non-invasive assessment of cardiac function in a mouse model of renovascular hypertension. *Hypertens. Res.* **36,** 770–775 (2013).

184. Hermans, H. *et al.* Murine pressure overload models: a 30-MHz look brings a whole new ‘sound’ into data interpretation. *J. Appl. Physiol.* **117,** 563–571 (2014).

185. Hahurij, N. D. *et al.* Echocardiographic assessment of embryonic and fetal mouse heart development: a focus on haemodynamics and morphology. *ScientificWorldJournal.* **2014,** 531324 (2014).

186. Guasch, E. *et al.* Atrial fibrillation promotion by endurance exercise: demonstration and mechanistic exploration in an animal model. *J. Am. Coll. Cardiol.* **62,** 68–77 (2013).

187. Pratt, S. J. P., Valencia, A. P., Le, G. K., Shah, S. B. & Lovering, R. M. Pre- and postsynaptic changes in the neuromuscular junction in dystrophic mice. *Front. Physiol.* **6,** 252 (2015).

188. Vachon, P. H. *et al.* Integrins (alpha7beta1) in muscle function and survival. Disrupted expression in merosin-deficient congenital muscular dystrophy. *J. Clin. Invest.* **100,** 1870–81 (1997).